Calcium-Activated Chloride Currents in Salamander Cone Photoreceptors

by

Mélanie Renée Lalonde

Submitted to the Faculty of Graduate Studies in partial fulfillment of the requirements for the degree of Doctor of Philosophy

at

Dalhousie University
Halifax, Nova Scotia
Canada

March 2005

Your file Votre référence
ISBN: 0-494-00973-X
Our file Notre référence
ISBN: 0-494-00973-X

DALHOUSIE UNIVERSITY

To comply with the Canadian Privacy Act the National Library of Canada has requested that the following pages be removed from this copy of the thesis:

Preliminary Pages
- Examiners Signature Page (pii)
- Dalhousie Library Copyright Agreement (piii)

Appendices
- Copyright Releases (if applicable)

For Mom and Dad

Table of Contents

Signature Page ii

Copyright Agreement Page iii

Dedication Page iv

List of Tables xii

List of Figures xiii

Abstract xvii

List of Abbreviations and Symbols Used xviii

Acknowledgements xxiii

Chapter 1 Introduction 1

1.1 Organization of the vertebrate retina 3

1.2 Visual Pathways 6

1.3 Photoreceptor classification 11

1.3.1 Tiger salamander photoreceptor classification 11

1.4 Photoreceptors are morphologically polarized neurons 13

1.4.1 The cone pedicle 18

1.5 Photoreceptors are non-spiking neurons that hyperpolarize in response to light stimulation 22

1.6 Ca^{2+} dynamics in cone photoreceptors 23

1.6.1 Ca^{2+} regulation at the inner segment 24

1.6.1.1 Ca^{2+} influx via voltage-gated Ca channels 27

1.6.1.2 Ca^{2+} extrusion via plasma membrane Ca^{2+}-ATPases (PMCAs) 34

1.6.1.3 Ca^{2+} sequestration into endoplasmic reticulum Ca^{2+} stores 36

1.7 Chloride channels 45

1.7.1 The ClC family of Cl channels 46

1.7.2 Ca^{2+}-activated Cl channel family 52

1.7.2.1 Properties of Cl(Ca) channels 52

1.7.2.2 Molecular structure of Cl(Ca) channels 54

1.8 Goals and hypotheses 56

Chapter 2 Methods **59**

2.1 Isolation of cone photoreceptors 60

2.2 Solutions 63

2.3 Drugs 65

2.4 Whole-cell current recordings 66

2.5 Instruments 72

2.6 Quantitative evaluation 73

Chapter 3 Characterization of $I_{Cl(Ca)}$ in Isolated Tiger Salamander Cone Photoreceptors 77

3.1 $I_{Cl(Ca)}$ is activated by depolarization-evoked Ca^{2+} influx 78

3.2 Free $[Ca^{2+}]_i$ sets the amplitude and kinetics of Ca^{2+}-activated Cl^- tail currents, which deactivate following a saturated exponential function 81

3.3 Cone photoreceptor $I_{Cl(Ca)}$ is characterized by outward rectification 86

3.4 Increased Cl(Ca) channel activation by Ca^{2+} influx through voltage-gated L-type Ca channels 94

3.5 Barium increases depolarization-induced current but inhibits Ca^{2+}-activated Cl^- tail currents 98

3.6 $I_{Cl(Ca)}$ in salamander cone photoreceptors is blocked by the Cl channel blocker NPPB 101

3.7 $I_{Cl(Ca)}$ is not modulated by calmodulin or by calmodulin inhibitors 104

3.8 Cl(Ca) channels are not vesicular ClC-3 channels 110

3.9 Summary 116

Chapter 4 Role of Ca^{2+} Released from Ca^{2+} Stores in Gating Salamander Cone Photoreceptor Cl(Ca) Channels **119**

4.1 Blocking Ca^{2+}-reuptake mechanisms into Ca^{2+} stores does not modulate $I_{Cl(Ca)}$ 120

4.2 IP_3-sensitive Ca^{2+} stores do not generally contribute to Cl(Ca) channel activation 125

4.3 Ryanodine-sensitive Ca^{2+} stores do not contribute to $I_{Cl(Ca)}$ activation 129

4.3.1 The source of Ca^{2+} for $I_{Cl(Ca)}$ activation during depolarization is not ryanodine-sensitive 130

4.3.2 Caffeine has no effect on $I_{Cl(Ca)}$ elicited by the standard depolarizing protocol 133

4.4 Inhibition of $I_{Cl(Ca)}$ by lanthanum (La^{3+}) 137

4.5 $I_{Cl(Ca)}$ is significantly increased by repeated depolarizing pulses in the presence of caffeine 140

4.6 Summary 146

Chapter 5 High $[Ca^{2+}]_i$-Induced Inhibition of $I_{Cl(Ca)}$ **148**

5.1 Enhancement of $I_{Cl(Ca)}$ followed by inhibition during repeated depolarizing pulses at 1 sec intervals in the presence of caffeine 149

5.2 $I_{Cl(Ca)}$ is inhibited following repeated strong depolarizations 153

5.3 $I_{Cl(Ca)}$ inhibition following repeated strong depolarizations is increased in the presence of SERCA pump inhibitors 156

5.4 $I_{Cl(Ca)}$ inhibition following repeated strong depolarizations is increased and becomes irreversible in the presence of H-8, a protein kinase inhibitor 159

5.5 $I_{Cl(Ca)}$ is enhanced by okadaic acid, a protein phosphatase inhibitor, and is inhibited by its washout 168

5.6 Enhancement of $I_{Cl(Ca)}$ is followed by inhibition in the presence of ionomycin 171

5.7 A transient conductance is observed at -60 mV holding potential in the presence of ionomycin 178

5.8 In the absence of extracellular Ca^{2+}, ionomycin does not activate $I_{Cl(Ca)}$ 181

5.9 Summary 185

Chapter 6 Discussion 189

6.1 Cl(Ca) channels are activated by submembrane $[Ca^{2+}]_i$ 190

6.1.1 $I_{Cl(Ca)}$ activation is tightly coupled to Ca^{2+} influx 191

6.1.2 Deactivation of Ca^{2+}-activated Cl^- tail currents reflects changing submembrane Ca^{2+} levels 192

6.1.3 Cone photoreceptor Cl(Ca) channels may be co-localized with L-type Ca channels at the plasma membrane 193

6.1.4 Cone Cl(Ca) channels may be directly activated by Ca^{2+} 194

6.2 Negligible role of Ca^{2+} released from Ca^{2+} stores in gating of salamander cone $I_{Cl(Ca)}$ 194

6.2.1 Ca^{2+} responsible for $I_{Cl(Ca)}$ activation is not amplified by calcium-induced Ca^{2+}-release from ryanodine-sensitive Ca^{2+} stores 195

6.2.2 RyR channels may be spatially distant from Cl(Ca) channels in salamander cone photoreceptors 196

6.2.3 Ca^{2+} release from internal stores may not contribute to submembrane Ca^{2+} levels 197

6.2.4 Cl(Ca) channels are likely not regulated by IP_3-sensitive Ca^{2+} stores 198

6.3 Ca^{2+} released from caffeine-sensitive stores contributes to $I_{Cl(Ca)}$ regulation only when Ca^{2+} levels are increased 199

6.4 High $[Ca^{2+}]_i$-induced inhibition of $I_{Cl(Ca)}$ 201

6.4.1 Caffeine-sensitive stores regulate $I_{Cl(Ca)}$ when submembrane $[Ca^{2+}]_i$ is overloaded 201

6.4.2 Mechanisms involved in $I_{Cl(Ca)}$ activation may be disrupted by high $[Ca^{2+}]_i$ 202

6.4.3 Phosphorylation mechanisms affect Cl(Ca) channel activation 203

6.4.4 Direct Cl(Ca) channel inhibition may explain $I_{Cl(Ca)}$ inhibition when submembrane Ca^{2+} levels are elevated 204

Chapter 7 Conclusion 206

7.1 Future studies 208

7.2 Finding the major functional role for Cl(Ca) channels in cone photoreceptors 210

7.2.1 $I_{Cl(Ca)}$ may play a significant role in mediating the effects of synaptic feedback from horizontal cells during surround illumination of a cone 210

7.2.2 The role of $I_{Cl(Ca)}$ during the feedback response depends on E_{Cl} 212

7.3 Finding the molecular identity for Cl(Ca) channels in cone photoreceptors 213

7.3.1 Is the channel responsible for $I_{Cl(Ca)}$ a member of the CLCA family? 214

Appendix 1 Ionomycin Increases $[Ca^{2+}]_i$ in a Sustained Manner in Salamander Cone Photoreceptors 216

Appendix 2 IP_3-Induced Oscillations in $I_{Cl(Ca)}$ 219

References 224

List of Tables

2.1	Composition of extracellular solutions (mM)	64
2.2	Composition of intracellular solutions (mM)	64

List of Figures

1.1	Schematic representation of a cross section through the vertebrate retina, showing the neuronal architecture	5
1.2	A simplified schematic of the rod and cone retinal visual pathways	8
1.3	A schematic structure of a cone photoreceptor showing two distinct compartments: the outer segment and the inner segment	16
1.4	Electron micrograph of two invaginating synapses within a cat cone pedicle	21
1.5	In the cone pedicle, Ca^{2+} is regulated by voltage-gated Ca channels, PMCAs, SERCAs, IP_3Rs, and RyRs	26
1.6	Dendrogram comparing the human amino acid sequences of $\alpha 1$ subunits of voltage-gated Ca channels	29
1.7	Structural organization of multi-subunit voltage-gated Ca channels	32
1.8	The mammalian ClC family of Cl channels	50
2.1	Typical salamander cone photoreceptors examined during patch-clamp experiments	62
2.2	Diffusion of ions from the patch-pipette into the cell cytoplasm following the whole-cell patch-clamp configuration	68
2.3	Simplified circuit for the whole-cell patch-clamp configuration	71
2.4	A representative example of whole-cell voltage-clamp recording and analysis obtained from a salamander cone photoreceptor	75

3.1 $I_{Cl(Ca)}$ activates following depolarization-evoked Ca^{2+} influx in isolated tiger salamander cone photoreceptors 80

3.2 Salamander cone Ca^{2+}-activated Cl^- tail currents, which deactivates following a saturated exponential function, are regulated by free $[Ca^{2+}]_i$ 84

3.3 Step depolarizations in the presence of ionomycin (IONO; 5 or 10 μM; n=3) evoked sustained $I_{Cl(Ca)}$ activation in cone photoreceptors 88

3.4 Calcimycin (ionophore A23187) did not modify $I_{Cl(Ca)}$ in cone photoreceptors 91

3.5 Repeated strong depolarizations (0 mV pulses of 100 ms duration, repeated at 2 Hz) elicited sustained $I_{Cl(Ca)}$ activation, characterized by outward rectification at positive potentials 93

3.6 Cone photoreceptor Cl(Ca) channels are activated by Ca^{2+} influx through voltage-gated L-type Ca channels 96

3.7 Ca^{2+} substitution with barium (Ba^{2+}) in the extracellular solution increases the current measured during depolarizing voltage steps and abolishes Ca^{2+}-activated Cl^- tail currents 100

3.8 The chloride channel blocker NPPB (100 μM) reduced $I_{Cl(Ca)}$ and Ca channel currents in salamander cone photoreceptors 103

3.9 Activation of Cl(Ca) channels by Ca^{2+} is not regulated via an intermediate mechanism involving calmodulin (CaM), a Ca^{2+}-binding protein 106

3.10 CaM inhibitors, trifluoperazine and calmidazolium, had insignificant effects on $I_{Cl(Ca)}$ 109

3.11 Cl(Ca) channels responsible for $I_{Cl(Ca)}$ are not vesicular ClC-3 channels that integrate with the plasma membrane upon Ca^{2+} influx 113

3.12 Blocking vesicle docking with Tetanus toxin did not modulate $I_{Cl(Ca)}$ 115

4.1 Inhibiting Ca^{2+}-reuptake into Ca^{2+} stores via SERCA pump blockade using cyclopiazonic acid and thapsigargin did not modulate $I_{Cl(Ca)}$ 124

4.2 $I_{Cl(Ca)}$ was insensitive to Ca^{2+}-release from IP_3-sensitive Ca^{2+} stores (n=5) 128

4.3 CICR from ryanodine-sensitive stores does not contribute to depolarization-evoked $I_{Cl(Ca)}$ activation since ryanodine (Ry; 10 μM; n=7) had little effect on $I_{Cl(Ca)}$ 132

4.4 Superfusion of caffeine (1 mM; n=4, 10 mM; n=5) does not modulate $I_{Cl(Ca)}$, suggesting that Ca^{2+} release from caffeine-sensitive Ca^{2+} stores does not contribute to Cl(Ca) channel activation in cone photoreceptors 135

4.5 The PMCA and Ca channel antagonist, lanthanum (La^{3+}; 1 mM; n=5), inhibits $I_{Cl(Ca)}$ without immediate recovery 139

4.6 The increase in $I_{Cl(Ca)}$ induced by repetitive depolarizing pulses was enhanced in the presence of caffeine (3 mM and 10 mM) 143

4.7 Example of current increase elicited by repetitive depolarizing pulses in control conditions and in the presence of 3 mM caffeine 145

5.1 Repetitive depolarizing steps at 1 sec intervals induce a transient $I_{Cl(Ca)}$ increase in the presence of caffeine 152

5.2 $I_{Cl(Ca)}$ is inhibited in a reversible manner following repeated strong depolarizations 155

5.3 $I_{Cl(Ca)}$ inhibition following repeated strong depolarizations seen in control conditions was increased in the presence of the SERCA pump blocker, thapsigargin 158

5.4 Inhibition of $I_{Cl(Ca)}$ following repeated strong depolarizations seen in control conditions was increased in the presence of cyclopiazonic acid 161

5.5 H-8 alone did not modulate $I_{Cl(Ca)}$ (n=5) 165

5.6 H-8 increased the repeated strong depolarization-induced inhibition effect on $I_{Cl(Ca)}$ and prevented current recovery (n=4) 167

5.7 When dephosphorylation mechanisms are inhibited or activated, $I_{Cl(Ca)}$ is increased and inhibited via negative and positive shifts in activation curves, respectively 170

5.8 $I_{Cl(Ca)}$ is enhanced then subsequently inhibited in the presence of ionomycin (5 or 10 μM; n=3) 174

5.9 Ionomycin (5 or 10 μM) transiently increases $I_{Cl(Ca)}$ but inhibits the current measured during depolarizing voltage steps to -20 mV (repeated every 5 or 15 sec; n=5) 176

5.10 Cl(Ca) channels may also be inhibited by high $[Ca^{2+}]_i$ achieved via ionomycin superfusion 180

5.11 In the absence of extracellular Ca^{2+}, ionomycin (5 or 10 μM; n=6) does not activate $I_{Cl(Ca)}$ 183

Abstract

Calcium-activated chloride channels are present in cone photoreceptors but their physiological role has not clearly been defined. This dissertation characterizes the kinetics and regulation of Ca^{2+}-activated Cl^- currents ($I_{Cl(Ca)}$) in salamander cone photoreceptors and provides evidence for their functional role in the retina. $I_{Cl(Ca)}$, sensitive to the Cl channel blocker NPPB, activates in response to depolarization-evoked Ca^{2+} influx. The slow and complex deactivation kinetics of Ca^{2+}-activated Cl^- tail currents following repolarization is considered to reflect the changing submembrane concentration of intracellular calcium ($[Ca^{2+}]_i$). The dihydropyridine Ca channel agonist BayK increased $I_{Cl(Ca)}$, demonstrating the importance of Ca^{2+} entry through L-type Ca channels for Cl(Ca) channel activation. The deactivation kinetics of $I_{Cl(Ca)}$ were resistant to manipulations of Ca^{2+} uptake and release from Ca^{2+} stores. The sarcoplasmic/endoplasmic reticulum Ca^{2+}-ATPase (SERCA) pump inhibitors, cyclopiazonic acid and thapsigargin, had no significant effect on tail current kinetics. IP_3 and the Ca^{2+}-induced Ca^{2+} release (CICR) modulators, caffeine and ryanodine, also had no discernable effect on the tail current. However, the submembrane $[Ca^{2+}]_i$-dominated deactivation kinetics of $I_{Cl(Ca)}$ were altered by increased $[Ca^{2+}]_i$ when modulating agents of Ca^{2+} stores were combined with repetitive depolarizations to induce Ca^{2+}-loading. Under these conditions, $I_{Cl(Ca)}$ became strongly inhibited. Thus, the normal activation and deactivation of $I_{Cl(Ca)}$ appears to be dominated by fast Ca^{2+} diffusion and buffering, but stores provide essential regulation of $[Ca^{2+}]_i$ when Ca^{2+} influx is very high. High $[Ca^{2+}]_i$-induced inhibition of $I_{Cl(Ca)}$, which involves dephosphorylation mechanisms within the cell, may reflect fast inhibition of Ca channels, followed by a slower inhibition of Cl(Ca) channels. In darkness, when intracellular Ca^{2+} levels are highest within cone photoreceptors, $I_{Cl(Ca)}$ may prevent strong depolarizations; however, in overloaded Ca^{2+} conditions, Ca and Cl(Ca) channel inhibition likely represents an effective protective mechanism for the cells.

List of Abbreviations and Symbols Used

A	amacrine
Amp	amplifier
AMPA	alpha-amino-3-hydroxy-5-methyl-4-isoxazole propionate
ANOVA	analysis of variance
ATP	adenosine triphosphate
B	bipolar
BAPTA	1,2-bis(-aminophenoxy)ethane-N,N,N',N'-tetraacetic acid
Ba	barium
Ba^{2+}	barium ion
$BaCl_2$	barium chloride
BayK	(±)-Bay K 8644
(±)-Bay K 8644	1,4-Dihydro-2,6-dimethyl-5-nitro-4-(2-[trifluoromethyl]phenyl)pyridine-3-carboxylic acid methyl ester
C	cone
Ca	calcium
Ca^{2+}	calcium ion
$[Ca^{2+}]_i$	intracellular calcium concentration
$CaCl_2$	calcium chloride
CICR	calcium-induced calcium release
Ca_f	cytosolic Ca^{2+}
CAF	caffeine
CaM	calmodulin
CaMK	calmodulin-dependent protein kinase
cAMP	cyclic adenosine monophosphate
Cd^{2+}	cadmium ion
cGMP	cyclic guanosine monophosphate
Cl	chloride
Cl^-	chloride ion
Cl(Ca)	calcium-activated chloride

C_m	membrane capacitance
CNG	cyclic nucleotide-gated
CPA	cyclopiazonic acid
Cs^+	cesium ion
CsCl	cesium chloride
CsOH	cesium hydroxyde
DAG	diacylglycerol
DMSO	dimethyl sulfoxide
E_{Cl}	equilibrium potential for chloride
EGTA	ethylene glycol bis(2-aminoethyl ether)-N,N,N'N'-tetraacetic acid
EtOH	ethanol
ER	endoplasmic reticulum
GABA	gamma-aminobutyric acid
GCL	ganglion cell layer
GΩ	gigaohm
GTP	guanosine 5' triphosphate
H	horizontal cell
H-8	N-[2-Methlamino)ethyl]-5-isoquinolinesulfonamide hydrochloride
HCl	hydrochloric acid
HEPES	N-(2-hydroxyethyl-piperazine-N'-(2-ethanesulphonic acid)
hr	hour
Hz	hertz
I	interplexiform
I	membrane current
I_{Ca}	calcium current
$I_{Cl(Ca)}$	calcium-activated chloride current
iCSNB	incomplete congenital stationary night blindness
I_{deact}	deactivating current
I_{exp}	exponential current
I_h	hyperpolarizing current
I_K	potassium current

I_{max}	saturation amplitude
INL	inner nuclear layer
IONO	ionomycin
IP_3	inositol trisphosphate
IP_3R	inositol trisphosphate receptor
IPL	inner plexiform layers
IS	inner segment
I-V	current-voltage
K	potassium
K^+	potassium ion
KCl	potassium chloride
kHz	kilohertz
La^{3+}	lanthanum ion
Lu-ECAM	lung-endothelial cell adhesion molecule
LVA	low-voltage-activated
m	slope factor
Mg^{2+}	magnesium ion
$MgCl_2$	magnesium chloride
mg	milligram
min	minute
ml	milliliter
mm	millimeter
mV	millivolt
MΩ	megaohm
n	cooperativity constant (Hill coefficient)
NA	noradrenaline
Na	sodium
Na^+	sodium ion
NaCl	sodium chloride
NaOH	sodium hydroxyde
NCKX	sodium/calcium, potassium (Na^+/Ca^{2+}, K^+) exchanger

NFL	nerve fiber layer
Ni^{2+}	nickel ion
nm	nanometer
nM	nanomolar
NPPB	5-Nitro-2-(3-phenylpropylamino)benzoic acid
OA	okadaic acid
OH	hydroxide
ONL	outer nuclear layer
OPL	outer plexiform layer
OS	outer segment
pC	picocoulomb
pF	picofarad
PKA	protein kinase A
PKC	protein kinase C
PIP2	phosphatidylinositol 4,5 biphosphate
PLC	phospholipase C
PMCA	plasma membrane calcium-ATPase
PP	protein phosphatase
pS	picosiemen
Q	charge
R	rod
R_c	cell membrane resistance
R_f	feedback resistor
RPE	retinal pigment epithelium
R_s	series resistance
Ry	ryanodine
RyR	ryanodine receptor
sec	second
s.e.m	standard error of the mean
SR	synaptic ribbon
TeTox	tetanus toxin

TG	thapsigargin
μL	microliter
μm	micrometer
μM	micromolar
V	voltage
Vc	command potential
Vm	membrane potential

Acknowledgements

I would like to acknowledge a number of people who have directly or indirectly contributed to the present dissertation. I must first acknowledge my supervisor, Steven Barnes, for taking the risk of taking on a PhD student with no biophysical background. Thank you Steve for your confidence, help, and support throughout the past 3 years. I feel privileged to have learned the patch-clamp technique from you. I would like to recognize other members of the Laboratory for Retina & Optic Nerve Research: Francois Tremblay, Bal Chauhan, and especially Melanie Kelly and Bill Baldridge. Thank you so much for our numerous scientific discussions and your assistance with all lab-related problems. I am particularly thankful for the day-to-day interactions with lab technicians, Michele Archibald, Terry Levatte, Kelly Stevens, and Christine Jollimore. Thank you guys for being my family away from home. I will really miss you all! I would also like to thank fellow students and postdocs who were instrumental in my learning process. Thank you Andy Hartwick for your help with calcium imaging experiments, 'John John' Vessey for ongoing stimulating conversations, Nicole Welch for your help with work-related stress, and Manuel Arias for sharing your electrophysiological expertise. Michael Jonz deserves special recognition for all his input and corrections for this dissertation, especially the 'frenchisms' (and believe me, there were many!).

On a more personal note, I would like to thank a close friend of mine, Hari Nair. Thanks Guz for the numerous intellectual conversations. I really wished that we had published our 'quotes' book. We would so be famous by now! I would like to thank my good friend, Anna Stratis, for her positive energy. Anna, I really feel privileged to know you! I am especially grateful to all my family members. Mom and Dad, thank you for

making things easier with your constant support. My brother, Jean Lalonde, is so incredibly intelligent. I wish that I were a natural like you are! Thank you to my sister Ninon Lalonde and to Yvan Pilon, as well as my two nephews, Cédric and Jacob Pilon, for reminding me what life is all about. Finally, a special thank you to Martin Marion and his family for their encouragement. Thank you 'puce' for your love. I cannot wait to be with you...

Chapter 1

Introduction

The retina is a highly organized layer of neuronal tissue that functions to detect environmental stimuli by analyzing the spatial and temporal patterns of light. Cone photoreceptors are fundamental neurons involved in the capture and conversion of photons into electrochemical signals, which are then transmitted to the brain. The ion channel composition of cone photoreceptors has been previously studied (Maricq and Korenbrot, 1988; Barnes and Hille, 1989; Lasater and Witkovsky, 1991; Maricq and Korenbrot, 1990a; Maricq and Korenbrot, 1990b; Yagi and MacLeish, 1994). Among important conductances involved in cone function is a chloride conductance activated by intracellular Ca^{2+}, called Ca^{2+}-activated Cl^- current, or $I_{Cl(Ca)}$. It is generally considered that a key role of $I_{Cl(Ca)}$ in cone photoreceptors is to stabilize membrane potential and prevent strong depolarizations (Bader et al., 1982; Maricq and Korenbrot, 1988; Thoreson and Burkhardt, 1991; Barnes and Deschenes, 1992). The characterization of $I_{Cl(Ca)}$ activation is the focus of this dissertation, and the results bear on the question of the role of $I_{Cl(Ca)}$ in visual processing.

Chapter 1 will highlight the anatomical and physiological properties of the vertebrate retina, with particular emphasis on cone photoreceptors, the cells of interest for the present research. More specifically, Ca^{2+} dynamics at the cone inner segment will be presented and $I_{Cl(Ca)}$ will be introduced. Chapter 2 consists of the detailed methods, including a description of the whole-cell patch-clamp recording technique, used to study $I_{Cl(Ca)}$ in freshly isolated salamander cone photoreceptors. Chapter 3 will outline important characteristics unique to $I_{Cl(Ca)}$ and demonstrate how the gating of Cl(Ca) channels depends on intracellular Ca^{2+} concentration ($[Ca^{2+}]_i$). The data from Chapter 4 will describe the role of intracellular Ca^{2+} stores in $I_{Cl(Ca)}$ activation. Chapter 5 will

introduce the hypothesis that excessive $[Ca^{2+}]_i$ leads to $I_{Cl(Ca)}$ inhibition, a phenomenon not previously described in cone photoreceptors. Chapter 6 consists of a general discussion of the findings presented in this dissertation and will explain how they contribute to the overall understanding of cone function. Finally, Chapter 7 summarizes all findings and outlines proposals for future research.

1.1 Organization of the vertebrate retina

The vertebrate retina is a portion of the central nervous system (CNS) consisting of a well-structured arrangement of neurons and glia (see review by Wassle and Boycott, 1991). The laminar organization of the retina is shown in Figure 1.1. Two layers of synaptic contacts, called the outer and inner plexiform layers (OPL and IPL, respectively), separate three distinct layers of neuronal cell bodies, called the outer nuclear layer (ONL), inner nuclear layer (INL), and ganglion cell layer (GCL). The cell bodies of the photoreceptors, rods (R) and cones (C), are located in the outer nuclear layer. The synaptic terminals of photoreceptors contact second-order neurons, bipolar (B) and horizontal (H) cells (Dowling, 1987). Whereas bipolar cells are involved in the vertical transmission pathway, relaying information from photoreceptors to retinal ganglion cells (G), horizontal cells are responsible for lateral interactions within the outer retina. The inner nuclear layer contains the cell bodies of those second order neurons, as well as amacrine (A), and interplexiform (I) cells. Amacrine cells are known to be responsible for interactions within the inner retina, whereas interplexiform cells link the two plexiform layers by receiving synaptic input in the inner plexiform layer and making synapses upon neurons at the outer plexiform layer. Müller cells, the principal type of

Figure 1.1 Schematic representation of a cross section through the vertebrate retina, showing the neuronal architecture. The cell bodies of retinal neurons are located in three layers: the outer nuclear layer (ONL), the inner nuclear layer (INL), and the ganglion cell layer (GCL). Whereas the outer nuclear layer contains the cell bodies of rod (R) and cone (C) photoreceptors, the inner nuclear layer includes those of horizontal (H), bipolar (B), amacrine (A), and interplexiform (I) cells. Synaptic contacts between retinal neurons located in the outer and inner nuclear layers occur in the outer plexiform layer (OPL). Retinal ganglion cell (G) bodies are located in the ganglion cell layer. Retinal neurons found in the inner nuclear layer make synaptic contacts with these cells in the inner plexiform layer (IPL). Retinal ganglion cells are the output neurons of the retina, as their axons form the nerve fiber layer (NFL), which projects to higher visual centers in the brain via the optic nerve. (Adapted from Dowling, 1996).

Figure 1.1

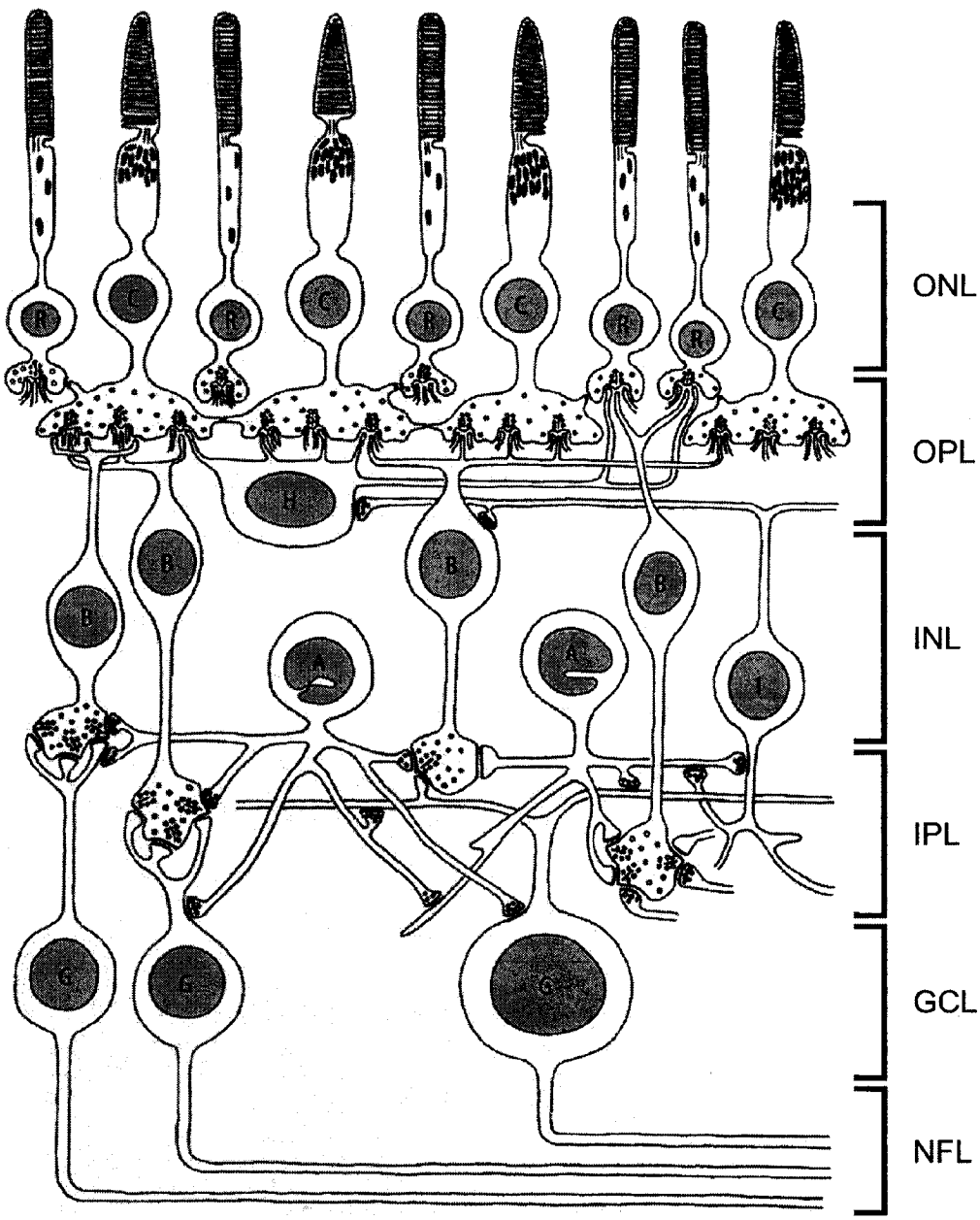

retinal glia, extend throughout the entire depth of the retina. Their cell bodies, however, are usually located in the inner nuclear layer. The cell bodies of the retinal ganglion cells form the innermost nuclear layer of the retina, called the ganglion cell layer. Displaced amacrine cells are also found in the ganglion cell layer and can comprise as much as 20% of the total amacrine cell population of the macaque monkey retina (Koontz et al., 1993). Retinal ganglion cell axons form the nerve fiber layer (NFL) and, via the optic nerve, are responsible for the transmission of visual information from the retina to higher visual centers located in the brain.

1.2 Visual pathways

Visual information is channeled to the brain via multiple synaptic pathways. Figure 1.2 illustrates the vertical pathway, which consists of information transfer from photoreceptors to retinal ganglion cells via bipolar cells. Retinal neurons responding with sign-preserving (hyperpolarizing) and sign-inverting (depolarizing) responses to light are shown in grey and white, respectively. The cone (C) circuitry through the retina differs from that of the rod (R). Cone photoreceptors connect with two basic types of bipolar cell, referred to as ON- and OFF-cone bipolar cell (ON- and OFF Cone BC). They make sign-inverting synapses with ON-cone bipolar cells and sign-preserving synapses with OFF-cone bipolar cells. This subdivision of cone bipolar cells can be related to the type of connection that they make with the output synapse of cone photoreceptors, called the cone pedicles (described in Section 1.4.1). ON-cone bipolar cell dendrites are inserted centrally into the invaginating synapses of the cone pedicles (see Fig. 1.4). On the other hand, OFF-cone bipolar cells make flat contacts with the base

Figure 1.2 A simplified schematic of the rod and cone retinal visual pathways. Retinal cells that respond with sign-preserving and sign-inverting synapses are shown in grey and white, respectively. The cone (C) and rod (R) retinal circuitry differ. Cone photoreceptors make sign-preserving synapses with horizontal cells (HC) and OFF-cone bipolar cells (OFF-Cone BC), and sign-inverting synapses with ON-cone bipolar cells (ON-cone BC). ON- and OFF-cone bipolar cells relay the visual information to ON- and OFF-ganglion cells (ON- and OFF-GC), establishing a parallel ON and OFF-cone pathway. Rod photoreceptors synapse with one type of bipolar cell called the ON-rod bipolar cell (ON-Rod BC), which does not directly contact the retinal ganglion cells. Rather, they make synaptic connections with AII amacrine cells (AII AC). AII amacrine cells relay excitatory and inhibitory input from the rod signal to the established parallel ON- and OFF-cone pathways, respectively.

Figure 1.2

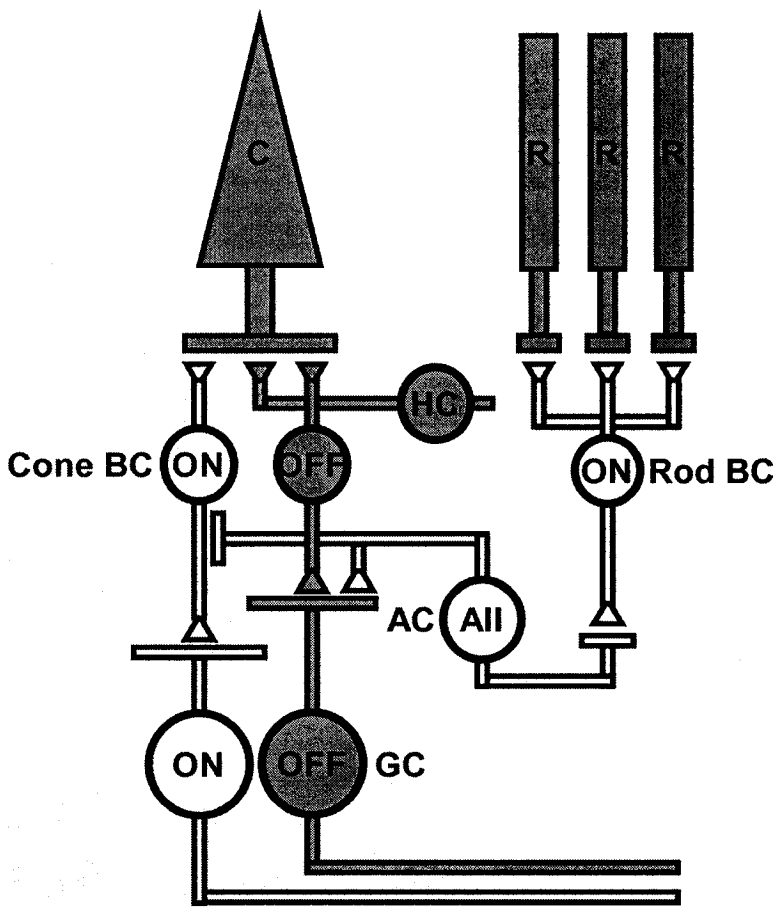

of the cone pedicles (Dowling and Boycott, 1966; Boycott and Kolb, 1973; Vardi et al., 1998). Cone photoreceptors also make sign-preserving synapses with horizontal cells. Horizontal cells are coupled to each other via gap junctions (see reviews by Kaneko, 1971; Naka, 1971). These cells have large receptive fields, as their dendrites form a dense network in the outer plexiform layer, and provide a surround-induced inhibition to the central cone response (Baylor et al., 1971; Naka, 1971; Lasansky, 1981).

The response of ON- or OFF-cone bipolar and horizontal cells to the release of glutamate from the presynaptic cone terminal is determined by their corresponding glutamate receptors (Slaughter and Miller, 1985; Brandstatter et al., 1998). Glutamate receptors are divided into two major groups: metabotropic receptors (mGluR), which activate a second messenger signal cascade via a G-protein (Pin and Duvoisin, 1995), and ionotropic receptors (iGluR), which are integral membrane proteins responsible for the opening of non-selective cation channels when activated by glutamate (Dingledine et al., 1999). Metabotropic glutamate receptors embedded in ON-bipolar cell dendrites link glutamate to the closure of cation channels, which causes these cells to hyperpolarize in the dark (Nawy and Jahr, 1991; Yamashita and Wässle, 1991). The specific G-protein-coupled receptor located at the ON-bipolar cell is thought to be mGluR6 (Nomura et al., 1994; Vardi and Morigiwa, 1997). Whereas ON-bipolar cells have metabotropic glutamate receptors, ionotropic AMPA and kainate glutamate receptors are expressed on the postsynaptic OFF-cone bipolar and horizontal cell dendrites (Schultz et al., 1997; Morigiwa and Vardi, 1999; Qin and Pourcho, 1999; Yazulla and Studholme, 1999). Glutamate released from the presynaptic cone terminals causes sodium (Na^+) influx through ionotropic glutamate receptors, thereby depolarizing these cells in the dark.

Cone bipolar cells make direct synaptic connections with ganglion cell dendrites (Kolb, 1974). ON- and OFF-cone bipolar cells connect ON- and OFF-ganglion cells (ON- and OFF-GC), respectively, and these contacts are made in different sublamina of the inner plexiform layer (Nelson et al., 1978). These direct parallel ON and OFF pathways in the cone circuitry differ, at least in mammals, from those of the rod visual circuitry. Rod photoreceptors make synaptic connections with a single type of bipolar cell, called the ON-rod bipolar cell (ON Rod BC). The rod synaptic terminal, called the rod spherule, has two synaptic ribbons, which are associated with two laterally positioned horizontal cell axon terminals and two centrally invaginating ON-rod bipolar cell dendrites. The synaptic connection between rod photoreceptors and ON-rod bipolar cells is sign-inverting and consequently these cells depolarize to light, although rod photoreceptors are in a hyperpolarized state. ON-rod bipolar cell axons terminate in the inner plexiform layer of the retina, close to retinal ganglion cell bodies. Unlike cone bipolar cells, which make direct contacts with retinal ganglion cells, ON-rod bipolar cells form sign-preserving synaptic contacts onto a type of amacrine cell, the ON-center AII amacrine cell (AII AC) (Kolb and Famiglietti, 1974; Famiglietti and Kolb, 1975; Kolb and Nelson, 1983; Chun et al., 1993). Amacrine cells relay information to both classes of cone bipolar cells. They make sign-inverting synapses with OFF-cone bipolar cells, inhibiting these cells via a conventional glycinergic synapse. Excitatory input originating from the rods is conducted through gap junctions between AII amacrine cells and ON-cone bipolar cells. Cone bipolar cells can subsequently convey rod input to retinal ganglion cells via the established parallel ON and OFF pathways.

1.3 Photoreceptor classification

Two types of photoreceptors, rods and cones, transduce light stimuli into an electrical signal. Most vertebrates, including humans, have a rod-dominated retina. Rod photoreceptors respond to dim light and mediate vision in dimly lit environments (scotopic vision). They have a higher level of photopigment than cones and are therefore more sensitive to light. Although relatively slow in their response to light stimulation, rods can reliably detect single photons. Cones only represent 3% of all photoreceptors in the human adult retina. They are concentrated at the center of the retina, a region called the fovea, but are dramatically outnumbered by rods in the periphery. Cone photoreceptors operate optimally in daylight (photopic vision). They are less sensitive than rods but are faster to respond and provide high acuity vision due to their close packing. Whereas rods only contain the photopigment rhodopsin, trichromatic species, such as humans, have three isoforms of opsin expressed in distinct cone types. The three human cone types have peak wavelength sensitivities at 440-450 nm (blue cones), 535-555 nm (green cones), and 570-590 nm (red cones). Due to their different spectral sensitivities, cones are responsible for colour vision. Other mammalian species, such as mice, are dichromatic and lack the long wavelength cone. Some lower vertebrates, including the tiger salamander, lack green-sensitive cones but have a cone subtype that expresses an opsin molecule responsible for detection of ultraviolet light.

1.3.1 Tiger salamander photoreceptor classification

The retina of the tiger salamander, *Ambystoma tigrinum*, is commonly used to study both retinal physiology and circuitry, mainly due to the large size and excellent

survival of their retinal cells. Photoreceptor subtype identification has been extensively studied in these animals using a combination of morphological- and immunocytochemical-based techniques (Harosi, 1975; Mariani, 1986; Makino et al., 1991; Perry and McNaughton, 1991; Braekevelt, 1993; Makino and Dodd, 1996; Sherry et al., 1998). Six morphological types of photoreceptors, which appear to be distributed in all retinal regions, can be distinguished in the tiger salamander retina: two rod subpopulations, identified as M- and S-rods, and four cone subpopulations, called small single cones, large single cones, and principal and accessory members of double cones (Mariani, 1986; Sherry et al., 1998).

Rods are the most abundant type of photoreceptor in the tiger salamander retina, comprising 62% of the total photoreceptor population (Mariani, 1986; Sherry et al., 1998). They are larger than cones and easily distinguished by their long, rod-shaped outer segments. M- and S-rods (medium and short wavelength-sensitive) respectively correspond to the 'red' and 'green' rods previously reported in frog retinas (Liebman and Entine, 1968; Hicks and Molday, 1986). They can be discriminated based on their morphology and spectral sensitivity. M-rods are larger and far more numerous than S-rods, representing ~98% of the total rod population (Bader et al., 1982; Mariani, 1986; Sherry et al., 1998). Their maximum sensitivity (~520 nm) is in the medium wavelength range. S-rods are smaller than M-rods, due to their smaller outer segment size (Sherry et al., 1998), and are quite rare, representing only 1% of the total photoreceptor population. S-rods respond best to shorter wavelength light, as they show peak sensitivity at 430 nm (Cornwall et al., 1984; Makino and Dodd, 1996).

Tiger salamander cones make up 38% of the total photoreceptor population (Mariani, 1986; Sherry et al., 1998). Two types of single cones have been described based on morphological criteria: a small single cone and a large single cone (Mariani, 1986). Small single cones can be distinguished by their shorter and smaller inner segment, and are somewhat more numerous than S-rods, making up to 5% of the total photoreceptor population. This least common type of cone in salamander retina can be further divided into three subtypes based on their maximal spectral sensitivity: red- (610 nm), blue- (440 nm), and UV- (380 to 400 nm) sensitive (Makino et al., 1990; Perry and McNaughton, 1991; Makino and Dodd, 1996; Sherry et al., 1998). The largest and best-characterized population of cones is the large single cone. With their short conical outer segment, and their elongated inner segment, they can be morphologically distinguished from the double cones and the smaller and less numerous small single cones. Double cones, identified by paired somata, inner segments, and small outer segments (see Fig. 2.1), are not electrically coupled (Atwell et al., 1984). The principal member of the double cone has a slender inner segment, and can therefore be distinguished from the accessory member. Similar to red-sensitive small single cones, large single and double cones are red-sensitive with a peak sensitivity at 610 nm (Mariani, 1986; Perry and McNaughton, 1991; Makino and Dodd, 1996; Sherry et al., 1998).

1.4 Photoreceptors are morphologically polarized neurons

Photoreceptors are divided into two main compartments: the outer segment and the inner segment, which includes the ellipsoid region, the cell body, and the synaptic terminal. A diagram of cone photoreceptor morphology is shown in Figure 1.3. The

photoreceptor outer segments are positioned in close proximity to a specialized monolayer of opaque cells, collectively termed the retinal pigment epithelium (RPE). Located behind the RPE layer is a vascularized choroid, which offers nutrients vital to photoreceptor survival and function. In addition to providing necessary trophic support fundamental to photoreceptor function, the RPE cells also facilitate the transport of both nutrients and metabolic waste between the vasculature of the choriocapillaris and the photoreceptors. Another important role served by RPE cells is to absorb photons that have not been absorbed by photopigment.

The cone outer segment is filled with uniformly spaced lamellar membranes, which are continuously renewed by invaginations of the plasma membrane at the base of the outer segment, and which shed from the apical surface. Photon capture by opsin molecules embedded within the phospholipid bilayer of the outer segment disk initiates the phototransduction cascade. Phototransduction is the process by which photons of light are absorbed by visual pigment molecules in a photoreceptor cell and translated into an electrochemical signal that is sent to the brain (see review by Burns and Baylor, 2001).

Numerous organelles are located in the cone inner segment at specific subdivisions. The mitochondria, responsible for the cell's energy production, and the endoplasmic reticulum (ER), the main source of Ca^{2+} stores, are predominantly located at the ellipsoid and subellipsoid regions, respectively. Opsin molecules are synthesized in the inner segment and translocated to the outer segment via a vesicular transport system. A physically distinguishable part of the inner segment is the synaptic terminal, or cone pedicle. Cone pedicles consist of a number of invaginating synapses, which contain

Figure 1.3 A schematic structure of a cone photoreceptor showing the two distinct compartments: the outer segment and the inner segment. The outer segment is embedded within a layer of opaque cells called retinal pigment epithelium (RPE). Inserted into folds of the outer segment plasma membrane are photopigments, which are responsible for capturing light photons and initiating the phototransduction cascade. The inner segment can be further divided into three different compartments: the ellipsoid region, the cell body, and the synaptic terminal, also called the cone pedicle. The ellipsoid region is the energy-producing center of the cell due to the large amount of mitochondria. The main location of Ca^{2+} stores, the endoplasmic reticulum (ER), is mainly found in the subellipsoid region, which also contains the Golgi complex. The synaptic terminal consists of many invaginating synapses and is the site of glutamatergic neurotransmission from cones to second order neurons. It contains dense structures known as synaptic ribbons, which direct the flow of glutamate-filled vesicles to release sites at the plasma membrane. Only one invaginating synapse, exaggerated in size, is shown in the diagram for simplification. (Adapted from Krizaj and Copenhagen, 2002).

Figure 1.3

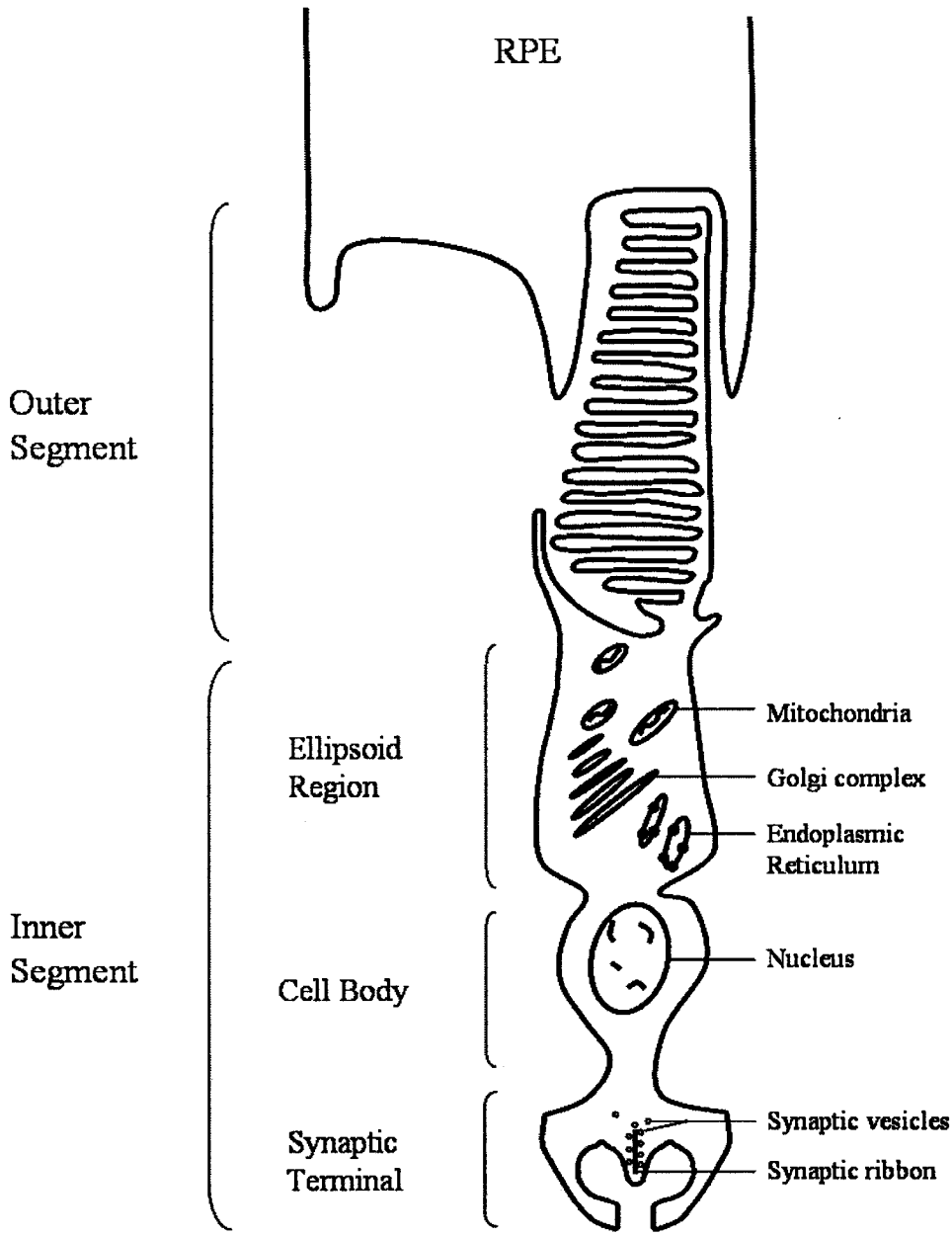
RPE
Outer Segment
Inner Segment
Ellipsoid Region
Cell Body
Synaptic Terminal
Mitochondria
Golgi complex
Endoplasmic Reticulum
Nucleus
Synaptic vesicles
Synaptic ribbon

glutamate-filled vesicles. These output synapses are the site of glutamatergic neurotransmission from photoreceptors to second order neurons and will be reviewed in the next section.

The membrane protein composition of the outer and inner segment also differs. The photoreceptor outer segment only contains one class of ion channel, which are non-selective cation channels called the cyclic-nucleotide gated channels (CNGCs or cyclic guanosine 5'-monophosphate (cGMP)-gated channels). Also located at the outer segment is an electrogenic Na^+:K^+, Ca^{2+} exchanger (also called NCKX), responsible for Ca^{2+} extrusion (Cervetto et al., 1989; Reid et al., 1990; Krizaj and Copenhagen, 1998). Conversely, a number of different classes of ion channels are localized to the inner segment plasma membrane. In salamander cone photoreceptors, these channels are responsible for the following five conductances: a Ca^{2+}-activated Cl^- current ($I_{Cl(Ca)}$), the focus of the present study, a voltage-gated Ca^{2+} current (I_{Ca}), a voltage-gated K^+ current (I_{Kx}), a Ca^{2+}-activated K^+ current ($I_{K(Ca)}$), and a current activated by hyperpolarization (I_h) (Barnes and Hille, 1989). $I_{Cl(Ca)}$ was first identified in salamander rod inner segments (Bader et al., 1982) and *Xenopus* oocytes (Miledi, 1982; Barish, 1983). The presence of $I_{Cl(Ca)}$ was first detected in salamander cones by Lasansky (1981) and then described in lizard (Maricq and Korenbrot, 1988), salamander (Barnes and Hille, 1989) and primate (Yagi and MacLeish, 1994) retina. I_{Ca} activates at potentials positive to -40 mV and peaks at membrane potentials close to -10 mV. Salamander cone Ca channels do not show inactivation; however, in general, different Ca channel subtypes differ in their inactivation (Hille, 2001). I_{Ca} was also described in lizard (Maricq and Korenbrot, 1988), turtle (Lasater and Witkovsky, 1991), and primate (Yagi and MacLeish, 1994) cone

photoreceptors. Beech and Barnes (1989) discovered I_{Kx} in isolated salamander rods. This conductance, which was also described in lizard cone inner segments (Maricq and Korenbrot, 1990a), is a calcium-insensitive outwardly rectifying K channel that is blocked by tetraethylammonium (TEA). $I_{K(Ca)}$ activates positive to -30 mV, but only becomes prominent close to 0 mV, outside the normal operating range of the cell. I_h is a non-selective inward current that activates and deactivates at membrane potentials negative and positive to -50 mV, respectively. Maricq and Korenbrot (1990b) described a similar I_h, responsible for shaping the recovery phase of the photoreceptor light response, in isolated lizard cones. In addition to the five conductances described above, a glutamate-activated Cl channel exists in tiger salamander cone photoreceptors (Picaud et al., 1995; Larsson et al., 1996). Due to its ionic dependence and pharmacology, this glutamate-elicited current has been suggested to be generated by a glutamate transporter coupled to a Cl channel (Grant and Werblin, 1996). Furthermore, high densities of ion transporters, such as plasma membrane Ca^{2+}-ATPases (PMCAs), are located at the inner segment (Krizaj and Copenhagen, 1998; Morgans et al., 1998; Krizaj et al., 2002).

1.4.1 The cone pedicle

Cone pedicles, the location of the multiple output synapses of a single cone photoreceptor, have been previously described in the primate retina (Missoten, 1965; Dowling and Boycott, 1966; Calkins et al., 1996; Chun et al., 1996). Each pedicle is 6 to 10 μm in diameter and is characterized by invaginating synapses that vary in number depending on the location of a cone photoreceptor within the retina. For example, approximately twenty and forty invaginating synapses have been estimated in macaque

cones located in the fovea and periphery, respectively (Chun et al., 1996). Each cone invaginating synapse typically contains three postsynaptic dendrites: two laterally positioned horizontal cell dendrites and one centrally positioned ON-cone bipolar cell dendrite. It is therefore referred to as a triad (Dowling and Boycott, 1966). Figure 1.4, an electron micrograph by Kolb (1974), illustrates this organization. Altogether, a single cone pedicle is thought to be associated with several hundred individual synaptic contacts (Missotten, 1965; Chun et al., 1996; Haverkamp et al., 2000). Braekevelt (1993) studied the tiger salamander photoreceptor population via light and electron microscopy. His observations indicate that, like in mammals, cones have synaptic pedicles, which show several invaginated and superficial synapses.

The photoreceptor synaptic terminals are concentrated with glutamate-filled vesicles (Lasansky, 1973; Adly et al., 1999). Associated with each invaginating synapse is a dense structure known as synaptic ribbon, which directs the flow of glutamate-filled vesicles to release sites at the plasma membrane of synaptic terminals (Rao-Mirotznik et al., 1995). In vertebrates, synaptic ribbons have also been described in rods, bipolar cells, and the cochlear hair cells of the auditory system (Wagner, 1997). The sustained high rate of tonic neurotransmitter release from photoreceptor terminals requires the presence of ribbon synapses. At these sites, as in conventional synapses, Ca^{2+} influx following presynaptic depolarization triggers exocytosis of vesicles docked at the active zone.

Figure 1.4 Electron micrograph of two invaginating synapses within a cat cone pedicle. Each cone pedicle is characterized by many invaginating synapses, but only two are pictured here. Each invaginating synapse exists as a triad due to the presence of two horizontal cell dendrites (HC), and one ON-bipolar cell dendrite (ON-BC). Each triad holds a single synaptic ribbon (SR), located at glutamate release sites. Synaptic ribbons facilitate the rapid fusion of synaptic vesicles to the synaptic terminal plasma membrane and maintain the high rate of glutamate release from photoreceptors in darkness. Scale bar is 100 nm. (Adapted from Kolb, 1974).

Figure 1.4

1.5 Photoreceptors are non-spiking neurons that hyperpolarize in response to light stimulation

The physiology of different retinal cell types, including photoreceptors, has been extensively reviewed (Kolb, 1994; Masland, 2001). An important feature of photoreceptors is that they do not signal with action potentials but instead relay changes in the intensity of the light stimulus as graded variations in membrane potential, which allows for the optimal rate of information transfer to second order neurons (Laughlin, 1989; Juusola et al., 1996). Vertebrate photoreceptors are in a depolarized state in darkness and are thus continuously releasing glutamate, the neurotransmitter of the vertical pathway in the retina (Copenhagen and Jahr, 1989). Glutamate release from photoreceptors is suppressed following their hyperpolarizing response to light. The cone resting potential is somewhere between -30 mV and -46 mV (Baylor and Fuortes, 1970; Attwell et al., 1982; Wu, 1991; Thoreson and Bryson, 2004) due to the steady-state cation influx through cyclic-nucleotide gated channels (CNGCs). Similar to other ligand-gated cation channels, ion permeation through CNGCs is relatively non-specific with approximately 80% of the inward current carried by Na^+ and the remainder carried primarily by Ca^{2+} (Detwiler and Gray-Keller, 1992). Light stimulation activates a G-protein-mediated enzymatic cascade that hydrolyzes cGMP, causing the CNGCs in the outer segment to close. Following the closure of CNGCs, Ca^{2+} influx ceases while extrusion via the Na^+:K^+, Ca^{2+}-exchanger continues. This results in a decrease in $[Ca^{2+}]_i$ (Yarfitz and Hurley, 1994) and the cone membrane potential hyperpolarizes to -60 or -50 mV (Toyoda et al., 1970). At the photoreceptor synaptic terminal, this hyperpolarization leads to the closure of voltage-gated Ca channels and a decrease in Ca^{2+}-dependent

glutamate release into the synaptic cleft (Rieke and Schwartz, 1996; Schmitz and Witkovsky, 1996; Witkovsky et al., 1997).

1.6 Ca^{2+} dynamics in cone photoreceptors

Ca^{2+} regulates a number of different processes within a cell including the gating of certain channels (e.g., Cl(Ca) channels), and the regulation of a wide variety of intracellular second messenger-mediated pathways. Steady-state $[Ca^{2+}]_i$ is regulated by Ca^{2+} entry, extrusion, buffering via a number of Ca^{2+}-binding proteins including calmodulin, and sequestration into internal stores (Berridge et al., 2000). Cells are able to maintain a large Ca^{2+} concentration gradient between the cytosol and the extracellular media. Basal cytosolic $[Ca^{2+}]_i$ (~50 nM) is usually 30,000-fold less than extracellular Ca^{2+} levels (~1.5 mM). However, large fluctuations of free cytosolic Ca^{2+} (Ca_f) can be achieved via Ca^{2+} influx and Ca^{2+} released from intracellular stores. A localized change in $[Ca^{2+}]_i$ is an important characteristic for Ca^{2+} signaling in different parts of the cell. Ca^{2+} function and homeostasis is greatly compartmentalized in photoreceptors due to the spatial distribution of Ca^{2+} effector proteins, such as Ca channels and pumps, cytoplasmic buffers, and intracellular Ca^{2+} stores (Krizaj and Copenhagen, 1998). Since transport and diffusion of Ca^{2+} between the outer and inner segment appears to be limited, the signaling action of Ca^{2+} may be restricted to the level of micro-, and even nanodomains.

In the outer segment, Ca^{2+} regulates photoreceptor light adaptation and recovery by independently adjusting the gain of phototransduction at different steps in the cascade (Nakatani and Yau, 1988; Fain et al., 2001). In the inner segment, which is subdivided into the ellipsoid region, cell body, and the synaptic terminal, Ca^{2+} controls several

processes including energy metabolism, gene expression, and neurotransmitter release, respectively. Steady-state $[Ca^{2+}]_i$ at the photoreceptor inner segment also controls many key Ca^{2+}-dependent cellular events, including protein kinase and phosphatase activity (Krizaj and Copenhagen, 2002). Cl(Ca) channels, the channels of interests in the present dissertation, are also thought to be dependent on $[Ca^{2+}]_i$ in the inner segment, where voltage-gated Ca channels and Cl(Ca) channels are preferentially localized at the plasma membrane.

1.6.1 Ca^{2+} regulation at the inner segment

$[Ca^{2+}]_i$ measurements at the photoreceptor inner segment and synaptic terminal have been estimated at ~50 nM in bright light and between ~300 to ~500 nM in the dark (Ratto et al., 1988; Gray-Keller and Detwiler, 1996; Sampath et al., 1999). In the dark, $[Ca^{2+}]_i$ levels are high enough to regulate transmitter release in the inner segment, but low enough to prevent Ca^{2+}-mediated cytotoxicity and the triggering of apoptosis (He et al., 2000). A simplified cartoon of Ca^{2+} regulation at the inner segment is shown in Figure 1.5. As previously mentioned, the operating voltage range of photoreceptors is between approximately -70 mV in saturating light and approximately -35 mV in the dark. Voltage-gated Ca channels located at the photoreceptor inner segment are hence activated in the dark, at depolarized resting potentials, leading to a large Ca^{2+}influx (Rieke and Schwartz, 1996; Witkovsky et al., 1997). This influx of Ca^{2+} is offset by Ca^{2+} extrusion, buffering, and uptake into internal stores. Extrusion of Ca^{2+} from the cone occurs by means of plasma membrane Ca^{2+}-ATPases (PMCAs). Via sarcoplasmic/endoplasmic

Figure 1.5 In the cone pedicle, Ca^{2+} is regulated by voltage-gated Ca channels, PMCAs, SERCAs, IP_3Rs, and RyRs. Following depolarization, Ca^{2+} enters the pedicle via voltage-gated Ca channels (green). Intracellular Ca^{2+} may be sequestered by Ca^{2+} stores through sarcoplasmic/endoplasmic reticulum Ca^{2+}-ATPases (SERCAs) or extruded via plasma membrane Ca^{2+}-ATPases (PMCAs). Two different types of Ca^{2+}-release stores exist in the cone photoreceptor: an IP_3-sensitive Ca^{2+}-store and a ryanodine-sensitive Ca^{2+}-store. The ryanodine receptor channel is also sensitive to caffeine, and mediates Ca^{2+}-induced Ca^{2+} release within the cell. HC: horizontal cells, IP_3R: inositol trisphosphate receptor, RyR: ryanodine receptor. The arrows represent movement of Ca^{2+} ions.

Figure 1.5

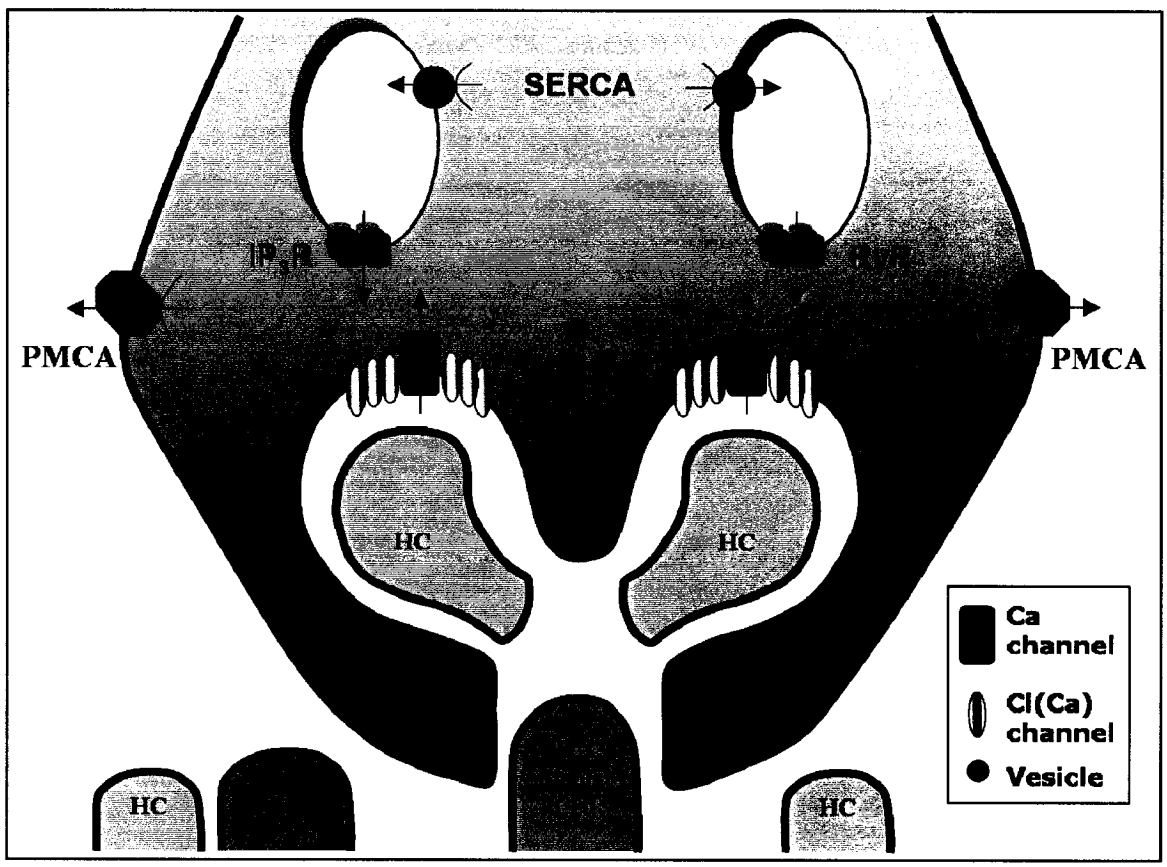

reticulum Ca^{2+}-ATPases (SERCAs), Ca^{2+} is thought to be sequestered into two different types of Ca^{2+} stores. One type is sensitive to inositol trisphosphate (IP_3) and the other to ryanodine (Ry) and caffeine, and is responsible for Ca^{2+}-induced Ca^{2+} release (CICR). Voltage-gated Ca channels, PMCAs, SERCAs, IP_3 receptors (IP_3Rs), and Ry receptors (RyRs) have all been shown to be expressed in the tiger salamander cone photoreceptor inner segment, and will be reviewed in further details in following sections.

1.6.1.1 Ca^{2+} influx via voltage-gated Ca channels

Voltage-gated Ca channels form a broad and diverse family of ion channels. They are a major route by which Ca^{2+} enters cells down a steep electrochemical gradient ($E_{Ca} \cong +150$ mV), and contribute to a variety of cellular functions ranging from membrane depolarization, neurotransmitter release, and initiation of intracellular signaling cascades. A classification scheme for voltage-activated Ca channels is shown in Figure 1.6. Based on their electrophysiological properties and pharmacological profile, different nomenclatures have been used to identify Ca channel subtypes (Tsien et al., 1988; Snutch et al., 1990; Birnbaumer et al., 1994; Ertel et al., 2000). According to the Tsien nomenclature (Tsien et al., 1988), voltage-gated Ca channels may be subdivided into five different groups. Four of them, L, P/Q, N and R-type, have a high-voltage threshold for activation (HVA), whereas the T-type Ca channels display low-voltage threshold for activation (LVA).

The molecular structure of voltage-gated Ca channels reveals that they are multi-subunit proteins. The $\alpha 1$ subunit forms the channel pore, whereas $\alpha 2$, β, and δ are

Figure 1.6 Dendrogram comparing the human amino acid sequences of $\alpha 1$ subunits of voltage-gated Ca channels. The family tree is divided into three branches, leading to the nomenclature Ca_v1-3. Based on the Tsien nomenclature, five different Ca channels can be distinguished: L- P/Q-, N- and R-type Ca channels, which have a high-voltage of activation (HVA) (branches Ca_v1 and 2), and T-type Ca channels which display low-voltage activation (LVA) (branch Ca_v3) (Tsien et al., 1988). (Adapted from Ertel et al., 2000).

Figure 1.6

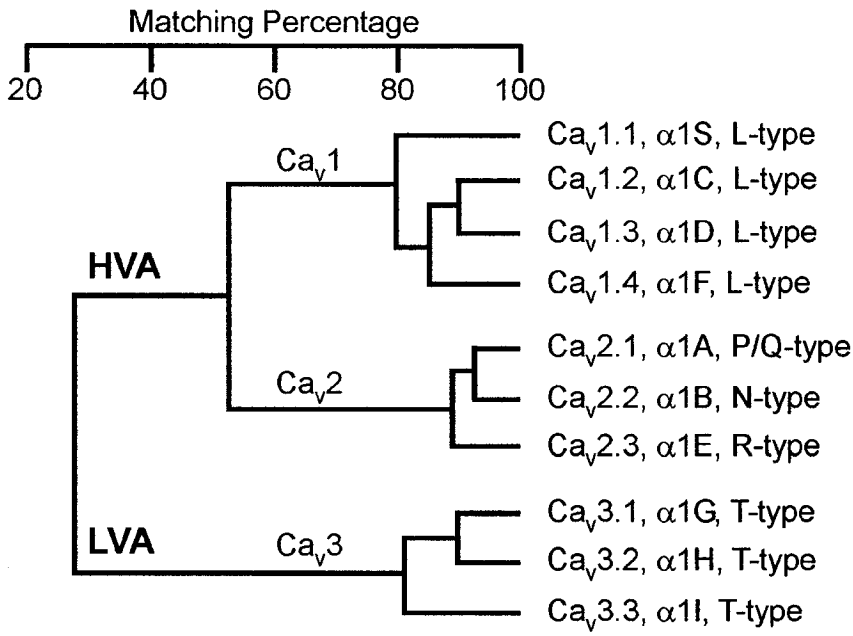
Matching Percentage
20
40
60
80
100
HVA
LVA
Ca_V1
Ca_V2
Ca_V3
$Ca_V1.1$, α1S, L-type
$Ca_V1.2$, α1C, L-type
$Ca_V1.3$, α1D, L-type
$Ca_V1.4$, α1F, L-type
$Ca_V2.1$, α1A, P/Q-type
$Ca_V2.2$, α1B, N-type
$Ca_V2.3$, α1E, R-type
$Ca_V3.1$, α1G, T-type
$Ca_V3.2$, α1H, T-type
$Ca_V3.3$, α1I, T-type

auxiliary subunits (Fig. 1.7). The α_1 subunit is characterized by four homologous repeats (domains I to IV) containing six membrane-spanning regions (S1-S6). S4 holds positively charged amino acids and forms part of the voltage sensor, while the pore region of the channel is created by two additional domains between S5 and S6. To date, ten α_1 subunits (α_1A-I, and S) have been cloned and described (Fig. 1.6). L-type Ca channels are formed by α1S, α1C, α1D, and α1F and are coded by specific Ca_v1 genes. The α1A, α1B, and α1E form P/Q, N, and R channels, respectively, and are coded by genes of the Ca_v2 family. T-type Ca channels, which carry a transient current and thus characterized by fast inactivation, consist of α1G, α1H, and α1I, and are coded by Ca_v3 genes. It is important to note that low voltage-activated Ca channels are not present in salamander cone photoreceptors (Barnes and Hille, 1989).

Wilkinson and Barnes (1996) have characterized the Ca channel current in tiger salamander cone photoreceptor inner segments using the patch-clamp technique. Their study suggested that the majority of HVA Ca channel currents are dihydropyridine (DHP)-sensitive, implying a prevalence of L-type Ca channels. A small fraction of the current was sensitive to ω-conotoxin GVIA, an N-type Ca channel blocker; however, the inhibition was reversible, which is unusual for N-type Ca channels, and the authors suggested that this reflects 'non-specific' block of L-type Ca channels by the toxin. Immunohistochemical and electrophysiological studies in amphibian and mammalian photoreceptors have demonstrated that α1D and α1F L-type Ca channels are localized in high densities at the pre-synaptic membrane terminal, which implies that they are involved in Ca^{2+}-dependent exocytosis of synaptic vesicles (Taylor and Morgans, 1998).

Figure 1.7 Structural organization of multi-subunit voltage-gated Ca channels. The α1 subunit consists of four homologous domains (I-IV) and forms the channel pore. The α1 subunit is also the location where many pharmacological agents bind. The cytoplasmic loops are labeled according to the domains they link. α2, β, and δ are auxiliary subunits important in controlling the structure and activity of the α1 subunit. The β subunit corresponds to a series of α helices. The yellow barrels indicate hydrophobic regions of the α2-δ. The branched structures represent predicted glycosylation sites. (Adapted from Walker and DeWaard, 1998).

Figure 1.7

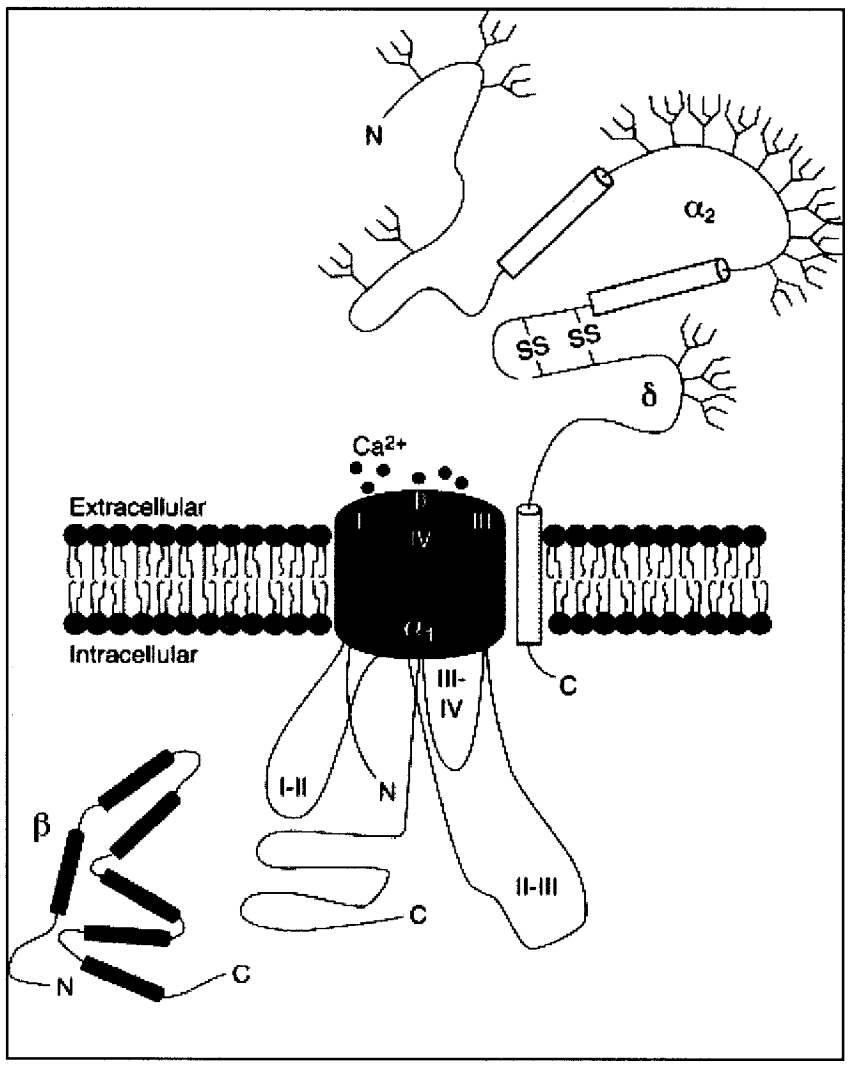
N
α_2
SS SS
δ
Ca^{2+}
Extracellular
I
II
III
IV
α_1
Intracellular
III-IV
C
I-II
N
β
II-III
C
N
C

The dihydropyridine-sensitive L-type Ca channels have long lasting open states activated at relatively high voltages, usually positive to -30 mV. The canonical L-type Ca channels inactivate relatively slowly (τ >500 ms) and their activation range is between -60 and -10 mV. However, cone photoreceptor Ca channels are non-inactivating, a property essential to sustaining tonic transmitter release (Taylor, 1998; Yagi and MacLeish, 1994). L-type Ca channels are characterized by large single channel conductances (~25 pS) compared to other family members (~8 to 13 pS), are blocked by divalent ions such as Cd^{2+} and Ni^{2+}, and usually have a relatively greater Ba^{2+} conductance than Ca^{2+} (see review by Hille, 2001). Different tissues express L-type Ca channels with different α1 subunits. Immunohistochemical data demonstrate that the α1F subunit is localized to rod photoreceptor active zones in rat retinal sections, supporting its role in synaptic transmission (Morgans, 2001). The retina-specific Ca channel α1-subunit gene (*Cacna1f*) was also identified in human rod photoreceptors (Bech-Hansen et al., 1998; Strom et al., 1998). Mutations in this gene (also called $Ca_v1.4$), which encodes the α1F protein, result in incomplete congenital stationary night blindness (iCSNB). A mouse model of iCSNB was shown to have impaired photoreceptor Ca^{2+} signaling and synaptic transmission (Mansergh et al., submitted). Immunohistochemical data collected from mammalian retinas demonstrate that cone Ca channels localized at the synaptic terminal appear to possess the α1D subunit (Taylor and Morgans, 1998; Morgans, 1999; Morgans, 2000), which is in agreement with the previously described pharmacological profile of salamander HVA Ca channel currents by Wilkinson and Barnes (1996). Unlike the α1F subunit, which is also found in cones (Morgans, 2001), the α1D subunit has been found to be expressed in different neurons.

1.6.1.2 Ca^{2+} extrusion via plasma membrane Ca^{2+}-ATPases (PMCAs)

Ca^{2+} is extruded from the cone outer segment by the Na^+/Ca^{2+}, K^+ exchangers (NCKXs). NCKX1, the isoform expressed in photoreceptors (Haase et al., 1990; Kim et al., 1998), exchanges four Na^+ for one Ca^{2+} and one K^+ (Schnetkamp et al., 1989; Szerencsei et al., 2001). Unlike the outer segment, there is little evidence for the presence of Na^+/Ca^{2+}, K^+ exchangers in the photoreceptor inner segment (Kim et al., 1998; Krizaj and Copenhagen, 1998; Krizaj et al., 2004). Ca^{2+} extrusion from the photoreceptor inner segment mainly occurs via the high-Ca^{2+} affinity membrane potential-independent plasma membrane Ca^{2+}-ATPase (PMCA) (Krizaj and Copenhagen, 1998; Morgans et al., 1998; Krizaj et al., 2002). Auditory hair cells, also characterized by graded, sustained responses, use PMCAs for Ca^{2+} extrusion as well (Yamoah et al., 1998). In mammals, PMCAs have been suggested to be localized to the lateral walls of the photoreceptor synaptic terminal, away from the active zone (Morgans et al., 1998; Morgans, 2000). PMCAs may be responsible for setting $[Ca^{2+}]_i$ at the plasma membrane where they could influence Ca^{2+} signaling events (Monteith and Roufogalis, 1995; Thayer et al., 2002). The regulation of neurotransmitter exocytosis likely depends on Ca^{2+} microdomains at the plasma membrane and not on longitudinal Ca^{2+} gradients, and therefore, others have suggested their co-localization with Ca channels close to the active zone (Schaeffer et al., 1982; Krizaj et al., 2002).

PMCAs, which are known to be effectively inhibited by lanthanides, are characterized by ten transmembrane regions, with both cytoplasmic N- and C-terminals (see review by Strehler and Treiman, 2004). The phosphorylation domain is located in the second cytosolic loop, which is found between transmembrane domains four and five.

The high affinity of PMCAs for Ca^{2+} relies on the fact that calmodulin (CaM) is constitutively attached to these pumps, at the CaM-binding site near the C-terminus (James et al., 1988; Enyedi et al., 1989; Guerini et al., 1998). PMCAs are also tightly regulated by Ca^{2+} itself. They remain in an auto-inhibited inactive state as long as the local Ca^{2+} concentration remains low (<50-100 nM). In its inactive state, the C-terminus tail is in contact with the two cytoplasmic loops, preventing high affinity Ca^{2+}-binding to the CaM-binding site. In its active state, Ca^{2+}-loaded calmodulin is bound to the regulatory C-terminus.

The PMCA family of Ca^{2+} pumping-ATPases includes four members (PMCA1-4). In mammals, the different PMCA isoforms are coded by four separate genes (Strehler and Treiman, 2004). These isoforms differ in their affinities for Ca^{2+}, calmodulin, and ATP (Guerini et al., 1998; Strehler and Zacharias, 2001). The distribution of PMCA isoforms, which has been studied via immunohistochemistry, reveals that they are ubiquitously expressed in retinal cells. PMCA1 has been shown to be expressed in photoreceptor inner segments of the mouse (Krizaj et al., 2002) and tiger salamander retina (Krizaj et al., 2004). These studies revealed that this isoform was expressed primarily at the synaptic terminal, suggesting a role for PMCAs in regulating synaptic transmission. Weak expression of PMCA1 was found in salamander rod photoreceptors, which may explain faster Ca^{2+} extrusion from cone inner segments as demonstrated by Ca^{2+}-imaging studies (Krizaj and Copenhagen, 1998; Krizaj et al., 2003). Of the four PMCA isoforms, PMCA2 has the highest affinity for Ca^{2+} (Guerini et al., 1998), and it is typically found in neuronal tissues. PMCA2 is also expressed in cone photoreceptors; however, the expression, which was only observed occasionally, was confined to the

outer segments (Krizaj et al., 2004). In addition, PMCA4 was also shown to be expressed in salamander cones at the inner segment cell body and synaptic terminals, and therefore, this isoform could also contribute to Ca^{2+} extrusion (Krizaj et al., 2004).

1.6.1.3 Ca^{2+} sequestration into endoplasmic reticulum Ca^{2+} stores

The removal of cytoplasmic Ca^{2+} by sequestration into intracellular stores is a critically important physiological process. In addition to providing rapid Ca^{2+} removal, Ca^{2+} stores are also sources of localized and fast acting Ca^{2+} signals. Therefore, the balance between two opposed Ca^{2+} fluxes, via Ca^{2+} pumps and Ca^{2+}-release channels, determines the net contribution of Ca^{2+} stores in modulating $[Ca^{2+}]_i$ dynamics. In most cells, the primary intracellular Ca^{2+} storage/release organelle is the ER, which represents a complex system of endomembranes, forming a continuous network. Photoreceptors, as do most neurons, sequester Ca^{2+} in both the rough and smooth ER, which are abundantly present within the photoreceptor inner segment (Ungar et al., 1984; Somlyo and Walz, 1985; Freihofer et al., 1990). Although the smooth ER has sometimes also been found in the synaptic terminal region (Mercurio and Holtzmann, 1982; Ungar et al., 1984), the distribution of the ER cisternae in lower vertebrate photoreceptors is mostly confined to the subellipsoid space of the inner segment (Mercurio and Holtzmann, 1982; Townes-Anderson et al., 1985; Ripps and Chappell, 1991).

In addition to intraluminal Ca^{2+}-binding proteins (i.e. calsequestrin), responsible for keeping the concentration of free ions low, several families of proteins are localized to the endomembrane, including Ca^{2+}-release channels. Ca^{2+} is released from ER Ca^{2+} stores through the activation of specific receptors. Two different families of Ca^{2+}-release

channels, each consisting of three members, are responsible for Ca^{2+} release from ER stores (see review by Berridge, 1993; Coronado et al., 1994; Furuichi et al., 1994; Mikoshiba et al., 1994; Sorrentino, 1995; Taylor, 1998; Patel et al., 1999; Fill and Copello, 2002). Inositol trisphosphate (IP_3) binds to one family of Ca^{2+}-release channels, called IP_3 receptors or IP_3R. The second family includes channels that are modulated by the alkaloid, ryanodine, and are therefore called ryanodine receptors or RyR. Each Ca^{2+}-release channel represents a large oligomeric structure formed by the association of four proteins. In addition, both IP_3 and Ry receptors are activated by $[Ca^{2+}]_i$.

IP_3-sensitive Ca^{2+} stores

The IP_3 intracellular signaling pathway was first discovered in the early 1980s (Streb et al., 1983; Berridge and Irvine, 1984). Since then, a number of studies have characterized IP_3Rs and the pathways leading to IP_3-dependent Ca^{2+} release in neurons. The formation of IP_3 occurs via two major receptor-mediated pathways, which require the activation of phospholipase C (PLC) (see review by Rhee and Bae, 1997). In response to different stimuli (such as neurotransmitters, hormones, and growth factors), PLC catalyzes the hydrolysis of phosphatidylinositol biphosphate (PIP_2), an inositol lipid stored in the plasma membrane, to produce two intracellular messengers, IP_3 and diacylglycerol (DAG). Whereas DAG mediates the activation of protein kinase C (PKC), IP_3 released into the cytoplasm mobilizes Ca^{2+} from internal stores (Berridge et al., 2000). PKC can influence neurotransmitter release as well as modulate ion channels and receptor function, and is therefore important in neuronal signaling.

One of the pathways leading to the formation of IP_3 is initiated by a family of G protein-coupled receptors and involves PLC-β. Several G protein-coupled receptors exist, and include receptors for acetylcholine, histamine, noradrenaline (NA), serotonin (5-HT), glutamate, endothelin, as well as light. These agonists induce a conformational change in the G protein-coupled receptor leading to the dissociation of heterotrimeric G proteins into G_α and $G_{\beta\gamma}$ subunits, which can activate different PLC-β isozymes. The other pathway responsible for the production of IP_3 begins with the activation of tyrosine kinase receptors, which interact with the γ-form of PLC. Upon binding of an agonist, such as a growth factor, two tyrosine kinase receptors are brought together, enabling their cytoplasmic kinase domains to autophosphorylate tyrosine residues and create docking sites for PLC-γ. Cytoplasmic PLC-γ translocates to the membrane, binds the activated receptors via its Src homology 2 (SH2) domain, and is phosphorylated on specific tyrosine residues. Activated PLC-γ may then hydrolyze PIP_2 at the membrane to give rise to DAG and IP_3.

The molecular structure of members of the IP_3R family is diverse. Three different IP_3R isoforms, with alternative splice variants, have thus far been identified (Danoff et al., 1991; Nakagawa et al., 1991; Nucifora et al., 1995). IP_3Rs are Ca^{2+}-permeant channels assembled from four subunits. The subunits combine to form homo- or hetero-tetrameric channels. Each subunit has an IP_3-binding site positioned towards the large cytoplasmic N-terminus (see review by Taylor et al., 2004). The membrane-spanning domains located in the C-terminus, anchor the protein in the membrane and form the channel pore. IP_3-induced Ca^{2+} release occurs in a quantal manner, meaning that a fixed proportion of the stored Ca^{2+} is released as the level of IP_3 rises (Bootman et al., 1992;

Ferris et al., 1992). Although not fully understood, IP_3 is thought to work by producing a conformational change in the IP_3R leading to an increase in channel-opening frequency (Mignery and Südhof, 1990). The sensitivity of IP_3R increases as the stores fill with Ca^{2+} (Missiaen et al., 1992). Ca^{2+} ions also regulate IP_3R in that they function as co-agonists with IP_3 to release stored Ca^{2+}. IP_3 bound to the receptor is thought to open the pore by promoting the binding of Ca^{2+}, thereby destabilizing an inhibitory interaction between N-terminus residues and a C-terminal 'gatekeeper' sequence (Taylor et al., 2004).

An immunohistochemical study by Peng et al. (1991) investigated the presence of the IP_3R protein in the vertebrate retina using an antibody against purified brain IP_3Rs. The study revealed that the IP_3R protein is present almost exclusively in the synaptic layers of the salamander retina. Using dissociated retinal neurons, high density IP_3Rs were further localized to presynaptic terminals of photoreceptors and bipolar cells, as well as the synaptic processes of amacrine cells. Although IP_3Rs have also been found at ribbon synapses in mammalian photoreceptors and bipolar cells (Stella et al., 2003), the specific isoform expressed in tiger salamander cone photoreceptors remains unclear. The IP_3R3 isoform has been shown to be expressed in pancreatic islets, kidney, and gastrointestinal tract, but rarely in neurons (Sorrentino and Rizzuto, 2001). Consistent with these findings, the IP_3R3 isoform was shown to be absent from tiger salamander retina (Krizaj et al., 2004). The IP_3R1 has been shown to be the predominant neuronal isoform in mammals (Furuichi et al., 1993), and Wang et al. (1999) demonstrated the expression of IP_3R1 in mammalian cone (especially red- and green- sensitive) outer segments, at their plasma and disk membrane. However, IP_3R2, but not IP_3R1, was detected in tiger salamander cone inner segments at the subellipsoid space, but not at the

synaptic terminal (Krizaj et al., 2004). This is consistent with the finding that most of the ER is distributed within the subellipsoid region (Mercurio and Holtzman, 1982). In central neurons, IP_3 receptor-mediated Ca^{2+} store-release plays a critical role in regulating excitatory transmitter release and plasticity. The functional role of IP_3R has yet to be confirmed in the photoreceptor inner segment. Although IP_3 does not seem to be involved in the phototransduction cascade (Jindrova and Detwiler, 1998), a light stimulus to mammalian and amphibian rod outer segments has been shown to increase intracellular IP_3 levels (Ghalayini and Anderson, 1984; Hayashi and Amakawa, 1985; Brown et al., 1987). The localization reported by Peng et al. (1991) suggests that Ca^{2+} stores within the synaptic terminals of retinal neurons may be involved in synaptic transmission.

Ryanodine-sensitive Ca^{2+} stores

The alkaloid ryanodine is naturally found in the stem and roots of the plant *Ryania speciosa*. Ryanodine modulates Ca^{2+} release from stores via high affinity binding to a ryanodine receptor (RyR) located in the ER membrane. RyRs, although larger in size, share considerable structural and molecular homology with IP_3Rs. The architecture of RyRs is reviewed in Rossi and Sorrentino (2002) and Wagenknecht and Samso (2002), and a brief overview will be presented here. RyRs consist of a tetrameric complex forming a large conductance channel. The large cytoplasmic portion of the protein accounts for more than 80% of its mass. The membrane-spanning domains, clustered near the C-terminus, suggests that very little of the protein is present on the luminal side of the ER. Although also expressed in smooth muscle and many non-muscle tissues, the highest density of RyR protein is found in striated muscle. Three different RyR isoforms

(RyR1, RyR2, and RyR3) have been defined in fish, amphibians, birds, and mammals via molecular cloning studies. The RyR2 isoform has recently been identified in salamander photoreceptor inner segments (Krizaj et al., 2004).

Fill and Copello (2002) have reviewed the regulation of ryanodine receptor Ca^{2+} release channels, which are characterized by different conductance states. The mechanism of action of ryanodine is very complex and dose dependent. Low (~10 nM) concentrations of ryanodine increase the frequency of single channel opening to the normal conductance level (Buck et al., 1992). By binding to its receptor, intermediate concentrations (~1 μM) of ryanodine locks the ER Ca channel in a slow-gating subconductance state (Fill and Coronado, 1988). The long-duration open events are accompanied by a reduced ion conductance through the pore (Rousseau et al., 1987; Buck et al., 1992). Higher concentrations of ryanodine (~10-100 μM) lock the channel in a closed configuration (Zimanyi et al., 1992). The ryanodine binding site is thought to be located in or near the RyR channel pore, thereby altering the permeation pathway, possibly by changing the diameter of the channel pore (Tinker and Williams, 1993). In fact, the ryanodine binding site has been localized to the C-terminus of the protein in skeletal muscle (Callaway et al., 1994). The possibility of multiple ryanodine binding sites (high vs. low affinity binding sites) may also explain its complex dose-dependent action (Chu et al., 1990; Pessah and Zimanyi, 1991).

RyR channels can also be regulated by the pharmacological agent caffeine (Jenden and Fairhurst, 1969; Endo, 1977). Caffeine acts on RyRs to induce Ca^{2+} release (Pozzan et al., 1994; Berridge, 1998). In neurons, caffeine-sensitive intracellular pools are thought to be distinct from the IP_3-gated pools (McPherson et al., 1991). However,

some studies have suggested that caffeine can also induce Ca^{2+} release from ryanodine-insensitive stores (Schmid et al., 1990; McNulty and Taylor, 1993; Orkand and Thomas, 1995). In rod photoreceptors, caffeine-sensitive stores have been proposed to coexist with IP_3-gated Ca^{2+} stores (Peng et al., 1991). However, caffeine acts to inhibit and not activate Ca^{2+} release from IP_3-gated stores (Ehrlich et al., 1994). Caffeine induces the release of Ca^{2+} from the ER in a quantal fashion (Cheek et al., 1993). Caffeine-induced Ca^{2+} release from stores is typically observed as a transient increase in $[Ca^{2+}]_i$, which can be blocked by ryanodine in some cell types (McPherson et al., 1991; Friel and Tsien, 1992; Garaschuk et al., 1997). Ca^{2+} release from caffeine-sensitive stores, blocked by ryanodine, was also described in salamander rod inner segments and synaptic terminals (Krizaj et al., 1999). Rapid transient reductions in ER Ca^{2+} levels have been shown with caffeine, as well as with Ca^{2+} currents triggered by depolarization, indicating Ca^{2+}-induced Ca^{2+} release (CICR). CICR following Ca^{2+} influx was shown to be blocked by ryanodine and potentiated by caffeine in sensory neurons (Solovyova et al., 2002). Loading the Ca^{2+} stores with Ca^{2+} via a conditioning depolarization greatly enhances the ability of low doses of caffeine to produce full depletion of the stores, indicating that after an increase in the ER Ca^{2+} content, the same low concentration of caffeine recruits more RyRs (Shmigol et al., 1996).

In addition to conducting through the channel pore, Ca^{2+} can also modulate the RyR channel. Similar to IP_3R, ryanodine Ca^{2+}-release channels have a bell-shaped dependence on the cytoplasmic Ca^{2+} level. Low (1-10 μM) concentrations of cytosolic Ca^{2+} activate the RyR channel, whereas these receptors are generally inhibited in the presence of high (1-10 mM) cytosolic Ca^{2+} concentrations (Hille, 2001). The gating of

RyRs can be regulated by both cytoplasmic and ER free Ca^{2+} levels (Shmigol et al., 1996). In fact, caffeine is thought to work by increasing the affinity of the RyRs for cytoplasmic Ca^{2+} (Pozzan et al., 1994; Hernandez-Cruz et al., 1995). Ca^{2+} binding sites are thought to exist on the luminal surface of the RyR channel. High luminal Ca^{2+} levels, which have been demonstrated to be on the order of 500-800 μM in a neuronal preparation (Alonso et al., 1999; Solovyova et al., 2002), are thought to increase the sensitivity of RyR channel (Sitsapesan and Williams, 1997; Györke and Györke, 1998). The luminal Ca^{2+} effects may also be mediated via associated luminal proteins, such as calsequestrin (Szegedi et al., 1999; Zhang et al., 2001; Beard et al., 2002), or feed-through regulation, which consist of luminal Ca^{2+} moving through the channel and interacting with cytosolic Ca^{2+}-binding sites (Tripathy and Meissner, 1996).

Ca^{2+}-reuptake via the sarcoplasmic/endoplasmic Ca^{2+}-ATPases (SERCAs)

Similar to PMCAs, sarcoplasmic/endoplasmic reticulum Ca^{2+}-ATPases (SERCAs) are capable of pumping Ca^{2+} against its large concentration gradient to buffer the cytosolic free Ca^{2+} concentration at the resting level. Whereas PMCAs pump Ca^{2+} out of the cell, SERCAs sequester Ca^{2+} into Ca^{2+} stores. These pumps may maintain large (three orders of magnitude) Ca^{2+} concentration gradient between the ER lumen and the cytosol (Meldolesi and Pozzan, 1998). The maintenance of high $[Ca^{2+}]$ in the lumen of the ER, in the range of hundreds of micromolar to one milimolar, is important for normal cell function, including Ca^{2+}-mediated cytosolic signals. SERCA transporters, together with PMCAs, have been suggested to reduce the amplitude of depolarization-

evoked $[Ca^{2+}]_i$ transients in the cytoplasm of salamander photoreceptors (Krizaj et al., 2003).

The SERCA family consists of three genes (SERCA 1, 2, and 3), each generating differentially spliced isoforms (see review by Wuytack et al., 2002; Strehler and Treiman, 2004). SERCA pumps are characterized by four major domains, a transmembrane (M) domain, and three cytosolic domains. The P (phosphorylation) and N (nucleotide binding) domains contain the phosphorylation and ATP binding site, respectively. The A (actuator or anchor) domain, is composed of a smaller cytoplasmic loop facing the cytosolic side. Ten transmembrane α-helices form the M domain, which contain two Ca^{2+}-binding sites (Toyoshima et al., 2000). Two Ca^{2+} ions are translocated into the ER lumen for each ATP molecule hydrolyzed. Although the catalytic cycle of SERCA pumps remains a controversy, most models suggest two major conformational states, called E1 and E2. In the E1 conformation, the two high-affinity Ca^{2+}-binding sites face the cytoplasm. Both cytosolic Ca^{2+} and ATP bind and the high-energy phosphorylated intermediate is formed. The $2Ca^{2+}$-E1-ATP complex undergoes a conformational change where some transmembrane helices are rearranged, including those contributing to the Ca^{2+}-binding site. This conformational change into the E2 state results in the reorientation of the complex, which now faces the lumen of the ER. The two Ca^{2+}-binding sites are then converted to a low-affinity state and Ca^{2+} is released. E2-ATP dephosphorylates and the cycle ends with another conformational change from the E2 to the E1 state. The SERCA pump activity is increased by elevated levels of Ca^{2+} outside the ER and inhibited by high luminal Ca^{2+} concentrations. In fact, depletion of ER Ca^{2+}

stores has been shown to increase the rate of SERCA-mediated Ca^{2+} uptake by several fold (Mogami et al., 1998; Solovyova et al., 2002).

Of the three SERCA family isoforms, SERCA2 is thought to be predominantly expressed in most brain regions (Wu et al., 1995; Baba-Aissa et al., 1996). Two different splice variants (a and b), which differ in their turnover rates and their affinity for Ca^{2+}, can be produced from the SERCA2 gene (Verboomen et al., 1992; Wuytack et al., 2002). An immunohistochemical study by Krizaj et al. (2004) demonstrated that salamander photoreceptor inner segments label for the SERCA2a isoform (Krizaj et al., 2004). SERCA2a labeling was localized to the subellipsoid space and cell body, which is consistent with the previously suggested distribution of the ER cisternae in amphibian photoreceptors (Mercurio and Holtzman, 1982).

1.7 Chloride channels

Chloride channels are of central importance to the present dissertation and therefore, this large and highly diverse group of anion channels will be reviewed in this section. Although permeable to various anions, such as iodide, bromide, nitrates, phosphates, and negatively charged amino acids, anion channels are mostly referred to as Cl channels because Cl^- is the most abundant and predominant permeating anion in all organisms. Cl channels are ubiquitously expressed in all eukaryotic cells, plant cells, protozoa, bacteria, and yeast; and their functions range from ion homeostasis to cell volume regulation, transepithelial transport, and regulation of electrical excitability. An excellent review by Jentsch et al. (2002) outlines the molecular structure and physiological function of Cl channels. Since several classes of Cl channels have not yet

been identified at the molecular level, these channels are commonly classified based on their function. According to their gating mechanisms, Cl channels may be classified into five distinct families: 1) the ClC family is gated by changes in transmembrane voltage, 2) Members of the Cl(Ca) family are activated by an increase in cytosolic Ca^{2+} concentration ($[Ca^{2+}]_i$), 3) c-AMP activates Cl channels of the cystic fibrosis transmembrane conductance regulator (CFTR) family (see reviews by Dawson et al., 1999; Gadsby and Nairn, 1994; Sheppard and Welsh, 1999), 4) the volume-regulated anion channel (VRAC) family is activated by cell swelling, 5) the glycine or γ-aminobutyric acid (GABA)-activated Cl channel family is ligand-gated, as the neurotransmitter GABA or glycine is required for channel activation (see review by Jentsch and Günter, 1997). Like GABA-activated Cl channels, Cl(Ca) channels are sometimes classified as ligand-operated channels. The molecular identity responsible for the Cl^- conductance studied in this dissertation is not yet resolved, and therefore, the channel responsible for this conductance could belong to any of these families. Since there is no evidence that cone Cl(Ca) channels are activated by c-AMP, cell swelling, or GABA, only the ClC and Cl(Ca) channel family will be further discussed. In particular, the ClC family member ClC-3 will be reviewed since this channel was shown to be distributed in the outer plexiform layer of the retina, and ClC-3 knockout mice suffer from photoreceptor degeneration (Strobrawa et al., 2001).

1.7.1 The ClC family of Cl channels

The ClC chloride channel family was originally identified via expression cloning of ClC-0 from the electric organ of *Torpedo marmorata* (Jentsch et al., 1990). This

relatively new family of voltage-gated ion channels, which are found in nearly all cells, is by far the best studied and understood family of Cl channels. Chloride-conducting ion channels of the ClC family are fundamentally different in their molecular structure and mechanism from the well-known cation-selective channels and other known anion channels (see review by Fong and Jentsch, 1995). The ClCs are α-helical transmembrane proteins predicted to span the membrane 10 to 12 times, with cytoplasmic N- and C-terminals (see review by Jentsch et al., 1999; Maduke et al., 2000). These channels are structurally unique, as they are thought to exist as two-pore homodimers, each pore shaped like an hourglass with a narrow constriction at the center (Ludewig et al., 1996; Middleton et al., 1996). This model of two identical ion conducting pores formed by separate subunits, thus forming a homodimeric membrane protein, was confirmed when Dutzler et al. (2002) reported the three-dimensional crystal structure of bacterial ClC proteins. High-resolution images of the two-dimensional crystal structure of a bacterial ClC homolog also supported this double-barrel configuration (Mindell et al., 2001). Unlike other ion channels, the gating charge of the ClC-type Cl channels may be carried by the Cl^- ion itself (see review by Maduke et al., 2000) and not by charged transmembrane domains on the channel protein, such as the S4 segment that acts as a voltage sensor in a superfamily of cation channels (Stühmer et al., 1989). More specifically, a glutamate amino acid residue with a negatively charged side chain is thought to act as a gate at the narrowest point of the conduction pathway, which is displaced following Cl^- ion entry into the pore region due to electrostatic repulsion.

In mammals, at least nine members of the ClC gene family are expressed in the plasma membrane or intracellular compartments (see review by Jentsch et al., 1999;

Fahlke, 2001). The ClC channel family dendrogram, which is based on the sequence homology of different gene products in mammals, can be grouped into three branches (Fig. 1.8). The first subfamily encodes ClC-1, -2, -Ka and -Kb, which are plasma membrane Cl channels expressed in a variety of tissues. ClC-1, a muscle specific Cl channel, is activated by depolarization and is responsible for stabilizing the membrane potential (Steinmeyer et al., 1991; Koch et al., 1992). ClC-2 is activated by hyperpolarization (Thiemann et al., 1992). It is broadly expressed, and is usually localized to the apical membrane of secretory epithelia, where it may play a role in cell volume regulation (Grunder et al., 1992). Tissues of ClC-2 expression include the retina, where it has been mainly localized to rod bipolar cells in rat (Enz et al., 1999). ClC-2 deficient mice display postnatal degeneration of the retina (Bosl et al., 2001). However, retinal degeneration may also be due to disruption of normal RPE cell functioning. Barttin, a beta subunit, is essential for the functional expression of both the ClC-Ka (apical) and ClC-Kb (basolateral) (Estevez et al., 2001). ClC-K channels are almost exclusively found in the kidney, where they are essential for transepithelial transport (Simon et al., 1997; Matsumura et al., 1999). Their expression in the retina has thus far not been investigated. The other two branches comprise ClC-3 to -7, which are channels predominantly residing in intracellular membranes. ClC-4 and -6 are poorly characterized channels and have not been shown to reside in cells of the retina. ClC-5 is predominantly expressed in the kidney and its mutation leads to renal failure (Piwon et al., 2000). ClC-7 is a lyzosomal Cl channel. Although ubiquitously expressed, its function remains unclear (Jentsch et al., 1999). ClC-7 deficient mice show severe

Figure 1.8 The mammalian ClC family of Cl channels. Based on homology sequence, nine members of the ClC family have been found in mammals and are grouped into three main branches. Channels of the first branch, which comprises ClC-1, -2, and -K, are predominantly plasma membrane proteins. The channels from the other two branches, which include ClC-3, -4, -5, -6, and -7, are though to be mainly located on intracellular membranes. Also indicated in the figure is the main tissue of distribution. (Adapted from Jentsch et al., 2002).

Figure 1.8

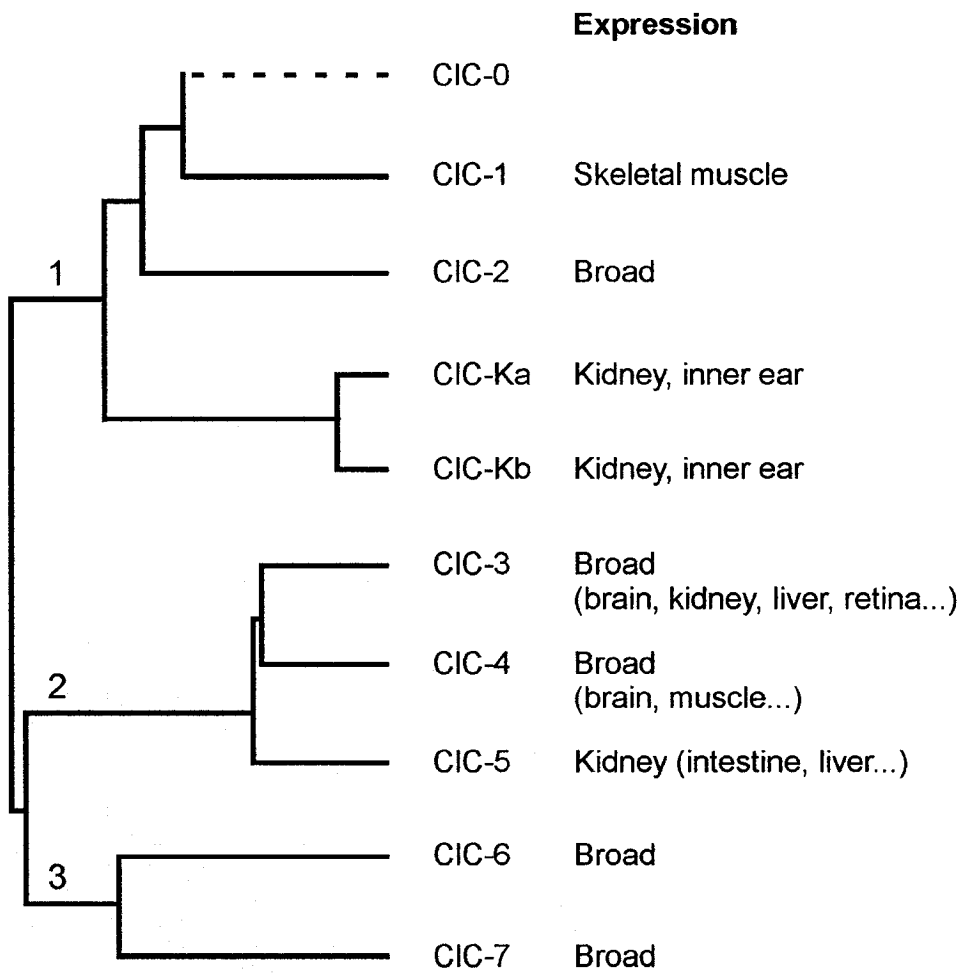
Expression
ClC-0
ClC-1
Skeletal muscle
1
ClC-2
Broad
ClC-Ka
Kidney, inner ear
ClC-Kb
Kidney, inner ear
ClC-3
Broad
(brain, kidney, liver, retina...)
ClC-4
Broad
(brain, muscle...)
2
ClC-5
Kidney (intestine, liver...)
ClC-6
Broad
3
ClC-7
Broad

osteopetrosis and retinal degeneration (Kornak et al., 2001); however, the cause of blindness has not been investigated.

ClC-3 channels are of importance for this dissertation because of their expression pattern and biophysical properties. They are intracellular Cl channels present in endosomes and synaptic vesicles. A study by Stobrawa et al. (2001) demonstrated via immunohistochemistry that ClC-3 is distributed in the outer plexiform layer of the mouse retina. In addition, this study also shows that ClC-3 knockout mice suffer from retinal degeneration with complete loss of photoreceptors after four weeks. ClC-3 is highly expressed in the brain and its disruption results in a loss of the hippocampus (Stobrawa, 2001). It was first cloned from rat brain cells by Kawasaki et al. (1994) and was then functionally expressed and studied in electrophysiological experiments, which demonstrated an outwardly rectifying Cl^- current (Kawasaki et al., 1994; Duan et al., 1997). The main function of ClC-3 is thought to involve the acidification of intracellular vesicles by providing an electrical shunt that is needed for the efficient action of the electrogenic H^+-ATPase (Duan et al., 1997; Stobrawa et al., 2001). Although ClC-3 is thought to mainly reside in intracellular membranes, such as synaptic vesicles and endosomes, a role for ClC-3 as a volume-sensing anion channel located at the plasma membrane has been put forth (Duan et al., 1997; Vessey et al., 2004). However, ClC-3 knockout studies in mice reveal a normal regulating Cl^- conductance, arguing against a function for ClC-3 as a cell-swelling activated Cl channel (Stobrawa et al., 2001).

1.7.2 Ca^{2+}-activated Cl channel family

The physiological role of Cl channels activated by intracellular Ca^{2+} (i.e. Cl(Ca) channels) in signal processing remains ambiguous given that the Cl^- equilibrium potential (E_{Cl}) is unknown. However, these channels are thought to contribute to the electrical excitability of neurons. Cl(Ca) channels consist of at least two functionally distinct groups, suggesting an underlying molecular diversity of Cl(Ca) channels. The typical Ca^{2+}-gated Cl^- channel is activated when Ca^{2+} binds to specific binding sites on the cytosolic side of the channel pore. The second type of Cl(Ca) channels are called Ca^{2+}/calmodulin-dependent protein kinase II (CaMK II)-activated Cl channels. They also open in response to an increase in $[Ca^{2+}]_i$, but channel activation is mediated by CaMK II-dependent phosphorylation (Jentsch et al., 2002; Matchkov et al., 2004). CaMK II-activated Cl channels, which have been proposed to regulate transepithelial transport in a number of epithelial cells (Kidd and Thorn, 2000), differ from neuronal Cl(Ca) channels (see review by Frings et al., 2000). CaMK II-activated Cl channels expressed in epithelial cells have a single channel conductance of 25-30 pS, which is much larger than that of Cl(Ca) channels, are weakly outwardly rectifying, and are rather voltage independent. On the other hand, neuronal Cl(Ca) channels are typically characterized by a small single channel conductance, they show an outward rectification, and are activated by voltage-dependent increases in $[Ca^{2+}]_i$.

1.7.2.1 Properties of Cl(Ca) channels

The permeability sequence of Cl(Ca) channels is as follows: $I^- > NO_3^- > Br^- > Cl^- > F^- > CH_3SO_4^-$. Cl(Ca) channels have relatively small unitary conductances, usually

between 0.5-3 pS. For example, single channel records of $I_{Cl(Ca)}$ have been documented at 3 pS in *Xenopus* oocytes (Takahashi et al., 1987a), 2.5 pS in cultured mammalian endocrine cells (Taleb et al., 1988), 0.5 pS in olfactory sensory neurons (Kleene, 1997), 2.8 pS in human smooth muscle cells (Klohkner, 1993), and 1-2 pS in lacrimal gland cells, which were assessed by analysis of current fluctuations recorded from large numbers of channels (noise analysis) (Marty et al., 1984). They are often functionally coupled with Ca^{2+} influx via voltage-gated Ca channels, as demonstrated in smooth muscle and oocytes, where they are involved in vasoconstriction and the prevention of polyspermy, respectively (Frings et al., 2000; Kidd and Thorn, 2000). In addition to their small single channel conductance, Cl(Ca) channels are characterized by an outward rectification and show time-dependent activation upon depolarization. However, a linear *I-V* curve and a time-independent activation is seen with increasing $[Ca^{2+}]_i$ (Evans and Marty, 1986). The voltage-dependence of Cl(Ca) channels is thought to primarily reside in the binding of Ca^{2+} to the channel. Transient local changes in $[Ca^{2+}]_i$ close to the membrane during activation of voltage-gated Ca channels are believed to rise over 10 μM to 100 μM (see review by Berridge, 1998; Neher, 1998). However, a number of studies in secretory cells indicate that Cl(Ca) channels are activated in the low micromolar range (0.1-1 μM) (Marty et al., 1984; Korn and Weight, 1987; Ishikawa and Cook, 1993). The value of the Hill coefficient (>1) suggests binding of more than one Ca^{2+} ion to the channel. A kinetic model implies activation of the channel by two identical, independent, sequential Ca^{2+} binding steps preceding a final Ca^{2+} independent transition from the closed to the open state (Arreola et al., 1996, Nilius et al., 1997a).

1.7.2.2 Molecular structure of Cl(Ca) channels

The molecular identity of Cl(Ca) channels remains unsolved. However, two different families of molecules have been proposed to form Cl(Ca) channels when expressed in heterologous systems: the CLCA family of putative Ca^{2+}-activated Cl channels and the bestrophins (Sun et al., 2002).

CLCA family

CLCAs are broadly distributed and tissue expressions include epithelia, endothelia, smooth muscle, and neurons. CLCA proteins serve a variety of important physiological roles, including ion channel, cell adhesion, and tumor suppressor function. Several members of the CLCA gene family, which behave as Cl channels when exposed to Ca^{2+}, have been cloned from different mammalian species, including mouse (m), bovine (b), and human (h). The very first gene encoding a CLCA channel was cloned by Cunningham et al. (1995) from bovine tracheal epithelium (*bCLCA1*). The primary structure of bCLCA1 shows no similarity to any other cloned Cl^--selective channel. Analysis of the primary amino acid sequence of bCLCA1 predicts at least four putative transmembrane domains with an extracellular N-terminus. Structural models suggest that it co-assembles as a homotetrameric protein complex (see review by Jentsch et al., 2002). A similar quaternary structure was proposed for the homologs of bCLCA1 cloned from mouse (mCLCA1, Gandhi et al., 1998; Gruber et al., 1998a) and for the human homolog hCLCA1 (Gruber et al., 1998b). The likely topology of the CLCA channel protein is four or five transmembrane domains with an extracellular N-terminus, containing a number of conserved cysteine residues and an extracellular (if four transmembrane domains) or

intracellular (if five transmembrane domains) C-terminus (Gruber et al., 1998b, 1999; Gruber and Pauli, 1999; Fuller et al., 2001; Elble et al., 2002).

When expressed in *Xenopus* oocytes, bCLCA1 is characterized by an outwardly rectifying Cl^- conductance, which is observed without raising $[Ca^{2+}]_i$ (Qu and Hartzell, 2000). However, currents in transfected COS-7 cells were characterized by a linear *I-V* relation and were only observed upon raising $[Ca^{2+}]_i$ (Cunningham et al., 1995). A second epithelial Cl(Ca) channel, hCLCA2, has now been cloned from human lung, trachea, and mammary gland. This channel, when expressed in HEK293 cells, also requires high $[Ca^{2+}]_i$ to be activated and was slightly outwardly rectifying (Gruber et al., 1999). Although CLCA proteins are characterized by several consensus sites for PKC phosphorylation, the mechanism of activation of CLCA channels, either directly by Ca^{2+} or by phosphorylation, is still unknown. In general, whole-cell patch-clamp experiments have used very high Ca^{2+} concentrations in the pipette solution, far beyond physiological relevance, to elicit CLCA-associated currents (Gandhi et al., 1998; Gruber et al., 1998b; Gruber and Pauli, 1999). The possibility that CLCA proteins activate endogenous Cl channels rather than being channels themselves has not been excluded by several workers (Gruber and Pauli 1999; Romio et al., 1999). Whether these epithelial channels are part of the same Cl channel family as the Cl(Ca) channels of interest in the present study is unknown.

Bestrophins

Potential Cl(Ca) channels include members of the bestrophin family. Bestrophins have been described recently as a new family of putative Cl channels (Sun et al., 2002).

They are protein products of the vitelliform macular dystrophy (*VMD2*) gene. Mutations in bestrophins induce the autosomal dominant disorder called Best disease, a vitelliform macular dystrophy in which accumulation of lipofuscin-like material in the retinal pigment epithelium causes a progressive loss of central vision (Marmostein et al., 2000; Sun et al., 2002). The characteristic accumulation of fluid in Best disease is consistent with abnormal fluid transport. Bestrophins have recently been identified in humans and include hbest1, located on retinal cell membranes. They are ~500 amino acid retina-specific proteins, shown to be expressed on the basolateral plasma membrane in retinal pigment epithelial cells (Marmorstein et al., 2000). Bestrophins were thought to consist of four transmembrane spanning domains, forming multimeric Cl channels; however, two bestrophins were recently cloned from *Xenopus* oocytes and six transmembrane domains were predicted following their expression in a variety of tissues (Qu et al., 2003). The human bestrophin is sensitive to intracellular Ca^{2+} and is physically and functionally coupled to the protein phosphatase 2A (Marmorstein et al., 2002). Whether this family of Cl channels, which are sensitive to $[Ca^{2+}]_i$, is related to the Cl(Ca) channels of interest here remains to be investigated.

1.8 Goal and hypotheses

$I_{Cl(Ca)}$ is a prominent ionic conductance in cone photoreceptors, and is thought to be responsible for stabilizing membrane potential, possibly during the surround illumination-induced feedback response from horizontal cells to cone photoreceptors. The overall goal of this dissertation was to describe features governing the gating of $I_{Cl(Ca)}$ to better understand their physiological function in cone photoreceptors. The

Results section is divided into three chapters (Chapter 3-5). Chapter 3 characterizes $I_{Cl(Ca)}$ and demonstrates the modulation of this conductance by $[Ca^{2+}]_i$, for example by changing the intracellular buffering capacity. The first guiding hypothesis was that Cl(Ca) channels are activated by a rise in intracellular Ca^{2+} ($[Ca^{2+}]_i$) close to the cell membrane, such as during Ca^{2+} entry through voltage-gated Ca channels at the synaptic terminal. The deactivating kinetics of Ca^{2+}-activated Cl^- tail currents were suggested to reflect Ca^{2+} diffusion and buffering away from Cl(Ca) channels located at the plasma membrane. Aside from investigating the importance of Ca^{2+} influx for $I_{Cl(Ca)}$ activation using both protocols and agents known to increase $[Ca^{2+}]_i$, Chapter 3 also examined possible intermediate modulators of Cl(Ca) channels, such as the Ca^{2+}-binding protein, calmodulin. Since the molecular identity of Cl(Ca) channels has not been revealed, it was hypothesized that $I_{Cl(Ca)}$ could arise from Cl channels located in synaptic vesicles (i.e. ClC-3) that integrate with the plasma membrane during periods of depolarization (hence the Ca^{2+} dependence).

The contribution of Ca^{2+} stores in $I_{Cl(Ca)}$ activation was investigated in Chapter 4. It was hypothesized that $I_{Cl(Ca)}$ would follow $[Ca^{2+}]_i$ levels and that Ca^{2+} stores would contribute to channel gating. The activation of $I_{Cl(Ca)}$ by Ca^{2+}-induced Ca^{2+}-release and by agents such as IP_3 and caffeine, which directly release Ca^{2+} from internal stores, was investigated. None of the agents used to affect the stores modified $I_{Cl(Ca)}$. The results suggested that Ca^{2+} release from Ca^{2+} stores does not increase submembrane $[Ca^{2+}]_i$ level high enough to modulate $I_{Cl(Ca)}$. Cl(Ca) and Ca channels at the plasma membrane of cone synaptic terminals may be physically distant from Ca^{2+} stores, such as those of the endoplasmic reticulum, and/or Ca^{2+} derived from stores may be rapidly buffered and/or

sequestered via intracellular mechanisms. Only during conditions where repetitive depolarizing pulses, likely increasing $[Ca^{2+}]_i$, did the Ca^{2+} stores participate in Cl(Ca) channel gating. In this case, Cl(Ca) channel activation first increased and then an inhibition of $I_{Cl(Ca)}$ followed.

In Chapter 5 it is demonstrated that $I_{Cl(Ca)}$ was typically inhibited following sustained activation. It was hypothesized that Cl(Ca) channel inhibition was caused by high levels of $[Ca^{2+}]_i$, referred in the present dissertation as 'high $[Ca^{2+}]_i$-induced inhibition of $I_{Cl(Ca)}$', and that this effect was mediated by the phosphorylation state of intracellular proteins. Dephosphorylation mechanisms were shown to be involved in high $[Ca^{2+}]_i$-induced inhibition of $I_{Cl(Ca)}$. Voltage-gated Ca channels involved in $I_{Cl(Ca)}$ activation were proposed to be possible targets of this inhibition. In addition, mechanisms involving Cl(Ca) channels themselves were also suggested responsible for high $[Ca^{2+}]_i$-induced inhibition of $I_{Cl(Ca)}$.

Chapter 2

Methods

2.1 Isolation of cone photoreceptors

Larval tiger salamanders, *Ambystoma tigrinum* (Kons Scientific Supply, Germantown, WI), typically 10-20 cm in length were stored at 4°C under a 12 hr light/dark cycle. In accordance with guidelines provided by the Canadian Council for Animal Care, salamanders were decapitated, pithed, and the eyes enucleated. One eye was placed in amphibian standard bath solution (Table 2.1) and stored in darkness at 4°C for later use. The other eye was used immediately for retinal cell isolation using the following procedure. The cornea, iris, and lens were extracted and the retina was gently peeled from the eyecup in standard bath solution. The isolated retina was incubated for 15-20 min at ~28°C in a Ca^{2+}-free solution (Table 2.1) and rinsed several times in standard bath solution. The retina was then mechanically triturated with a fire-polished glass Pasteur pipette to dissociate the cells. Aliquots of the resulting cell suspension were plated in 0.2-0.5 ml recording chambers formed with Sylgard 182 (Dow Corning, Midland, MI) in 35 x 10 mm polystyrene tissue culture dishes (Becton Dickinson Labware, Franklin Lakes, NJ). The dishes were pre-coated with Sal-1, a mouse monoclonal antibody produced against salamander retinal membranes (a kind gift from Dr. Peter MacLeish; see MacLeish et al., 1983). Briefly, the dishes were coated with 100 μL of 0.2 mg/ml goat anti-mouse IgG (Jackson ImmunoResearch Laboratories, Inc., West Grove, PA) followed by 100 μL of Sal-1 (1:100), both for 1 hr at room temperature. Isolated retinal cells were kept on ice and allowed to settle to the bottom of dishes for 15-30 min before each experiment. Whole-cell patch-clamp recordings were mainly obtained from double cones with intact synaptic terminals (Fig. 2.1); however, large

Figure 2.1 Typical salamander cone photoreceptors examined during patch-clamp experiments. Whole-cell patch-clamp recordings were mainly performed on tiger salamander double cones with intact synaptic terminals, where L-type Ca channels and Cl(Ca) channels are likely located. The principal member (right) of the pair of cells is characterized by a slender inner segment and can easily be distinguished from the accessory member (left). The patch electrode is approaching from the left, onto the accessory member of the double cone. Scale bar: 10 μm.

Figure 2.1

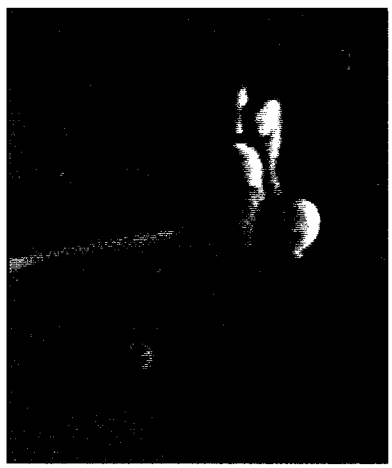

single cones in an aggregate were also used. Large single cones as well as both members of the double cones are positive for L-cone opsin immunolabeling (Sherry et al., 1998) and have a maximum sensitivity to red light (610 nm) (Mariani, 1986; Perry and McNaughton, 1991; Makino and Dodd, 1996; Sherry et al., 1998). At the beginning of each experiment, retinal cells were brightly illuminated with a 50 W Nikon inverted microscope lamp supplied with ~6 V, which was turned off during recordings to reduce noise.

2.2 Solutions

The ionic composition of both the standard bath and pipette solutions used to isolate I_{Ca} and $I_{Cl(Ca)}$ are shown in Table 2.1 and 2.2, respectively. Free intracellular Ca^{2+} concentration ($[Ca^{2+}]_i$) was calculated at 15 nM using Max Chelator software (www.stanford.edu/~cpatton/maxc.html) (Bers et al., 1994). These recording solutions, which contained symmetrical $[Cl^-]$, set the equilibrium potential for Cl^- ions (E_{Cl}) close to 0 mV. I_K and I_h, the other two most prominent ionic conductances in cone photoreceptors (Barnes and Hille, 1989), were blocked with intracellular and extracellular Cs^+, respectively. On some occasions, where indicated in text and figure legends, 3 mM Ca^{2+} contained in the standard bath solution was replaced with the same concentration of Ba^{2+} to isolate Ca channel currents and to eliminate any contribution from $I_{Cl(Ca)}$ to whole-cell current recordings (Table 2.1). In addition, for Ca^{2+} free experiments performed in the presence of ionomycin, 3 mM Mg^{2+} and 2 mM BAPTA was added to the standard bath solution. Solutions were applied at room temperature (between 21°C and 25°C) via a

Table 2.1 Composition of extracellular solutions (mM)			
Ionic composition	Standard bath solution	Ca^{2+} free solution	Ba^{2+} solution
NaCl	90	90	90
KCl	2.5	2.5	2.5
$CaCl_2$	3.0	0	0
$BaCl_2$	0	0	3.0
Glucose	10	10	10
HEPES	10	10	10
CsCl	1.0	0	0
pH (adjusted with NaOH)	7.6	7.6	7.6

Table 2.2 Composition of intracellular solution (mM)	
Ionic composition	Standard pipette solution
CsCl	95
$MgCl_2$	0.8
$CaCl_2$	0.01
BAPTA:CsOH	0.1:0.4
HEPES	5
Mg^{2+}-ATP	1
Na^{+}-GTP	0.2
pH (adjusted with CsOH)	7.2

gravity-driven perfusion system through an eight-way valve at an approximate rate of 2 ml/min, and were removed using a vacuum pump.

The pH of each solution was adjusted with NaOH or CsOH (see Table 2.1 and 2.2) before each experiment and measured with a pH meter (Corning model 240). HEPES, BAPTA, ATP, and GTP were obtained from Sigma-Aldrich (St. Louis, MO). Drugs (see below), diluted from concentrated stocks, were added to the standard bath solution, or included in the pipette solution.

2.3 Drugs

Bay K 8644 (BayK), caffeine (CAF), calcimycin (ionophore A23187), calmidazolium chloride, calmodulin (CaM), cyclopiazonic acid (CPA), D-myo-Inositol 1,4,5-trisphosphate sodium salt (IP_3), ionomycin (IONO), lanthanum chloride heptahydrate (La^{3+}), 5-Nitro-2-(3-phenylpropylamino)benzoic acid (NPPB), N-[2-Methlamino)ethyl]-5-isoquinolinesulfonamide hydrochloride (H-8), ryanodine (Ry), Tetanus toxin (TeTox) from *Clostridium tetani*, thapsigargin (TG), and trifluoperazine dihydrochloride were all obtained from Sigma-Aldrich (St. Louis, MO). Anti-ClC-3 (Alomone Labs, Jerusalem, Israel) was dialyzed into the cell via the pipette solution to assess the contribution of ClC-3 channels in the activation of $I_{Cl(Ca)}$. More specifically, intracellular dialysis of 5 μg/ml of this polyclonal antibody directed against one of the cytoplasmic domains of the C-terminus (residues 592-661) of the rat ClC-3 was used (Kawasaki et al., 1994). This epitope is highly conserved in all known vertebrate ClC-3 proteins, and the anti-ClC-3 antibody recognizes a full-length ClC-3 voltage-gated Cl channel. Okadaic acid (OA) was obtained from Calbiochem (San Diego, CA). All

chemicals were dissolved as stock solutions in distilled water, dimethyl sulfoxide (DMSO), or ethanol (EtOH) and were diluted to the final concentrations designated in the text and figure. The final DMSO and EtOH concentrations never exceeded 0.1%. Experiments with 0.1% DMSO in the bathing solution produced no change in whole-cell current parameters when compared to control, and 0.1% EtOH alone has previously been shown to have no effect (Barnes and Deschenes, 1992).

2.4 Whole-cell current recordings

Ca^{2+}-activated Cl^- currents ($I_{Cl(Ca)}$) were recorded from cone photoreceptors using the ruptured patch-clamp technique (Hamill et al., 1981). This whole-cell recording configuration allows measurement of two different electrical parameters: the membrane potential (V_m) at a given current (current clamp) and the current across the membrane (I) at a given voltage (voltage clamp). The voltage-clamp technique allows the identification and characterization of ion channels by measuring the current required to hold the membrane potential at a desired voltage. The data presented in the present dissertation consists of measurements of changes in current through ion channels of the total cell membrane (see Fig. 2.2) following different voltage-step protocols. This macroscopic current corresponds to the average of different simultaneously conducting channels.

The whole-cell patch-clamp configuration offers the advantage of controlling the composition of the solutions on both sides of the cell membrane, facilitating experiments involving ion substitution or drug application, or where intracellular access is required. To perform this technique, a seal is formed between a glass pipette and a small patch of

Figure 2.2 Diffusion of ions from the patch-pipette into the cell cytoplasm following the whole-cell patch-clamp configuration. (**A**) A high resistance seal (~1 GΩ) is formed when the pipette touches the cell membrane. This is called the cell-attached recording configuration. (**B**) Following suction application to the interior of the pipette, the cell membrane is ruptured and the pipette solution dialyzes the cellular interior. The concentration of ions within the cell equilibrates with those in the pipette within a few seconds due to the relatively small cytosolic volume of the cell compared to the volume of the patch pipette.

Figure 2.2

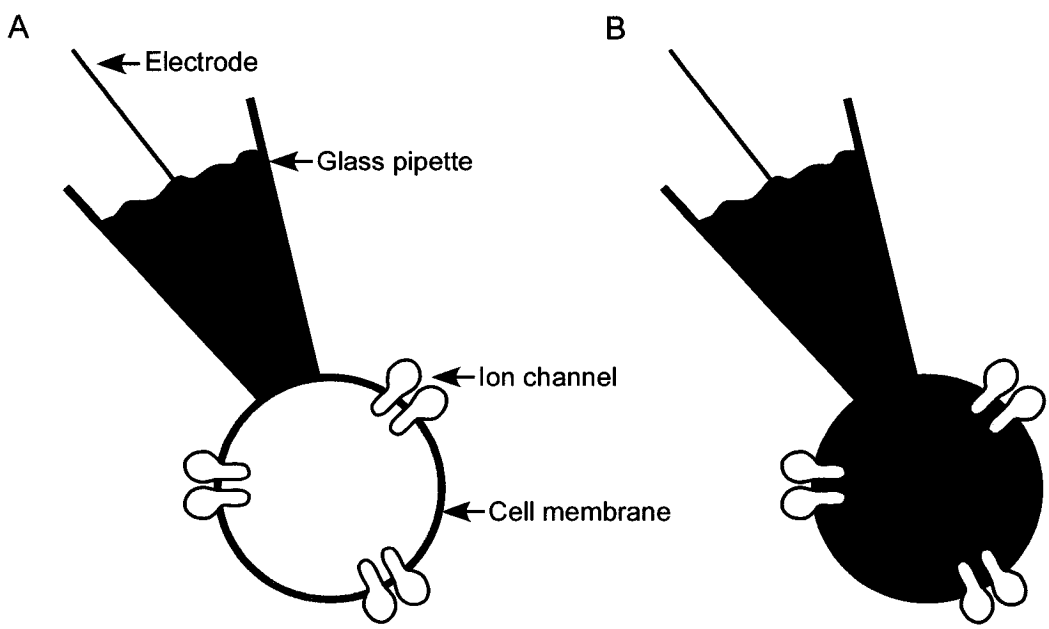

cellular membrane by lowering the pipette to the membrane surface and applying negative pressure. Once a seal of sufficiently high (gigaohm) resistance is established, a brief suction is applied again to the interior of the pipette to rupture the membrane patch underneath the pipette tip. After the cell is ruptured, there is a low resistance pathway for current through the pipette, and the patch-pipette solution dialyses the interior of the cell. Since the volume of the solution-filled pipette is large compared to the cytosolic compartment of the cells, ion concentrations within the cell cytoplasm rapidly equilibrate with those in the patch-pipette (Fig. 2.2). In this manner, experiments designed to assess the effects of cellular modulators were performed, in which compounds were introduced into the cell cytoplasm via the patch-pipette, or added to the bath solution by continuous perfusion, allowing rapid changes in the ionic composition outside the cell.

A schematic diagram for a whole-cell voltage-clamp circuit is shown in Figure 2.3. This scheme consists of a recording microelectrode inserted into a glass pipette filled with a known concentration of ions. In the whole-cell voltage-clamp configuration, electrical and chemical continuity exists between the recording microelectrode and the cytoplasm of the cell. In addition, the cell membrane resistance (R_m) must be larger than the series resistance (R_s) arising from the recording microelectrode. The actual cell membrane potential (V_m) is fed into the negative input of the amplifier, whereas the command potential (V_c) is fed into the positive input. The cell membrane potential is voltage clamped to the electrode potential or command voltage. A feedback amplifier (Amp) continuously compares the measured V_m and V_c. When current flows through membrane ion channels, a difference in the measured V_m and V_c is detected by

Figure 2.3 Simplified circuit for the whole-cell patch-clamp configuration. The circuit clamps the membrane potential (V_m) at the value of the command potential (V_c), and measures the required compensatory current. When a difference is detected between V_m and V_c, the amplifier generates a current to null the difference. The recorded current is equal but opposite to the current flowing through channels located in the cell membrane. Amp: amplifier; R_c: cell membrane resistance; R_f: feedback resistor; R_s: series resistance arising from the recording microelectrode; V_m: membrane potential; V_c: command potential.

Figure 2.3

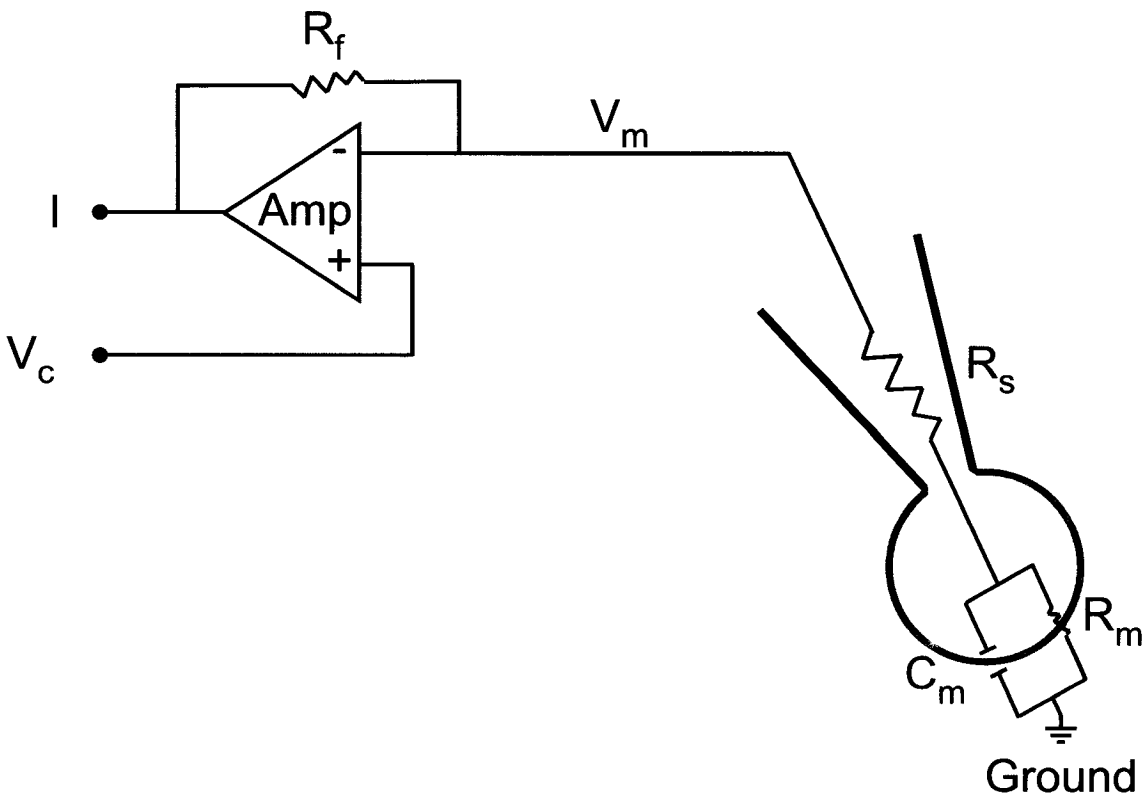

the amplifier and a compensatory current (I) to zero the difference is generated at the output of the amplifier. Because of the high resistance of the feedback resistor (R_f), the current will flow across R_f into the recording pipette and not back into the amplifier. The current injected via the recording microelectrode to clamp V_m at V_c is equal but opposite to the actual current flowing through the plasma membrane ion channels.

2.5 Instruments

Patch electrodes were pulled from fire polished micro-hematocrit capillary tubes (VWR Scientific, West Chester, PA) using a two-step vertical pipette puller (Kopf model 730, David Kopf Instruments, Tujunga, CA). Pipette tips were first dipped in and then back-filled with filtered (0.22 μm pore) standard pipette solutions. Filled pipettes had 5-10 MΩ tip resistances, measured in the standard bath. The bath reference electrode consisted of a bath solution-filled agar bridge with an AgCl wire (World Precision Instruments, Inc., Sarasota, FL). Offset currents were nulled before seals were made. Whole-cell voltage was clamped with an Axopatch-1D amplifier (Axon Instruments, Foster City, CA) using whole-cell membrane capacitance (C_m) and series resistance (R_s) compensation to reduce capacitive artifacts. The averaged C_m was calculated at 16.4 ± 0.4 pF and R_s was 21.5 ± 0.8 MΩ (n=102). Signals were filtered (0.5-1 kHz) (Ithaco 4302 Dual 24dB/octave filter, Ithaca, NY) and digitized (1 kHz) with an Indec Systems interface (Sunnyvale, CA) for storage on the hard disk of a computer running BASIC-FASTLAB acquisition software. BASIC-FASTLAB generated the voltage-clamp commands, and provided some data analysis. Several successive points were averaged together in some records where currents changed slowly in time to reduce the storage

requirements. For illustration, one to three points at the peak of each capacitance current transient have been removed from some records.

2.6 Quantitative evaluation

In all experiments described, the holding potential was set at -60 mV. The standard depolarizing protocol consisted of voltage steps from -70 mV to +60 mV that were changed in increments of 10 mV, and were applied for a duration of 100 ms every 3 or 5 sec. Ca^{2+}-activated Cl^- tail currents were recorded at -60 mV (i.e. upon repolarization) for 800 ms after each step (Fig. 2.4A). Repetitive depolarizing pulses, consisting of 100 ms steps from -60 mV to -20 mV at 1, 2, and 5 sec intervals were used also used on occasions where indicated in the text and figure legends. An increase in the current (~100% on average) up to 5 min following rupture of the whole-cell patch in control conditions was observed, as is typically observed in ruptured patch recordings (Barnes and Bui, 1991). Therefore, recordings were obtained a few minutes post-rupture, after the current had stabilized. For experiments where intracellular drugs were applied via the recording patch-pipette solution, control recordings were taken ~5 min following rupture of the whole-cell patch. Current-voltage (*I-V*) relations were measured by calculating the mean current between 90-94 ms into each voltage step (Fig. 2.4B measured from Fig. 2.4A; black arrowhead), and 12-15 ms after the return to -60 mV (Fig. 2.4C measured from Fig. 2.4A; grey arrowhead). Occasionally, where indicated in the text and figure legend, the current during depolarizing steps was measured early, between 3 and 6 ms following depolarizing voltage steps (white arrowhead; Fig. 2.4A). Tail currents were also quantified by calculating the integral of the current, which

Figure 2.4 A representative example of whole-cell voltage-clamp recording and analysis obtained from a salamander cone photoreceptor. (**A**) Current traces obtained with the standard depolarizing protocol, consisting of 10 mV increments from -70 mV to +60 mV from a holding potential of -60 mV, under the conditions used in this study to isolate I_{Ca} and $I_{Cl(Ca)}$. (**B**) Leak-subtracted current-voltage (*I-V*) relation collected from the mean current measured at the end depolarizing voltage steps, a region indicated by the black arrow in (**A**). The current measured at depolarizing voltage steps, which comprises both I_{Ca} and $I_{Cl(Ca)}$, was typically inward between -30 mV and +10 mV, and outward positive to +10 mV. (**C**) Leak-subtracted Ca^{2+}-activated Cl^- tail currents, recorded at -60 mV and plotted against the voltage of the preceding step, were measured at the area indicated by the grey arrow in (**A**). The Ca^{2+}-activated Cl^- inward tail currents were typically elicited during depolarizing voltage steps positive to -30 mV. The amplitude of the tail currents increased as the voltage was stepped to positive potentials in 10 mV increments, until the maximum amplitude, following voltage steps between 0 mV and +10 mV, was reached. When voltage potentials were stepped positive to +10 mV, the Ca^{2+}-activated Cl^- tail currents decreased in amplitude. (**D**) Offset subtracted charge-voltage (*Q-V*) relation, calculated from the integral of the Ca^2-activated Cl^- tail currents and plotted against the voltage of the preceding steps, were also calculated to estimate the amount of charge entry (*Q* in pC).

Figure 2.4

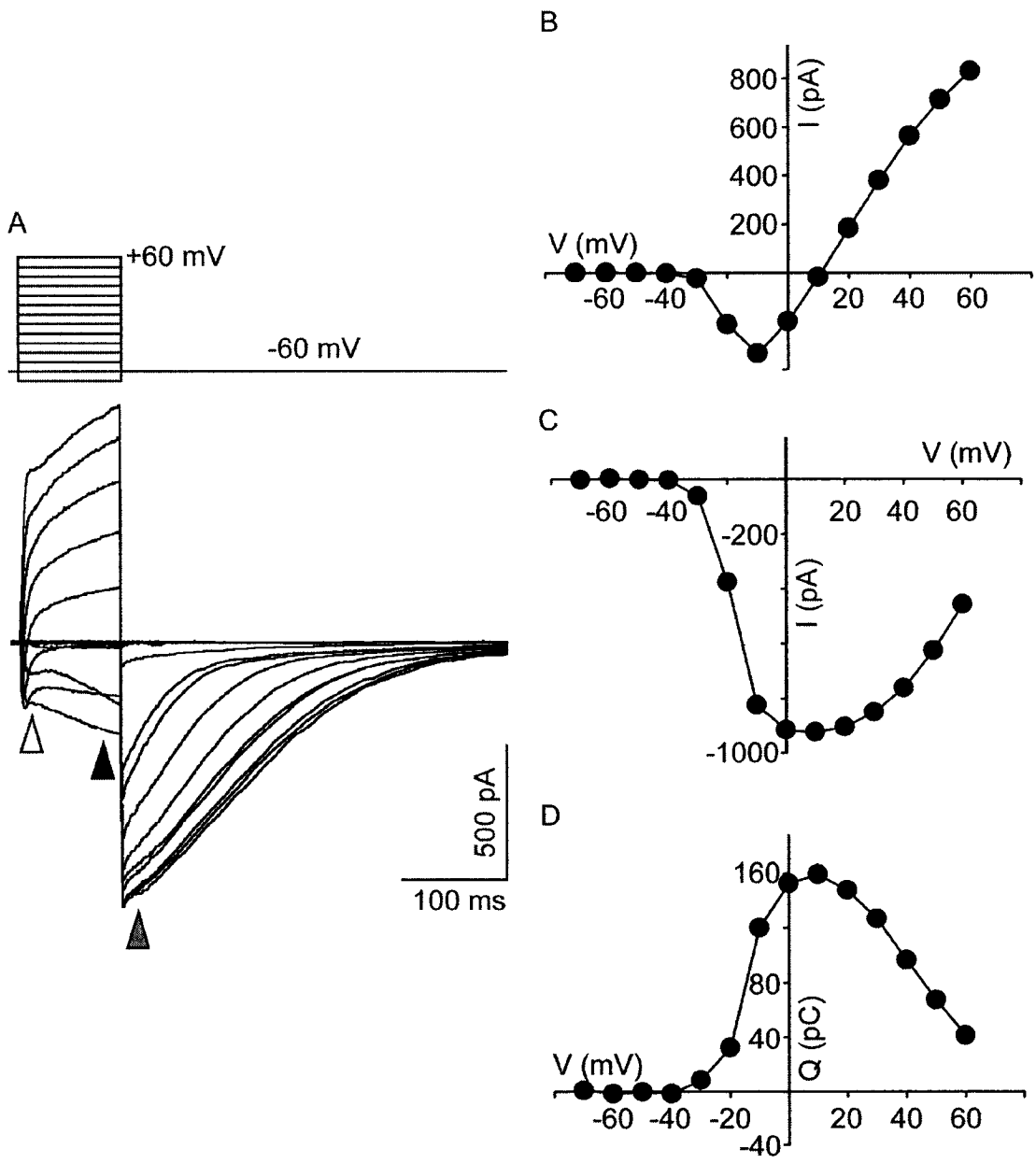
A
+60 mV
-60 mV
500 pA
100 ms
B
800
600
400
200
I (pA)
V (mV)
-60 -40
20 40 60
C
V (mV)
-60 -40
-200
20 40 60
I (pA)
-1000
D
160
80
40
Q (pC)
V (mV)
-60 -40 -20
20 40 60
-40

estimates the amount of charge entry (Q in pC) (Fig. 2.4D). Another voltage-clamp protocol, referred to as 'repeated strong depolarizations' was used in the present dissertation. Repeated strong depolarizations consisted of 100 ms prepulses to 0 mV, each followed by 100 ms steps changing from +20 mV to -80 mV in decrements of 10 mV, applied at 2 Hz (Chapter 3 and Chapter 5). *I-V* relations for this particular protocol were obtained from the mean current 25 ms before the end of the voltage steps.

Changes in currents following drug application were expressed as a percentage of control, defined as $[I-(I_{test})/(I_{control})] \times 100$, and were assessed at the peak current measured during depolarizing voltage steps and during repolarization following those steps, unless otherwise indicated. Activation curves were constructed from leak subtracted *I-V* relations by dividing by the driving force. Activation curves were fitted with the Boltzmann function $1/\{1+ \exp((V-V_{1/2})/m)\}$ to characterize the voltage for half activation (activation midpoint, $V_{1/2}$) and slope factor (m). Summarized data are expressed as mean ± s.e.m (where n represents the number of cells). Data were plotted in Sigma Plot 2001 for Windows and were presented in Canvas 9.0 (Deneba Software, Miami, FL). Statistical analyses of drug effect were performed on raw data using Student's paired *t*-tests. One-way repeated measures ANOVA was also used where more than one treatment was applied. Differences between mean current remaining from two different samples were compared with the non-parametric Mann-Whitney Rank Sum Test. Probability (P) values of less than 0.05 were considered statistically significant (*$P<0.05$ and **$P<0.01$) (SigmaStat 2.03).

Chapter 3

Characterization of $I_{Cl(Ca)}$ in Isolated Tiger Salamander Cone Photoreceptors

Parts of this chapter have been previously published in the following publications:

Lalonde MR, Barnes S. 2003. Contribution of Calcium Stores to Activation of Chloride Current in Cone Photoreceptors. Society for Neuroscience, E-Abstract 791.18.

Lalonde MR, Barnes S. 2004. Inhibition of Cl(Ca) Channels in Response to High Intracellular Calcium Levels Due to Dephosphorylation-Mediated Ca channel Inhibition in Cone Photoreceptors. Society for Neuroscience, E-Abstract 65.12.

Parts of this chapter are submitted to be in the following publication:

Lalonde MR, Barnes S. 2004. Contribution of Calcium Stores to Activation of Calcium-Activated Chloride Currents in Cone Photoreceptors. European Journal of Neuroscience.

The present chapter describes the activation of Ca^{2+}-activated Cl^- currents ($I_{Cl(Ca)}$), in isolated tiger salamander cone photoreceptors. $I_{Cl(Ca)}$ is thought to arise from the activation of Cl(Ca) channels, which have not previously been described in salamander cone photoreceptors. A model in which Ca^{2+}-activated Cl^- tail currents decay in a manner that reflects the diffusion of Ca^{2+} ions from submembrane microdomains will be introduced. Changes in Ca^{2+}-activated Cl^- tail current amplitude and kinetics in response to various voltage protocols and drugs known to modify $[Ca^{2+}]_i$ were investigated.

3.1 $I_{Cl(Ca)}$ is activated by depolarization-evoked Ca^{2+} influx

This first section describes how $I_{Cl(Ca)}$ can be elicited by depolarization-evoked Ca^{2+} influx. Figure 3.1 demonstrates a typical voltage-clamp recording of an isolated salamander cone photoreceptor, responding to a 100 ms voltage step to 0 mV from a holding potential of -60 mV. For this cell, the membrane capacitance (C_m) was 26 pF and the series resistance (R_s) was 15 MΩ after ~4.5 min of dialysis with intracellular solution. The voltage step to 0 mV first opens voltage-gated Ca channels, which leads to an influx of Ca^{2+} ions. Cl(Ca) channels responsible for $I_{Cl(Ca)}$ are activated following this increased $[Ca^{2+}]_i$, which I show later to be localized to the local submembrane area. Hence, during depolarizing voltage steps, the early current (measured between 3-6 ms into each voltage step) is predominantly a Ca^{2+} current (I_{Ca}) whereas both I_{Ca} and $I_{Cl(Ca)}$ contribute to the late current (measured between 90-94 ms into each voltage step). Since E_{Cl} is set at 0 mV, a depolarizing step to that potential should elicit I_{Ca} uncontaminated by movement of Cl^- ions into or out of the cell. As seen in the example shown in Figure 3.1,

Figure 3.1 $I_{Cl(Ca)}$ activates following depolarization-evoked Ca^{2+} influx in isolated tiger salamander cone photoreceptors. During the depolarizing stimulus (-60 mV to 0 mV for 100 ms) both a Ca current (I_{Ca}) and $I_{Cl(Ca)}$ are activated. The depolarizing voltage step first leads to an influx of Ca^{2+} through voltage-gated Ca channels, which then activate Cl(Ca) channels. During a depolarizing voltage step, the early current is predominantly I_{Ca}, whereas the late current consists of both I_{Ca} and $I_{Cl(Ca)}$. Upon repolarization of the membrane to a holding potential of -60 mV, voltage-gated Ca channels quickly deactivate and a large slowly decaying Ca^{2+}-activated Cl^- tail current develops due to the increased $[Ca^{2+}]_i$ and the large driving force for Cl^- ions (E_{Cl} is set at 0 mV). The complex time course of Ca^{2+}-activated Cl^- tail current decay is thought to reflect the closure of Cl(Ca) channels as submembrane $[Ca^{2+}]_i$ falls. The dashed line represents zero current.

Figure 3.1

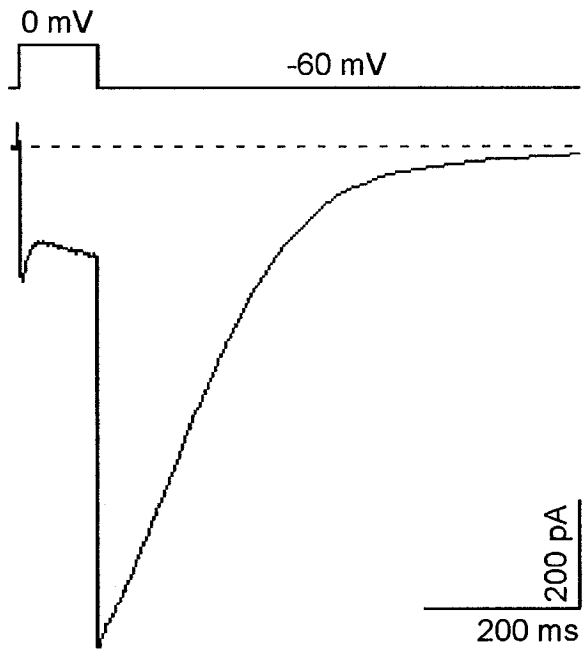

the inward current during the step declined sharply at first but then increased slowly as the depolarization persisted. The reason for the early decrease is unknown but could be due to vesicular proton release inhibiting presynaptic Ca channels (Devries, 2001; Palmer et al., 2003). In addition, the increase seen in the late current could be due to a small difference between E_{Cl} and 0 mV. Following the return of the membrane potential to -60 mV, voltage-gated Ca channels responsible for I_{Ca} in these cells deactivate within 5 ms (Wilkinson and Barnes, 1996) but a large inward Ca^{2+}-activated Cl^- tail current develops in response to both the elevated $[Ca^{2+}]_i$ from the preceding depolarizing voltage step, and the increased driving force for Cl^- ions. The amplitude of Ca^{2+}-activated Cl^- tails is determined not only by $[Ca^{2+}]_i$ at the submembrane level, but also by the number of Cl(Ca) channels activated by Ca^{2+}, and the electrochemical gradient for Cl^- ions. Since neuronal Ca^{2+}-activated Cl^- tail currents do not show evidence of inactivation (see reviews by Scott et al., 1995; Frings et al., 2000), the complex time course of decay following repolarization is proposed here to reflect the slow deactivation of Cl(Ca) channels as submembrane $[Ca^{2+}]_i$ decreases due to Ca^{2+} handling and restoration to normal resting levels via a variety of cellular processes.

3.2 Free $[Ca^{2+}]_i$ sets the amplitude and kinetics of Ca^{2+}-activated Cl^- tail currents, which deactivate following a saturated exponential function

The importance of $[Ca^{2+}]_i$ for Cl(Ca) channel activation can be readily demonstrated by changing the Ca^{2+} buffering capacity in the patch-pipette solution. The kinetics of the Ca^{2+}-activated Cl^- tail current have previously been shown to be modulated in different cells by changing the buffering capacity of the intracellular environment (Bader et al., 1987; Korn and Weight, 1987). In isolated salamander cone

photoreceptors, relatively larger Ca^{2+}-activated Cl^- tail currents (0.1 mM BAPTA, 146 ± 13 pC; n=8) with slower deactivation kinetics were obtained in the presence of a low-capacity buffering system, whereas smaller Ca^{2+}-activated Cl^- tail currents (1 mM BAPTA, 13 ± 3 pC; n=4) with faster kinetics were present when the free $[Ca^{2+}]_i$ was reduced (Fig. 3.2). Figure 3.2A, B, and C demonstrate a representative example of a family of current traces, recorded with the standard depolarizing protocol, as described above, in the presence of intracellular BAPTA at concentrations of 0.001, 0.1, and 1 mM. Differences in the amplitude of Ca^{2+}-activated Cl^- tail currents as the BAPTA concentration was increased in the patch-pipette solution can be easily discerned. For each experimental condition, differences in $I_{Cl(Ca)}$ kinetics were further investigated by fitting the largest Ca^{2+}-activated Cl^- tail currents with a saturated exponential function. Deactivating Cl(Ca) tail currents were fit with a saturating exponential function of the following form to emphasize possible features governing $I_{Cl(Ca)}$ activation:

$$I_{deact} = I_{max} * \{1\text{-}1/(1+([Ca^{2+}]/EC_{50})^n)\}, \text{ where } [Ca^{2+}] \propto I_{exp} = I_{inst} * e^{(-t/\tau)}$$

A single exponential, I_{exp}, was first fit to the late stage of the deactivating current, a region typically well suited for exponential fitting. However, the amplitude of the exponential function exceeded by a large margin the amplitude of the tail current at times immediately following the voltage step back to -60 mV, and frequently deviated in this manner for tens of milliseconds. Convolution of the exponential function with a modified Hill equation (expressed as a function of current, not concentration) reduced or saturated the early large amplitude region of the tail current decay, yet had no effect on the late smaller amplitude stage. Since the magnitude of the exponential current, I_{exp}, was

Figure 3.2 Salamander cone Ca^{2+}-activated Cl^- tail currents, which deactivate following a saturated exponential function, are regulated by free $[Ca^{2+}]_i$. (**A**) Representative example of a family of current traces recorded with the standard depolarizing protocol in the presence of a low-capacity buffering system, which consisted of 0.001 mM BAPTA in the patch- pipette solution (free $[Ca^{2+}]_i$ calculated at 99 nM). Large amplitude Ca^{2+}-activated Cl^- tail currents with slow kinetics were observed. The peak Ca^{2+}-activated Cl^- tail current was fit with a τ value of 220 ms, and the Hill parameters for this fit were a saturation level of 2050 pA, a half saturation of 1500 pA, and a slope coefficient of 1.1. (**B**) Smaller Ca^{2+}-activated Cl^- tail currents with faster decay kinetics were present when $[Ca^{2+}]_i$ was buffered by increasing the BAPTA concentration to 0.1 mM in the patch-pipette solution (free $[Ca^{2+}]_i$ calculated at 15 nM). The peak Ca^{2+}-activated Cl^- current, which was recorded following a 0 mV depolarizing step from a holding potential of -60 mV, was fit with a saturating exponential function, which is shown as a dotted line in (**D**). The exponential portion was fit with a τ value of 98 ms and the parameters of the Hill-type equation that produced appropriate deviance from the exponential were: a saturation level of 2600 pA, a half saturation value of 1700 pA, and a Hill coefficient of 1.15. (**C**) Although calculated free $[Ca^{2+}]_i$ was the same as in (**B**), i.e. 15 nM, the Ca^{2+}-activated Cl^- tail currents were much smaller due to the higher concentration of BAPTA (1 mM) in the patch-pipette solution. The exponential fit for peak Ca^{2+}-activated Cl^- current had a τ value of 43 ms, and almost no saturation was applied (the same parameters as in Fig. 3.2A were used).

Figure 3.2

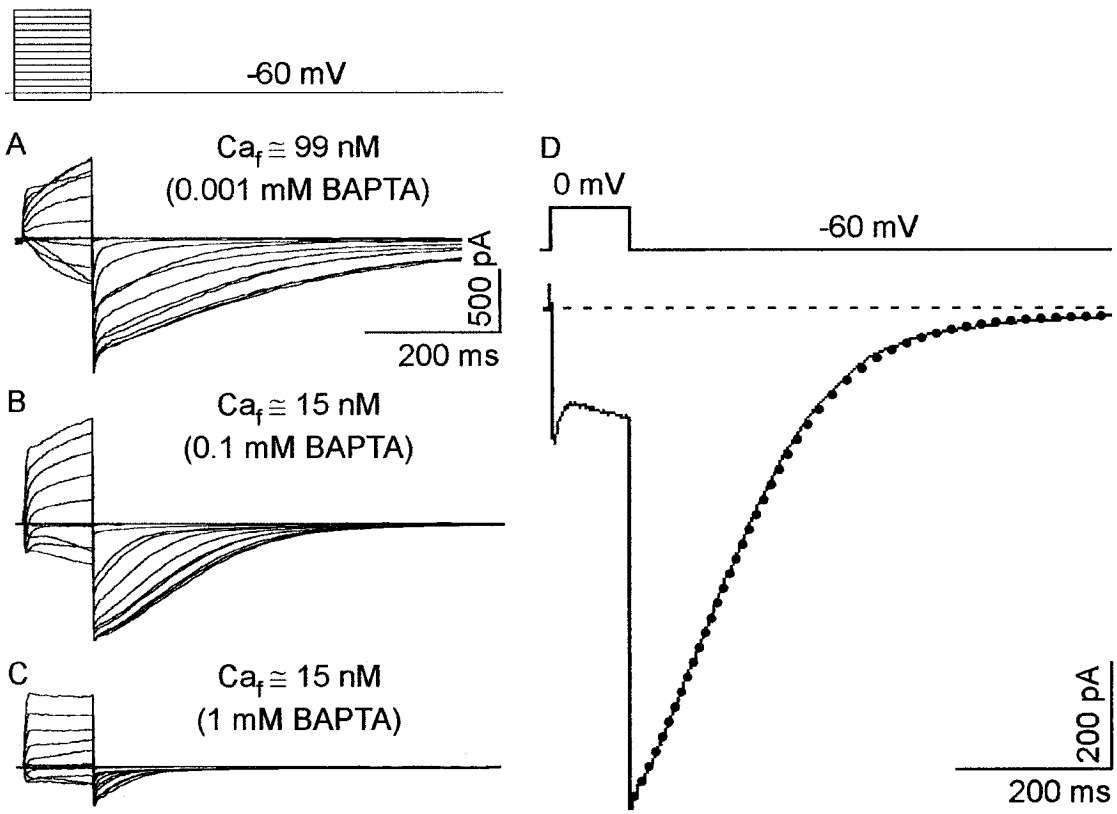
-60 mV
A
$Ca_f \cong$ 99 nM
(0.001 mM BAPTA)
500 pA
200 ms
B
$Ca_f \cong$ 15 nM
(0.1 mM BAPTA)
C
$Ca_f \cong$ 15 nM
(1 mM BAPTA)
D
0 mV
-60 mV
200 pA
200 ms

assumed to be proportional to the concentration of a gating factor (e.g., $[Ca^{2+}]$), this component replaced the concentration variable in the Hill equation. Adjusting the midpoint value for I_{exp} saturation (EC_{50}), the saturation amplitude (I_{max}), and cooperativity constant (Hill coefficient, n) optimized the fit.

After a duration of ~200 ms following the return to -60 mV, the decay followed an exponential time course. However, before this time, convolution with a sigmoidal dose-response function produced saturation of the exponential curve. At the lowest concentration of intracellular BAPTA tested (0.001 mM; example cell shown in Fig. 3.2A), the exponential portion of the peak Ca^{2+}-activated Cl^- tail current was fit with a mean τ value of 190 ± 17 ms (n=5), a relatively slow rate of deactivation. Figure 3.2B shows a family of current traces recorded with 0.1 mM BAPTA in the patch-pipette solution. The averaged τ calculated when this buffering system was used was 109 ± 10 ms (n=8). The saturated exponential fit of the largest Ca^{2+}-activated Cl^- tail current, which was recorded at 0 mV (and previously shown in Fig. 3.1), is shown as a dotted line in Figure 3.2D. At the highest concentration of intracellular BAPTA tested (1 mM; Fig. 3.2C), the averaged τ value calculated was 57 ± 6 ms (n=4). These results indicate that when free $[Ca^{2+}]_i$ is high, Ca^{2+}-activated Cl^- tail currents deactivate slowly. This agrees with the proposed model that the Ca^{2+}-activated Cl^- tail current decay reflects Ca^{2+} ions diffusing away from the Cl(Ca) channels located at the plasma membrane. A relatively faster rate of Ca^{2+}-activated Cl^- tail current deactivation was observed when a high-capacity buffering system was used, in agreement with a fast decrease in free $[Ca^{2+}]_i$ near Cl(Ca) channels after the voltage-gated Ca channels had closed. These results also suggest good dialysis of the patch-pipette solution approximately two minutes following

the rupture of salamander cone photoreceptors, the time at which the data were recorded. Unless otherwise indicated in the text or figure legends, all subsequent experiments were conducted using 0.1 mM BAPTA (Fig. 3.2B), since this offered the best manageable conditions to record $I_{Cl(Ca)}$.

3.3 Cone photoreceptor $I_{Cl(Ca)}$ is characterized by outward rectification

The current-voltage (*I-V*) relation of Cl(Ca) channels was investigated using ionomycin, a Ca^{2+} ionophore that induces a sustained increase in $[Ca^{2+}]_i$ (see Appendix 1). Superfusion with 5 μM or 10 μM ionomycin activated an outwardly rectifying current that reversed close to 0 mV (Fig. 3.3C). Figures 3.3A and B show representative examples of a family of current traces from a cone photoreceptor before and approximately 3 min after 5 μM ionomycin superfusion, respectively. Ionomycin evoked a sustained $I_{Cl(Ca)}$ activation probably reflecting increased $[Ca^{2+}]_i$. Figure 3.3C shows the constructed *I-V* relations from the recording before (Control; black circles) and after (IONO; white circle) ionomycin superfusion. The *I-V* relation in the presence of ionomycin approaches linearity and reverses close to E_{Cl}. This steady-state *I-V* relation was normalized at -40 mV (potential generating largest Ca^{2+}-activated Cl^- tail current) to correct for changes in current at the holding potential ($IONO_{norm}$; grey circles). The normalized *I-V* relation in the presence of ionomycin also indicates outward rectification at positive potentials. Similar results were obtained from other cone photoreceptors (n=3).

Figure 3.3 Step depolarizations in the presence of ionomycin (IONO; 5 or 10 μM; n=3) evoked sustained $I_{Cl(Ca)}$ activation in cone photoreceptors. (**A**) Current traces elicited with the standard depolarizing protocol in control conditions and (**B**) in the presence of ionomycin (5 μM). Zero current is indicated by the dotted line. Ca^{2+}-activated Cl^- tail currents show little deactivation in the presence of ionomycin. (**C**) Constructed *I-V* relations from the same cone measured during depolarizing voltage steps in control conditions (Control; black circles; leak-subtracted) and in the presence of ionomycin before (IONO; white circles), and after normalization ($IONO_{NORM}$; grey circles). With ionomycin, the current reverses close to E_{Cl} and is characterized by some outward rectification at positive potentials.

Figure 3.3

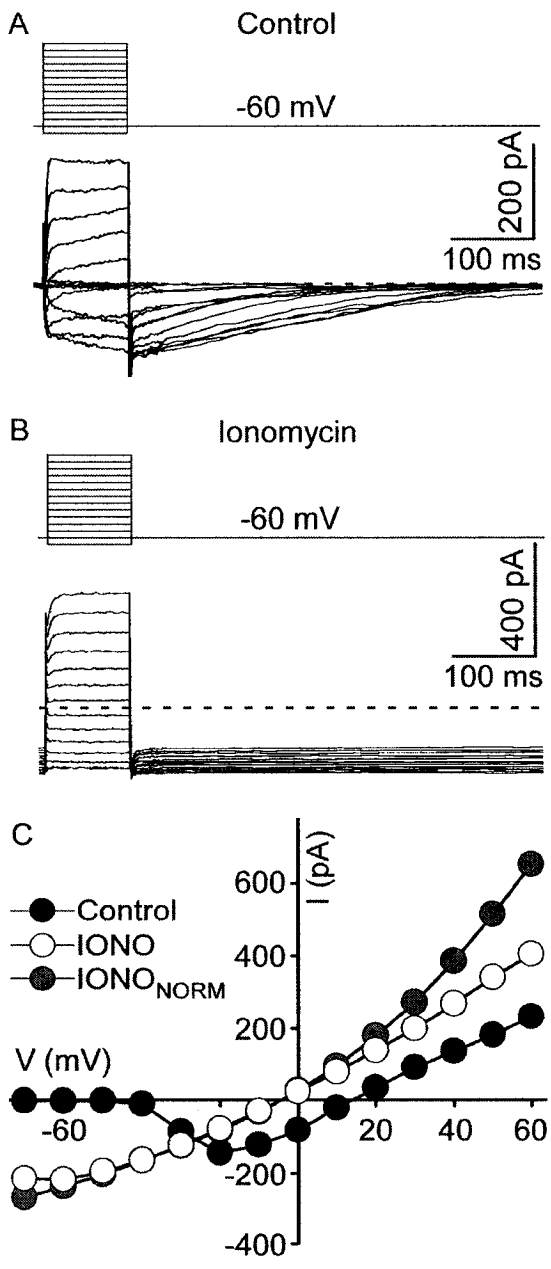
A
Control
-60 mV
200 pA
100 ms
B
Ionomycin
-60 mV
400 pA
100 ms
C
Control
IONO
IONO$_{NORM}$
I (pA)
600
400
200
-200
-400
V (mV)
-60
20
40
60

Another Ca^{2+} ionophore called calcimycin (or ionophore A23187) has been used at a concentration bellow 5 μM to elevate $[Ca^{2+}]_i$ and activate $I_{Cl(Ca)}$ in secretory cells and *Xenopus* oocytes (Marty et al., 1984; Boton et al., 1989). Unlike ionomycin, calcimycin (10 μM) failed to increase the amplitude of $I_{Cl(Ca)}$ in salamander cone photoreceptors. A family of current traces recorded in control conditions (Fig. 3.4A) remained unchanged after calcimycin was added to the standard bath solution (Fig. 3.4B). Figure 3.4C shows the corresponding *I-V* relations. The averaged peak current remaining in the presence of calcimycin was 82 ± 18% (n=3), measured during depolarizing voltage steps, and 87 ± 16% (n=3), measured during repolarization following those steps (i.e. Ca^{2+}-activated Cl^- tails).

Repeated strong depolarizations also elicited currents characterized by an *I-V* relation displaying outward rectification that reversed close to E_{Cl}. This protocol, which was applied at a frequency of 2 Hz, consisted of a 100 ms prepulse to 0 mV from a holding potential of -60 mV, followed by 100 ms voltage steps that were changed by decrements of 10 mV from +20 mV to -80 mV (see Fig. 3.5B). This voltage-clamp protocol most likely increases intracellular Ca^{2+} levels since it generated similar *I-V* relations to the ones obtained in the presence of ionomycin, which has been shown to induce sustained $[Ca^{2+}]_i$ elevation in salamander cone photoreceptors (see Appendix 1). Figure 3.5A demonstrates a recording from a cone photoreceptor held at -60 mV and depolarized from -80 mV to +20 mV, in 10 mV increments at a rate of 0.5 Hz. The *I-V* relation from this recording is typical of voltage-gated Ca channel, with an $I_{Cl(Ca)}$ component (reverses near E_{Cl} at 0 mV) (Control; black circles; Fig. 3.5C). A large Cl^-

Figure 3.4 Calcimycin (ionophore A23187) did not modify $I_{Cl(Ca)}$ in cone photoreceptors. (**A**) Representative example of a family of current traces elicited with the standard depolarizing protocol before and (**B**) after calcimycin (10 μM) was added to the extracellular solution. $I_{Cl(Ca)}$ remained unchanged. (**C**) *I-V* relations (not leak-subtracted) constructed from the current measured during depolarizing voltage steps obtained from the same cone photoreceptor in control conditions (black circles) and in the presence of calcimycin (white circles).

Figure 3.4

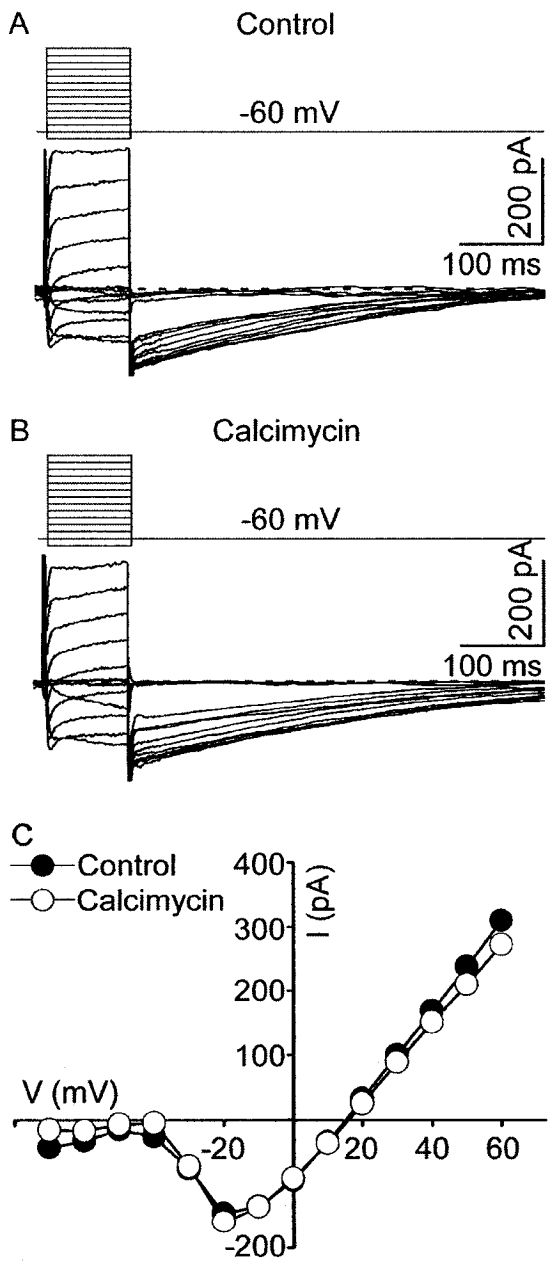
A
Control
-60 mV
200 pA
100 ms
B
Calcimycin
-60 mV
200 pA
100 ms
C
Control
Calcimycin
400
300
200
100
I (pA)
V (mV)
-20
20
40
60
-200

Figure 3.5 Repeated strong depolarizations (0 mV pulses of 100 ms duration, repeated at 2 Hz) elicited sustained $I_{Cl(Ca)}$ activation, characterized by outward rectification at positive potentials. (**A**) Typical family of current traces obtained from a cone photoreceptor held at -60 mV and depolarized with 10 mV increments from -80 mV to +20 mV at 0.5 Hz. (**B**) The same cone generated a large inward conductance when a 100 ms prepulse to 0 mV was added to the voltage-clamp protocol, which consisted of 10 mV decrements from +20 mV to -80 mV applied at 2 Hz. The dashed line indicates zero current. (**C**) Without the fast-paced depolarizing prepulses to 0 mV, the *I-V* relation measured from the mean current 25 ms before the end of the voltage steps represents a combination of both I_{Ca} and $I_{Cl(Ca)}$ (Control; black circles; leak-subtracted). Following repeated strong depolarizations, the characteristic outward rectification of $I_{Cl(Ca)}$ is revealed (Prepulse; white-circles). The *I-V* relation remains outwardly rectifying following normalization ($Prepulse_{NORM}$). This cell was recorded using a low-capacity buffering system (1 μM BAPTA and 0.1 mM $CaCl_2$).

Figure 3.5

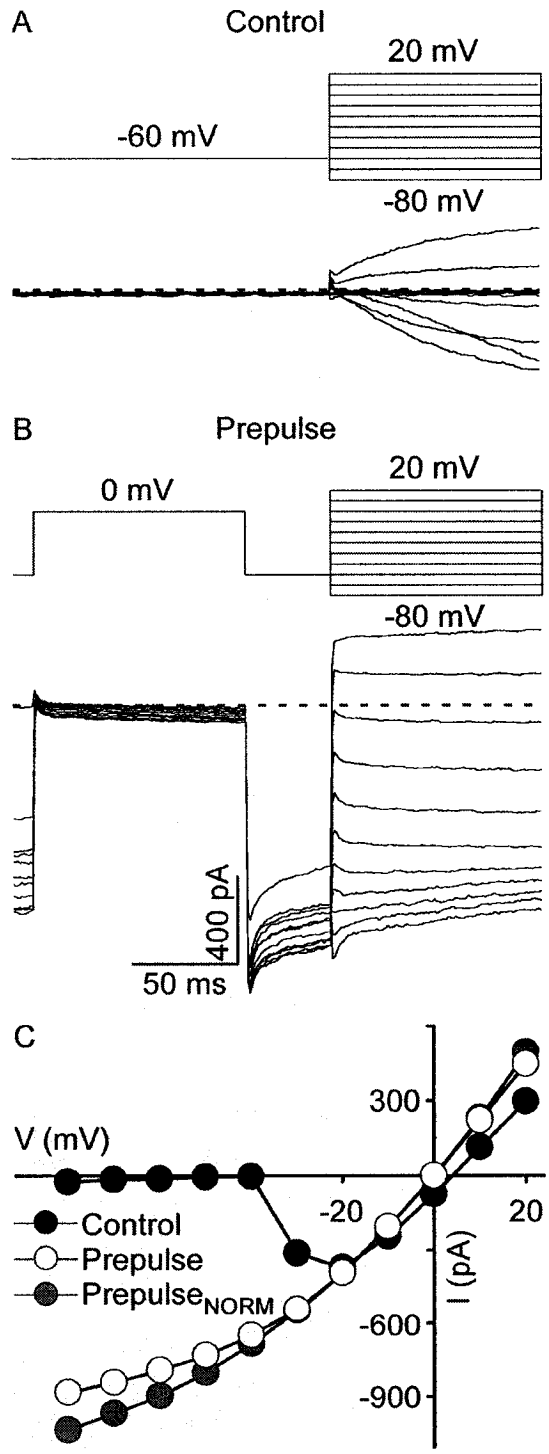
A
Control
20 mV
-60 mV
-80 mV
B
Prepulse
0 mV
20 mV
-80 mV
400 pA
50 ms
C
V (mV)
300
-20
20
Control
Prepulse
Prepulse NORM
-600
-900
I (pA)

conductance developed from the repeated strong depolarization protocol (Fig. 3.5B). The 0 mV prepulse used in this protocol most likely induced Ca^{2+} influx through voltage-gated Ca channels, resulting in increased submembrane $[Ca^{2+}]_i$ and $I_{Cl(Ca)}$ activation. The sustained $I_{Cl(Ca)}$ activation is characterized by some outward rectification at positive test potentials (Prepulse; white circles; Fig. 3.5C). The normalized *I-V* relation (corrected for changes in current at holding potential) also shows some outward rectification ($Prepulse_{NORM}$; grey circles; Fig. 3.5C). Similar recordings were obtained from other isolated salamander cone photoreceptors (n=4). Superfusion with ionomycin and repeated strong depolarizations first caused an increase in $I_{Cl(Ca)}$, as shown in Figure 3.3 and 3.5, but this enhancement was followed by inhibition of $I_{Cl(Ca)}$. This will be discussed in more detail in Chapter 5.

3.4 Increased Cl(Ca) channel activation by Ca^{2+} influx through voltage-gated L-type Ca channels

Voltage-gated Ca channels play a key role in sustaining glutamate release at the photoreceptor synapse. Dihydropyridine-sensitive L-type Ca channels have been identified and characterized in cone photoreceptors (Wilkinson and Barnes, 1996). The activation of Cl(Ca) channels by Ca^{2+} influx specifically through voltage-gated L-type Ca channels was investigated with (±)-Bay K8644 (BayK), a well-known agonist of dihydropyridine-sensitive Ca channels. In cone photoreceptors, BayK significantly ($P<0.01$) increased peak $I_{Cl(Ca)}$ (Steps: 62 ± 7%; Tails: 27 ± 8%; n=5). Figure 3.6A demonstrates a representative example of a voltage-clamp recording from an isolated cone photoreceptor. Figure 3.6B shows a constructed *I-V* relation in control conditions

Figure 3.6 Cone photoreceptor Cl(Ca) channels are activated by Ca^{2+} influx through voltage-gated L-type Ca channels. (**A**) Representative current traces from a cone photoreceptor held at -60 mV and depolarized to -20 mV in control conditions (Control; solid line) and in the presence of 1 μM (±)-Bay K8644 (BayK; dotted line), added to the extracellular solution. Both I_{Ca} and $I_{Cl(Ca)}$ were increased by BayK. (**B**) Leak subtracted *I-V* relations from the same cell comparing the current measured during depolarizing voltage steps in control conditions and (**C**) in the presence of BayK, showing that the difference between the current measured early vs. later during depolarizing steps intersect at 0 mV for both conditions. (**D**) Leak-subtracted *I-V* relations from the same cone measured early on during depolarizing voltage steps reflect the increase in I_{Ca} in the presence of BayK (white circles) when compared to control (black circles). (**E**) Ca^{2+}-activated Cl^- *Q-V* relations (offset-subtracted) from the same cell demonstrate an increase in $I_{Cl(Ca)}$ with application of BayK. (**F**) Summary of the cumulative data showing the significant increase in the peak current remaining (expressed as a percentage of control) in the presence of BayK. The peak current remaining measured early on during depolarizing voltage steps (Early voltage step) was increased by 54 ± 15% (n=4) while the Ca^{2+}-activated Cl^- tail current integral (Tail integral) was enhanced by 40 ± 10% (n=4). *$P<0.05$.

Figure 3.6

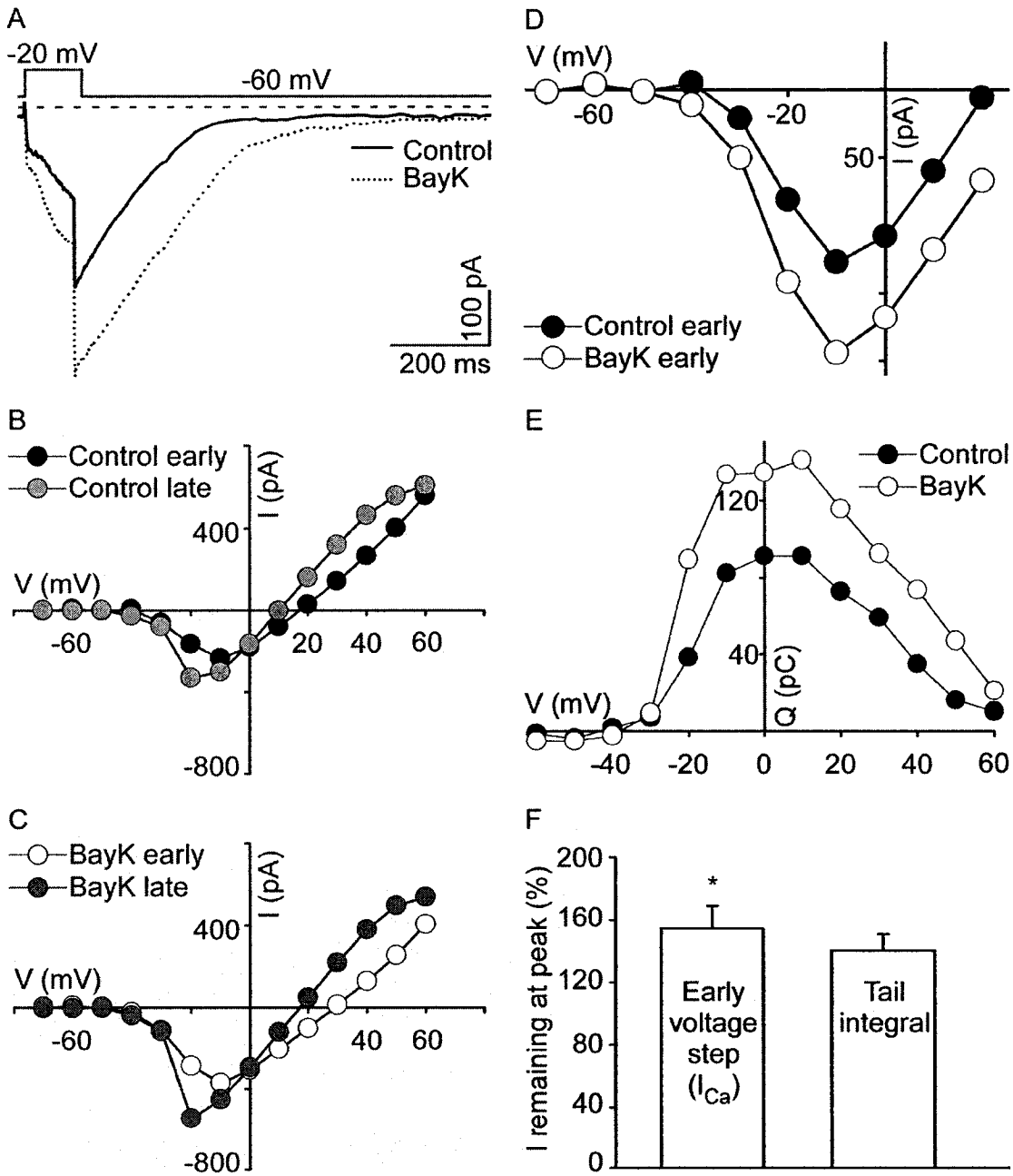
A
-20 mV
-60 mV
Control
BayK
100 pA
200 ms
B
Control early
Control late
I (pA)
400
V (mV)
-60
20
40
60
-800
C
BayK early
BayK late
I (pA)
400
V (mV)
-60
40
60
-800
D
V (mV)
-60
-20
50
I (pA)
Control early
BayK early
E
Control
BayK
120
40
Q (pC)
V (mV)
-40
-20
0
20
40
60
F
I remaining at peak (%)
200
160
120
80
40
0
*
Early voltage step (I_{Ca})
Tail integral

measured early on into each depolarizing voltage step (between 3-6 ms; black circles), where there is less contamination from $I_{Cl(Ca)}$, and later (between 90-94 ms into each voltage step; light grey circles). The difference between the two *I-V* relations, which reflects the contribution of $I_{Cl(Ca)}$ alone, reverses at E_{Cl}. Figure 3.6C compares the *I-V* relations in the presence of BayK measured early (white circles) and later (dark grey circles) during depolarizing voltage steps. The difference between these two *I-V* relations also reverses at 0 mV. The *I-V* relations from control conditions and in the presence of BayK, measured at the beginning of the voltage steps are shown in Figure 3.6D and demonstrate an increase in the presence of BayK. In addition, the Ca^{2+}-activated Cl^- *Q-V* relations also show an increase in the presence of BayK (Fig. 3.6E). A 54 ± 15% (n=4; $P<0.05$) increase was observed in the current measured early on in the voltage steps, whereas $I_{Cl(Ca)}$ measured from the integral of the Ca^{2+}-activated Cl^- tail current was enhanced by 40 ± 10% (n=4) (Fig. 3.6F), suggesting a near one-to-one correspondence between Ca^{2+} entry and Cl(Ca) channel activation.

The potentiation of $I_{Cl(Ca)}$ by BayK has also been previously observed in dorsal root ganglia (DRG) neurons (Scott et al., 1988). The activation of voltage-gated Ca^{2+} currents most likely increases Ca^{2+}-activated Cl^- tail currents by increasing the Ca^{2+} available to activate Cl(Ca) channels. The results of this study suggest that Cl(Ca) channels are activated by local Ca^{2+} microdomains located at the plasma membrane as a result of Ca^{2+} entering via voltage-activated L-type Ca channels in cone photoreceptors. Cl(Ca) channels may therefore be co-localized with high voltage-gated Ca channels at the plasma membrane, to ensure efficient activation by localized domains of elevated Ca^{2+} (Chad and Eckert, 1984; Llinás et al., 1992).

3.5 Barium increases depolarization-induced current but inhibits Ca^{2+}-activated Cl^- tail currents

Barium (Ba^{2+}) ions permeate Ca channel pores more readily than Ca^{2+} ions, and are commonly used as charge carriers to study voltage-gated Ca channels. Thus, the ionic specificity of cone photoreceptor Cl(Ca) channel activation was investigated by equimolar replacement of Ca^{2+} with Ba^{2+} in the standard bath solution. In the presence of 3 mM Ba^{2+}, peak current measured during depolarizing voltage steps was significantly ($P<0.05$) enhanced by 35 ± 7% (n=3), while peak Ca^{2+}-activated Cl^- tail current was significantly ($P<0.05$) inhibited by 84 ± 12% (n=3). This is demonstrated in a representative cell shown in Figure 3.7A during a voltage-step protocol when 3 mM Ca^{2+} (solid line) was replaced with 3 mM Ba^{2+} (dotted line). Figures 3.7B and C show *I-V* relations from another cell, measured during depolarizing voltage steps and during repolarization following those steps, respectively, in the presence of either 3 mM Ca^{2+} (black circles) or Ba^{2+} (white circles). The increased current during depolarization reflects more current through voltage-gated Ca channels when Ba^{2+} was used as a charge carrier. The inhibition of Ca^{2+}-activated Cl^- tail currents with Ba^{2+} suggests that Ca^{2+} ions are required for the activation of Cl(Ca) channels. Another possibility is that Ba^{2+} also activates Cl(Ca) channels but these ions are buffered faster from submembrane microdomains.

Figure 3.7 Ca^{2+} substitution with barium (Ba^{2+}) in the extracellular solution increases the current measured during depolarizing voltage steps and abolishes Ca^{2+}-activated Cl^- tail currents. (**A**) Current traces from a cone photoreceptor held at -60 mV and depolarized to 0 mV in control conditions (3 Ca^{2+}; solid line), and after extracellular Ca^{2+} was replaced with equimolar Ba^{2+} (3 Ba^{2+}; dotted line). In 3 mM Ba^{2+}, the current measured during depolarization was increased, whereas the Ca^{2+}-activated Cl^- tail current was inhibited. (**B**) Leak-subtracted *I-V* relations from a different cell, measured during depolarizing voltage steps elicited with the standard depolarizing protocol, shows the increased inward current after substitution of Ca^{2+} with Ba^{2+}. (**C**) From the same cell, leak-subtracted *I-V* relations measured during repolarization and plotted against the corresponding voltage from the steps. The Ca^{2+}-activated Cl^- tail current was inhibited in the presence of Ba^{2+}. For this set of data, the buffering system for the intracellular solution was 1 mM EGTA and 0.1 mM Ca^{2+} (calculated free $[Ca^{2+}]_i$ of 17.8 nM).

Figure 3.7

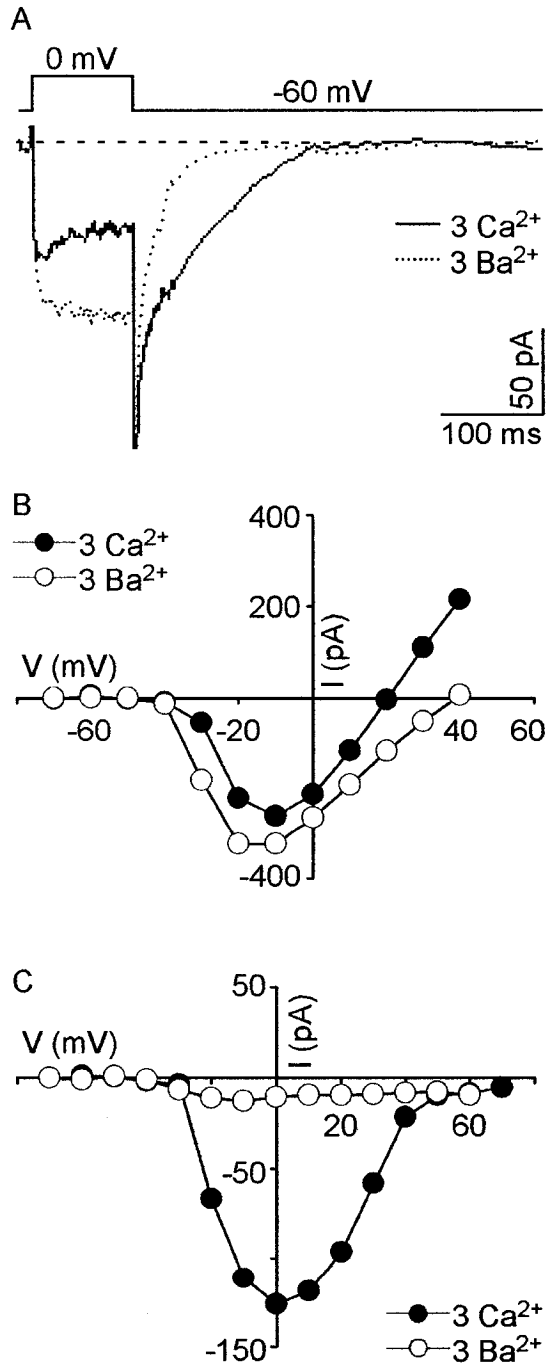
A
0 mV
-60 mV
3 Ca2+
3 Ba2+
50 pA
100 ms
B
3 Ca2+
3 Ba2+
400
200
I (pA)
V (mV)
-60
-20
40
60
-400
C
50
I (pA)
V (mV)
20
60
-50
-150
3 Ca2+
3 Ba2+

3.6 $I_{Cl(Ca)}$ in salamander cone photoreceptors is blocked by the Cl channel blocker NPPB

5-Nitro-2-(3-phenylpropylamino)benzoic acid (NPPB), a commonly used Cl channel blocker, was used to test the biophysical properties of Cl(Ca) channels. At 100 μM, NPPB has previously been shown to block Cl(Ca) channels in bovine pulmonary artery endothelial cells (Nilius et al., 1997b). In the present study, a reversible inhibition of $I_{Cl(Ca)}$ in cone photoreceptors was observed when 100 μM NPPB was added to the superfusate, which typically contained 3 mM Ca^{2+} (Figs. 3.8A-C, F). On average, NPPB significantly ($P<0.05$) inhibited the current induced at a test potential of -20 mV by 80 ± 2% (3 mM Ca^{2+}; black; n=3) and the corresponding Ca^{2+}-activated Cl^- tails by 71 ± 8% (3 mM Ca^{2+}; white; n=3) (Fig. 3.8F). The time course of current remaining, measured during depolarizing voltage steps (Steps; black circles) and during repolarization following those steps (Tails; white circles), indicates the inhibition upon NPPB application (Fig. 3.8A). The current traces (Fig. 3.8B) and Ca^{2+}-activated Cl^- tail *Q-V* relations (Fig. 3.8C) also demonstrate the decrease in $I_{Cl(Ca)}$.

The inward current measured early on during -20 mV voltage steps, which is less contaminated with $I_{Cl(Ca)}$ (i.e. contains more Ca^{2+} current) was also significantly ($P=0.01$) inhibited (mean inhibition of 72 ± 5%; n=3) in 3 mM extracellular Ca^{2+}. Therefore, similar experiments were performed by replacing extracellular Ca^{2+} with equimolar Ba^{2+} to investigate if NPPB also inhibits Ca channels. Although NPPB is a commonly used Cl channel blocker, application of this drug also resulted in reduction of the Ca channel current (Figs. 3.8D, E, and F). Measured in 3 mM Ba^{2+}, NPPB induced a 44 ± 7% (n=3) Ca channel blockade induced at a test potential of -20 mV (Fig. 3.8F), which likely

Figure 3.8 The chloride channel blocker NPPB (100 μM) reduced $I_{Cl(Ca)}$ and Ca channel currents in salamander cone photoreceptors. (**A**) Time course of current remaining measured during depolarizing steps to -20 mV (Steps; black circles) and during repolarization following those steps (Tails; white circles), showing the NPPB-induced inhibition. (**B**) Current traces from a -20 mV depolarizing voltage step recorded in control conditions (solid line), in the presence of NPPB (dotted line), and during wash of NPPB (dashed line). The current was markedly increased when NPPB was removed from the superfusing solution and overshot control levels. (**C**) Offset-subtracted Ca^{2+}-activated Cl^- *Q-V* relations, obtained from the same cone, show reduced charge entry during NPPB superfusion (white circles) when compared to control (black circles). (**D**) Ca channel current traces (3 mM extracellular Ca^{2+} was replaced with Ba^{2+}) recorded from a cone held at -60 mV and depolarized to -20 mV in control conditions (solid line) and in the presence of NPPB (dotted line). NPPB caused a reduction in the Ca channel current. (**E**) Leak-subtracted *I-V* relations of the Ca channel current from the same cone showing the reduction in the presence of NPPB (white circles) when compared to control (black circles). (**F**) Summary of the average current remaining at -20 mV following the application of NPPB. In 3 mM Ca^{2+}, NPPB blocked 80 ± 2% (n=3) of the current measured at -20 mV (Steps; black bar) and 71 ± 8% (n=3) of the corresponding Ca^{2+}-activated Cl^- tail current measured at -60 mV (Tails; white bar). The Ca channel current, tested in 3 mM Ba^{2+}, was reduced to 56 ± 7% (n=3) during NPPB superfusion. *$P<0.05$.

Figure 3.8

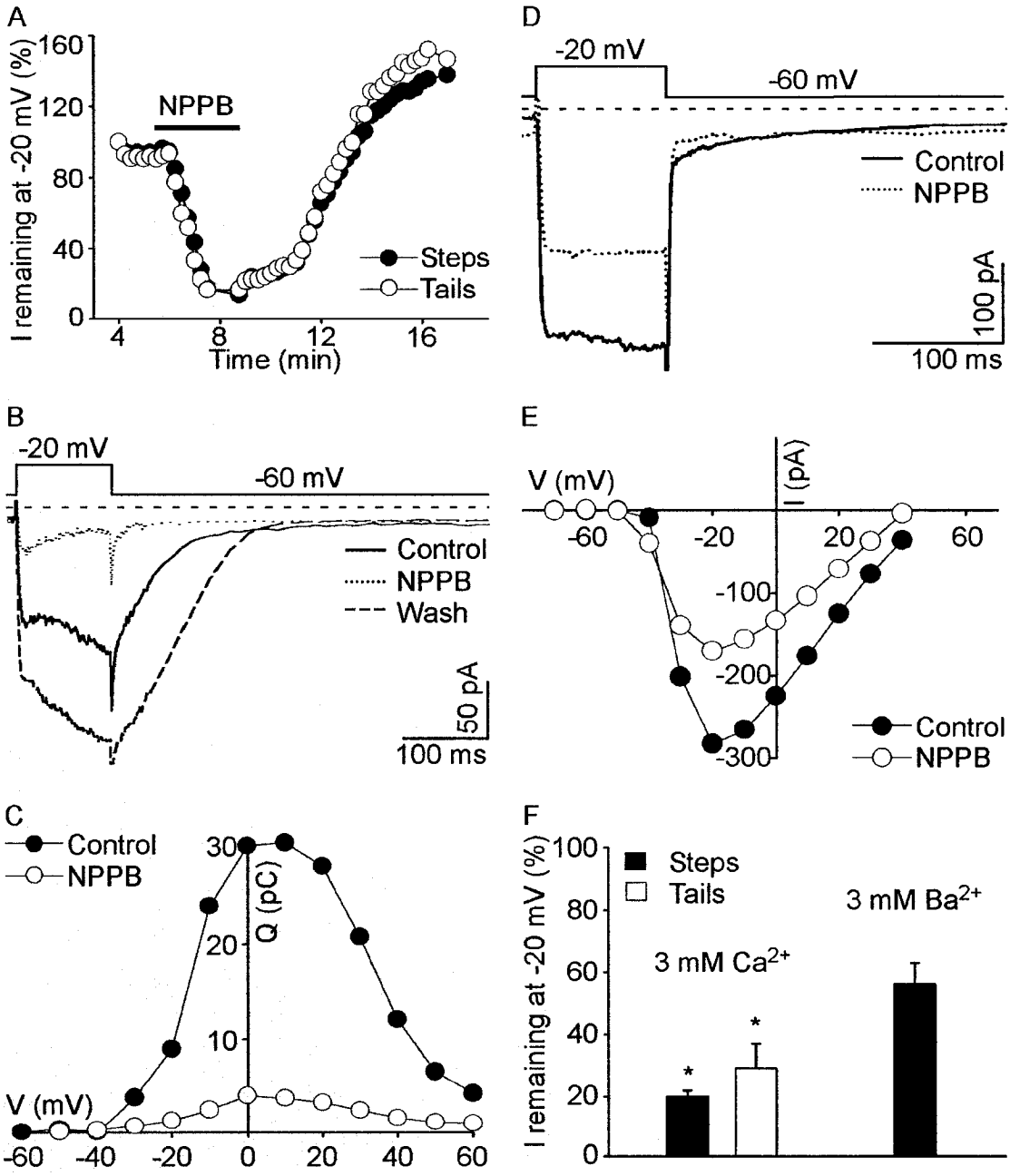
A
I remaining at -20 mV (%)
160
120
80
40
0
NPPB
Steps
Tails
4
8
12
16
Time (min)
B
-20 mV
-60 mV
Control
NPPB
Wash
50 pA
100 ms
C
Control
NPPB
30
20
10
Q (pC)
V (mV)
-60
-40
-20
0
20
40
60
D
-20 mV
-60 mV
Control
NPPB
100 pA
100 ms
E
V (mV)
I (pA)
-60
-20
20
60
-100
-200
-300
Control
NPPB
F
I remaining at -20 mV (%)
100
80
60
40
20
0
Steps
Tails
3 mM Ca2+
3 mM Ba2+
*
*

contributed to the inhibition of $I_{Cl(Ca)}$, in addition to the direct block of Cl(Ca) channels. The reduction in Ca channel currents by NPPB was irreversible; however, $I_{Cl(Ca)}$ recovered above baseline levels following washout of NPPB. For example, as shown in the figure, $I_{Cl(Ca)}$ was increased by ~60% of its original value when NPPB was removed from the superfusate (Figs. 3.8A and B). The factors responsible for over-recovery of $I_{Cl(Ca)}$ were not further investigated in the present series of experiments.

3.7 $I_{Cl(Ca)}$ is not modulated by calmodulin or by calmodulin inhibitors

In addition to ion channels and pumps, many key Ca^{2+}-dependent cellular enzymes, such as protein kinases and phosphatases, are localized at the inner segment of cone photoreceptors. Within the inner segment, Ca^{2+} may activate calmodulin (CaM) kinases that in turn could phosphorylate a number of targets within the synaptic terminal, including Cl(Ca) channels. Alternatively, CaM could be a direct intermediate between Cl(Ca) channel activation mediated by $[Ca^{2+}]_i$. The effect of CaM on salamander cone $I_{Cl(Ca)}$ was investigated by including 1 μM CaM in the recording pipette solution. Figure 3.9 demonstrates a representative example in which a cell was subjected to intracellular CaM. Ca^{2+}-activated Cl^- tail currents were present and unchanged as seen from the current traces (Fig. 3.9A). The *I-V* relation from the current measured during depolarizing voltage steps (Fig. 3.9B), and Ca^{2+}-activated Cl^- *Q-V* relation (Fig. 3.9C) are also illustrated. Similar results were obtained in three other cone photoreceptors. Currents recorded ~5 min following rupture of the whole-cell patch were compared to recordings obtained ~10 min post-rupture. After this time, the peak current remaining

Figure 3.9 Activation of Cl(Ca) channels by Ca^{2+} is not regulated via an intermediate mechanism involving calmodulin (CaM), a Ca^{2+}-binding protein. The presence of calmodulin (CaM; 1 μM in pipette solution; n=5) did not alter $I_{Cl(Ca)}$. (**A**) Representative current traces elicited by the standard depolarizing protocol in the presence of CaM (~10 min) in the recording pipette solution. Zero current is indicated by the dashed line. (**B**) Constructed *I-V* (leak-subtracted) and (**C**) Ca^{2+}-activated Cl^- *Q-V* (offset-subtracted) relations from the same cone, were unmodified in the presence of CaM.

Figure 3.9

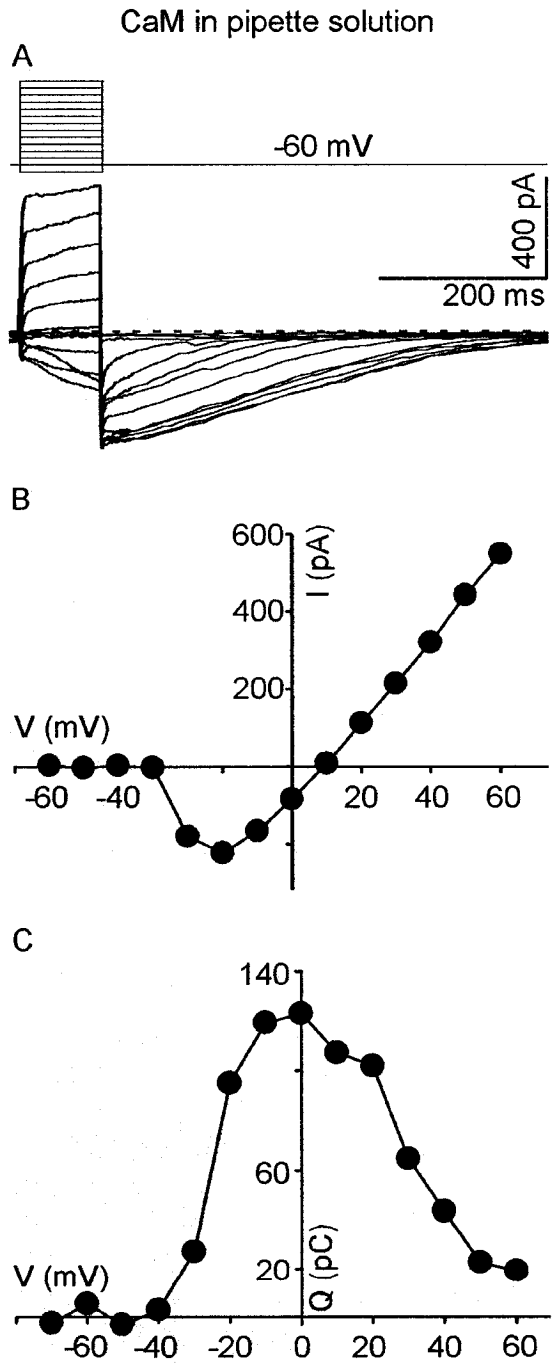
CaM in pipette solution
A
-60 mV
400 pA
200 ms
B
600
400
200
I (pA)
V (mV)
-60
-40
20
40
60
C
140
60
20
Q (pC)
V (mV)
-60
-40
-20
0
20
40
60

during depolarizing voltage steps and during repolarization following those steps was 95 ± 7% (n=4) and 97 ± 5% (n=4), respectively.

The effect of the CaM inhibitors, trifluoperazine and calmidazolium, on salamander cone photoreceptor $I_{Cl(Ca)}$ was also tested by adding these drugs to the superfusate (Fig. 3.10). Although both of these CaM inhibitors have been shown to reduce $I_{Cl(Ca)}$ in pulmonary artery endothelial cells (Nilius et al., 1997a), these drugs failed to modify $I_{Cl(Ca)}$ in salamander cone photoreceptors. Figure 3.10A demonstrates unchanged current traces to a 0 mV depolarizing step before (solid line) and after trifluoperazine (dotted line) was added to the standard bath solution. Figure 3.10B and C also demonstrate unchanged *I-V* and *Q-V* relations obtained from the same cell in the presence of trifluoperazine. Figure 3.10D illustrates the cumulative data of the current remaining (expressed as a percentage of control) in the presence of both CaM inhibitors trifluoperazine and calmidazolium. The peak current remaining measured during depolarizing voltage steps and during repolarization following those steps was 99 ± 20% (n=5) and 106 ± 15% (n=5), respectively, when superfusing trifluoperazine (5 μM). In the presence of calmidazolium (10 μM), the peak current remaining during depolarization was 92 ± 6% (n=5) and 109 ± 8% (n=5), measured at the tail. $I_{Cl(Ca)}$ was also unchanged when 10 μM calmidazolium was added to the recording pipette solution (n=2; data not shown). These results suggest that CaM may not have an significant role in the activation of Cl(Ca) channels in salamander cone photoreceptors. However, a number of Ca^{2+}-binding proteins are found in cone photoreceptors and the modulation of Cl(Ca) channels via Ca^{2+}-binding proteins other than CaM can not be ruled out.

Figure 3.10 CaM inhibitors, trifluoperazine and calmidazolium, had insignificant effects on $I_{Cl(Ca)}$. Cone photoreceptors, held at -60 mV, were depolarized following the standard depolarizing protocol under control conditions and in the presence of trifluoperazine (5 μM; n=5) and calmidazolium (10 μM; n=5). (**A**) Representative example of current traces elicited by a 0 mV depolarizing voltage step in control conditions (solid line) and in the presence of trifluoperazine (dotted line), showing no changes. (**B**) Leak-subtracted *I-V* and (**C**) offset-subtracted Ca^{2+}-activated Cl^- *Q-V* relations from the same cone showing no changes in the presence of trifluoperazine (white circles) compared to control (black circles). (**D**) Summary of the average peak current remaining after trifluoperazine and calmidazolium were added to the extracellular solution. In the presence of trifluoperazine, the average peak current remaining was 99 ± 20% (n=5), measured during depolarizing voltage steps (Steps; black bar) and 106 ± 15% (n=5), measured during repolarization following those steps (Tails; white bar). Similar values were obtained when superfusing with calmidazolium. The peak current remaining was 92 ± 6% (n=5), measured during depolarizing voltage steps, and 109 ± 8% (n=5), measured during repolarization following those steps. For these experiments, the buffering system consisted of 1 μM BAPTA and 0.1 mM $CaCl_2$.

Figure 3.10

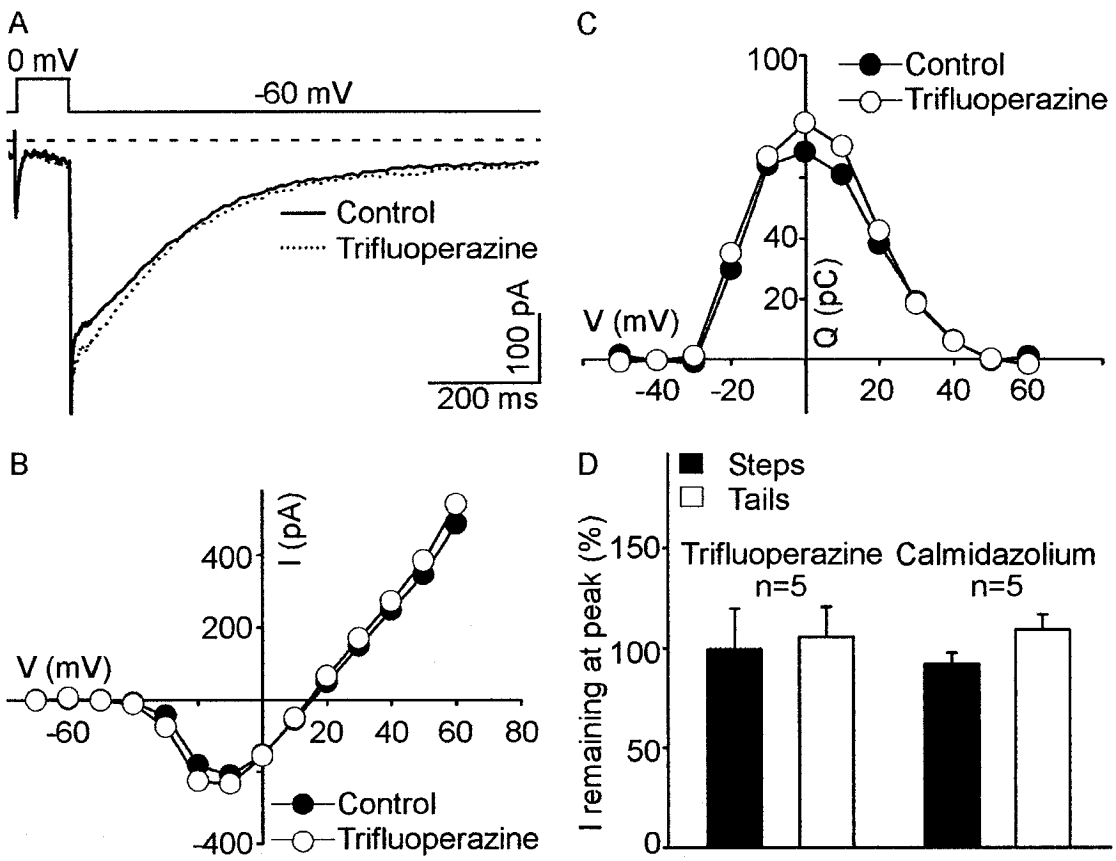
A
0 mV
-60 mV
Control
Trifluoperazine
100 pA
200 ms
B
I (pA)
400
200
V (mV)
-60
20
40
60
80
Control
-400
Trifluoperazine
C
100
Control
Trifluoperazine
40
20
Q (pC)
V (mV)
-40
-20
20
40
60
D
Steps
Tails
I remaining at peak (%)
150
100
50
0
Trifluoperazine
n=5
Calmidazolium
n=5

3.8 Cl(Ca) channels are not vesicular ClC-3 channels

ClC-3 channels are possible candidates for the Cl(Ca) channels of interest in the present study since ClC-3 antibodies label photoreceptors (Stobrawa et al., 2001). ClC-3 primarily resides in intracellular organelles, such as synaptic vesicles. Synaptic vesicle docking is mediated by a complex between components of the synaptic vesicle membrane (synaptobrevin and synaptotagmin) and the presynaptic plasma membrane (syntaxin and SNAP-25) (Bennett and Scheller, 1994). Synaptobrevin has been shown to be present in the other plexiform layer of the rat retina (Morgans, 2000). Since Ca^{2+} is required for the fusion of synaptic vesicles with the presynaptic plasma membrane, ClC-3 channels in vesicles may fuse with the plasma membrane in response to Ca^{2+} influx, giving rise to increased whole-cell Cl^- conductance. Stobrawa et al. (2001) generated a ClC-3 knockout mouse, which showed selective postnatal degeneration of the hippocampus and photoreceptors, and impaired acidification of synaptic vesicles, supporting the presence of ClC-3 channels in photoreceptors and a role for intracellular ClC-3.

Since the molecular identity of Cl(Ca) channels has yet to be determined, the present study tested the hypothesis that Cl(Ca) channels are vesicular ClC-3 channels that are integrated with the plasma membrane upon Ca^{2+} influx following depolarization. The effect of a polyclonal antibody directed towards ClC-3 (anti-ClC-3) on $I_{Cl(Ca)}$ in salamander cone photoreceptors was examined by including the antibody in the recording pipette solution. Current traces in response to the standard depolarizing protocol were recorded at ~5 min following rupture of the whole-cell patch, and up to 15 min later to ensure thorough diffusion of the antibody into the cell interior. ClC-3 antibodies have been shown to completely inhibit the expressed ClC-3 current as well as its outwardly

rectifying anion conductance in a variety of cell types (Duan et al., 2001). Electrophysiological properties of $I_{Cl(Ca)}$ when anti-ClC-3 antibodies were added to the pipette solution were not different from control recordings (Fig. 3.11). Figures 3.11A and B show similar family of current traces ~5 min and ~10 min after dialysis with anti-ClC-3 added to the intracellular solution. The corresponding *I-V* and Ca^{2+}-activated Cl^- *Q-V* relations are shown in Figure 3.11C and Figure 3.11D, respectively. Similar results were obtained from four other cones. The peak current remaining was 103 ± 2% (n=5), measured during depolarizing voltage steps, and 101 ± 6% (n=5), measured during repolarization following those steps. The results of this study also indicate that ClC-3 does not contribute to whole-cell Cl(Ca) channel currents in salamander cone photoreceptors.

To further examine whether Cl(Ca) conductances are due to another Cl channel that fused with the cell membrane during Ca^{2+} dependent vesicle docking, tetanus toxin was tested. Tetanus toxin, a neurotoxin produced by bacteria of the genus *Clostridium*, is a potent inhibitor of neurotransmitter release (Schiavo et al., 1994). This toxin functions as an endoprotease that selectively targets synaptobrevin for cleavage, inhibiting vesicle docking and fusion. Tetanus toxin was tested in a similar fashion than anti-ClC-3, as it was also included in the pipette solution. Tetanus toxin, introduced to the pipette solution, generated normal Ca^{2+}-activated Cl^- tail currents following the standard depolarizing protocol up to ~15 min post-rupture (Fig. 3.12). The peak current remaining was 107 ± 11% (n=5), measured during depolarizing voltage steps, and 110 ± 6% (n=5),

Figure 3.11 Cl(Ca) channels responsible for $I_{Cl(Ca)}$ are not vesicular ClC-3 channels that integrate with the plasma membrane upon Ca^{2+} influx. Adding anti-ClC-3 (1:100; n=5) to the recording pipette solution did not modify $I_{Cl(Ca)}$. (**A**) A family of current traces ~5 min and (**B**) ~10 min following rupture of the whole-cell patch in the presence of anti-CLC-3 in the pipette solution are similar. (**C**) Leak-subtracted *I-V* and (**D**) offset-subtracted Ca^{2+}-activated Cl^- *Q-V* relations from the same cell also show no significant changes in current (~5 min: black circles; ~10 min: white circles).

Figure 3.11

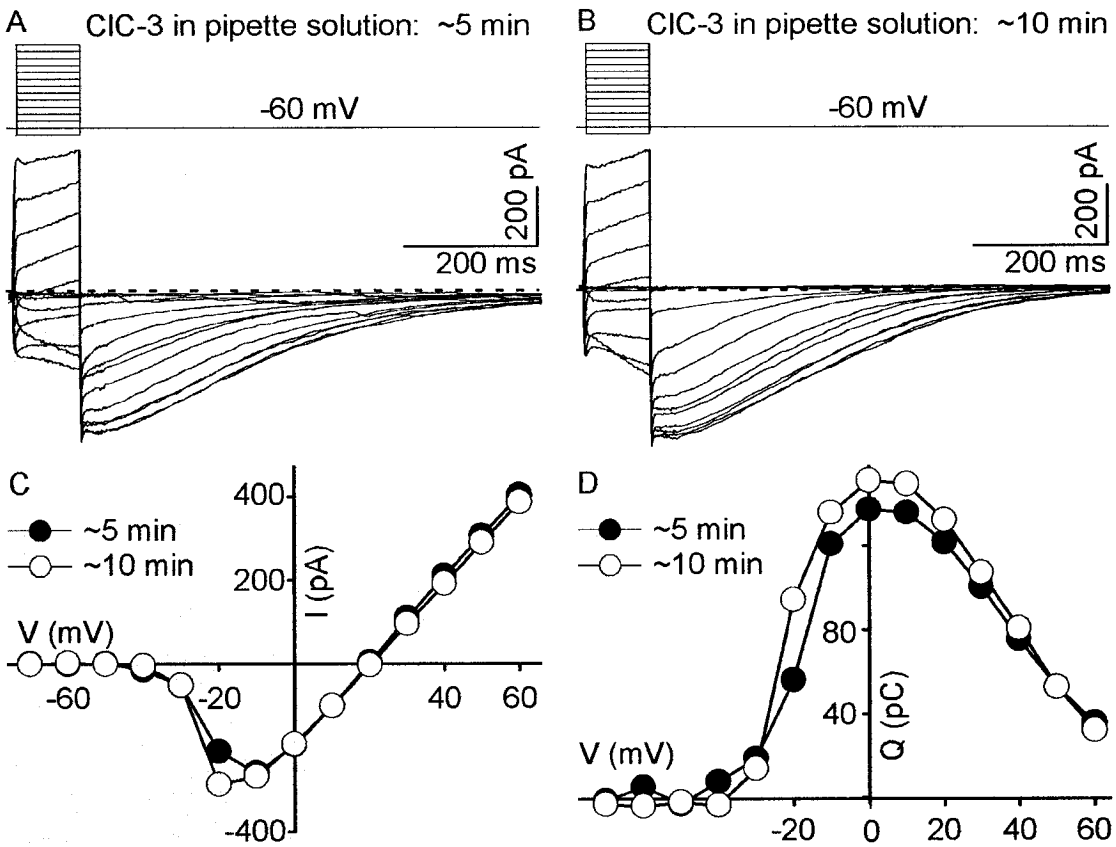
A
ClC-3 in pipette solution: ~5 min
-60 mV
200 pA
200 ms
B
ClC-3 in pipette solution: ~10 min
-60 mV
200 pA
200 ms
C
~5 min
~10 min
V (mV)
-60
-20
40
60
400
200
-400
I (pA)
D
~5 min
~10 min
V (mV)
-20
0
20
40
60
80
40
Q (pC)

Figure 3.12 Blocking vesicle docking with Tetanus toxin did not modulate $I_{Cl(Ca)}$. Adding Tetanus toxin (TeTox 4 μM; n=5) to the recording pipette solution did not alter $I_{Cl(Ca)}$. (**A**) Current traces in response to the standard depolarizing protocol are similar ~5 min and (**B**) ~10 min post-rupture. (**C**) Constructed *I-V* (leak-subtracted) and (**D**) Ca^{2+}-activated Cl^- *Q-V* (offset-subtracted) relations from the same cell in the presence of Tetanus toxin show no significant changes ~5 min (black circles) vs. ~10 min (white circles) following rupture of the whole-cell patch.

Figure 3.12

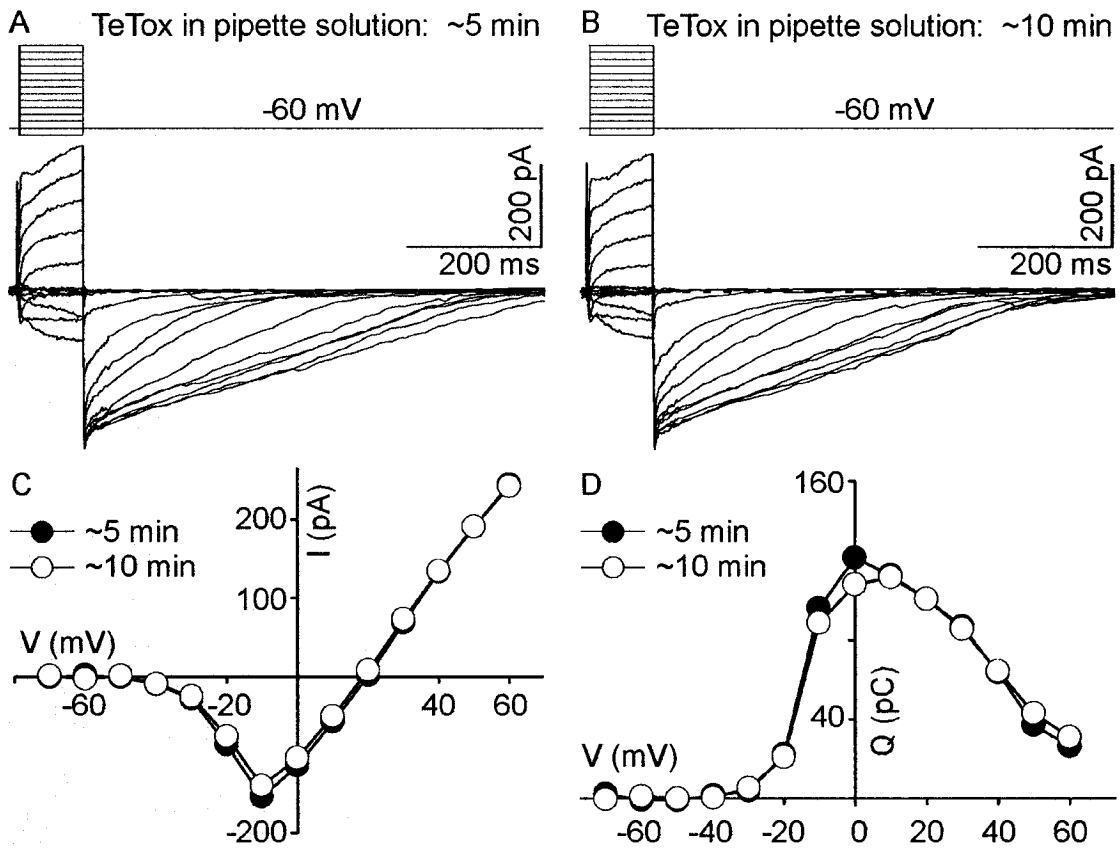
A
TeTox in pipette solution: ~5 min
-60 mV
200 pA
200 ms
B
TeTox in pipette solution: ~10 min
-60 mV
200 pA
200 ms
C
~5 min
~10 min
I (pA)
200
100
V (mV)
-60
-20
40
60
-200
D
~5 min
~10 min
160
Q (pC)
40
V (mV)
-60
-40
-20
0
20
40
60

measured during repolarization following those steps. Figures 3.12A and B show similar current traces obtained ~5 min vs. ~10 min following rupture of the whole-cell patch in the presence of 4 μM tetanus toxin. The constructed *I-V* and Ca^{2+}-activated *Q-V* relations from this cell is shown in Figure 3.12C and D, respectively. The Ca^{2+}-activated Cl^- tail current integral, measured up to 20 min after membrane rupture was also unchanged (mean charge remaining of 106 ± 8%; n=5). This suggests that the $I_{Cl(Ca)}$ conductance is not generated by a Cl channel localized to the synaptic vesicle membrane.

3.9 Summary

To summarize, Ca^{2+}-activated Cl^- currents ($I_{Cl(Ca)}$) are elicited by depolarizing steps known to open voltage-gated Ca channels in cone photoreceptors. The decaying Ca^{2+}-activated Cl^- tail currents exhibit several features characteristic of a saturated exponential, namely, adherence to a single exponential function when the amplitude is low and deviance from that exponential when the amplitude is high. The saturated exponential function fit suggests that Ca^{2+}-activated Cl^- tail currents are saturated by Ca^{2+} ions at the submembrane level and deactivate as the submembrane $[Ca^{2+}]_i$ level decreases due to Ca^{2+} buffering and one-dimensional diffusion from the plasma membrane. Increasing free $[Ca^{2+}]_i$ is likely to activate more Cl(Ca) channels, and contribute to larger $I_{Cl(Ca)}$, provided there are available Cl(Ca) channels to be activated. Salamander cone photoreceptors $I_{Cl(Ca)}$ were larger in amplitude and deactivated at a slower rate when dialyzed with a weak buffered pipette solution.

Sustained Cl(Ca) channel activation could be achieved following the superfusion of the Ca^{2+} ionophore ionomycin, but not with calcimycin, which had no effect on $I_{Cl(Ca)}$.

Ionomycin elicited a conductance characterized by an *I-V* relation displaying outward rectification. A similar *I-V* relation was elicited with a repeated strong depolarization protocol that included a 0 mV prepulse. Therefore, this protocol presumably increased intracellular Ca^{2+} levels and allowed persistent activation of Cl(Ca) channels, thereby demonstrating a characteristic outward rectification of the channel.

The dependence of $I_{Cl(Ca)}$ on submembrane $[Ca^{2+}]_i$ can be readily demonstrated by replacing Ca^{2+} ions with Ba^{2+} in the extracellular solution. Ba^{2+} is commonly used as a charge carrier through voltage-gated Ca channels. It increased the Ca channel conductance but inhibited $I_{Cl(Ca)}$. The present data are consistent with results obtained from a number of studies, which have reported that Ba^{2+} is ineffective in inducing Ca^{2+}-activated Cl^- tail currents in neurons (Owen et al., 1986; Bader et al., 1987; Korn and Weight, 1987; Johansen and Kleinhaus, 1988; Maricq and Korenbrot, 1988; Rogawski et al., 1988; Akasu et al., 1990; McBride and Roper, 1991; Taylor and Roper, 1994; Okada et al., 1995; Taylor and Morgans, 1998). While it is likely that Ba^{2+} ions do not activate Cl(Ca) channels, other explanations may account for the inhibited Ca^{2+}-activated Cl^- tail current. Ba^{2+} ions could be activating Cl(Ca) channels, but the diffusion of Ba^{2+} from the submembrane area may be faster than that of Ca^{2+}, which may account for the lack of tail currents. Further evidence suggesting activation of $I_{Cl(Ca)}$ by submembrane $[Ca^{2+}]_i$ comes from experiments using the L-type Ca channel agonist BayK, where an increase in $I_{Cl(Ca)}$ was observed. These results suggest that Cl(Ca) channels in salamander cone photoreceptors may be co-localized with voltage-gated Ca channels at the plasma membrane.

Salamander cone $I_{Cl(Ca)}$ was inhibited by the Cl channel blocker NPPB. In addition to blocking Cl(Ca) channels, a modest voltage-gated Ca channel current inhibition was also observed. Finding a selective Cl(Ca) channel blocker that will discriminate between $I_{Cl(Ca)}$ and I_{Ca} is essential to evaluate the role of $I_{Cl(Ca)}$ in neurons. In light of the unexpected inhibition of Ca channel current by NPPB, the present study suggests that the effect of NPPB on $I_{Cl(Ca)}$, should be carefully interpreted.

The molecular identity of Cl(Ca) channels in cone photoreceptors is unknown. Although $[Ca^{2+}]_i$ is required for $I_{Cl(Ca)}$ to be elicited, the mechanism by which Ca^{2+} ions are responsible for the activation of Cl(Ca) channels is also unknown. The $[Ca^{2+}]_i$ buffering mechanisms in neurons include a variety of Ca^{2+}-binding proteins, such as calmodulin. Calmodulin and calmodulin antagonists, calmidazolium and trifluoperazine, did not modulate $I_{Cl(Ca)}$ in cones, suggesting that these molecules may not play a role in $I_{Cl(Ca)}$ activation. Cl(Ca) channels may possibly be directly gated by Ca^{2+} ions, but interactions from other Ca^{2+}-binding proteins or Ca^{2+} regulated protein kinases may be involved. The present study also investigated the possibility that $I_{Cl(Ca)}$ is generated by a Cl channel located in synaptic vesicular membranes. Anti-ClC-3 and Tetanus toxin were used to confirm that $I_{Cl(Ca)}$ is not elicited by a Cl channel (i.e. ClC-3) located in the synaptic vesicular membrane that integrates with the plasma membrane following Ca^{2+} entry.

Chapter 4

Role of Ca^{2+} Released from Ca^{2+} Stores in Gating Salamander Cone Photoreceptor Cl(Ca) Channels

Parts of this chapter have been previously published in the following publications:

Lalonde MR, Barnes S. 2003. Contribution of Calcium Stores to Activation of Chloride Current in Cone Photoreceptors. Society for Neuroscience, E-Abstract 791.18.

Lalonde MR, Barnes S. 2004. Inhibition of Cl(Ca) Channels in Response to High Intracellular Calcium Levels Due to Dephosphorylation-Mediated Ca channel Inhibition in Cone Photoreceptors. Society for Neuroscience, E-Abstract 65.12.

Parts of this chapter are submitted to be in the following publication:

Lalonde MR, Barnes S. 2004. Contribution of Calcium Stores to Activation of Calcium-Activated Chloride Currents in Cone Photoreceptors. European Journal of Neuroscience.

The results from the previous chapter suggest that Ca^{2+} entry through voltage-gated Ca channels activates $I_{Cl(Ca)}$ in salamander cone photoreceptors. Depolarization-evoked Ca^{2+} influx likely increases submembrane Ca^{2+} microdomains to activate Cl(Ca) channels. The present chapter investigates if Ca^{2+} stores also contribute to $I_{Cl(Ca)}$ activation. In cone photoreceptors, $[Ca^{2+}]_i$ is regulated via release and sequestration from Ca^{2+} stores, which are located mainly in the endoplasmic reticulum (ER). Whereas Ca^{2+} is mainly extruded from the cone inner segment via plasma membrane Ca^{2+}-ATPases (PMCAs), sequestration into ER Ca^{2+} stores is achieved via the sarcoplasmic/ endoplasmic reticulum Ca^{2+}-ATPase (SERCA) pumps. Two different intracellular Ca^{2+} store release-channels exist: IP_3- and Ry-gated channels. The contribution of Ca^{2+} stores to $I_{Cl(Ca)}$ activation was investigated by blocking Ca^{2+}-reuptake via SERCA pumps and by testing IP_3R and RyR-modulating agents. The effect of the PMCA blocking agent, lanthanum, on $I_{Cl(Ca)}$ was also tested. Finally, the effect of repetitive depolarizing pulses, a protocol previously suggested to cause localized accumulation of Ca^{2+} at the photoreceptor terminal (Barnes and Hille, 1989), was investigated in control conditions and in the presence of the RyR agonist, caffeine.

4.1 Blocking Ca^{2+}-reuptake mechanisms into Ca^{2+} stores does not modulate $I_{Cl(Ca)}$

SERCA pumps are responsible for Ca^{2+}-reuptake within intracellular Ca^{2+} stores (see review by MacLennan et al., 1997). A dynamic state that balances Ca^{2+}-reuptake via the SERCA pumps and constant passive Ca^{2+} leak from intracellular Ca^{2+} stores exists ('pump-leak' concept). Although the mechanism responsible for the Ca^{2+} leak from intracellular Ca^{2+} stores is still unknown, SERCAs must continuously pump Ca^{2+} to

oppose this Ca^{2+} permeability at the ER membrane. Cyclopiazonic acid and thapsigargin are two of the most commonly used compounds that have inhibitory actions on SERCA pumps in part due to their high membrane permeability and efficient cell penetration (Inesi and Sagara, 1992). Cyclopiazonic acid and thapsigargin-sensitive SERCA pumps have been shown to be located at Ca^{2+} store compartments, including IP_3-sensitive Ca^{2+} stores, of both muscle cells and neurons (Verma et al., 1990; Bian et al., 1991). By inhibiting SERCA pumps, these two structurally unrelated compounds have been demonstrated to increase Ca^{2+} concentration levels within cells, including rod photoreceptors (Krizaj et al., 2003).

Cyclopiazonic acid, a mycotoxin produced by certain species of the common fungal genera *Aspergillus* and *Penicillium*, was used in the present study to investigate the extent to which Ca^{2+} stores participate in $I_{Cl(Ca)}$ activation. Cyclopiazonic acid is an inhibitor of the Ca^{2+}-activated ATPase activity of the Ca^{2+} pump (Goeger and Riley, 1989). The specific mechanism of action of this compound appears to be a reversible competitive inhibition of ATP binding to the SERCA pumps (Seidler et al., 1989). SERCA pump inhibition by cyclopiazonic acid seems to be specific as no inhibition of the Na^+/K^+-ATPase, H^+/K^+-ATPase, mitochondrial ATPase or PMCAs have been reported (Seidler et al., 1989). However, the passive Ca^{2+} efflux from the ER has also been reported to be inhibited by this compound (Missiaen et al., 1992). Complete inhibition of ER SERCAs can be achieved with 1-2 μM cyclopiazonic acid (half-maximal inhibitory concentration (IC_{50}) is ~300-500 nM). In the present study, 5 μM cyclopiazonic acid failed to modify the amplitude and kinetics of Ca^{2+}-activated Cl^- tail currents in all cone photoreceptors tested (n=4). In the presence of cyclopiazonic acid

(~4 min superfusion), the peak current remaining was 107 ± 16% (n=4), measured during depolarizing voltage steps, and 99 ± 3% (n=4), measured during repolarization following those steps. A representative example of the time course of current remaining (Fig. 4.1A) and current traces (Fig. 4.1B) from the same cone demonstrate unmodified $I_{Cl(Ca)}$ in the presence of cyclopiazonic acid.

Thapsigargin, a sesquiterpene lactone extract isolated from the umbelliferous plant, *Thapsia garganica*, was also used to investigate the contribution of Ca^{2+} stores to $I_{Cl(Ca)}$ activation. Thapsigargin has no detectable action on any other ion-motive ATPase, including PMCAs. It offers specific and potent inhibition by tightly interacting with the ER SERCA, yielding a 1:1 stoichiometric complex referred to as a 'dead end complex' (Thastrup et al., 1990; Sagara et al., 1992). This irreversible interaction is thought to cause the global disruption of the SERCA structure and activity by specifically stabilizing the enzyme in the E2 state, a structural conformation characterized by a greatly diminished Ca^{2+} sensitivity (Wictome et al., 1992). The recognition site at which thapsigargin interacts is unknown. However, in addition to inhibiting steady state enzyme activity, thapsigargin has been shown to inhibit Ca^{2+} binding and phosphorylation (two individual partial reactions of the ATPase cycle), which occur at domains relatively distant from each other in the protein structure (Inesi and Sagara, 1992). This indicates that the perturbation caused by the binding of this compound involves the entire enzyme. Thapsigargin has the highest potency of all known SERCA inhibitors, blocking these pumps with an IC_{50} of 10-20 nM (Lytton et al., 1991). A concentration as low as 100 nM is usually sufficient to completely inhibit the ER SERCA

Figure 4.1 Inhibiting Ca^{2+}-reuptake into Ca^{2+} stores via SERCA pump blockade using cyclopiazonic acid and thapsigargin did not modulate $I_{Cl(Ca)}$. Cone photoreceptor whole-cell currents were elicited with -20 mV pulses from a holding potential of -60 mV in control conditions and during superfusion of cyclopiazonic acid (5 μM; n=4) and thapsigargin (1 μM; n=7). (**A**) Representative example of the time course of current remaining (expressed as a percentage of control), showing that cyclopiazonic acid (CPA; indicated by the horizontal bar) had no effect on the current measured during depolarizing voltage steps (Steps; black circles) and associated Ca^{2+}-activated Cl^- tails (Tails; white circles). (**B**) Current traces from the same cone recorded in control conditions (Control; solid line) and in the presence of cyclopiazonic acid (CPA; dotted line) are similar. (**C**) Representative example of the time course of current remaining (expressed as a percentage of control) measured during steps to -20 mV (Steps; black circles) and during repolarization following those steps (Tails; white circles), recorded at -60 mV. No significant changes were observed in the presence of thapsigargin (TG; indicated by the horizontal bar). (**D**) Current traces from the same cone in control conditions (Control; solid line) and in the presence of thapsigargin (TG; dotted line) are similar.

Figure 4.1

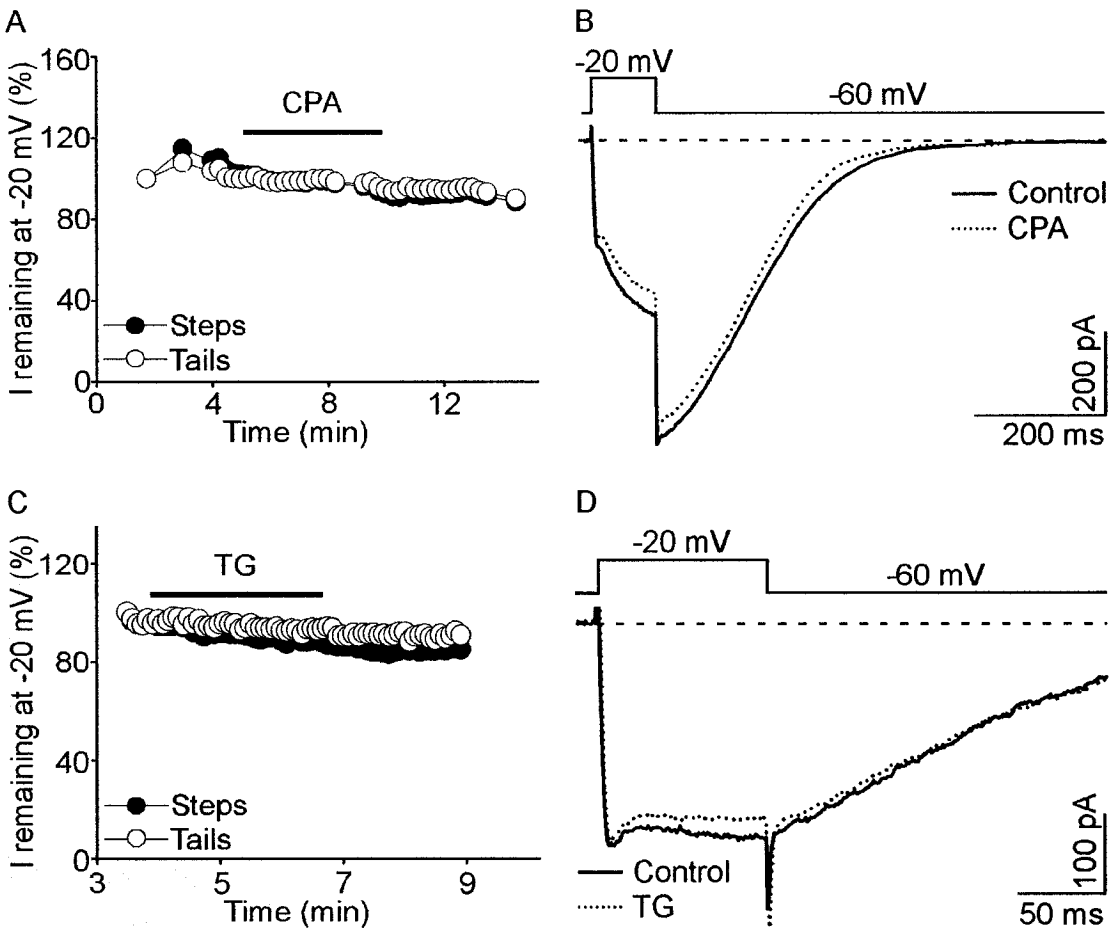
A
I remaining at -20 mV (%)
160
120
80
40
0
CPA
Steps
Tails
0
4
8
12
Time (min)
B
-20 mV
-60 mV
Control
CPA
200 pA
200 ms
C
I remaining at -20 mV (%)
120
80
40
0
TG
Steps
Tails
3
5
7
9
Time (min)
D
-20 mV
-60 mV
Control
TG
100 pA
50 ms

pumps; however, 1 μM is frequently used to ensure maximal Ca^{2+}-reuptake inhibition. Similar to cyclopiazonic acid, inhibiting Ca^{2+}-reuptake into stores using thapsigargin (1 μM) did not modulate $I_{Cl(Ca)}$ in any of the cone photoreceptor tested (n=7). A representative example from a cone photoreceptor demonstrates that thapsigargin does not produce any significant change in the time course of current remaining (Fig. 4.1C) and current traces (Fig. 4.1D). In the presence of thapsigargin (~4 min of superfusion), the peak current remaining was 93 ± 3% (n=7), measured during depolarizing voltage steps, and 100 ± 3% (n=7), measured during repolarization following those steps. These results suggest that inhibiting Ca^{2+}-reuptake into Ca^{2+}-stores does not contribute to an increase in submembrane Ca^{2+} levels in isolated salamander cone photoreceptors. Effective pathways for the clearance of high $[Ca^{2+}]_i$ when SERCAs are blocked may exist in these cells. These findings therefore do not support a role for stores in Cl(Ca) channel gating and instead are consistent with a closer link between Cl(Ca) channels and voltage-gated Ca channels at the plasma membrane.

4.2 IP_3-sensitive Ca^{2+} stores do not generally contribute to Cl(Ca) channel activation

Endogenous IP_3, produced by the activation of phospholipase C (PLC), acts at IP_3 receptors to release Ca^{2+} from intracellular stores. Peng et al. (1991) have demonstrated localization of the IP_3 receptor (IP_3R) exclusively at synaptic terminals of cone photoreceptor of vertebrates, including salamander. Stella et al. (2003) have also suggested the localization of IP_3Rs within terminals of photoreceptors and bipolar cells, specifically at ribbon synapses in the mammalian retina. In the present study, $I_{Cl(Ca)}$ in cone photoreceptors was generally (five out of six recordings) unmodified by IP_3 (100

μM) introduced in the recording pipette solution (Fig. 4.2). Only one recording from a cone photoreceptor showed significant modulation in the presence of IP_3 (see Appendix 2). Recordings obtained in response to the standard depolarizing protocol, taken ~5 min following rupture of the whole-cell patch to ensure thorough diffusion of IP_3 in the pipette solution, were compared to recordings obtained ~15 min (up to ~28 min) post-rupture (Fig. 4.2). The peak current remaining measured during depolarizing voltage steps was 95 ± 4% (n=5); whereas the peak Ca^{2+}-activated Cl^- tail current was 107 ± 8% (n=5). Current recorded immediately after and up to 5 min following rupture of the whole-cell patch in the presence of IP_3 in the pipette solution also did not differ from control recordings (when IP_3 was omitted from the pipette solution; data not shown; n=4). Figures 4.2A and B demonstrate a representative family of current records in the presence of IP_3 at ~5 min and ~15 min following rupture. Leak-corrected *I-V* (Fig. 4.2C) and Ca^{2+}-activated *Q-V* relations (Fig. 4.2D) from the same isolated cone photoreceptor are of normal appearance.

Ca^{2+}-activated Cl^- conductances have been evoked by IP_3 in guinea-pig isolated hepatocytes (Ogden et al., 1990). However, the use of IP_3 to release Ca^{2+} from stores has generally been unsuccessful even at high (100 μM) intracellular concentrations (Currie et al., 1992). Several possibilities may account for the lack of change in $I_{Cl(Ca)}$. A possible explanation is that only modest Ca^{2+} release arises from IP_3-sensitive Ca^{2+} stores. For example, IP_3-sensitive stores have been found to release as little as 110 nM Ca^{2+} in DRG neurons, as directly assessed using the Ca^{2+}-sensitive dye fura-2 (Thayer et al., 1988a). In addition, a low responsiveness to IP_3 was also shown in cerebellar Purkinje neurons, hippocampal neurons, and striatal neurons (Khodakhah and Ogden, 1993). Another

Figure 4.2 $I_{Cl(Ca)}$ was insensitive to Ca^{2+}-release from IP_3-sensitive Ca^{2+} stores (n=5). (**A**) A family of current traces ~5 min and (**B**) ~15 min following rupture of the whole-cell patch in the presence of 100 μM IP_3 added in the recording pipette solution. Current traces elicited with the standard depolarizing protocol are similar. (**C**) Leak-subtracted *I-V* and (**D**) offset-subtracted Ca^{2+}-activated *Q-V* relations from the same cone ~5 min (black circles) and ~15 min (white circles) post-rupture, demonstrating that IP_3 did not modulate $I_{Cl(Ca)}$.

Figure 4.2

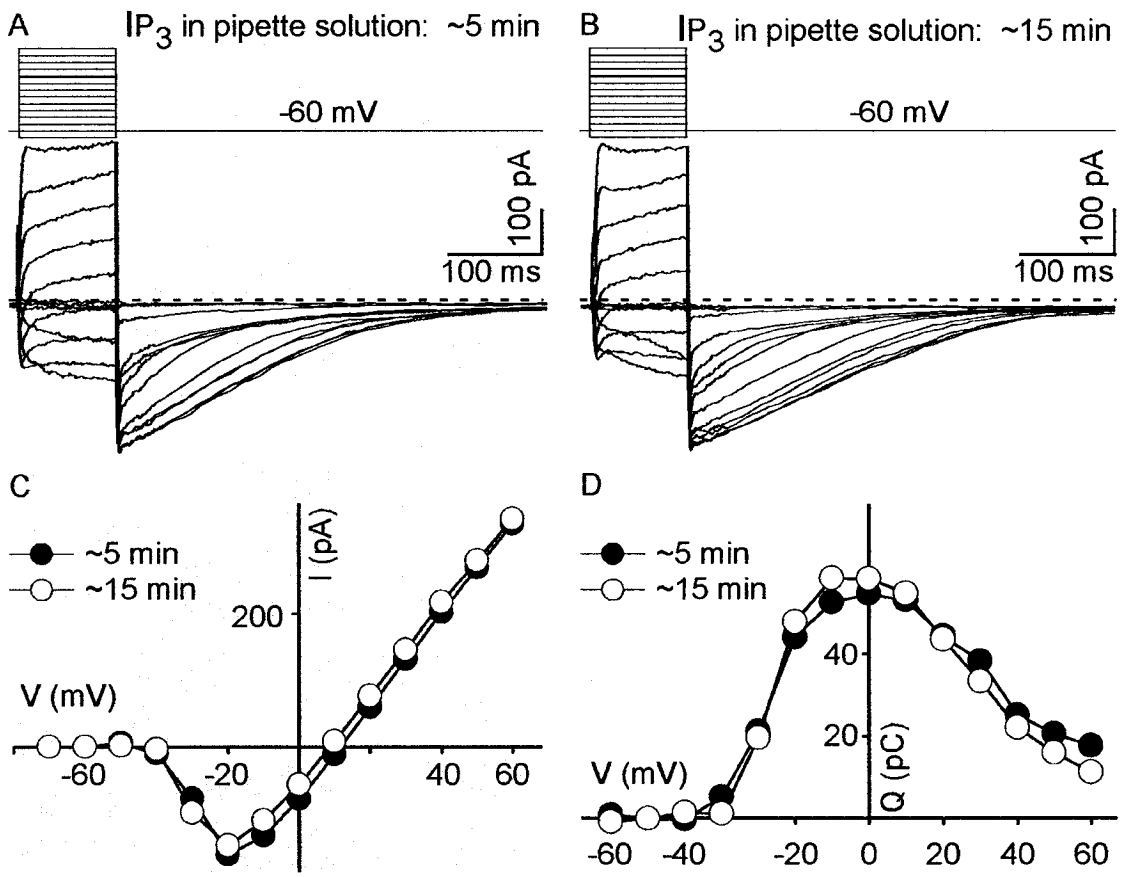
A
IP3 in pipette solution: ~5 min
-60 mV
100 pA
100 ms
B
IP3 in pipette solution: ~15 min
-60 mV
100 pA
100 ms
C
~5 min
~15 min
I (pA)
200
V (mV)
-60
-20
40
60
D
~5 min
~15 min
40
20
Q (pC)
V (mV)
-60
-40
-20
0
20
40
60

possible explanation for unchanged $I_{Cl(Ca)}$ in the presence of IP_3 is that the IP_3-sensitive Ca^{2+} stores are spatially distant from Cl(Ca) channels at the membrane. Although IP_3Rs have been shown to be located at synaptic terminal regions, the ER of salamander cones is mainly localized at the subellipsoid region; and therefore, Ca^{2+} release from IP_3-sensitive stores may not contribute to submembrane $[Ca^{2+}]_i$ levels. It seems likely that Cl(Ca) channels are unaffected by the Ca^{2+} released from the stores due to their distance from the site of release coupled with rapid Ca^{2+} buffering, extrusion via PMCAs and/or sequestration. Other explanations, such as insufficient amount of Ca^{2+} stored, could also explain the lack of $I_{Cl(Ca)}$ modulation with IP_3.

4.3 Ryanodine-sensitive Ca^{2+} stores do not contribute to $I_{Cl(Ca)}$ activation

The second family of intracellular Ca^{2+}-release channels, the ryanodine receptors (RyRs), is associated with Ca^{2+}-induced Ca^{2+}-release (CICR) in neurons. Depending on its concentration, the plant alkaloid ryanodine has differential effects when binding to its putative target located in the ER membrane. Whereas low concentrations activate Ca^{2+} release from ryanodine-sensitive Ca^{2+} stores by locking the channel in a low conductance opened state (Sutko et al., 1985; Smith et al., 1988), high ryanodine concentrations (10 μM) inhibit channel opening (Lattanzio et al., 1987; Hille, 2001). The increase in $[Ca^{2+}]_i$, following depolarization-evoked Ca^{2+} influx may stimulate CICR from ryanodine-sensitive stores. In order to investigate if ryanodine-sensitive Ca^{2+} stores were continuously contributing to $I_{Cl(Ca)}$ activation, 10 μM ryanodine, a concentration commonly used to block Ca^{2+} release from ryanodine-sensitive Ca^{2+} stores (Ivanenko et

al., 1993; Alonso et al., 1999; Collier et al., 2000), was added to the standard bath solution to block CICR.

Ryanodine-sensitive intracellular Ca^{2+} release channels are also putative targets for modulation by caffeine. The present study investigated the effect of caffeine on $I_{Cl(Ca)}$ in cones to see if Ca^{2+} released from ryanodine-sensitive Ca^{2+} stores contributes to submembrane $[Ca^{2+}]_i$. Caffeine potentiates CICR by reducing the threshold for Ca^{2+}-induced activation of the ryanodine receptor. Unlike Ca^{2+} release from IP_3-sensitive stores, caffeine-induced Ca^{2+} transients have been observed in a variety of neuronal preparations (Lipscombe et al., 1988; Brorson et al., 1991; Marrion and Adams, 1992; Mironov et al., 1993). The activation of $I_{Cl(Ca)}$ by caffeine has been demonstrated in rat dorsal root ganglia (Currie and Scott, 1992). In addition, an increase in $I_{Cl(Ca)}$ seen in the presence of caffeine in avian sensory neurons was shown to be blocked by ryanodine (Ivanenko et al., 1993).

4.3.1 The source of Ca^{2+} for $I_{Cl(Ca)}$ activation during depolarization is not ryanodine-sensitive

Although the presence of ryanodine receptors in photoreceptor inner segments and synaptic terminals has recently been identified via immunofluorescence (Krizaj et al., 2003), ryanodine did not modify $I_{Cl(Ca)}$ in cone photoreceptors under the conditions used in this study (Fig. 4.3). In the presence of ryanodine, a reduction of depolarization-activated $I_{Cl(Ca)}$ would be expected if increased $[Ca^{2+}]_i$, following Ca^{2+} influx via voltage-gated Ca channels, was amplified by Ca^{2+}-induced Ca^{2+}-release. Following the application of ryanodine, the average remaining peak current was 109 ± 6% (n=7),

Figure 4.3 CICR from ryanodine-sensitive stores does not contribute to depolarization-evoked $I_{Cl(Ca)}$ activation since ryanodine (Ry; 10 μM; n=7) had little effect on $I_{Cl(Ca)}$. **(A)** Current traces from a cone photoreceptor in response to a 0 mV depolarizing voltage step from a holding potential of -60 mV in the presence of ryanodine (Ry; dotted line) were similar to those of control recordings (Control; solid line). **(B)** Leak-subtracted *I-V* and **(C)** offset-subtracted Ca^{2+}-activated Cl^- *Q-V* relations from the same cone were unchanged during ryanodine superfusion (Control: black circles; Ry: white circles). **(D)** Summary of the average peak current remaining measured during depolarizing voltage steps and during repolarization following those steps. Differences between peak current recorded in control conditions and in the presence of ryanodine were non-significant.

Figure 4.3

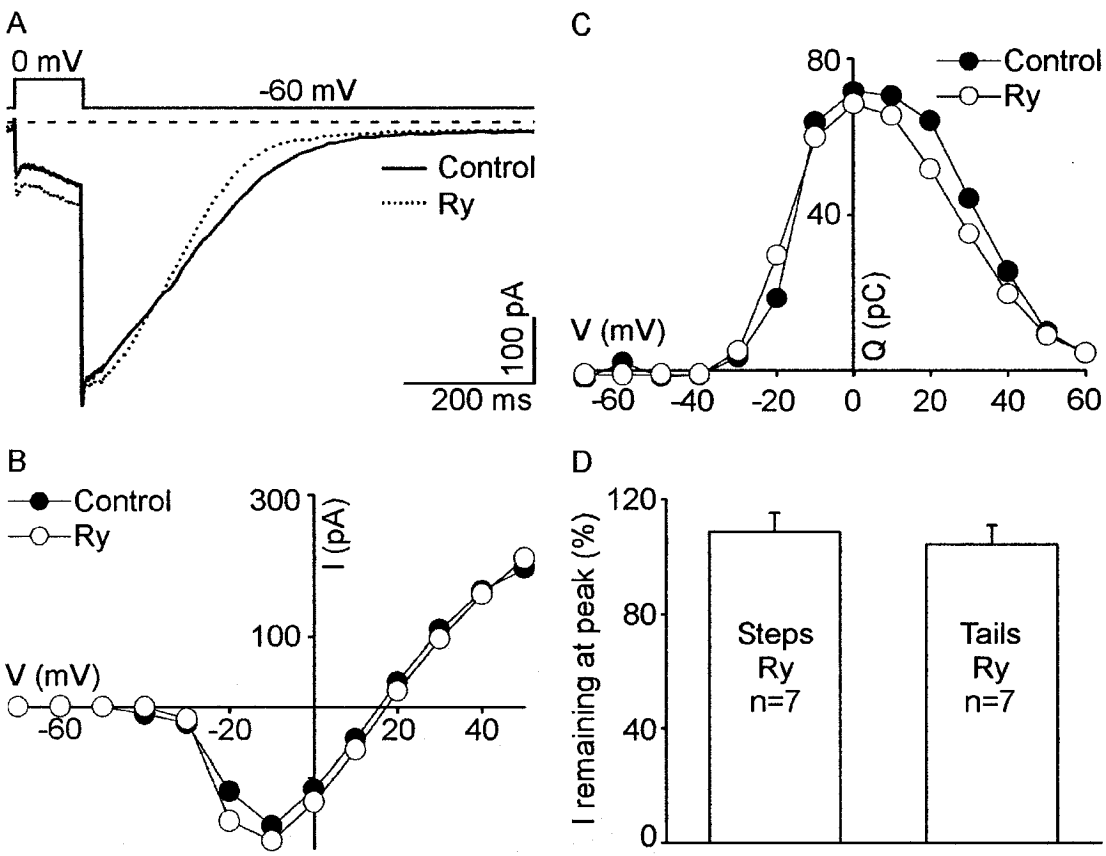
A
0 mV
-60 mV
Control
Ry
100 pA
200 ms
B
Control
Ry
300
I (pA)
100
V (mV)
-60
-20
20
40
C
80
Control
Ry
40
V (mV)
Q (pC)
-60
-40
-20
0
20
40
60
D
120
80
40
0
I remaining at peak (%)
Steps
Ry
n=7
Tails
Ry
n=7

measured during depolarizing voltage steps, and 104 ± 7% (n=7), measured during repolarization following those steps (Fig. 4.3D). Figure 4.3A shows a representative example of current records elicited by a 0 mV voltage-clamp step from a holding potential of -60 mV, demonstrating unchanged $I_{Cl(Ca)}$ in the presence of ryanodine. The leak-corrected *I-V* relation (Fig. 4.3B), and Ca^{2+}-activated Cl^- *Q-V* relations (Fig. 4.3C) from the same cone photoreceptors are the same before and during ryanodine application. These results suggest that ryanodine does not have any direct action on Cl(Ca) channels, and demonstrate that ryanodine-sensitive stores do not constitutively contribute to the activation of Ca^{2+}-activated Cl^- tail currents in cone photoreceptors. Similar to the results obtained from the present study, the amplitude of Ca^{2+}-activated Cl^- tail currents were not attenuated by ryanodine in avian sensory neurons (Ivanenko et al., 1993). The magnitude of depolarization-evoked $I_{Cl(Ca)}$ in isolated salamander cone photoreceptors was not affected by ryanodine, implying that the Ca^{2+} that activates Cl(Ca) channels in this protocol is supplied by the Ca^{2+} current through voltage-gated Ca channels without amplification by a ryanodine-sensitive mechanism, such as CICR. These results are therefore consistent with the idea that Ca^{2+} release from ryanodine-sensitive stores do not contribute to submembrane $[Ca^{2+}]_i$ levels. However, other explanations, such as unfilled Ca^{2+} stores, cannot be ruled out.

4.3.2 Caffeine has no effect on $I_{Cl(Ca)}$ elicited by the standard depolarizing protocol

Caffeine has a low potency and must be used at millimolar concentrations. At 1 mM, caffeine had no effect on the fast $I_{Cl(Ca)}$ kinetics in cone photoreceptors, even in the

Figure 4.4 Superfusion of caffeine (1 mM; n=4, 10 mM; n=5) does not modulate $I_{Cl(Ca)}$, suggesting that Ca^{2+} release from caffeine-sensitive Ca^{2+} stores does not contribute to Cl(Ca) channel activation in cone photoreceptors. (**A**) Current traces elicited by a -10 mV depolarizing voltage step from a holding potential of -60 mV in control conditions (Control; solid line) and in the presence of 1 mM caffeine (CAF; dotted line) are similar. (**B**) Leak-subtracted *I-V* and (**C**) offset-subtracted Ca^{2+}-activated Cl^- *Q-V* relations from the same cone before (Control; black circles) and during caffeine superfusion (CAF; white circles), showing no change in current. (**D**) Summary of the peak current remaining (expressed as a percentage of control) measured during depolarizing voltage steps (Steps; grey bars) and during repolarization following those steps (Tails; black bars) in the presence of both 1 mM and 10 mM caffeine. No significant differences between recordings in control conditions and in the presence of caffeine were observed. Intracellular solution was prepared with a low buffering system (0.1 mM $CaCl_2$ and 0.001 mM BAPTA).

Figure 4.4

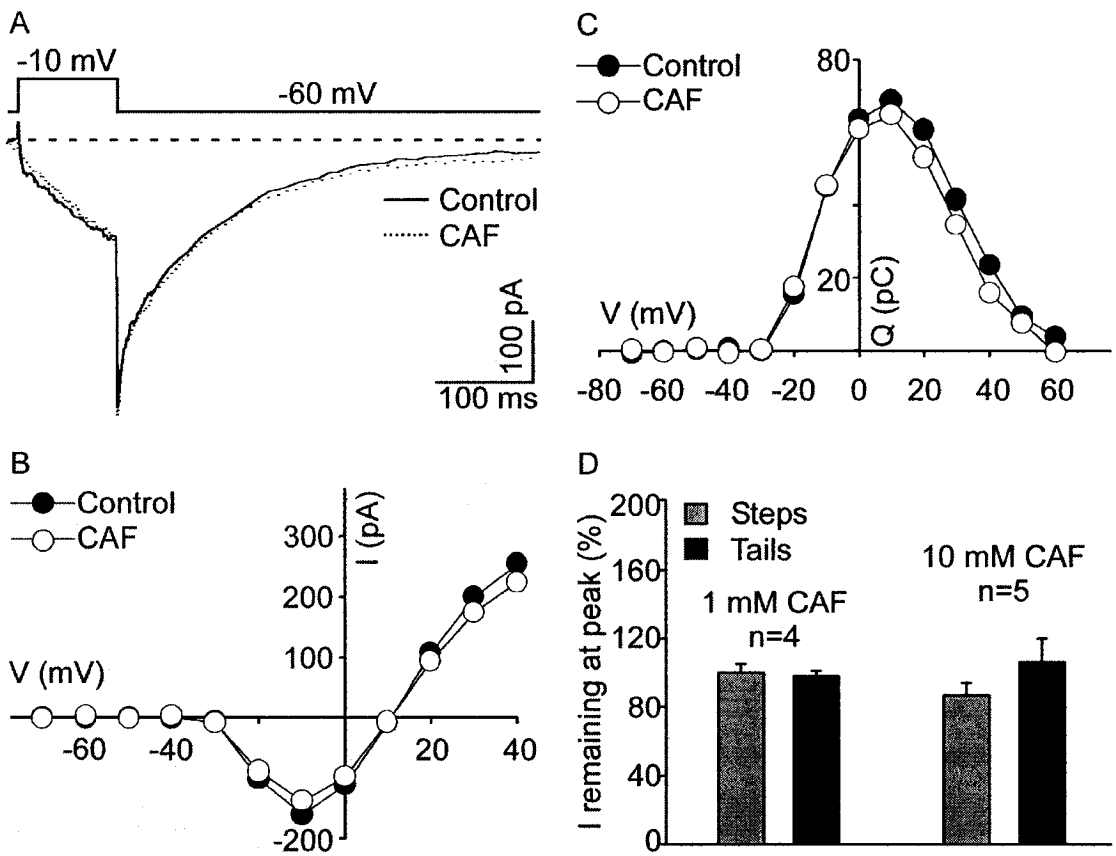
A
-10 mV
-60 mV
Control
CAF
100 pA
100 ms
B
Control
CAF
V (mV)
-60
-40
20
40
300
200
100
-200
I (pA)
C
Control
CAF
80
20
Q (pC)
V (mV)
-80 -60 -40 -20 0 20 40 60
D
Steps
Tails
1 mM CAF
n=4
10 mM CAF
n=5
I remaining at peak (%)
200
160
120
80
40
0

presence of a low-capacity buffering system (1 μM BAPTA and 0.1 mM $CaCl_2$) (Fig. 4.4). These results therefore suggest that caffeine-sensitive Ca^{2+} stores do not contribute to submembrane Ca^{2+} levels. In the presence of 1 mM caffeine, the mean peak current remaining measured during depolarizing steps was 100 ± 5% (n=4), and during Ca^{2+}-activated Cl^- tails was 98 ± 3% (n=4). The effect of caffeine-sensitive stores on $I_{Cl(Ca)}$ was also tested using 10 mM caffeine. At this high caffeine concentration, $I_{Cl(Ca)}$ also remained unchanged. The average peak current remaining was 87 ± 7% (n=5), measured at depolarizing voltage steps, and 106 ± 14% (n=5), measured during repolarization following those steps (Fig. 4.4D). This again raises the possibility that Ca^{2+} release from stores does not contribute to submembrane Ca^{2+} levels, which is known to activate $I_{Cl(Ca)}$. Although the amount of Ca^{2+} held in caffeine-sensitive stores is unknown, the physical separation between Ca^{2+} stores in the ER and Cl(Ca) channels at the plasma membrane may be the basis for the lack of $I_{Cl(Ca)}$ modulation. This negative finding is consistent with a model where Cl(Ca) channels are co-localized with high voltage-activated Ca channels at the plasma membrane, away from Ca^{2+} stores. Previous studies have reported that caffeine activates ryanodine sensitive Ca^{2+}-release channels in salamander rod but not cone photoreceptors (Krizaj et al., 1999; Krizaj et al., 2003). Krizaj et al. (2003) concluded that the release of Ca^{2+} from caffeine-sensitive Ca^{2+} stores in cone photoreceptors was masked by the highly active PMCAs that are responsible for Ca^{2+} extrusion at the inner segments.

4.4 Inhibition of $I_{Cl(Ca)}$ by lanthanum (La^{3+})

Lanthanum (La^{3+}) is a high-affinity inhibitor of the plasma membrane Ca^{2+}-ATPase (PMCA) transport system in a variety of cells. This inorganic compound is thought to effectively inhibit PMCAs by hindering the conformational change of the enzyme following phosphorylation (Herscher and Rega, 1996). Extrusion of released Ca^{2+} by PMCAs has been proposed to be relatively rapid in cone photoreceptors, so fast in fact that it masks caffeine-induced Ca^{2+} release from Ca^{2+} stores (Krizaj and Copenhagen, 1998; Krizaj et al., 2003). Caffeine-sensitive stores in cone photoreceptor inner segments do produce increases in $[Ca^{2+}]_i$ when PMCA-dependent Ca^{2+} extrusion is blocked with La^{3+} (Krizaj et al., 2003). In spite of the evidence that La^{3+} increases $[Ca^{2+}]_i$ in cones, in the present study, inhibiting Ca^{2+} extrusion via the PMCAs with La^{3+} did not produce an increase in $I_{Cl(Ca)}$. Although an increase in $[Ca^{2+}]_i$ in the presence of La^{3+} cannot be ruled out (see Krizaj and Copenhagen, 1998), Ca^{2+} levels within submembrane microdomains sufficient to activate Cl(Ca) channels were not achieved. In contrast, the results are more consistent with a reduction in submembrane $[Ca^{2+}]_i$ with the application of La^{3+} in cone photoreceptors because $I_{Cl(Ca)}$ was irreversibly abolished in all cells tested (n=5; Fig. 4.5). La^{3+} significantly ($P<0.01$) inhibited the current induced at a test potential of -20 mV by 98 ± 2% (n=5) and the corresponding Ca^{2+}-activated Cl^- tails by 96 ± 3% (n=5). La^{3+} is also known to block voltage-gated Ca channels. In the present study, La^{3+} produced the complete inhibition of $I_{Cl(Ca)}$ in a similar fashion to the effect of the widely used voltage-gated Ca channel blocker Cd^{2+} (data not shown; also see Barnes and Hille, 1989). In isolated salamander cone photoreceptors, the rapid inhibition of I_{Ca}

Figure 4.5 The PMCA and Ca channel antagonist, lanthanum (La^{3+}; 1 mM; n=5), inhibits $I_{Cl(Ca)}$ without immediate recovery. (**A**) Time course of current remaining (expressed as a percentage of control) measured during depolarizing voltage steps to -20 mV (Steps; black circles) and associated Ca^{2+}-activated Cl^- tails (Tails; white circles), recorded at -60 mV. Fast and irreversible inhibition was observed in the presence of La^{3+}, which was added to the standard bath solution. (**B**) Leak-subtracted current traces from the same cone (*1*) before, (*2*) during inhibition, and (*3*) after complete La^{3+}-induced inhibition of the current. (**C**) *I-V* relations (not leak-subtracted) from the same cone measured during depolarizing voltage steps before (Control; black circles) and after La^{3+}-induced inhibition of the current (La^{3+}; white circles).

Figure 4.5

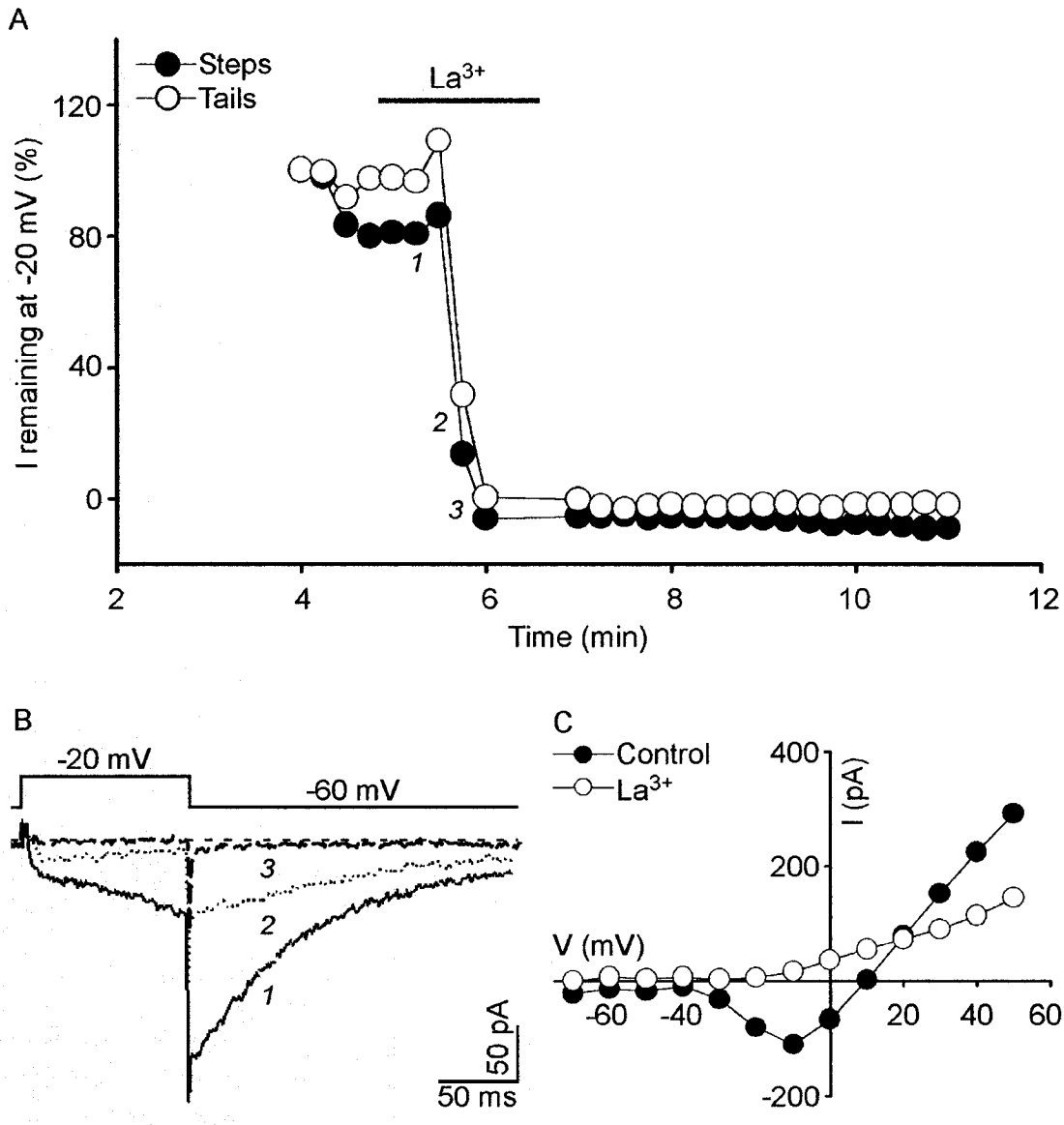
A
Steps
Tails
La3+
120
80
40
0
I remaining at -20 mV (%)
1
2
3
2
4
6
8
10
12
Time (min)
B
-20 mV
-60 mV
3
2
1
50 pA
50 ms
C
Control
La3+
400
200
I (pA)
V (mV)
-60
-40
20
40
60
-200

and $I_{Cl(Ca)}$ by La^{3+} suggests a direct Cl(Ca) and/or Ca channel blockade, which would reduce submembrane $[Ca^{2+}]_i$ during voltage steps. Figure 4.5A shows a representative example of the time course of current remaining measured during pulses to -20 mV from a holding potential of -60 mV (Steps) and from corresponding Ca^{2+}-activated Cl^- tails (Tails) throughout the application of bath-applied La^{3+}. The corresponding current traces for the same cone before, during, and following complete inhibition of the current are demonstrated in Figure 4.5B. In the presence of La^{3+}, the current measured during depolarizing voltage steps and during repolarization following those steps were reduced and subsequently abolished within a minute of La^{3+} application. These data suggest that La^{3+} may have blocked submembrane Ca^{2+} microdomains. The *I-V* relation, constructed from the current measured during depolarizing voltage steps elicited with the standard depolarizing protocol before (Control) and in the presence La^{3+}, demonstrates the inhibited inward current (Fig. 4.5C). An alternate explanation for the inhibition of I_{Ca} and $I_{Cl(Ca)}$ in the presence of La^{3+} is 'high-$[Ca^{2+}]_i$-induced inhibition', described in the next chapter.

4.5 $I_{Cl(Ca)}$ is significantly increased by repeated depolarizing pulses in the presence of caffeine

Previous experiments have shown that Ca^{2+} store modulating agents do not alter $I_{Cl(Ca)}$. The contribution of Ca^{2+}, blocked from reuptake into Ca^{2+} stores or released from Ca^{2+} stores, to submembrane $[Ca^{2+}]_i$ may be insufficient to increase $I_{Cl(Ca)}$, possibly due to fast Ca^{2+} buffering by Ca^{2+}-binding proteins and/or fast elimination through PMCAs. Test pulses applied several times in succession have previously been shown to cause a cumulative increase in $I_{Cl(Ca)}$ (Barnes and Hille, 1989). These repetitive pulses were

suggested to cause localized accumulation of submembrane $[Ca^{2+}]_i$, overloading intracellular sequestering mechanisms. The present study investigated the effect of repetitive depolarizations on $I_{Cl(Ca)}$ in the absence and presence of caffeine. The protocol used consisted of 100 ms steps from -60 mV to -20 mV repeated every 5 sec. In control conditions, $I_{Cl(Ca)}$ was enhanced by repetitive depolarizing pulses (Fig. 4.6), probably due to localized $[Ca^{2+}]_i$ accumulation within the cell (Barnes and Hille, 1989). The peak current increase was 15 ± 5% (n=4), measured at the -20 mV depolarizing step, and 12 ± 4% (n=4), measured at the corresponding Ca^{2+}-activated Cl^- tail current. In the presence of 3 mM caffeine, the increase in $I_{Cl(Ca)}$ elicited by repetitive depolarizing pulses was significantly ($P<0.05$) enhanced. A 52 ± 20% (n=4) increase was measured during depolarizing voltage steps and a 44 ± 11% (n=4) enhancement was observed during repolarization of those steps (Fig. 4.6). The current increase elicited by repetitive depolarizing pulses was also enhanced in the presence of 10 mM caffeine (Steps: 26 ± 18%; Tails: 35 ± 9%; n=3); however, significance level was not achieved. A representative example of current enhancement following repetitive depolarizing pulses (-20 mV steps from a holding potential of -60 mV repeated at 5 sec intervals) in the absence of caffeine is shown in Figure 4.7A. The corresponding current traces from the same cone photoreceptor demonstrate the baseline current (elicited by the first pulse; Baseline Control) and the current at the peak of the increase (Peak Control) (Fig. 4.7C). Figure 4.7B demonstrates an example where a large current enhancement, elicited by repetitive depolarizing pulses in the presence of 3 mM caffeine, was seen. Current traces from the same cone photoreceptor, measured from baseline (Baseline CAF) and from the

Figure 4.6 The increase in $I_{Cl(Ca)}$ induced by repetitive depolarizing pulses was enhanced in the presence of caffeine (3 mM and 10 mM). The bar graph summarizes the effect of -20 mV depolarizing voltage steps from a holding potential of -60 mV at 5 sec intervals, in the absence of caffeine (Control; n=4), and in the presence of 3 mM caffeine (CAF; n=4) as well as 10 mM caffeine (n=3). The peak current increase following 5 sec pulses was measured during depolarizing voltage steps (Steps; black bars) and during repolarization following those steps (Tails; white bars), recorded at -60 mV. The values correspond to 15 ± 5% (n=4) and 12 ± 4% (n=4) in control conditions, to 52 ± 20% (n=4) and 44 ± 11% (n=4) in the presence of 3 mM caffeine, and to 26 ± 18% (n=3) and 35 ± 9% (n=3) in the presence of 10 mM caffeine. *$P<0.05$.

Figure 4.6

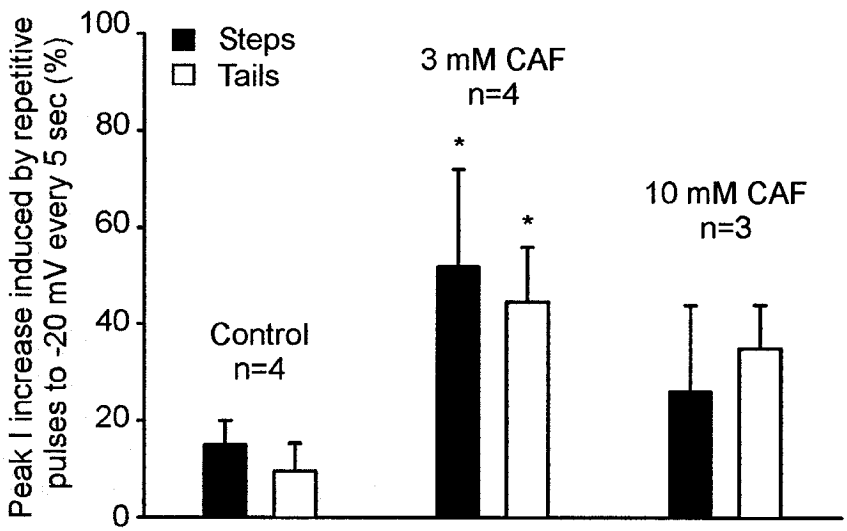
Peak I increase induced by repetitive pulses to -20 mV every 5 sec (%)
100
80
60
40
20
0
Steps
Tails
Control
n=4
3 mM CAF
n=4
10 mM CAF
n=3
*
*

Figure 4.7 Example of current increase elicited by repetitive depolarizing pulses in control conditions and in the presence of 3 mM caffeine. (**A**) Time course of current increase, measured during -20 mV depolarizing voltage steps (Steps; black circles) and during repolarization following those steps (Tails; white circles), in response to pulses repeated every 5 sec. (**B**) Repetitive depolarization-induced current enhancement in control conditions was increased in the presence of caffeine (CAF; 3 mM). Both the current measured during depolarizing voltage steps (Steps; black circles) and associated Ca^{2+}-activated Cl^- tails (Tails; white circles), were increased. (**C**) Current traces at baseline (solid line) and following depolarizing pulses at 5 sec intervals (dotted line) are shown in control conditions (in the absence of caffeine) and (**D**) in the presence of 3 mM caffeine. An increase in the current elicited by depolarizing voltage steps and by repolarization is seen.

Figure 4.7

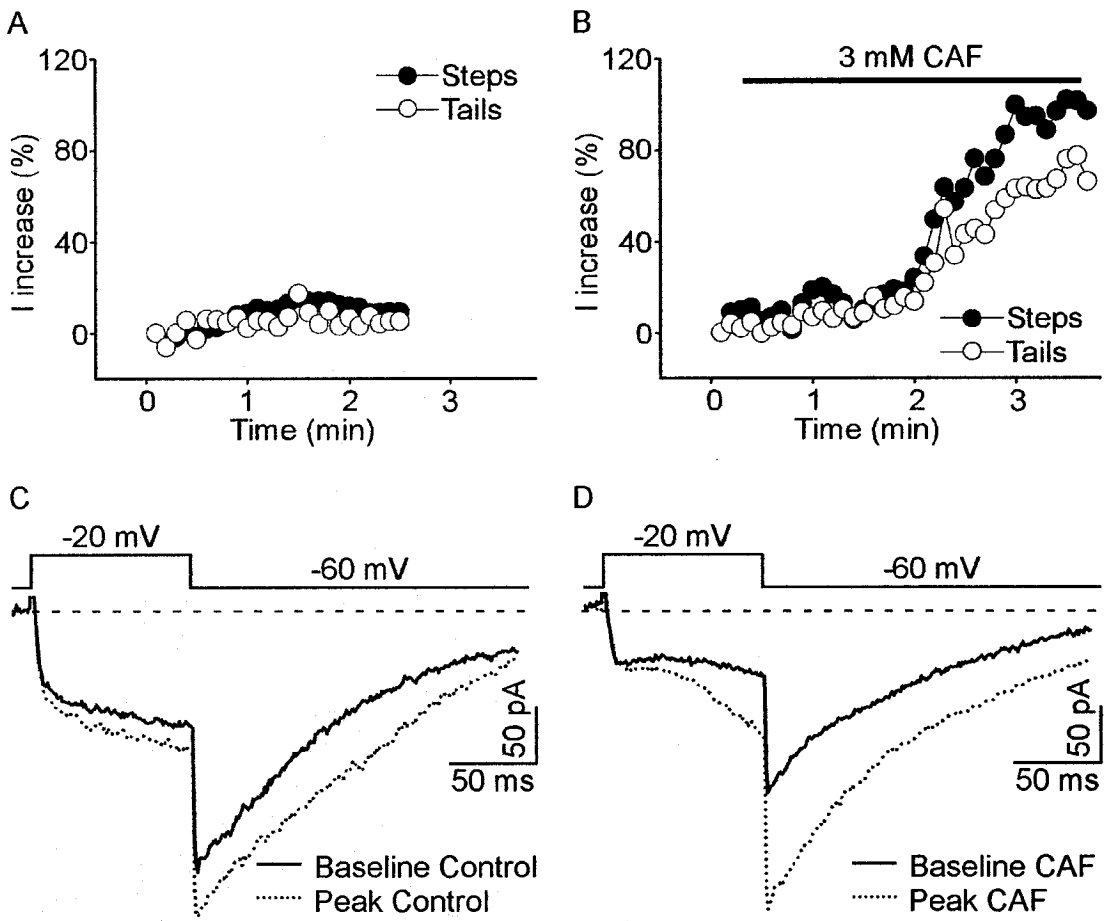
A
120
80
40
0
I increase (%)
Steps
Tails
0
1
2
3
Time (min)
B
120
80
40
0
I increase (%)
3 mM CAF
Steps
Tails
0
1
2
3
Time (min)
C
-20 mV
-60 mV
50 pA
50 ms
Baseline Control
Peak Control
D
-20 mV
-60 mV
50 pA
50 ms
Baseline CAF
Peak CAF

peak increase in the presence of caffeine (Peak CAF), indicate current enhancement (Fig. 4.7D). These results suggest that Ca^{2+} buffering and/or sequestration may be impaired during repeated depolarizations in the presence of caffeine, allowing $[Ca^{2+}]_i$ accumulation near the plasma membrane.

4.6 Summary

Ca^{2+} influx through voltage-gated Ca channels following membrane depolarization is known to produce Ca^{2+}-induced Ca^{2+}-release (CICR) from ryanodine-sensitive channels. In the present study, $I_{Cl(Ca)}$ elicited by depolarizing voltage steps remained unchanged in the presence of ryanodine, at a concentration known to block the ryanodine receptor. These results suggest that the source of Ca^{2+} for $I_{Cl(Ca)}$ elicited during depolarization is not from ryanodine-sensitive Ca^{2+} stores. In addition, blocking the SERCA pumps, responsible for Ca^{2+} sequestration into internal stores, and inducing Ca^{2+} release from IP_3 and ryanodine receptor-gated channels did not modulate $I_{Cl(Ca)}$. Taken together, the results suggest that Ca^{2+} stores do not contribute to submembrane $[Ca^{2+}]_i$ to activate $I_{Cl(Ca)}$. From Chapter 3, it is clear that Cl(Ca) channels are activated by Ca^{2+} influx through voltage-gated Ca^{2+} channels. Therefore, Cl(Ca) channels and voltage-gated Ca channels may be closely associated at the plasma membrane, away from Ca^{2+} stores. As previously mentioned, the ER has been localized mainly to the subellipsoid region of cone photoreceptors, and not to the synaptic terminal, where voltage-gated Ca channels are located (Mercurio and Holtzmann, 1982; Townes-Anderson et al., 1985; Ripps and Chappell, 1991). In addition, Ward and Kenyon (2000) have proposed that ryanodine-sensitive stores are relatively distant from the Cl(Ca) channels in avian sensory

neurons. Using a modeling system, they have concluded that the Cl(Ca) channels are approximately 50-400 nm from the voltage-gated Ca channels, and that the ryanodine receptors are more than 600 nm from the plasma membrane. Therefore, the fact that an increase in $I_{Cl(Ca)}$ was not observed in isolated salamander cone photoreceptors in the presence of SERCA pump blockers, IP_3, and caffeine, is not surprising. As suggested by Krizaj et al. (2003) the PMCAs (responsible for Ca^{2+} extrusion in cone inner segments) are very active, and these pumps could therefore prevent Ca^{2+}, released from Ca^{2+} stores, from increasing submembrane $[Ca^{2+}]_i$ high enough to modulate $I_{Cl(Ca)}$. In the present study, treatment with the well-known PMCA antagonist lanthanum, which is known to increase $[Ca^{2+}]_i$, inhibited $I_{Cl(Ca)}$ in an irreversible manner. With La^{3+}, submembrane Ca^{2+} levels were probably reduced due to its blocking effect on voltage-gated Ca channels. However, $I_{Cl(Ca)}$ inhibition could also result from Cl(Ca) channel inhibition in the presence of high $[Ca^{2+}]_i$, which is the focus of the next chapter. Finally, the result of this section demonstrate that repeated depolarizing pulses produce an increase in $I_{Cl(Ca)}$, probably due to $[Ca^{2+}]_i$ accumulation within the cell (Barnes and Hille, 1989). This increase in $I_{Cl(Ca)}$ was enhanced when the protocol was performed in the presence of caffeine. $I_{Cl(Ca)}$ increase elicited by Ca^{2+} influx through voltage-gated Ca channels, combined with Ca^{2+} release from caffeine-sensitive Ca^{2+} stores may reflect the inability of overloaded intracellular sequestering mechanisms to reduce free $[Ca^{2+}]_i$ at the submembrane microdomain where Cl(Ca) channels are located. These results suggest that the contribution of Ca^{2+} released from caffeine-sensitive stores to submembrane $[Ca^{2+}]_i$ may be revealed only when global Ca^{2+} levels are disturbed.

Chapter 5

High $[Ca^{2+}]_i$-Induced Inhibition of $I_{Cl(Ca)}$

Parts of this chapter have been previously published in the following publications:

Lalonde MR, Barnes S. 2003. Contribution of Calcium Stores to Activation of Chloride Current in Cone Photoreceptors. Society for Neuroscience, E-Abstract 791.18.

Lalonde MR, Barnes S. 2004. Inhibition of Cl(Ca) Channels in Response to High Intracellular Calcium Levels Due to Dephosphorylation-Mediated Ca channel Inhibition in Cone Photoreceptors. Society for Neuroscience, E-Abstract 65.12.

Previous chapters of the present study have argued that Ca^{2+}-activated Cl^- current ($I_{Cl(Ca)}$) is induced following depolarization-evoked Ca^{2+} influx, and that decay of Ca^{2+}-activated Cl^- tail currents reflect the time course of Ca^{2+} diffusion away from Cl(Ca) channels located at the plasma membrane. In this model, sustained activation of $I_{Cl(Ca)}$ is therefore expected to reflect persistently high submembrane Ca^{2+} levels. Surprisingly, as the present chapter will demonstrate, sustained $I_{Cl(Ca)}$ activation due to high Ca^{2+} levels is followed quickly by inhibition of $I_{Cl(Ca)}$. I hypothesize that this phenomenon, referred to here as 'high $[Ca^{2+}]_i$-induced' inhibition of $I_{Cl(Ca)}$, is caused by Ca^{2+} overload at the submembrane level. The following sections will describe the conditions where sustained activation of the Ca^{2+}-activated Cl^- current led to its own inhibition.

5.1 Enhancement of $I_{Cl(Ca)}$ followed by inhibition during repeated depolarizing pulses at 1 sec intervals in the presence of caffeine

Repetitive depolarizing pulses, consisting of -20 mV steps from a holding potential of -60 mV repeated at 5 sec intervals, were previously shown to cause an increase in $I_{Cl(Ca)}$, which was enhanced in the presence of 3 mM caffeine (see Chapter 4; Section 4.5, Figs. 4.6 and 4.7). It was proposed that the ability of local mechanisms to clear free $[Ca^{2+}]_i$ at the submembrane level was reduced when Ca^{2+} influx through voltage-gated Ca channels is combined with Ca^{2+} release from caffeine-sensitive stores. As a next step, the result of higher submembrane $[Ca^{2+}]_i$ on $I_{Cl(Ca)}$ was investigated by testing the effect of faster pulses in the presence of caffeine. As expected, repetitive depolarizing pulses at 1 or 2 sec intervals in the presence of 3 mM caffeine, increased $I_{Cl(Ca)}$ amplitude; however, this enhancement was subsequently followed by $I_{Cl(Ca)}$ inhibition. A representative example of the enhanced current elicited from 1 sec pulses in

the presence of 3 mM caffeine is shown in Figure 5.1A. The time course of current remaining is shown following depolarizing pulses from a holding potential of -60 mV to -20 mV repeated at different intervals (1, 2, 5, 10, 15, and 20 sec). In the absence of caffeine, an increase in the current (Step: ~75%; Tail: ~37%) was seen when pulses were repeated at 1 sec intervals. Control current traces at baseline and at the peak increase elicited by 1 sec pulses are shown in Figure 5.1B. In the presence of caffeine, the increase in the current (measured from baseline to the peak increase) elicited with 1 sec pulses was faster and twice as large in amplitude (Step: ~148%; Tail: ~79%). The current records at baseline and at the peak increase in the presence of caffeine show an increased amplitude and altered submembrane $[Ca^{2+}]_i$-dominated deactivation kinetics of $I_{Cl(Ca)}$ (Fig. 5.1C). In the presence of caffeine, the $I_{Cl(Ca)}$ enhancement was quick (peak reached in less than 15 sec) and was followed by inhibition. For example, repetitive pulses every 2 sec induced an increase in the current in control conditions (Step: ~62%; Tail: ~21%); however, current enhancement at the same interval could not be elicited following the inhibition of $I_{Cl(Ca)}$ in the presence of caffeine (Fig. 5.1A). $I_{Cl(Ca)}$ inhibition during repetitive depolarizing pulses in the presence 3 mM caffeine was seen in all cells tested (n=3).

Amplified $I_{Cl(Ca)}$ elicited with repetitive depolarizing pulses is thought to reflect localized $[Ca^{2+}]_i$ accumulation within the cell (Barnes and Hille, 1989). The enhanced current increase in the presence of caffeine is most likely due to increased submembrane $[Ca^{2+}]_i$. Although the cell has powerful mechanisms to maintain $[Ca^{2+}]_i$ at resting levels, the combination of depolarization-evoked Ca^{2+} influx and Ca^{2+}-release from caffeine-

Figure 5.1 Repetitive depolarizing steps at 1 sec intervals induce a transient $I_{Cl(Ca)}$ increase in the presence of caffeine. (**A**) Time course of current remaining (expressed as a percentage of control) in response to depolarizing pulses to -20 mV from a holding potential of -60 mV, repeated every 1, 2, 5, 10, 15, and 20 sec. The current measured during depolarizing voltage steps (Steps; black circles) and during repolarization following those steps (Tails; white circles), is shown. Depolarizing pulses repeated every 1 or 2 sec produced an increase in $I_{Cl(Ca)}$ in control conditions. In the presence of 3 mM caffeine (CAF; indicated by the horizontal bar), the increase in $I_{Cl(Ca)}$ elicited by repeated depolarizing pulses at 1 sec intervals was enhanced. This enhanced current increase was followed by a rapid inhibition without recovery. The cell was superfused with caffeine 1 min prior to the depolarizing pulses repeated at 1 sec intervals. Note that after the current was inhibited in the presence of caffeine, the increase seen during 2 sec pulses in control conditions could not be reproduced. (**B**) Current traces at baseline (Baseline; solid line) and at the peak increase elicited during 1 sec pulses (Peak (1s); dotted line) are shown in control conditions and (**C**) during the application of caffeine. The dashed lines indicate zero current.

Figure 5.1

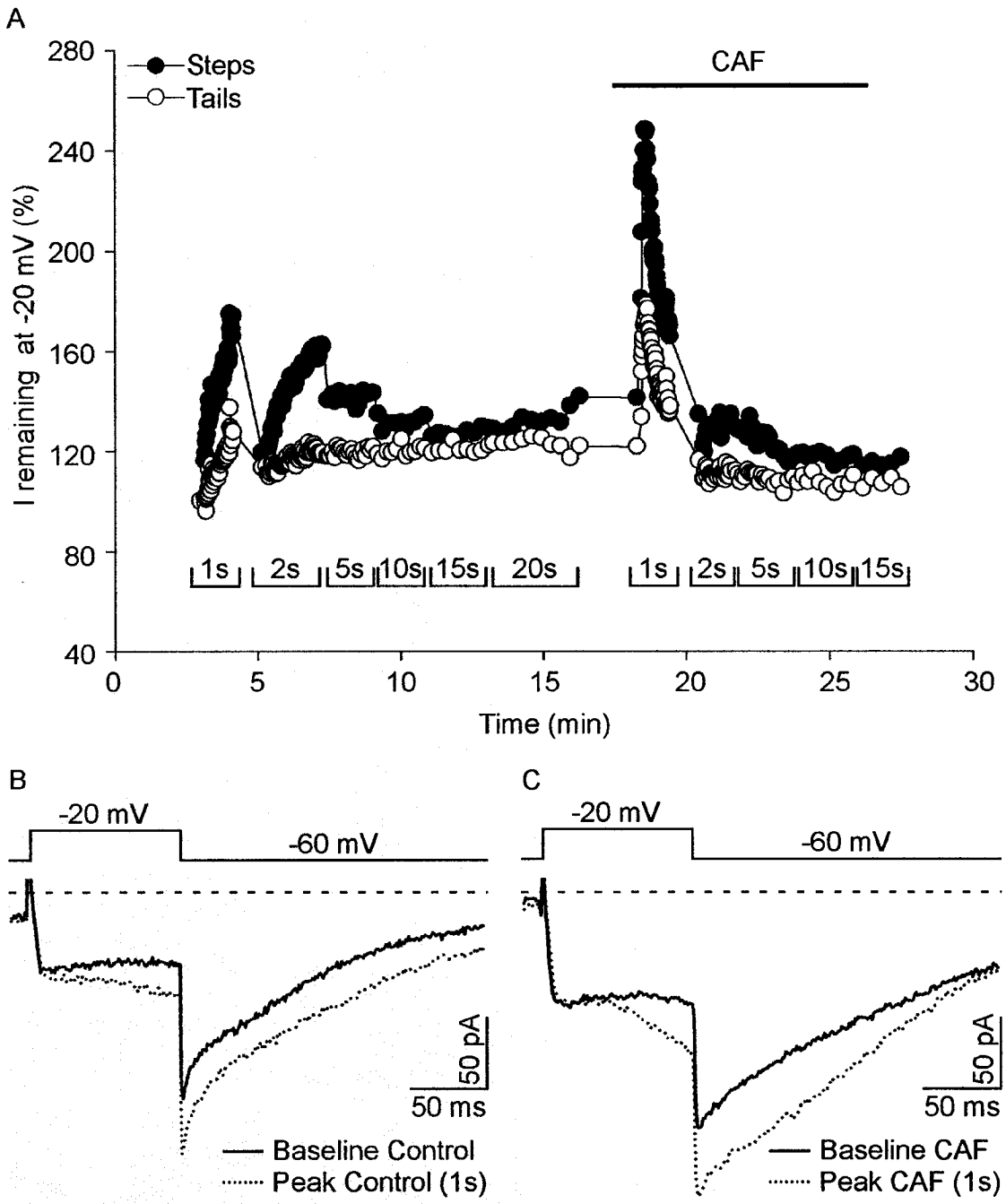
A
Steps
Tails
CAF
I remaining at -20 mV (%)
280
240
200
160
120
80
40
1s
2s
5s
10s
15s
20s
1s
2s
5s
10s
15s
0
5
10
15
20
25
30
Time (min)
B
-20 mV
-60 mV
50 pA
50 ms
Baseline Control
Peak Control (1s)
C
-20 mV
-60 mV
50 pA
50 ms
Baseline CAF
Peak CAF (1s)

sensitive Ca^{2+} stores seems to increase and accelerate accumulation of $[Ca^{2+}]_i$ within the cell. The enhanced current increase in the presence of caffeine was quickly followed by inhibition. Since this observation has not been previously described or explained, the mechanisms responsible for $I_{Cl(Ca)}$ inhibition are investigated in the following work. $I_{Cl(Ca)}$ inhibition could reflect decreased submembrane Ca^{2+} levels. For example, when Ca^{2+} levels are high, super-efficient mechanisms to buffer and/or sequester Ca^{2+} may be activated within the cell. In addition, a decreased depolarization-evoked Ca^{2+} influx through voltage-gated Ca channel would also explain reduced $[Ca^{2+}]_i$ at the submembrane. It is possible that $I_{Cl(Ca)}$ is the result of a protective mechanism used by the cell, where Ca channels become inactivated when the cell's capacity to buffer Ca^{2+} is depleted. On the other hand, mechanisms involved in Cl(Ca) channel activation could be inhibited by elevated levels of $[Ca^{2+}]_i$.

5.2 $I_{Cl(Ca)}$ is inhibited following repeated strong depolarizations

Repeated strong depolarizations (100 ms prepulses to 0 mV, each followed by a step to -60 mV for 40 ms and then 100 ms steps decrementing from +20 mV to -80 mV in 10 mV steps, applied at 2 Hz), has previously been shown to induce sustained $I_{Cl(Ca)}$ activation (see Chapter 3; Section 3.3, Fig. 3.5B). The *I-V* relation observed with repeated strong depolarizations was similar to the one obtained with ionomycin, and therefore, this protocol was suggested to increase submembrane Ca^{2+} levels. However, enhancement of $I_{Cl(Ca)}$ via repeated strong depolarization was followed by inhibition. The peak current remaining was 79 ± 8% (n=5), measured during depolarizing voltage steps

Figure 5.2 $I_{Cl(Ca)}$ is inhibited in a reversible manner following repeated strong depolarizations. A cone photoreceptor, held at -60 mV and depolarized following the standard depolarizing protocol, was subjected to repeated strong depolarization. (**A**) Time course of peak current remaining (expressed as a percentage of control) measured during depolarizing voltage steps (Steps; black circles) and during repolarization following those steps (Tails; white circles). Repeated strong depolarizations (indicated by the arrow), induced a reduction in current, which almost fully recovered. (**B**) Current traces from the same cone photoreceptor, elicited by the -10 mV depolarizing pulse. The current traces before (solid line) and after (dotted line) the repeated strong depolarization protocol demonstrate the inhibition. The dashed line indicates zero current. (**C**) *I-V* relations from the same cone, before (black circles) and after (white circles) repeated strong depolarizations, show a decrease in the current.

Figure 5.2

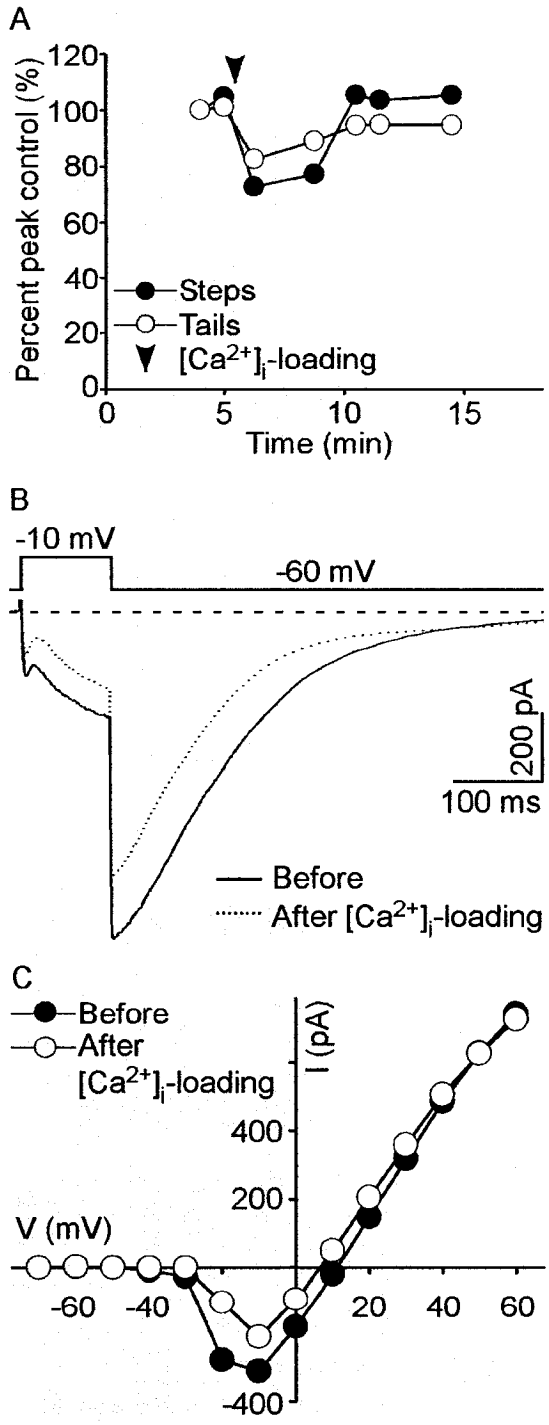
A
Percent peak control (%)
120
100
80
60
40
20
0
0
5
10
15
Time (min)
Steps
Tails
[Ca2+]i-loading
B
-10 mV
-60 mV
200 pA
100 ms
Before
After [Ca2+]i-loading
C
Before
After
[Ca2+]i-loading
I (pA)
400
200
V (mV)
-60
-40
20
40
60
-400

and 93 ± 5% (n=5), measured during repolarization following those steps. Figure 5.2A shows an example of $I_{Cl(Ca)}$ reduction following repeated strong depolarizations. The inhibition was reversible as the current measured during depolarizing voltage steps to -20 mV recovered to 96 ± 5% (n=5) of its original value. Current traces during a -10 mV depolarizing step (Fig. 5.2B) and *I-V* relations (Fig. 5.2C) from the same cell show the decreased current following repeated strong depolarizations. Since repeated strong depolarizations seems to increase $[Ca^{2+}]_i$ at the submembrane level, the inhibition in $I_{Cl(Ca)}$ following this protocol is likely mediated by high $[Ca^{2+}]_i$; however, the specific mechanism by which this inhibition occurs is unknown.

5.3 $I_{Cl(Ca)}$ inhibition following repeated strong depolarizations is increased in the presence of SERCA pump inhibitors

Repeated strong depolarizations leads to a reversible inhibition of $I_{Cl(Ca)}$. This effect was significantly ($P<0.05$) enhanced in the presence of the SERCA pump inhibitor thapsigargin (Fig. 5.3). Thapsigargin alone was shown not to modulate $I_{Cl(Ca)}$ (see Chapter 4; Section 4.1, Figs. 4.1C and D). The cumulative data indicated that in the presence of thapsigargin (~4 min of superfusion) the peak current remaining measured during depolarizing voltage steps, and during repolarization following those steps, was 93 ± 3% (n=7) and 100 ± 3% (n=7), respectively. However, when cells were subjected to repeated strong depolarizations in the presence of thapsigargin, $I_{Cl(Ca)}$ was inhibited. The peak current measured during depolarizing voltage steps and during repolarization following those steps was significantly ($P<0.05$) inhibited by 48 ± 10% (n=5) and by 25 ± 5% (n=5), respectively. Figure 5.3A shows the inhibited current, which slowly recovered. $I_{Cl(Ca)}$ inhibition following repeated strong depolarizations in the presence of

Figure 5.3 $I_{Cl(Ca)}$ inhibition following repeated strong depolarizations seen in control conditions was increased in the presence of the SERCA pump blocker, thapsigargin. A cone photoreceptor was held at -60 mV and currents were elicited following the standard depolarizing protocol repeated consecutively. (**A**) Time course of peak current remaining measured during depolarizing voltage steps (Steps; black circles) and during repolarization following those steps (Tails; white circles). $I_{Cl(Ca)}$ was inhibited following repeated strong depolarizations (indicated by the arrow) in the presence of 1 μM thapsigargin (TG; indicated by the horizontal bar). (**B**) Current traces from the same cone obtained in the presence of thapsigargin, demonstrating the current elicited by a -30 mV depolarizing voltage step before (solid line) and after (dotted line) repeated strong depolarizations. The dashed line indicates zero current. (**C**) Leak-corrected *I-V* and (**D**) offset-subtracted Ca^{2+}-activated Cl^- *Q-V* relations, from the same cone before (black circles) and after (white circles) repeated strong depolarization in the presence of thapsigargin, also show the inhibition.

Figure 5.3

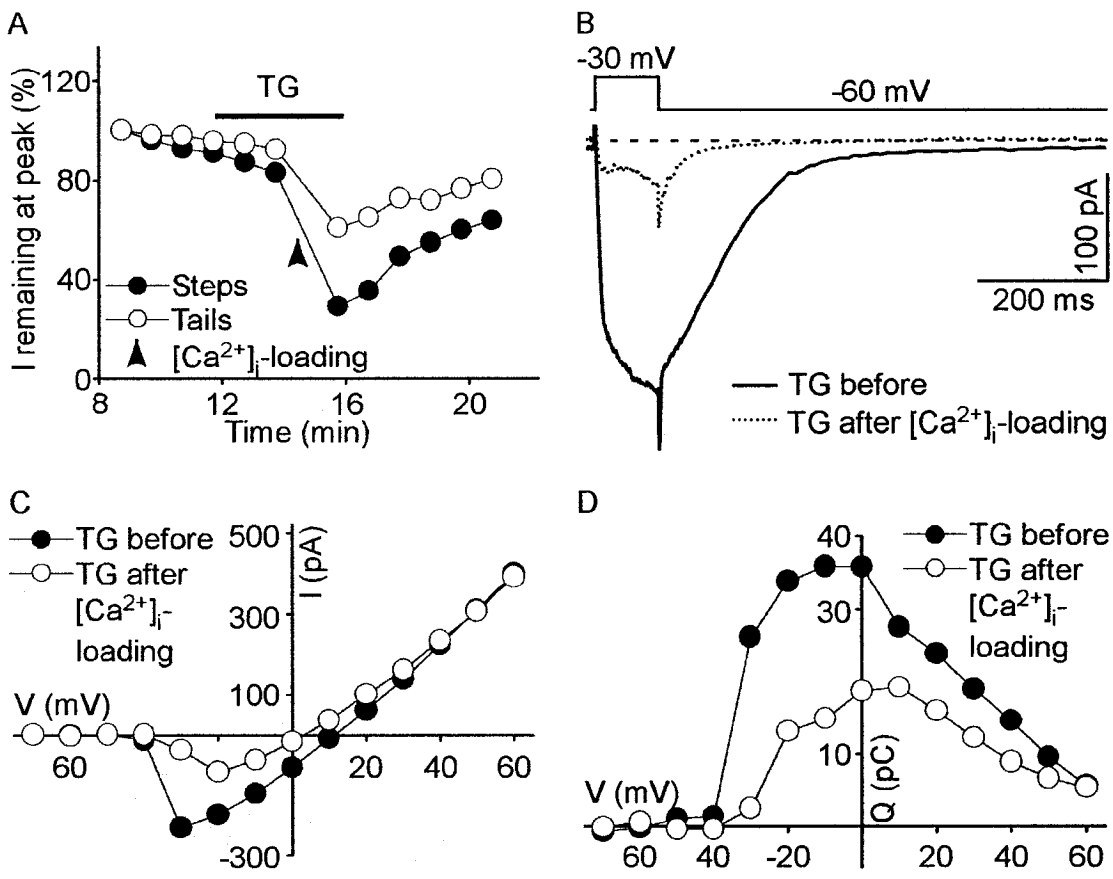
A
I remaining at peak (%)
120
80
40
0
TG
Steps
Tails
[Ca2+]i-loading
8
12
16
20
Time (min)
B
-30 mV
-60 mV
100 pA
200 ms
TG before
TG after [Ca2+]i-loading
C
TG before
TG after [Ca2+]i-loading
V (mV)
60
500
300
100
-300
I (pA)
20
40
60
D
TG before
TG after [Ca2+]i-loading
40
30
10
Q (pC)
V (mV)
60
40
-20
20
40
60

thapsigargin is also illustrated in the current traces (Fig. 5.3B), and constructed *I-V* (Fig. 5.3C) and Ca^{2+}-activated Cl^- *Q-V* (Fig. 5.3D) relations from the same cone photoreceptor. Similar results were obtained with another commonly used SERCA pump inhibitor, cyclopiazonic acid (Fig. 5.4).

$I_{Cl(Ca)}$ shows reversible inhibition following repeated strong depolarizations in control conditions. This inhibition, which was also reversible, was enhanced in the presence of SERCA pump inhibitors, thapsigargin and cyclopiazonic acid. These data suggest that Ca^{2+} reuptake inhibition into Ca^{2+} stores, which may have participated in increasing global Ca^{2+} levels, are responsible for the increased $I_{Cl(Ca)}$ inhibition following repeated strong depolarizations. The present results suggest that in the presence of high $[Ca^{2+}]_i$, resulting from both Ca^{2+} entry via voltage-gated Ca channels and from Ca^{2+} reuptake inhibition into Ca^{2+} stores, subsequent inhibition of $I_{Cl(Ca)}$ occurred. It seems that a higher $[Ca^{2+}]_i$ induces greater $I_{Cl(Ca)}$ inhibition. The mechanism by which high $[Ca^{2+}]_i$ could cause the inhibition of $I_{Cl(Ca)}$ is unknown but could involve direct inhibition of Cl(Ca) channels or indirect inhibition of voltage-gated Ca channels.

5.4 $I_{Cl(Ca)}$ inhibition following repeated strong depolarizations is increased and becomes irreversible in the presence of H-8, a protein kinase inhibitor

In cone photoreceptors, $I_{Cl(Ca)}$ is inhibited following repeated strong depolarization, when Ca^{2+} levels appear to be increased. Mechanisms involved in 'high $[Ca^{2+}]_i$-induced' inhibition of $I_{Cl(Ca)}$ are not known, but as described earlier in this dissertation, could arise following voltage-gated Ca channel inhibition. Previous studies have shown that photoreceptor Ca channel currents can be modulated by cAMP-

Figure 5.4 Inhibition of $I_{Cl(Ca)}$ following repeated strong depolarizations seen in control conditions was increased in the presence of cyclopiazonic acid. Whole-cell currents elicited by the standard depolarizing protocol were recorded from a cone photoreceptor held at -60 mV. (**A**) Time course of peak current remaining (expressed as a percentage of control) measured during depolarizing voltage steps (Steps; black circles) and during repolarization following those steps (Tails; white circles). In the presence of 5 μM cyclopiazonic acid (CPA; indicated by the horizontal bar), $I_{Cl(Ca)}$ was inhibited following repeated strong depolarizations (indicated by the arrow). (**B**) Current traces from the same cone elicited by a -20 mV depolarizing voltage step before (solid line) and the after (dotted line) repeated strong depolarizations in the presence of cyclopiazonic acid. Zero current is indicated by the dashed line. (**C**) Leak-subtracted *I-V* and (**D**) offset-subtracted Ca^{2+}-activated Cl^- *Q-V* relations, before (black circles) and after (white circles) repeated strong depolarizations in the presence of cyclopiazonic acid, also show the decrease.

Figure 5.4

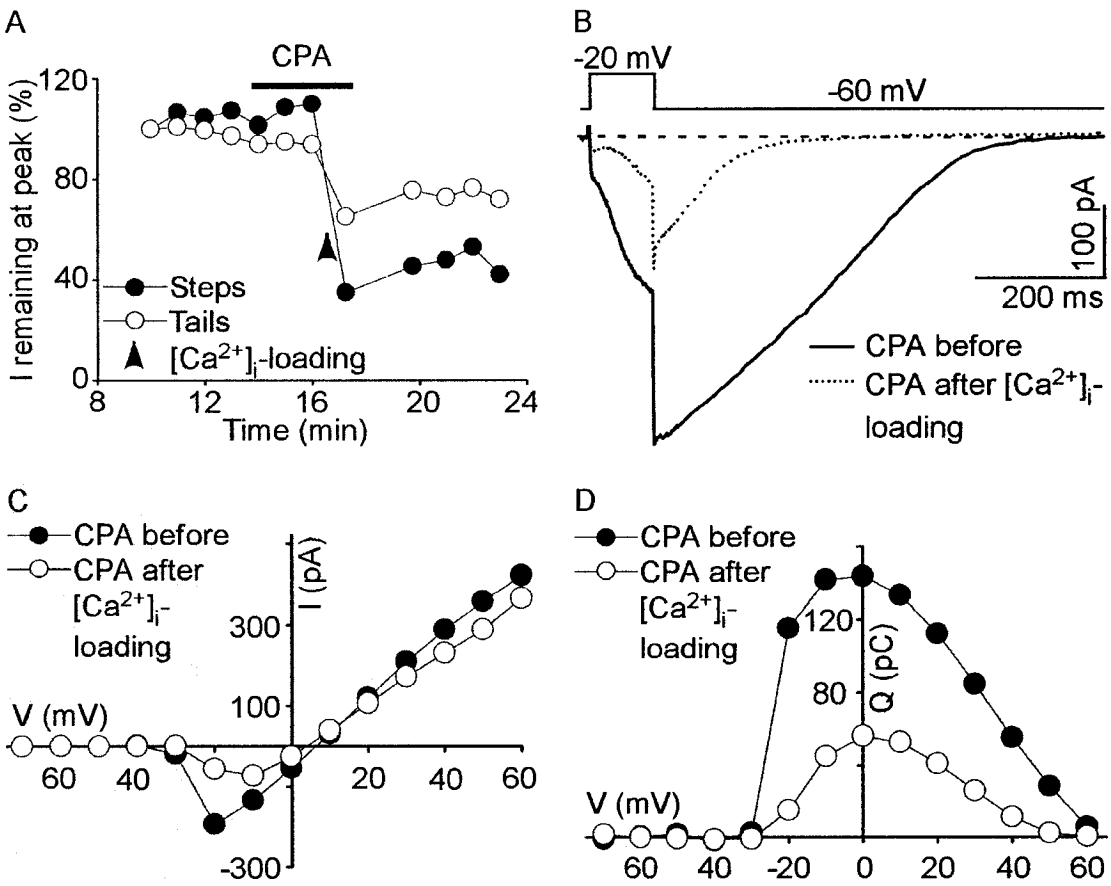
A
CPA
I remaining at peak (%)
120
80
40
0
Steps
Tails
[Ca2+]i-loading
8
12
16
20
24
Time (min)
B
-20 mV
-60 mV
100 pA
200 ms
CPA before
CPA after [Ca2+]i-loading
C
CPA before
CPA after [Ca2+]i-loading
V (mV)
60
40
I (pA)
300
100
-300
20
40
60
D
CPA before
CPA after [Ca2+]i-loading
120
80
Q (pC)
V (mV)
60
40
-20
0
20
40
60

dependent protein kinases (Stella and Thoreson, 2000; Stella et al., 2002). The following section tests the role of phosphorylation mechanisms in $I_{Cl(Ca)}$ inhibition following repeated strong depolarizations by subjecting cones to this voltage-clamp protocol in the presence of H-8, a cAMP and cGMP-dependent protein kinase inhibitor. The action of H-8 alone on $I_{Cl(Ca)}$ was first tested. H-8 (10 μM) did not significantly modulate $I_{Cl(Ca)}$. The average peak current remaining after application was 88 ± 7% (n=5), measured at depolarizing voltage steps, and 106 ± 6% (n=5), measured during repolarization following those steps. A representative example of leak-subtracted *I-V* relations recorded with the standard depolarizing protocol in control conditions (Control; black circles) and in the presence of H-8 (white circles) is shown in Figure 5.5A. Activation curves, constructed from these *I-V* relations by dividing by the driving force and then fitted with the Boltzmann function, indicate no changes in $I_{Cl(Ca)}$ by H-8 alone (Fig. 5.5B). However, when repeated strong depolarizations were elicited in the presence of H-8, much like in the presence of the SERCA pump inhibitors, the inhibition of $I_{Cl(Ca)}$ was enhanced. Following repeated strong depolarization, the Ca^{2+}-activated Cl^- tail current elicited by the -20 mV depolarizing step, which was reduced by 15 ± 12% (n=5) in control conditions, was inhibited by 69 ± 15% (n=3) in the presence of H-8. Figure 5.6 illustrates an example of a cone that was highly sensitive to repeated strong depolarizations in the presence of H-8. Figure 5.6A shows the time course of current remaining measured during depolarization to -20 mV (Steps; black circles), and from corresponding Ca^{2+}-activated Cl^- tails (Tails; white circles), recorded at -60 mV. A large inhibition of the current measured at both the depolarizing voltage step and associated Ca^{2+}-activated Cl^- tail was seen following repeated strong depolarizations (indicated by

the arrows) in the presence of H-8. Current traces (Fig. 5.6B) and *I-V* relations (Figs. 5.6C) from the same cone indicate a greater inhibition when compared to control conditions (Fig. 5.2). The present data indicate that when phosphorylation mechanisms are inhibited, a greater inhibition of $I_{Cl(Ca)}$ is observed following repeated strong depolarizations, when Ca^{2+} levels are likely increased. The shift in the *I-V* relation in the presence of H-8 after repeated strong depolarizations (Fig. 5.6C) suggests that voltage-gated Ca channels were inhibited due to a shift in the activation curve along the voltage axis. Changes in Ca channel activation were measured early into the voltage steps, a region less contaminated with Cl^- conductance, and activation midpoints were calculated from activation curves fitted with the Boltzmann function. In the cell shown in Figure 5.6, a rightward shift in the activation midpoint ($V_{1/2}$) from -13.8 mV to -10.6 mV was observed following repeated strong depolarizations in the presence of H-8. In a sample of cells, the activation midpoint following repeated strong depolarizations shifted from 1.6 ± 0.8 mV (n=4) in control condition (without H-8) to 2.0 ± 0.8 mV (n=3) in the presence of H-8; however, this shift was not statistically significant. In addition, $I_{Cl(Ca)}$ inhibition following repeated strong depolarizations in the presence of H-8 could not be recovered. These data suggest that when phosphorylation mechanisms are inhibited, 'high $[Ca^{2+}]_i$-induced' inhibition of $I_{Cl(Ca)}$, which is irreversible, is due, at least in part, to a shift in the Ca channel activation curve.

Figure 5.5 H-8 alone did not modulate $I_{Cl(Ca)}$ (n=5). Cone photoreceptors were held at -60 mV and subjected to the standard depolarizing protocol in control conditions and in the presence of H-8 (10 μM). (**A**) Representative example of *I-V* relations measured during depolarizing voltage steps, in control conditions (black circles) and in the presence of H-8 (white circles). H-8 had no effect on the whole-cell current. (**B**) Activation curves constructed using the driving force calculated from corresponding *I-V* relations, demonstrating that the control recording was very similar to the one obtained in the presence of H-8 (Boltzmann fit: $V_{1/2}$ = -17.7 vs. -20.2 mV and m = 6.9 vs. 6.4)

Figure 5.5

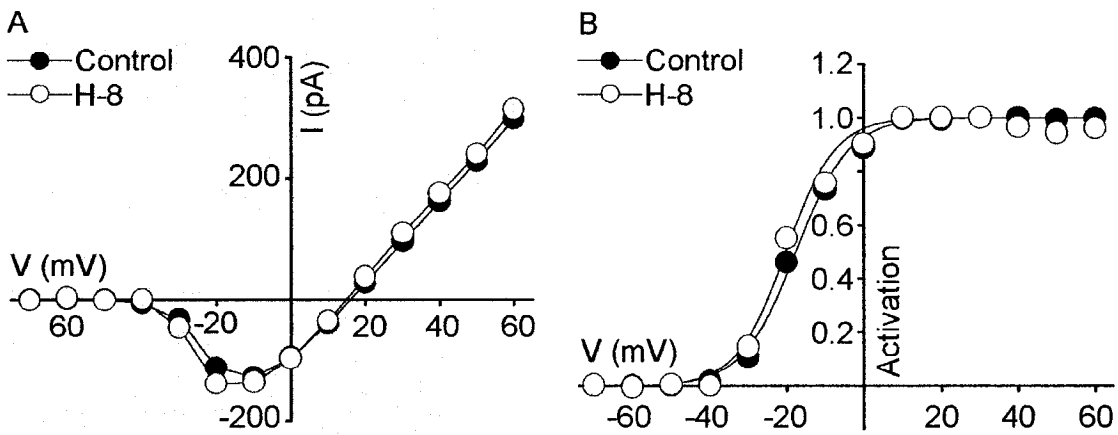
A
Control
H-8
400
200
I (pA)
V (mV)
60
-20
20
40
60
-200
B
Control
H-8
1.2
1.0
0.6
0.4
0.2
Activation
V (mV)
-60
-40
-20
20
40
60

Figure 5.6 H-8 increased the repeated strong depolarization-induced inhibition effect on $I_{Cl(Ca)}$ and prevented current recovery (n=4). (**A**) Time course of current remaining (expressed as a percentage of control) to -20 mV pulses measured during the standard depolarizing protocol (Steps; black circles) and during repolarization following those steps (Tails; white circles). $I_{Cl(Ca)}$ was strongly inhibited following repeated strong depolarization (indicated by the arrow) when superfusing with H-8 (10 μM; indicated by the horizontal bar). (**B**) Corresponding current traces from the same cone before (solid line) and after (dotted line) the repeated strong depolarization protocol in the presence of H-8. Zero current is indicated by the dashed line. (**C**) Corresponding leak-subtracted *I-V* relations of the current measured early during depolarizing voltage steps in the presence of H-8 before (black circles) and following (white circles) repeated strong depolarizations. The decrease is associated with a change in the activation curve, as readily seen from the constructed *I-V* relation.

Figure 5.6

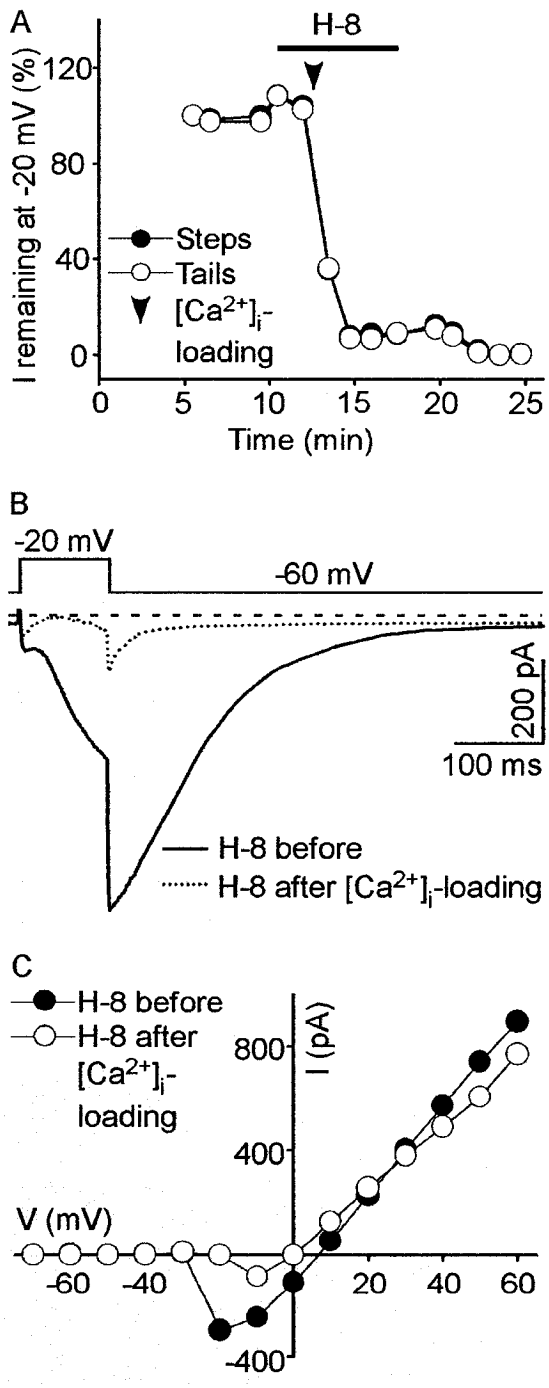
A
H-8
I remaining at -20 mV (%)
120
80
40
0
Steps
Tails
[Ca2+]i-
loading
0
5
10
15
20
25
Time (min)
B
-20 mV
-60 mV
200 pA
100 ms
H-8 before
H-8 after [Ca2+]i-loading
C
H-8 before
H-8 after
[Ca2+]i-
loading
800
400
I (pA)
V (mV)
-60
-40
20
40
60
-400

5.5 $I_{Cl(Ca)}$ is enhanced by okadaic acid, a protein phosphatase inhibitor, and is inhibited by its washout

The link between high $[Ca^{2+}]_i$-induced inhibition of $I_{Cl(Ca)}$ and dephosphorylation mechanisms was further explored with the use of okadaic acid, a protein phosphatase inhibitor. Okadaic acid (1 μM added to the standard bath solution) increased the peak current measured during depolarizing voltage steps (38 ± 17%; n=4; $P<0.05$) and during repolarization following those steps (18 ± 5%; n=4). The time course (current remaining plotted against time) of drug application is shown in Figure 5.7A. While current build up could have contributed to the increase seen in the presence of okadaic acid, $I_{Cl(Ca)}$ was irreversibly inhibited when the drug was washed out. A few minutes after okadaic acid was removed from the extracellular solution, complete reduction in $I_{Cl(Ca)}$ could not be reversed by re-applying the drug. This increase and inhibition, which occurred when okadaic acid was applied and removed from the extracellular solution, respectively, are also reflected in the current traces (Fig. 5.7B), leak-subtracted *I-V* relations (Fig. 5.7C), and offset-subtracted Ca^{2+}-activated Cl^- *Q-V* relations (Fig. 5.7D) from a different cell. Figure 5.7E shows Ca channel activation curves, fitted with the Boltzmann function, in control conditions (black circles), in the presence of okadaic acid (white circles), and a few minutes after washout of okadaic acid (black triangles). Okadaic acid caused an increase in $I_{Cl(Ca)}$, due to, at least in part, a negative shift in the Ca channel activation curve, whereas a positive shift was seen when this drug was removed from the extracellular solution. These observations were consistent among all cone photoreceptors tested (n=4). The negative shift in the activation midpoint ($V_{1/2}$) in the presence of okadaic acid was -1.8 ± 1.8 mV while the positive shift was 10.0 ± 2.8 mV ($P<0.05$)

Figure 5.7 When dephosphorylation mechanisms are inhibited or activated, $I_{Cl(Ca)}$ is increased and inhibited via negative and positive shifts in activation curves, respectively. (**A**) Time course of current remaining measured during depolarizing voltage steps to -20 mV (Steps; black circles) and during repolarization following those steps (Tails; white circles). Okadaic acid (OA; 1 μM) produced an increase in the current (mainly tail), which was later abolished when the drug was removed from the extracellular solution. Reapplication of okadaic acid during current decrease (indicated by the horizontal bar) could not recover the inhibition. (**B**) Current traces of a representative cone photoreceptor in control conditions (solid line), in the presence of okadaic acid (dotted line), and after okadaic acid was removed from the extracellular solution (dashed line), showing the okadaic-induced increase and washout-induced inhibition of the current. (**C**) Leak-subtracted *I-V* relations measured during depolarizing voltage steps, and (**D**) offset-subtracted Ca^{2+}-activated Cl^- *Q-V* relations, are shown in control conditions (black circles), during the first okadaic acid application (OA; white circles), and after okadaic washout (Wash; black triangles). (**E**) Compared to control conditions (black circles), a negative and positive shift in the Ca channel activation curve was observed in the presence of okadaic acid (white circles) and when okadaic acid was washed out (black triangles), respectively. (**F**) Cumulative data from four cone photoreceptors showing the average Ca^{2+}-activated Cl^- charge remaining in the presence of okadaic acid (OA; black bars) and after okadaic acid was removed from the superfusate (Wash; white bars). Data from both the -20 mV and 0 mV depolarizing voltage steps are shown. When okadaic acid was washed out, a significant decrease in the tail integral was observed at -20 mV but not at 0 mV, further confirming the shift in the activation curve. *$P<0.05$.

Figure 5.7

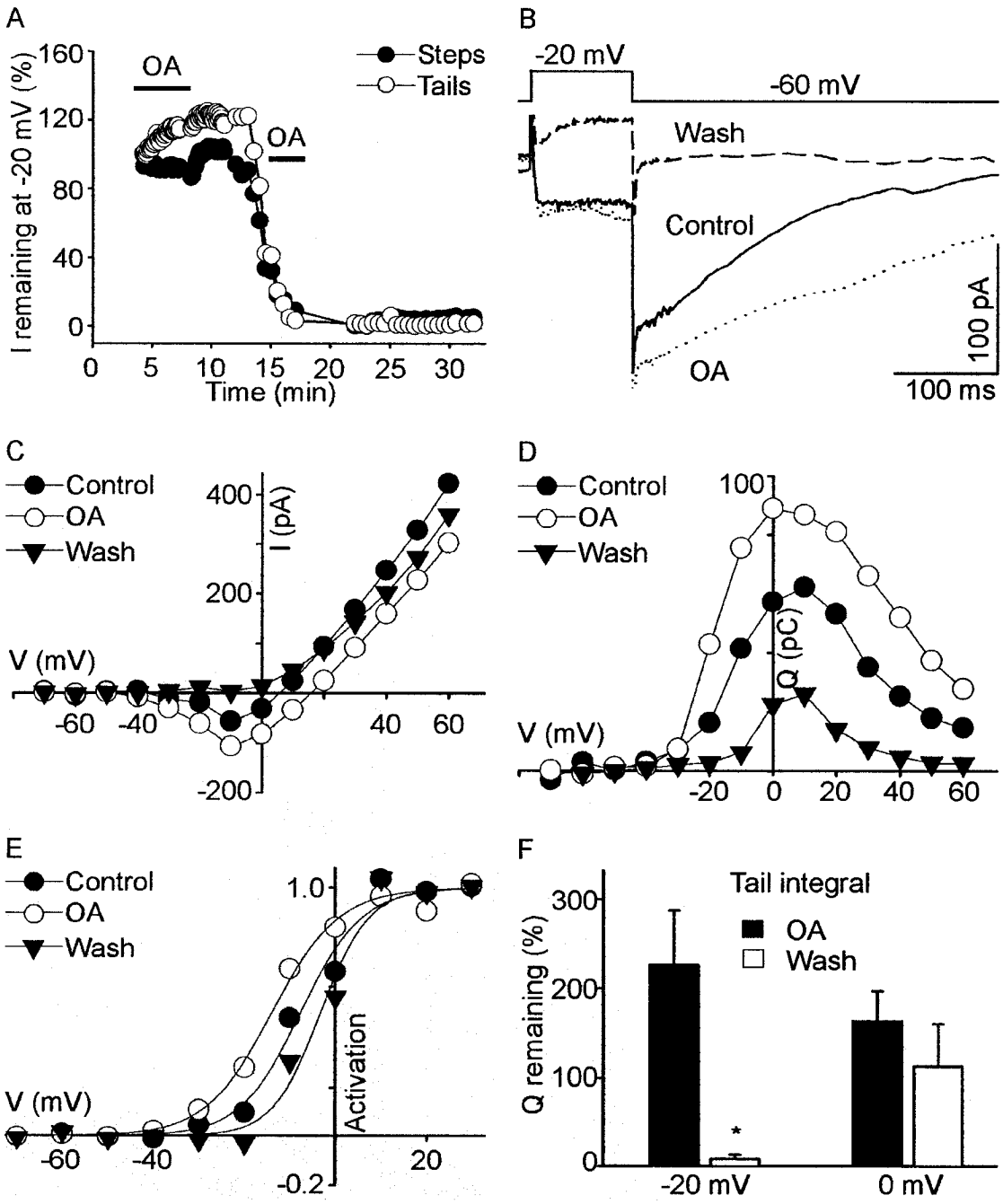
A
I remaining at -20 mV (%)
160
120
80
40
0
OA
OA
Steps
Tails
0 5 10 15 20 25 30
Time (min)
B
-20 mV
-60 mV
Wash
Control
OA
100 pA
100 ms
C
Control
OA
Wash
400
200
-200
I (pA)
V (mV)
-60 -40 40 60
D
Control
OA
Wash
100
Q (pC)
V (mV)
-20 0 20 40 60
E
Control
OA
Wash
1.0
-0.2
Activation
V (mV)
-60 -40 20
F
Tail integral
OA
Wash
Q remaining (%)
300
200
100
0
*
-20 mV
0 mV

when okadaic acid was washed out, suggesting recovery of phosphatase activity above control. Figure 5.7F further demonstrates the shifts in the activation curves. In the presence of okadaic acid, the mean charge (Q; calculated from the integral of the Ca^{2+}-activated Cl^- tails and expressed as a percentage of control) increase following the step to -20 mV was 126 ± 61% (n=4) and 63 ± 34% following the step to 0 mV. When okadaic acid was washed out, the charge passing was 8 ± 5% following the step to -20 mV and 113 ± 47% following the step to 0 mV. These results suggest that $I_{Cl(Ca)}$ inhibition occurs, at least in part, via a mechanism involving voltage-gated Ca channel inhibition.

5.6 Enhancement of $I_{Cl(Ca)}$ is followed by inhibition in the presence of ionomycin

As described in previous sections, repeated strong depolarization causes $I_{Cl(Ca)}$ inhibition, and this inhibition was increased in the presence of SERCA pump blockers. It was therefore hypothesized that $I_{Cl(Ca)}$ inhibition was induced by high $[Ca^{2+}]_i$. Ionomycin is an ionophore that forms lipid-soluble complexes with divalent metal cations. It has a greater sensitivity to Ca^{2+} ions over Mg^{2+} (by a factor of ~2), forming a 1:1 complex (Liu and Hermann, 1978) and is therefore commonly used to increase the Ca^{2+} permeability of biological membranes. Therefore, the 'high $[Ca^{2+}]_i$-induced' inhibition of $I_{Cl(Ca)}$ was tested by adding ionomycin to the extracellular solution. Although Ca^{2+}-imaging experiments demonstrate a sustained increase in $[Ca^{2+}]_i$ in salamander cone photoreceptors in the presence of ionomycin (see Appendix 1), the sustained $I_{Cl(Ca)}$ activation previously described (see Chapter 3; Section 3.3; Fig. 3.5B) was subsequently followed by inhibition. The application of 5 μM and 10 μM ionomycin generated similar results; therefore, the data acquired for both concentrations were combined. In the

presence of ionomycin, current records, whether obtained by subjecting cells to the standard depolarizing protocol (n=3; Fig. 5.8) or by depolarizing the cells to -20 mV every 5 sec or 15 sec from a holding potential of -60 mV (n=5; Fig. 5.9), showed that an increase in $I_{Cl(Ca)}$ was subsequently followed by inhibition. Figure 5.8A demonstrates a representative example of currents elicited by the -20 mV depolarizing voltage step in control conditions (Control; solid line), in the presence of ionomycin (2 min superfusion; IONO; dotted line), and after ionomycin-induced inhibition of $I_{Cl(Ca)}$ (4 min superfusion; Inhibition; dashed line). After two minutes of ionomycin superfusion, sustained $I_{Cl(Ca)}$ activation was observed while the current elicited by depolarizing voltage steps became smaller. Four minutes after ionomycin was added to the extracellular solution, both the voltage step current and the Ca^{2+}-activated Cl^- tail current were inhibited. Figure 5.8B and C show the constructed *I-V* and Ca^{2+}-activated Cl^- *Q-V* relations of the same cell, respectively. The large Ca^{2+}-activated Cl^- conductance generated by two minutes ionomycin superfusion is reflected in the *I-V* relation, where the current reverses close to 0 mV, near E_{Cl} (IONO; white circles). The inhibition in $I_{Cl(Ca)}$ caused by ionomycin is reflected in the *Q-V* relation, where the amount of charge crossing is significantly reduced (Inhibition; black triangles). After $I_{Cl(Ca)}$ inhibition in the presence of ionomycin, an outward current measured during depolarizing voltage-steps remained at positive potentials. On one occasion, in the example shown in Figure 5.8B, this outward current (black triangles) elicited at potentials positive to +20 mV was of nearly identical magnitude to the ionomycin-induced current before inhibition (white circles).

Figure 5.8 $I_{Cl(Ca)}$ is enhanced then subsequently inhibited in the presence of ionomycin (5 or 10 μM; n=3). Cone photoreceptors were held at -60 mV and subjected to the standard depolarizing protocol in control conditions and during superfusion of ionomycin. (**A**) Representative example of currents elicited by a -20 mV depolarizing voltage step in control conditions (Control; solid line), at the peak increase in the presence of 10 μM ionomycin (IONO; dotted line), and following ionomycin-induced inhibition (Inhibition; dashed line). Zero current is indicated by a dashed line. (**B**) Corresponding *I-V* relations and (**C**) Ca^{2+}-activated Cl^- *Q-V* relations from the same cone, recorded in control conditions (Control; black circles), in the presence of ionomycin (IONO; white circles), and after ionomycin-induced inhibition (Inhibition; black triangles). In the presence of ionomycin, a large Ca^{2+}-activated Cl^- conductance contribution can be detected in the *I-V* relation, where the current reverses close to E_{Cl} (0 mV). No inward current is seen after ionomycin-induced inhibition (4 min of ionomycin superfusion). The large $I_{Cl(Ca)}$ increase in the presence of ionomycin is reflected in the increased Ca^{2+}-activated Cl^- *Q-V* relation. After ionomycin-induced inhibition, the Ca^{2+}-activated Cl^- tails are significantly reduced

Figure 5.8

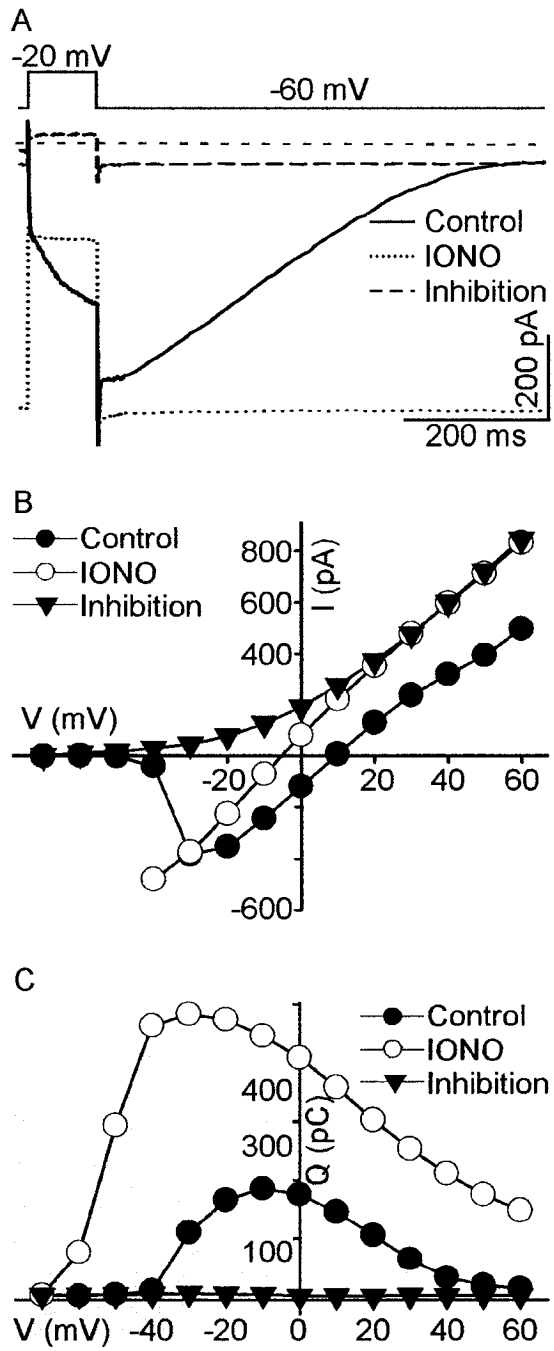
A
-20 mV
-60 mV
Control
IONO
Inhibition
200 pA
200 ms
B
Control
IONO
Inhibition
800
600
400
I (pA)
V (mV)
-20
20
40
60
-600
C
Control
IONO
Inhibition
400
300
100
Q (pC)
V (mV) -40 -20 0 20 40 60

Figure 5.9 Ionomycin (5 or 10 μM) transiently increases $I_{Cl(Ca)}$ but inhibits the current measured during depolarizing voltage steps to -20 mV (repeated every 5 or 15 sec; n=5). **(A)** Time course of current remaining from a cone photoreceptor, held at -60 mV and subjected to -20 mV depolarizing voltage steps every 15 sec in the presence of 10 μM ionomycin (indicated by the horizontal bar). The current measured during depolarizing voltage steps (Steps; black circles) decreased in amplitude in the presence of ionomycin. The Ca^{2+}-activated Cl^- tail current (Tails; white circles) was increased (peak reached after ~4 min superfusion) and then inhibited. Note that the inhibition was reduced before ionomycin was removed from the extracellular solution. **(B)** Current records from the same cone photoreceptor shown before the application of ionomycin (Control; solid line), at the peak increase created by ionomycin superfusion (Ionomycin; dotted line), and after ionomycin-induced inhibition (Inhibition; dashed line). In the presence of ionomycin, the reduced current measured during the pulses to -20 mV, and sustained $I_{Cl(Ca)}$ activation are shown. Zero current is indicated with a dashed line.

Figure 5.9

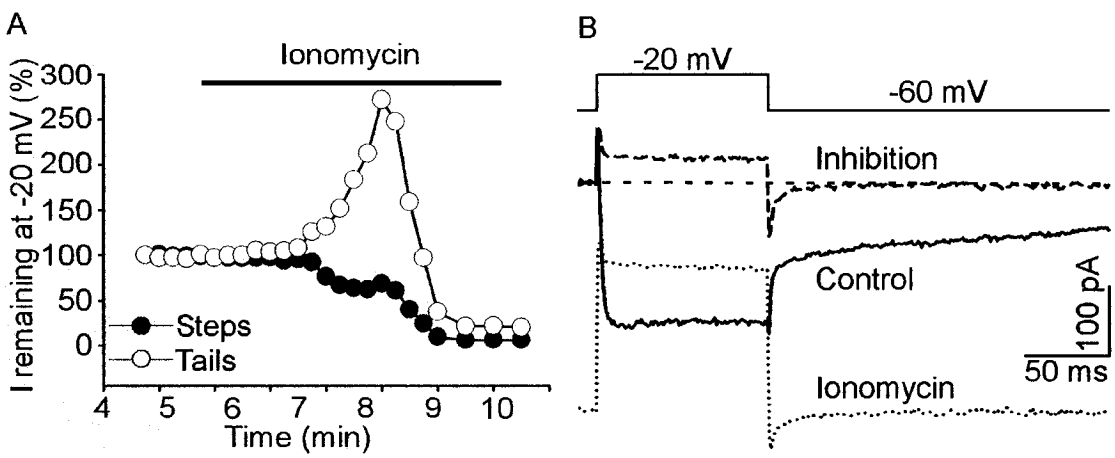
A
Ionomycin
I remaining at -20 mV (%)
300
250
200
150
100
50
0
Steps
Tails
4
5
6
7
8
9
10
Time (min)
B
-20 mV
-60 mV
Inhibition
Control
100 pA
50 ms
Ionomycin

Similar results were obtained with test pulses to -20 mV from a holding potential of -60 mV, repeated every 5 or 15 sec in the presence of ionomycin (n=5). Figure 5.9A demonstrates a representative example of the time course of current remaining measured during depolarizing voltage steps at 15 sec intervals in the presence of 10 μM ionomycin. The Ca^{2+}-activated Cl^- tail current increased in amplitude and then was inhibited by ionomycin (Tails; white circles). However, ionomycin inhibited the current measured during depolarizing voltage steps (Steps; black circles). These observations were seen in all cells tested. Current traces constructed from the same cell also illustrate the large $I_{Cl(Ca)}$ tail increase and concomitant reduction in the current recorded during the steps (Fig. 5.9B).

The initial enhancement of $I_{Cl(Ca)}$ in the presence of ionomycin likely reflects increased $[Ca^{2+}]_i$, as suggested by the Ca^{2+}-imaging experiments (Appendix 1). Whether the source of Ca^{2+} is from ionomycin-induced Ca^{2+} entry from the extracellular solution and/or from internal stores, along with depolarization evoked Ca^{2+} influx, is unknown. Also, although not identified in salamander cone photoreceptors, store-operated channels (SOCs), which are non-selective cation channels, may be contributing to increased $[Ca^{2+}]_i$ after ionomycin-induced Ca^{2+} store depletion. Mechanisms responsible for $I_{Cl(Ca)}$ inhibition following enhancement in the presence of ionomycin are unknown. Since Ca^{2+}-imaging experiments in salamander cone photoreceptors demonstrate sustained $[Ca^{2+}]_i$ increase in the presence of ionomycin, the inhibition of $I_{Cl(Ca)}$ following enhancement is likely not due to Ca^{2+} buffering and/or sequestration mechanism, reducing submembrane Ca^{2+} levels. Therefore, it seems likely that mechanisms involving Cl(Ca) channel activation may have been affected by high $[Ca^{2+}]_i$. The current

reduction during depolarizing steps indicate a decreased I_{Ca} precedes $I_{Cl(Ca)}$ inhibition. Although a change in driving force for Ca^{2+} ions is expected when $[Ca^{2+}]_i$ is high, inhibition of voltage-gated Ca channels is likely occurring.

5.7 A transient conductance is observed at -60 mV holding potential in the presence of ionomycin

For the purpose of ruling out the possibility that the transient effect of ionomycin was triggered by depolarization-evoked Ca^{2+} influx, the effect of ionomycin on current measured at -60 mV holding potential was tested. Since voltage-gated Ca channels are not open at -60 mV, $I_{Cl(Ca)}$ does not rely on Ca^{2+} influx through these channels for activation. A large transient conductance was observed at resting potential (-60 mV) when ionomycin was added to the extracellular solution (n=4). Figure 5.10 demonstrates a cone photoreceptor subjected to sample recordings at 15 sec intervals in the presence of 5 μM ionomycin. The increased conductance (40-fold) with ionomycin likely reflects Ca^{2+} entry from the extracellular solution and/or release from intracellular stores, activating Cl(Ca) channels. This increase in $I_{Cl(Ca)}$ was subsequently followed by inhibition. These results suggest that increased submembrane $[Ca^{2+}]_i$ in the presence of ionomycin is responsible for $I_{Cl(Ca)}$ activation, and possibly inhibition. Mechanisms involved in Cl(Ca) channel activation may have been affected by the increased $[Ca^{2+}]_i$.

Figure 5.10 Cl(Ca) channels may also be inhibited by high $[Ca^{2+}]_i$ achieved via ionomycin superfusion. Cone photoreceptor sample recordings were obtained every 15 sec at the holding potential of -60 mV before and during superfusion of 5 μM ionomycin. A representative example of the time course of the normalized current remaining is shown in the figure. Ionomycin caused a transient 40-fold increase in conductance. Similar results were obtained in three other cone photoreceptors.

Figure 5.10

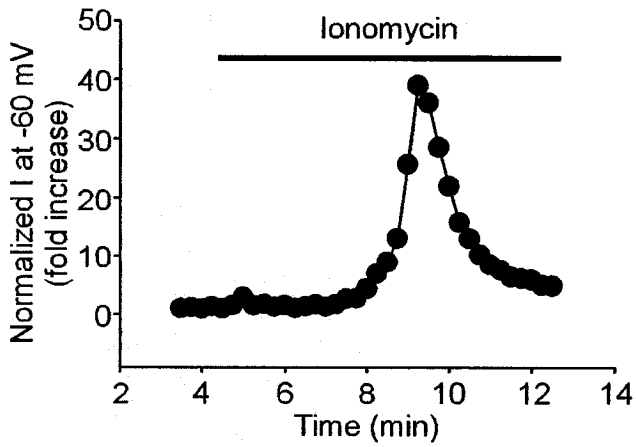
Ionomycin
Normalized I at -60 mV
(fold increase)
50
40
30
20
10
0
2
4
6
8
10
12
14
Time (min)

5.8 In the absence of extracellular Ca^{2+}, ionomycin does not activate $I_{Cl(Ca)}$

In addition to increasing Ca^{2+} flux across the plasma membrane, the hydrophobic Ca^{2+} ionophore, ionomycin, also empties intracellular Ca^{2+} stores by transporting Ca^{2+} out into the cytosol. Thus, the contribution of Ca^{2+} stores (without the influence of extracellular Ca^{2+} entry) to the enhancement of $I_{Cl(Ca)}$, which was followed by inhibition, described in the previous sections, was assessed by superfusing ionomycin in a Ca^{2+} free extracellular solution. For some of the recordings, 3 mM Mg^{2+} and 2 mM BAPTA were added to the standard bath solution. Extracellular Mg^{2+} was used to compensate for the total absence of Ca^{2+}, while BAPTA assured rapid and total elimination of Ca^{2+} ions. Figure 5.11A demonstrates the time course of current remaining during pulses to -20 mV from a holding potential of -60 mV, repeated every 15 sec. As expected, the current measured during depolarizing voltage steps, and during repolarization following those steps, both decreased when Ca^{2+} ions were removed from the extracellular solution. In cells where BAPTA was included into the superfusing solution, $I_{Cl(Ca)}$ started to decrease less then 2 min following the removal of Ca^{2+} from the extracellular solution, and no current remained after 4 min. Figure 5.11B demonstrates current traces before (Control; solid line), and 2 min (dotted line), 3 min (dashed line), and 4 min (dotted dashed line) after Ca^{2+} was removed from the extracellular solution. I-V and Ca^{2+}-activated Q-V relations are shown before (Control; black circles) and after (Ca^{2+} free; white circles) Ca^{2+} removal from the extracellular solution (Figs. 5.11D and E). When $I_{Cl(Ca)}$ inhibition was achieved in Ca^{2+} free solution, ionomycin was applied to empty the Ca^{2+} stores (Fig. 5.11A). In the absence of extracellular Ca^{2+}, ionomycin had no effect on $I_{Cl(Ca)}$ in all cell

Figure 5.11 In the absence of extracellular Ca^{2+}, ionomycin (5 or 10 μM; n=6) does not activate $I_{Cl(Ca)}$. **(A)** Representative example of the time course of current remaining (expressed as a percent of control) elicited by -20 mV pulses repeated every 15 sec. When Ca^{2+} was removed from the superfusing solution (for this example, Mg^{2+} and BAPTA were added), a decrease in both the current measured during depolarizing voltage steps (Steps; back circles) and during repolarization following those steps (Tails; white circles) was observed. When 10 μM ionomycin was introduced with the Ca^{2+} free superfusing solution, no changes in the current were observed after 10 min of superfusion. A transient conductance was seen when Ca^{2+} was re-introduced into the extracellular solution. **(B)** Current records from the same cell in control conditions (solid line) and 2 min (dotted line), 3 min (dashed line), and 4 min (dotted dashed line) after Ca^{2+} was removed from the extracellular solution. **(C)** Current traces showing a Ca^{2+} free recording (solid line; same recording that is illustrated at 4 min in **(B)**), and a recording after 10 min of ionomycin superfusion (Ca^{2+} free + IONO; dotted line). No differences were observed. The peak increase observed following the re-introduction of Ca^{2+} in the superfusate, which is characterized by sustained Ca^{2+}-activated Cl^- tails, is also shown (dashed line). Zero current is also indicated by a dashed line. **(D)** Leak-corrected *I-V* and **(E)** offset-subtracted Ca^{2+}-activated Cl^- *Q-V* relations constructed from recordings in control conditions (Control; black circles), 4 min after Ca^{2+} removal from the extracellular solution (Ca^{2+} free; white circles), 10 min after ionomycin superfusion in Ca^{2+} free solution (Ca^{2+} free + IONO; black triangles), and after $I_{Cl(Ca)}$ was reduced following re-introduction of Ca^{2+} in the extracellular solution (Inhibition; white triangles).

Figure 5.11

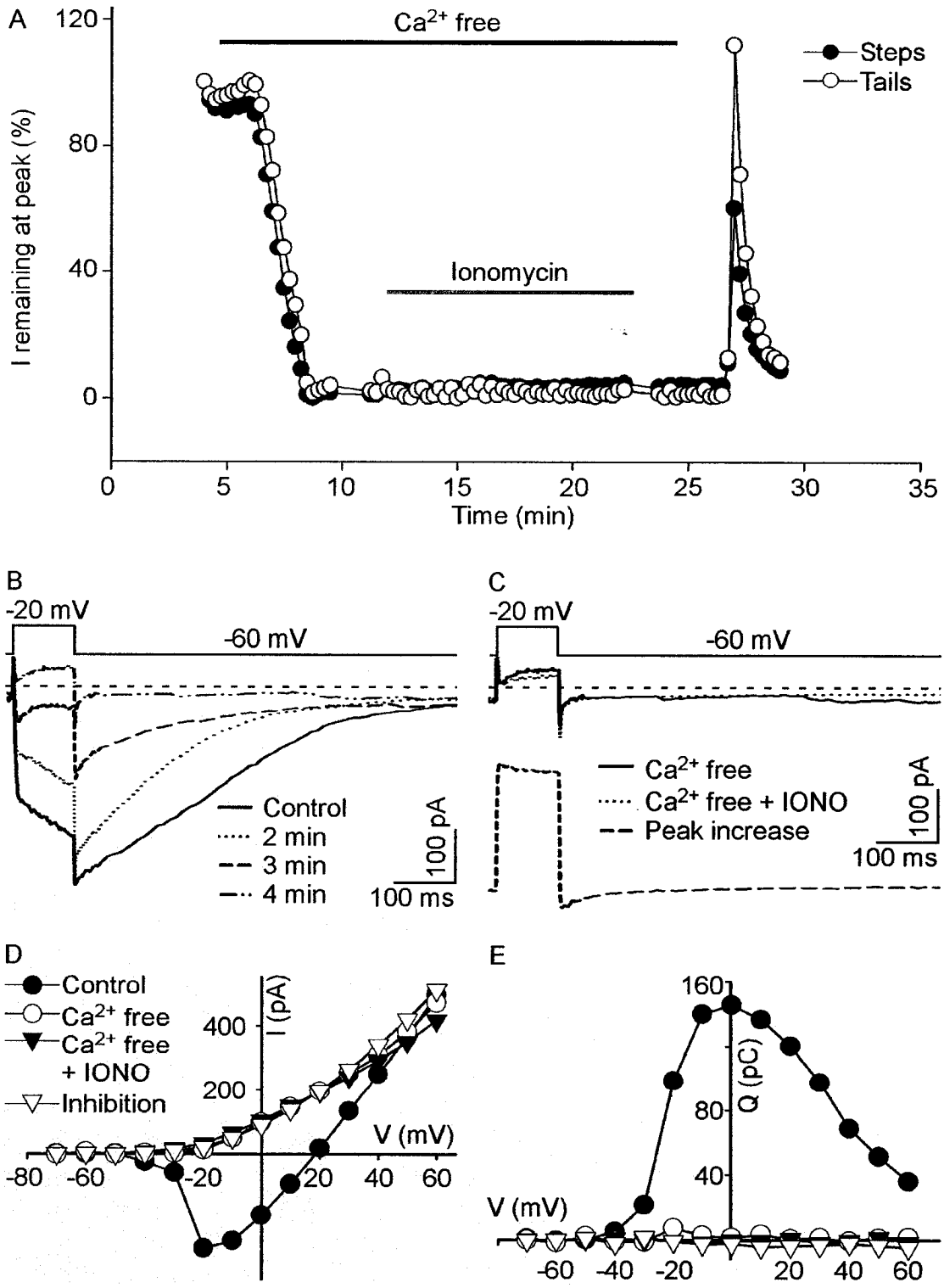
A
120
80
40
0
I remaining at peak (%)
Ca2+ free
Ionomycin
Steps
Tails
0
5
10
15
20
25
30
35
Time (min)
B
-20 mV
-60 mV
Control
2 min
3 min
4 min
100 pA
100 ms
C
-20 mV
-60 mV
Ca2+ free
Ca2+ free + IONO
Peak increase
100 pA
100 ms
D
Control
Ca2+ free
Ca2+ free + IONO
Inhibition
400
200
I (pA)
V (mV)
-80
-60
-20
20
40
60
E
160
80
40
Q (pC)
V (mV)
-60
-40
-20
20
40
60

tested (n=6). Current traces (Fig. 5.11C), *I-V* (Fig. 5.11D) and *Q-V* (Fig. 5.11E) relations recorded in Ca^{2+} free before (Ca^{2+} free) and after (Ca^{2+} free + IONO) ionomycin superfusion are unmodified. These data suggest that, similar to the results obtained in Chapter 4, Ca^{2+} release from internal stores does not participate in the activation of $I_{Cl(Ca)}$. A transient conductance similar to the effect of ionomycin superfusion in the presence of extracellular Ca^{2+} (Figs. 5.8, 5.9, and 5.10), was observed when Ca^{2+} ions were re-introduced to the extracellular solution (Fig. 5.11A). Shown in Figure 5.11C is the current trace at the peak increase (dashed line), which is characterized by sustained Ca^{2+}-activated Cl^- tail. *I-V* and Ca^{2+}-activated Cl^- *Q-V* relations (Figs. 5.11D and E), constructed from a recording after the inhibition of $I_{Cl(Ca)}$ (Inhibition; white triangles), which was induced when Ca^{2+} was re-introduced to the extracellular solution are shown in Figure 5.11D and E, respectively.

In the presence of extracellular Ca^{2+}, ionomycin superfusion induces an increase in $I_{Cl(Ca)}$, which is followed by inhibition (Figs. 5.8, 5.9, 5.10). The source of Ca^{2+} responsible for the increase in $I_{Cl(Ca)}$ could be extracellular (ionomycin-induced Ca^{2+} entry from extracellular solution) or intracellular (ionomycin-induced Ca^{2+} exit from internal stores). Since $I_{Cl(Ca)}$ was not activated by ionomycin in Ca^{2+} free extracellular solution, the present data further suggest that Ca^{2+} stores do not contribute to the activation of Cl(Ca) channels under these conditions. In addition, an increase in $I_{Cl(Ca)}$ was followed by inhibition when Ca^{2+} was re-introduced to the superfusing solution, similar to that observed with ionomycin in the presence of extracellular Ca^{2+}. These results suggest that the transient current, seen with ionomycin only when extracellular Ca^{2+} was present, is due to extracellular Ca^{2+} entry, and not release from the stores.

Whether Ca^{2+} released from Ca^{2+} stores in the presence of ionomycin when extracellular Ca^{2+} was absent was too small to increase the submembrane $[Ca^{2+}]_i$, or if the stores were too distant from the submembrane level, is unknown. Although unlikely, the possibility that the Ca^{2+} stores were depleted in the absence of Ca^{2+} in the extracellular solution cannot be ruled out. However, Krizaj et al. (1999) demonstrated, via Ca^{2+}-imaging experiments, that Ca^{2+} can be released from caffeine-sensitive stores up to 4 min in the absence of extracellular Ca^{2+}.

5.9 Summary

The activity of $I_{Cl(Ca)}$ reflects changes in submembrane $[Ca^{2+}]_i$. $I_{Cl(Ca)}$ increases during depolarization-induced Ca^{2+} influx, and decreases as Ca^{2+} diffuses away from the plasma membrane. However, as this chapter has shown, under conditions of high intracellular $[Ca^{2+}]$, $I_{Cl(Ca)}$ is inhibited instead of being persistently activated. Caffeine-sensitive Ca^{2+} stores were shown to increase submembrane Ca^{2+} levels but only during depolarizing pulses repeated at 1 sec intervals, a specific protocol that aimed to increase $[Ca^{2+}]_i$. Increased $I_{Cl(Ca)}$ amplitude presumably reflects high submembrane Ca^{2+} levels, caused by both depolarization-evoked Ca^{2+} influx and Ca^{2+} release from caffeine sensitive stores, combined with an overloaded Ca^{2+} buffering and sequestration. In these conditions, enhanced $I_{Cl(Ca)}$ was subsequently inhibited. Mechanisms involved in $I_{Cl(Ca)}$ inhibition can only be speculated, and could reflect decreased submembrane Ca^{2+} levels. For example, increased activation of pumps or transporters triggered by Ca^{2+} release from stores may explain $I_{Cl(Ca)}$ inhibition seen here (Schmid et al., 1990; Friel and Tsien, 1992; McNulty and Taylor, 1993; Orkand and Thomas, 1995). Krizaj et al. (1999) proposed the

presence of release-activated Ca^{2+} transporters (RACTs) in salamander photoreceptors. Although its identity is still unknown, RACT would be responsible for rapid Ca^{2+} reuptake into internal stores when high levels of Ca^{2+} are reached within the cell. Other mechanisms, such as rapid Ca^{2+} extrusion through plasma membrane Ca^{2+}-ATPases (PMCAs) and Ca^{2+} sequestration via Ca^{2+}-binding protein would explain a reduction of free $[Ca^{2+}]_i$ and $I_{Cl(Ca)}$ inhibition. In addition, inhibited Ca channel during conditions of high $[Ca^{2+}]_i$ would also explain reduced submembrane Ca^{2+} levels and the inability to activate Cl(Ca) channels upon depolarizations. Finally, other than reduced submembrane $[Ca^{2+}]_i$, other mechanisms, including Cl(Ca) channel down-regulation or an intermediate protein involved in the activation of $I_{Cl(Ca)}$, could explain $I_{Cl(Ca)}$ inhibition in conditions where Ca^{2+} levels seemed increased.

The voltage-clamp protocol termed 'repeated strong depolarizations' was described in Chapter 3 (Section 3.3; Fig. 3.5B). It consists of 100 ms prepulses to 0 mV from a holding potential of -60 mV applied at 2 Hz, each followed by 100 ms voltage steps decrementing every 10 mV from +20 mV to -80 mV. This protocol causes sustained Cl(Ca) channel activation and therefore presumably increases submembrane $[Ca^{2+}]_i$. When subjecting the cell to repeated strong depolarizations, persistent activation of $I_{Cl(Ca)}$ was followed by an inhibition period, which slowly recovered. Whether this inhibition is caused indirectly through voltage-gated Ca channel inhibition, directly through Cl(Ca) channel inhibition, or via a different mechanism is not clear. Cells have a necessity to move Ca^{2+} between the cytosol and storage sites by sequestration. This process is principally attributable to the action of SERCA pumps (Missiaen et al., 1991a). The inhibition of $I_{Cl(Ca)}$ following repeated strong depolarizations was increased in the

presence of SERCA pump blockers. These observations suggest that the higher the $[Ca^{2+}]_i$, the greater the inhibition of $I_{Cl(Ca)}$.

The inhibition of $I_{Cl(Ca)}$ following repeated strong depolarizations was also increased and became irreversible in the presence of the cAMP-dependent protein kinase inhibitor, H-8. This increased inhibition in the presence of H-8 is mediated by a positive shift in Ca channel activation kinetics. While phosphorylation mechanisms may increase $I_{Cl(Ca)}$ in cone photoreceptors, it seems likely that when dephosphorylation mechanisms are activated, voltage-gated Ca channels are the targets of inhibition. The protein phosphatase inhibitor, okadaic acid, increased $I_{Cl(Ca)}$ due to a negative shift of Ca channel activation. In addition, $I_{Cl(Ca)}$ was irreversibly inhibited due to a positive shift when okadaic acid was washed out. Therefore, Cl(Ca) channels are inhibited, at least in part, via a mechanism involving voltage-gated Ca channel inhibition.

Ionomycin incorporates into lipid bilayers where it operates as a Ca^{2+}/H^+ exchanger (Wheeler et al., 1994). Although $[Ca^{2+}]_i$ elevation is sustained in the presence of ionomycin (Appendix 1), superfusion with ionomycin caused a transient increase in $I_{Cl(Ca)}$, which was irreversibly inhibited. These results support a 'high $[Ca^{2+}]_i$-induced' inhibition of $I_{Cl(Ca)}$. In the presence of ionomycin, when Cl(Ca) channels were fully activated (sustained Ca^{2+}-activated Cl^- tail currents), the current measured during depolarizing voltage steps was decreased. Therefore, elevated $[Ca^{2+}]_i$ at the submembrane level seemed to first suppress voltage-gated Ca channel activity, although a change in the driving force for Ca^{2+} ions is also expected. In the absence of depolarization-evoked Ca^{2+} influx, ionomycin also caused enhancement of $I_{Cl(Ca)}$ followed by inhibition, suggesting that Ca^{2+} influx through voltage-gated Ca channels is

not responsible for the transient $I_{Cl(Ca)}$ activation. Since Cl(Ca) channels do not rely on depolarization-evoked Ca^{2+} influx for activation in the presence of ionomycin, the inhibition observed may be due to a more direct inhibition on Cl(Ca) channels or intermediate proteins involved in their activation. Ionomycin also causes Ca^{2+} extrusion from internal stores. However, in Ca^{2+} free extracellular solution, ionomycin failed to activate $I_{Cl(Ca)}$, suggesting that Ca^{2+} stores do not contribute to Cl(Ca) channel activation.

Chapter 6

Discussion

The overall goal of this dissertation was to describe features governing the gating of $I_{Cl(Ca)}$ to better understand their physiological function in cone photoreceptors. The first hypothesis tested if Cl(Ca) channels are activated by a rise in intracellular Ca^{2+} ($[Ca^{2+}]_i$) close to the cell membrane, such as during Ca^{2+} entry through voltage-gated Ca channels at the synaptic terminal. The deactivating kinetics of Ca^{2+}-activated Cl^- tail currents were suggested to reflect Ca^{2+} diffusion and buffering away from Cl(Ca) channels located at the plasma membrane. It was hypothesized that $I_{Cl(Ca)}$ would follow $[Ca^{2+}]_i$ levels and that Ca^{2+} stores would contribute to channel gating. The results suggest that Ca^{2+} release from Ca^{2+} stores does not increase the submembrane level high enough to modulate $I_{Cl(Ca)}$. Cl(Ca) and Ca channels at the plasma membrane of cone synaptic terminals may be physically distant from Ca^{2+} stores. It was also hypothesized that Cl(Ca) channel inhibition was caused by high levels of $[Ca^{2+}]_i$, and that this effect was mediated by the phosphorylation state of intracellular proteins. Dephosphorylation mechanisms were shown to be involved in high $[Ca^{2+}]_i$-induced inhibition of $I_{Cl(Ca)}$. Voltage-gated Ca channels involved in $I_{Cl(Ca)}$ activation, as well as the Cl(Ca) channels themselves, were proposed to be possible targets of this inhibition.

6.1 Cl(Ca) channels are activated by submembrane $[Ca^{2+}]_i$

A number of studies have proposed the exclusive regulation of Cl(Ca) channel activity by $[Ca^{2+}]_i$ in neurons (Mayer, 1985; Owen et al., 1986; Bader et al., 1987; Johansen and Kleinhaus, 1988; Rogawski et al., 1988; Barnes and Hille, 1989; Korn and Horn, 1989; Currie and Scott, 1992; Sanchez-Vives and Gallego, 1994; Currie et al., 1995). In salamander cone photoreceptors, the steep dependence of Cl(Ca) channels on $[Ca^{2+}]_i$ was linked to Ca^{2+} influx through voltage-gated Ca channels as the non-specific

Ca channel blocker, Cd^{2+}, inhibited Cl(Ca) channel activation (Barnes and Hille, 1989; Barnes and Bui, 1991; Morgans et al., 1998). Such relationships between Ca^{2+} entry through voltage-gated Ca channels and $I_{Cl(Ca)}$ activation have been observed in different systems including mammalian neurons and smooth muscles (Akasu et al., 1990; Akbarali and Giles, 1993). The present study extends this body of evidence and demonstrates $I_{Cl(Ca)}$ activation by submembrane $[Ca^{2+}]_i$ in cone photoreceptors.

6.1.1 $I_{Cl(Ca)}$ activation is tightly coupled to Ca^{2+} influx

This dissertation has demonstrated the dependence of $I_{Cl(Ca)}$ on $[Ca^{2+}]_i$ with several lines of evidence, such as current inhibition by Ca^{2+} chelators, lanthanum (a voltage-gated Ca channel blocker), and the substitution of Ca^{2+} with Ba^{2+} in the extracellular solution. In addition, depolarizations that induce Ca^{2+} influx through voltage-gated Ca channels activated $I_{Cl(Ca)}$ and the L-type Ca channel agonist, (±)-Bay K8644, enhanced the Ca^{2+}-activated Cl^- tails in a manner that mirrored enhancement of Ca currents. The same voltage dependence for Ca^{2+} influx is reflected in the bell-shaped *Q-V* relations for Ca^{2+}-activated Cl^- tail currents, which were maximal between the voltage ranges of 0 to +10 mV, near the peak of voltage-gated Ca channel currents in salamander cone photoreceptors. In addition, the amount of charge crossing the membrane carried by Cl^- ions was small following test pulses to very positive potentials (e.g., +60 mV). Such changes in potential do not elicit voltage-gated Ca channel currents due to the reduction in driving force for Ca^{2+} influx. Using brief depolarizing pulses of different durations and measuring Ca^{2+}-activated Cl^- tail current after repolarization, it has previously been shown in salamander cone photoreceptors (Barnes and Hille, 1989)

and in goldfish retinal bipolar cells (Okada et al., 1995) that Ca^{2+}-activated Cl^- tail currents follow $[Ca^{2+}]_i$ dynamics. In these studies, increasing the duration of the preceding depolarization, which prolongs the activation time of voltage-gated Ca channels and promotes Ca^{2+} accumulation (i.e. build up) in the cell, generated larger Ca^{2+}-activated Cl^- tail currents with a slower decline.

6.1.2 Deactivation of Ca^{2+}-activated Cl^- tail currents reflects changing submembrane Ca^{2+} levels

The saturated exponential approach used in the present work to fit the decay of $I_{Cl(Ca)}$ suggests that the predominant factor governing deactivation of Cl(Ca) channels is simple one-dimensional diffusion of $[Ca^{2+}]_i$ (Scott et al., 1995). That the decaying Ca^{2+}-activated Cl^- tail currents reflects a progressive decrease in $[Ca^{2+}]_i$, and not intrinsic inactivation of $I_{Cl(Ca)}$, was originally proposed by Currie et al. (1995). In that study, the authors observed the re-activation of declining Ca^{2+}-activated Cl^- tail currents in rat dorsal root ganglia (DRG) when generating a steep $[Ca^{2+}]_i$ increase via the photorelease of caged Ca^{2+}. In this dissertation, saturation of the exponential function, achieved by convolution with a modified Hill equation, is proposed to reflect occupancy of all available Ca^{2+} binding sites on Cl(Ca) channels or other regulatory partners. Single exponential behavior, as seen during the later part of the current trajectory, implies diffusion of Ca^{2+} away from the plane of the membrane, suggesting that Ca channels and Cl(Ca) channels are located in close proximity to each other at the membrane.

Since Ca^{2+} influx is required for vesicle fusion, Ca channels are presumably located in close proximity to the ribbon synapse, which orchestrates the flow of neurotransmitter-filled vesicles to the release site. Similarly, Cl(Ca) channels involved

may be localized at the cone pedicle. In fact, ion channels mediating $I_{Cl(Ca)}$ in salamander rods are thought to be preferentially located at the terminal (MacLeish and Nurse, 2000).

6.1.3 Cone photoreceptor Cl(Ca) channels may be co-localized with L-type Ca channels at the plasma membrane

Tightly linked $[Ca^{2+}]_i$-Cl(Ca) channel coupling that is only suppressed under a high-capacity buffering system provides evidence that Cl(Ca) channels and voltage-gated Ca channels lie in close proximity to one another and form a submembrane microsystem. The co-localization of other Ca^{2+}-dependent channels and voltage-gated Ca channels has also been suggested for Ca^{2+}-activated K channels (Gola and Crest, 1993) and Ca^{2+}-activated non-selective cation channels (Partridge et al., 1994) in *Helix* neurons. In addition, the coupling of specific types of Ca channels with Ca^{2+}-dependent channels has also been suggested. For example, the source of Ca^{2+} influx for the activation of Cl(Ca) and K(Ca) channels in mouse sympathetic neurons appeared different because Cl(Ca) channels are activated by Ca^{2+} influx through L- and P-type Ca channels while K(Ca) channels are activated by N-type Ca channels (Martinez-Pinna et al., 2000). Given the prevalence of L-type Ca channels in salamander cone photoreceptors (Wilkinson and Barnes, 1996), the specific co-localization of Cl(Ca) channels and L-type Ca channels is plausible. The activation of $I_{Cl(Ca)}$ following Ca^{2+} influx specifically through L-type Ca channels has also been proposed in other systems, including cardiac myocytes (Zygmunt and Gibbons, 1992) and oesophageal smooth muscle cells (Akbarali and Giles, 1993), where L-type Ca channels are predominant. In salamander cone photoreceptors, Cl(Ca) channels likely outnumber voltage-gated Ca channels. This postulation is based on single channel properties and maximum cell current amplitudes of both of these channels.

Voltage-gated Ca channels have a large conductance and small whole-cell I_{Ca}. On the other hand, Cl(Ca) channels have a small conductance, as judged from the smoothness of the current trajectories, and large whole-cell $I_{Cl(Ca)}$. Hence, a model in which a small number of Ca channels are closely surrounded by clusters of Cl(Ca) channels appears to be a reasonable proposal.

6.1.4 Cone Cl(Ca) channels may be directly activated by Ca^{2+}

In cone photoreceptors, the $[Ca^{2+}]_i$-Cl(Ca) channel coupling mechanism, whether it be direct or indirect via Ca^{2+}-binding proteins or via Ca^{2+}-dependent enzymes, is unknown. In the present study, calmodulin was excluded from being a possible intermediate between Ca^{2+} and Cl(Ca) channel activation, as also suggested in rat parotid secretory cells (Arreola et al., 1998), and therefore, direct Ca^{2+} binding to the channel protein is suggested. However, in the present dissertation, all recordings were performed with intracellular ATP, which is required for Ca channel activity, and therefore Cl(Ca) channel activation via a Ca^{2+}-dependent phosphorylation mechanism in not excluded. Other studies using excised patches have suggested direct Ca^{2+} binding to Cl(Ca) channel proteins in a variety of tissues, based on the fact that there was no evidence of rundown of channel activity in the absence of ATP (Martin, 1993; Koumi et al., 1994; Collier et al., 1996; Nilius et al., 1997b).

6.2 Negligible role of Ca^{2+} released from Ca^{2+} stores in gating of salamander cone $I_{Cl(Ca)}$

The present dissertation examined the role of intracellular Ca^{2+} stores in the activation of Cl(Ca) channels. The mitochondria and the endoplasmic reticulum (ER) are

two important regulators of $[Ca^{2+}]_i$. However, the present work only investigated the contribution of Ca^{2+} released from the latter by using agents that specifically activate or inhibit channels and pumps responsible for Ca^{2+} movement across the ER membrane. Since it is known that Ca^{2+} influx activates Ca^{2+} stores in cones (Krizaj et al., 1999), changes in Cl(Ca) channel relaxation kinetics after manipulating the ryanodine and IP_3 sensitive Ca^{2+} stores were investigated.

6.2.1 Ca^{2+} responsible for $I_{Cl(Ca)}$ activation is not amplified by calcium-induced Ca^{2+}-release from ryanodine-sensitive Ca^{2+} stores

Ca^{2+}-induced Ca^{2+}-release (CICR) is the mechanism of excitation-contraction coupling in cardiac myocytes where a tight coupling of Ca^{2+} influx and Ca^{2+} release is achieved by the positioning of ryanodine receptors (RyRs) within 100 nm of the voltage-gated Ca channels (Rios and Stern, 1997; Stern, 1998). One isoform of the ryanodine receptor, RyR2, has recently been identified in subellipsoid spaces and cell bodies of salamander photoreceptors (Krizaj et al., 2004). In the present study, blocking CICR from ryanodine-gated Ca^{2+} stores did not modulate the magnitude of $I_{Cl(Ca)}$ activated by depolarization. These results suggest that Cl(Ca) channels are activated by I_{Ca} without amplification by a ryanodine-sensitive mechanism, and that under the specific conditions used in the present dissertation, there is no evidence of CICR in salamander cone photoreceptors. Similar results were obtained in rat sympathetic neurons (Thayer et al., 1988b; Thayer and Miller, 1990) and in avian sensory neurons (Ivanenko et al., 1993). It is also possible (but unlikely, due to the appearance of the tail current) that $I_{Cl(Ca)}$ activation was saturated by I_{Ca} and CICR block could not be detected. In addition, the effect of blocking CICR may not have been detected by the sampling protocol used in

this dissertation. The standard depolarizing protocol used in this study consisted of voltage steps repeated every 3 or 5 sec, and therefore, increased $[Ca^{2+}]_i$ originating from CICR may not have been detected if it occurred between these sampling periods. However, Ca^{2+}-imaging studies revealed that the CICR response occurs over a duration of 1 min (Alonso et al., 1999; Collier et al., 2000; Solessio and Lasater, 2002).

6.2.2 RyR channels may be spatially distant from Cl(Ca) channels in salamander cone photoreceptors

$I_{Cl(Ca)}$ activation by Ca^{2+} release from caffeine-sensitive stores has been shown in isolated chick dorsal root ganglia (Ivanenko et al., 1993; Kenyon and Goff, 1998). Using a similar protocol, $I_{Cl(Ca)}$ was not modulated by Ca^{2+} release from caffeine-sensitive stores in the present dissertation. These results were surprising since previous studies have suggested penetration of the smooth ER into synaptic terminals of frog photoreceptors (Mercurio and Holtzman, 1982; Ungar et al., 1984), and Ca^{2+} release from caffeine-sensitive stores has also been reported in photoreceptor synaptic terminals (Steele et al., 2002). The present data, together with the fact that the deactivation kinetics of Ca^{2+}-activated Cl^- tail currents remained unchanged following Ca^{2+} reuptake inhibition via the blockade of sarcoplasmic/endoplasmic reticulum Ca^{2+}-ATPase (SERCA) pumps, suggest that intracellular Ca^{2+} release sites are physically distant from Cl(Ca) channels at the plasma membrane. In avian sensory neurons, where Cl(Ca) channels activate and deactivate in a manner similar to that shown here in cones, it was calculated that the Cl(Ca) channel activation site lies up to ~10 times closer to the Ca channel source than the Ca^{2+} stores (Ward and Kenyon, 2000). Ward and Kenyon (2000) developed a Ca^{2+} diffusion model that indicated that the distance between voltage-gated Ca channels

located at the plasma membrane and RyRs is greater than 600 nm. Thus, Ca channel-mediated Ca^{2+} influx dominates the gating of Cl(Ca) channels, and this model may provide an estimate for the physical separation of the channels and their source in photoreceptors. Although the data presented here do not exclude the possibility that some voltage-gated Ca channels and RyR channels are positioned close to each other in salamander cone photoreceptors, it seems unlikely that the activity of these RyRs will be tightly coupled to Ca^{2+} influx via voltage-gated Ca channels and Cl(Ca) activation.

6.2.3 Ca^{2+} release from internal stores may not contribute to submembrane Ca^{2+} levels

Other mechanisms may explain the lack of $I_{Cl(Ca)}$ modulation in the presence of caffeine. $I_{Cl(Ca)}$ in salamander cones seems to correlate with increased $[Ca^{2+}]_i$ near the plasma membrane, which could possibly reach concentrations in the micromolar range. For example, Ward and Kenyon (2000) have estimated persistent Cl(Ca) channel activation with 0.5 μM free Ca^{2+} in avian sensory neurons. The use of caffeine alone may not have increased submembrane $[Ca^{2+}]_i$ enough to increase $I_{Cl(Ca)}$ amplitude. In fact, some studies have suggested that caffeine only raises $[Ca^{2+}]_i$ by approximately 200-600 nM in neurons (Thayer et al., 1988b; Mironov et al., 1993; Shmigol et al., 1995; Yoshizaki et al., 1995), probably a concentration not high enough to activate $I_{Cl(Ca)}$. In addition, Ca^{2+}-imaging studies in neurons suggest that high $[Ca^{2+}]_i$ following exposure to caffeine does not reach submembrane regions (Hernandez-Cruz et al., 1990; Mironov et al., 1993). In salamander, Krizaj et al. (2003) demonstrated that caffeine did not evoke an increase in $[Ca^{2+}]_i$ in inner segments of cones. PMCAs extrude Ca^{2+} from the cone inner segment and synaptic terminal region (Krizaj and Copenhagen, 1998). It was

suggested that Ca^{2+} extrusion via PMCAs was particularly efficient in cone inner segments, thereby masking the caffeine-evoked increase in Ca^{2+} levels. The authors used the PMCA inhibitor lanthanum (La^{3+}) to reveal this effect. However, this unmasking technique could not be used in the present study, since La^{3+} produced complete and irreversible inhibition of $I_{Cl(Ca)}$, probably due to its well-known blocking effect on voltage-gated Ca channels (Hagiwara and Takahashi, 1967). Although caffeine- and ryanodine-sensitive Ca^{2+} stores in neurons may be subjected to CICR mechanisms (Friel and Tsien, 1992; Marrion and Adams, 1992), a physiological role for these stores in cone photoreceptors has not been described.

6.2.4 Cl(Ca) channels are likely not regulated by IP_3-sensitive Ca^{2+} stores

Phospholipase C beta (PLCβ) hydrolyzes membrane phospholipid PIP_2 to generate IP_3 and DAG (Berridge et al., 2000). Different studies suggest that PLC may be constitutively stimulated by cGMP and Ca^{2+} in the photoreceptor outer segment (Ghalayini and Anderson, 1987; Haque et al., 1998). It remains unclear, however, which isoform of PLC is expressed in cone photoreceptors and whether PLC is found at synaptic terminal. A study by Gan and Iuvone (1997) suggested the activation of PLC in photoreceptor inner segments, and possibly synaptic terminals, via Ca^{2+} influx through dihydropyridine-sensitive channels. In addition, different retinal neuromodulators, such as dopamine, could also contribute to IP_3 synthesis (Jin et al., 2003). Although dopamine D1, D2, and D4 receptor subtypes have been localized to both rod and cone photoreceptor inner segments (Cohen et al., 1992; Hare and Owen, 1995; Krizaj et al., 1998), dopamine-mediated IP_3 production has yet to be established in cone

photoreceptors. Dopamine production in the retina is thought to originate from specific subpopulations of amacrine, interplexiform, and bipolar cells (Krizaj and Witkovsky, 1993; Hare and Owen, 1995).

Although the production of IP_3 in cone photoreceptors remains unclear, Peng et al. (1991) localized expression of IP_3R to the salamander photoreceptor synaptic terminal. The specific association of IP_3 receptors with synaptic terminals suggests a role for IP_3 in synaptic modulation, especially with respect to transmitter release. However, Ca^{2+} release from IP_3-sensitive Ca^{2+} stores generally did not modulate $I_{Cl(Ca)}$ in this dissertation. Only on one occasion in my work, when cellular $[Ca^{2+}]_i$ was probably disturbed, did the presence of IP_3 modulate $I_{Cl(Ca)}$. Activation of $I_{Cl(Ca)}$ by Ca^{2+} released from IP_3-sensitive stores in cultured DRG neurons has also not been consistently demonstrated (Currie and Scott, 1992). The lack of IP_3-induced modulation of $I_{Cl(Ca)}$ in salamander cone photoreceptors could be due to the high level of Ca^{2+}-binding proteins in these neurons, low IP_3 receptor density, or the size and distribution of Ca^{2+} stores relatively far from the synaptic terminal. Photoreceptor ER in lower vertebrates is mostly located at the subellipsoid region and not at the synaptic terminal, which could explain the present results. In addition, rapid Ca^{2+} clearance upon release from internal stores via transporters and pumps, as previously mentioned, may contribute to Ca^{2+} buffering to resting levels in cone photoreceptors.

6.3 Ca^{2+} released from caffeine-sensitive stores contributes to $I_{Cl(Ca)}$ regulation only when Ca^{2+} levels are increased

Ca^{2+} stores in general do not contribute to submembrane $[Ca^{2+}]_i$ in salamander cone photoreceptors. However, caffeine-sensitive stores may influence submembrane

$[Ca^{2+}]_i$ when $[Ca^{2+}]_i$ is enhanced, such as during repetitive depolarizing pulses that cause Ca^{2+} influx through voltage-gated Ca channels. Repetitive depolarizing pulses (steps to -20 mV from a holding potential of -60 mV repeated between 1 and 5 sec) caused a cumulative increase in the Ca^{2+}-activated Cl^- tail currents, which has been referred to as current 'build up' (Barnes and Hille, 1989). This increase in current is thought to reflect a localized increase in $[Ca^{2+}]_i$, which is caused by reduced Ca^{2+}-buffering and/or diffusion. The available mechanisms for rapidly removing Ca^{2+} from the area near the membrane, the PMCAs, become saturated by the repeated depolarizations, which continually allow Ca^{2+} to enter the cell (Barnes and Bui, 1991). In the present study, current increase caused by repetitive depolarizing pulses was enhanced in the presence of caffeine. Ca^{2+} release from caffeine-sensitive stores most likely modulated $I_{Cl(Ca)}$ by raising global free Ca^{2+} levels, thereby saturating mechanisms responsible for resetting $[Ca^{2+}]_i$ back to resting levels. Repetitive depolarizing pulses may also have increased luminal ER Ca^{2+} levels, which greatly enhance caffeine to produce full depletion of stores (Shmigol et al., 1996). In addition, store-operated channels (SOCs) may have contributed to the increased $I_{Cl(Ca)}$ under these conditions. Ca^{2+} influx through SOC occurs via an unknown mechanism when Ca^{2+} stores become depleted (Putney, 1986; Putney, 1990). Store-operated Ca^{2+} entry (also called capacitive Ca^{2+} entry) has not been described in salamander cone photoreceptors. Whatever the mechanism, sustained activation of $I_{Cl(Ca)}$ was followed by irreversible inhibition of the current. $I_{Cl(Ca)}$ inhibition following persistent activation, as seen in the present study, is suggested to be regulated in part by the Ca^{2+}-dependent phosphorylation state of the Ca channel or related proteins, which is described below.

6.4 High $[Ca^{2+}]_i$-induced inhibition of $I_{Cl(Ca)}$

When the overall $[Ca^{2+}]_i$ was strongly increased in cones, i.e. following $[Ca^{2+}]_i$ overload at the submembrane level, $I_{Cl(Ca)}$ was inhibited. This process, which was referred to as 'high $[Ca^{2+}]_i$-induced inhibition' in this dissertation, has so far not been addressed in the literature. Mechanisms underlying high $[Ca^{2+}]_i$-induced inhibition of $I_{Cl(Ca)}$ is in part mediated via the dephosphorylation of voltage-gated Ca channels at the plasma membrane. Inhibition of voltage-gated Ca channels would prevent depolarization-induced Ca^{2+} influx and subsequent Cl(Ca) channel activation. However, a more direct inhibitory pathway on the Cl(Ca) channels was suggested with experiments using ionomycin to activate $I_{Cl(Ca)}$. High $[Ca^{2+}]_i$-induced inhibition of $I_{Cl(Ca)}$ may therefore involve a fast inhibitory mechanism on voltage-gated Ca channels, followed by slower inhibition of Cl(Ca) channels.

6.4.1 Caffeine-sensitive stores regulate $I_{Cl(Ca)}$ when submembrane $[Ca^{2+}]_i$ is overloaded

Increased $I_{Cl(Ca)}$ followed by inhibition was observed with repetitive depolarizing pulses at 1 sec intervals in the presence of caffeine. Krizaj et al. (1999) showed via Ca^{2+}-imaging experiments that caffeine evoked a transient increase in $[Ca^{2+}]_i$, which was followed by a prolonged depression of $[Ca^{2+}]_i$ in salamander rods, somewhat similar to the present results in cones when protocols aimed at increasing $[Ca^{2+}]_i$ were used in the presence of caffeine. The authors rule out voltage-gated Ca channels as the only source of $[Ca^{2+}]_i$ depression and propose that a release-activated Ca^{2+} transporter (RACT), the identity of which is unknown, is responsible for the depressed $[Ca^{2+}]_i$ following Ca^{2+}-release from caffeine-sensitive stores. Caffeine-induced Ca^{2+} release from stores has

been suggested to stimulate Ca^{2+}-reuptake into the ER in other cells (Friel and Tsien, 1992; Orkand and Thomas, 1995; Cseresnyes et al., 1997; Lara et al., 1997; Golovina and Blaustein, 1998). Therefore, the inhibition seen after caffeine application during repetitive depolarizing pulses could reflect caffeine-induced depletion of Ca^{2+} stores, which stimulate Ca^{2+} reuptake into these compartments and removal from the cytosol. However, although RACTs have yet to be identified in salamander cones, this system alone is probably not responsible for the lack of Cl(Ca) channel activation, which likely reflects reduced submembrane $[Ca^{2+}]_i$. Therefore, the combined effects of systems responsible for Ca^{2+} clearance from submembrane levels, such as PMCAs and Ca^{2+}-binding proteins, would likely be needed to explain $I_{Cl(Ca)}$ inhibition. However, $I_{Cl(Ca)}$ inhibition may also be explained by high $[Ca^{2+}]_i$-induced inhibition of mechanisms involved in Cl(Ca) channel activation.

6.4.2 Mechanisms involved in $I_{Cl(Ca)}$ activation may be disrupted by high $[Ca^{2+}]_i$

Under control conditions, repeated strong depolarizations (believed to increase $[Ca^{2+}]_i$), resulted in sustained $I_{Cl(Ca)}$ activation, which was followed by a significant inhibition. The inhibition seen following this protocol was referred to as 'high $[Ca^{2+}]_i$-induced' inhibition of $I_{Cl(Ca)}$. $I_{Cl(Ca)}$ reduction following repeated strong depolarizations was greater in the presence of SERCA pump inhibitors, consistent with the idea that the inhibition of $I_{Cl(Ca)}$ is due to increased intracellular Ca^{2+} levels. Mechanisms responsible for high $[Ca^{2+}]_i$-induced inhibition of $I_{Cl(Ca)}$, however, can only be speculated. High submembrane Ca^{2+} levels may down-regulate voltage-gated Ca channels, thereby inhibiting depolarization-evoked Ca^{2+} influx and $I_{Cl(Ca)}$ activation. However, although

inhibited, $I_{Cl(Ca)}$ is not abolished after repeated strong depolarization, and therefore, Ca channels are not completely 'non-conducting'. Another explanation for high $[Ca^{2+}]_i$-induced inhibition of $I_{Cl(Ca)}$ involves the activation of some mechanisms that reduce the number of Cl(Ca) channels (internalization), reduce their open probability or lower their sensitivity to $[Ca^{2+}]_i$.

6.4.3 Phosphorylation mechanisms affect Cl(Ca) channel activation

The effects of phosphorylation on Cl(Ca) channel deactivation was also examined. Repetitive strong depolarizations were tested in the presence of the protein kinase inhibitor H-8. When phosphorylation was prevented with H-8, repetitive strong depolarizations induced a positive shift in Ca channel activation and irreversibly inhibited $I_{Cl(Ca)}$. The contribution of dephosphorylation mechanisms to voltage-gated Ca channel inhibition and subsequent $I_{Cl(Ca)}$ reduction with no recovery, was also shown with okadaic acid, a type 1 (PP1) and 2A (PP2A) protein phosphatase inhibitor. Ca channel activity was increased under phosphorylating conditions and inhibited under dephosphorylating conditions due to negative and positive shifts in the channel activation curve, respectively. This general view of the roles of phosphorylation and dephosphorylation in L-type Ca channel regulation, via a diversity of signaling pathways, is well established in different systems (Gutierrez, 1994; Groschner et al., 1995; Kamp and Hell, 2000). Equilibrium between levels of active PKA and phosphatases (PP1, PP2A) thus seems responsible for Ca channel tuning. L-type Ca channels in photoreceptors are regulated by G protein-coupled receptors via multiple cAMP/PKA pathways (Stella and Thoreson, 2000; Stella et al., 2002). For example, Stella et al. (2002) suggested that activation of

adenosine (A_2) receptors in salamander rods stimulates PKA, which inhibits L-type Ca channels. In addition, Rabl and Thoreson (2002) demonstrated Ca^{2+}-dependent inactivation of L-type Ca channels in rods, although phosphorylation and dephosphorylation were not investigated in this regard. The results presented in the present dissertation confirm that protein kinases and phosphatases regulate L-type Ca channels in cone photoreceptors. These results suggest the presence of basally active protein kinases and phosphatases regulating voltage-gated Ca channels in salamander cones. A balance between basal phosphorylation-dephosphorylation turnovers must be responsible for the modulation of synaptic transmission at the photoreceptor terminal. The specific mechanisms by which the Ca channel activation state is modulated by phosphorylation, either directly on the channel itself or through intermediate mechanisms, remains to be investigated. Dephosphorylation that leads to inhibition of Ca channels under conditions of high intracellular Ca^{2+} could represent an effective protective mechanism for photoreceptors.

6.4.4 Direct Cl(Ca) channel inhibition may explain $I_{Cl(Ca)}$ inhibition when submembrane Ca^{2+} levels are elevated

The Cl(Ca) channel *I-V* relation, which exhibited some outward rectification, was similar under the repeated strong depolarization paradigm and when $[Ca^{2+}]_i$ was increased with the Ca^{2+} ionophore ionomycin. The ionomycin-evoked current reversed near the predicted E_{Cl}. The increase in $I_{Cl(Ca)}$ in the presence of ionomycin could be explained by ionomycin-mediated Ca^{2+} movement across the plasma membrane; however, Ca^{2+} influx through SOCs may also be involved. The activation of SOC at the plasma membrane, following depletion of internal Ca^{2+} stores, has previously been

shown to modulate Cl(Ca) channels in *Xenopus* oocytes (Thurman, 2000). However, in the presence of ionomycin, oocyte $I_{Cl(Ca)}$ is characterized by a 'fast' and 'slow' component, quite different from what is seen in cones. The fast component reflects Ca^{2+} release from internal stores, whereas store-operated Ca^{2+} entry is responsible for the slow component (Yoshida and Plant, 1992; Morgan and Jacob, 1994). The presence or absence of SOCs remains to be investigated in salamander cone photoreceptors. In the present dissertation, although $[Ca^{2+}]_i$ was increased in a sustained manner in the presence of ionomycin, persistent $I_{Cl(Ca)}$ activation was followed by inhibition. Since $I_{Cl(Ca)}$ activation does not depend on depolarization-evoked Ca^{2+} influx in these conditions, mechanisms other than voltage-gated Ca channel dephosphorylation, including direct inhibition of Cl(Ca) channels or proteins involved in their activation, may contribute to 'high $[Ca^{2+}]_i$-induced' $I_{Cl(Ca)}$ inhibition.

Whether the mechanism by which $I_{Cl(Ca)}$ is inhibited following the different conditions used in the present study (i.e. repetitive depolarizing pulses, repeated strong depolarizations, and ionomycin) is the same is unknown. However, in all cases, abnormally high levels of $[Ca^{2+}]_i$ seemed to be required. Since I_{Ca} appeared to be reduced before $I_{Cl(Ca)}$, a fast inhibition on Ca channels followed by a slower Cl(Ca) channel inhibition is suggested.

Chapter 7

Conclusion

Although the dependence of $I_{Cl(Ca)}$ activation on $[Ca^{2+}]_i$ has been characterized, little is known about the role of Ca^{2+} stores in the gating of $I_{Cl(Ca)}$. The present dissertation investigated the contribution of both ryanodine and IP_3 receptor-gated Ca^{2+} stores in tiger salamander cone photoreceptors. The coupling of Ca^{2+} entry via L-type Ca channels, and Cl(Ca) channel activation was found to be saturable, but generally defined by diffusion from submembrane microdomains. The duration of $I_{Cl(Ca)}$ activation is suggested to be set by the rate at which the submembrane intracellular Ca^{2+} load is brought back to resting levels. $I_{Cl(Ca)}$ reflects the Ca^{2+} concentration close to the membrane and can therefore represent a physiological index of $[Ca^{2+}]_i$ and its handling in this microdomain. While the presence of caffeine- and IP_3-sensitive Ca^{2+} stores in cone photoreceptors was confirmed, it was found that the stores had little effect on normal Cl(Ca) channel gating. However, intracellular stores do contribute to cellular Ca^{2+} concentration and its effect on $I_{Cl(Ca)}$. When high levels of $[Ca^{2+}]_i$ were achieved via simultaneous $[Ca^{2+}]_i$-loading and store emptying, inhibition of the mechanisms underlying $I_{Cl(Ca)}$ activation occurred. This inactivation was shown to be due, at least in part, to disrupted dephosphorylation mechanisms on voltage-gated Ca channels. Cl(Ca) channel inhibition via mechanisms other than voltage-gated Ca channel inhibition is also proposed. This suggests a feedback mechanism by which sustained Ca^{2+} influx, which is maximal in darkness, can cause the release of Ca^{2+} from internal stores, but creates inhibition of Ca channels during periods of high intracellular Ca^{2+} and maintain a dynamic equilibrium.

7.1 Future studies

The data collected in the present dissertation were interpreted based on the following model: In cone photoreceptors, $I_{Cl(Ca)}$ activation arises following depolarization-evoked Ca^{2+} influx through voltage-gated L-type Ca channels, which are located in close proximity to Cl(Ca) channels at the plasma membrane. Upon Ca^{2+} influx, a 'microgradient' is formed as the concentration of Ca^{2+} ions extend away from the site of entry. The duration of $I_{Cl(Ca)}$ closely reflects the interval of elevated $[Ca^{2+}]_i$ close to the plasma membrane above threshold for current activation. When all available Cl(Ca) channels are activated and when all Ca^{2+} binding sites are saturated, sustained $I_{Cl(Ca)}$ activation follows. However, when global $[Ca^{2+}]_i$ is excessively elevated, $I_{Cl(Ca)}$ is inhibited. To test the regulation of $I_{Cl(Ca)}$ by $[Ca^{2+}]_i$, high temporal and spatial resolution Ca^{2+}-imaging techniques are needed to measure differences in submembrane Ca^{2+} levels and correlate them with changes in whole-cell $I_{Cl(Ca)}$. Combined patch-clamp and Ca^{2+}-imaging experiments are necessary to observe expected simultaneous changes in $[Ca^{2+}]_i$ and whole-cell $I_{Cl(Ca)}$ during different voltage-step protocols, as used in the present study. In addition, understanding the state of the Ca^{2+} stores (degree of loading vs. rate of leakage) will allow a more accurate interpretation of the present results. Free $[Ca^{2+}]_i$ measurements inside the endoplasmic reticulum have previously been reported (Montero et al., 1995; Barrero et al., 1997; Montero et al., 1997), suggesting that accurate measurement in highly restricted cellular compartments are feasible. The authors used a recombinant form of the Ca^{2+} binding photoprotein, aequorin, to measure Ca^{2+} subcompartments in the ER of HeLa Cells. However, very high ER Ca^{2+} levels (>100 μM) cannot be accurately measured with this technique.

Although the results from the present dissertation have addressed some characteristics of $I_{Cl(Ca)}$, additional work is needed to better understand their role in cone photoreceptors and recognize Cl^--dependent functions at the inner segments and synaptic terminals. However, a thorough pharmacological profile cannot be developed in the absence of highly specific blockers. Specific channel blockers with high binding affinity and high selectivity are currently unavailable for different classes of Cl channels, including Cl(Ca) channels. Although the venoms of various animals have developed highly effective toxins against other channel types (i.e. Na, K, and Ca channels), none have yet been discovered for Cl(Ca) channels. Given the low specificity of available Cl channel blockers, pharmacological studies should be interpreted with care. A potent and selective pharmacological tool would greatly help in the identification of the physiological function of Cl(Ca) channels in neurons (see below). Another important future study, also discussed below, will be to determine the molecular identity of channels responsible for $I_{Cl(Ca)}$. The mechanism of activation (i.e. directly by Ca^{2+} or by phosphorylation) of Cl(Ca) channels is still unknown. Finding regulatory sites (phosphorylation, Ca^{2+} itself and Ca^{2+}-binding protein sites) will contribute to our understanding of channel activation and inactivation. Investigations incorporating the techniques of molecular biology will be to identify functionally relevant areas on the protein, or additional subunits required for Ca^{2+} sensitivity, and to identify the physiological role of these channels in the nervous system.

7.2 Finding the major functional role for Cl(Ca) channels in cone photoreceptors

$I_{Cl(Ca)}$ is a prominent ionic current in cone photoreceptors. Although some of the pharmacological and biophysical properties of $I_{Cl(Ca)}$ have been characterized (Maricq and Korenbrot, 1988; Barnes and Hille, 1989; Barnes and Bui, 1991; Thoreson and Burkhardt, 1991), the major role of Cl(Ca) channels is still unclear. Photoreceptors are hyperpolarized by light. Following light stimulation, cyclic-nucleotide gated channels (CNGCs) in the outer segment close and Ca^{2+} influx ceases, but extrusion at the inner segment continues, greatly decreasing $[Ca^{2+}]_i$. In saturating light, Ca^{2+} levels in cone inner segments may be as low as 10-50 nM (Krizaj and Copenhagen, 1998; Sampath et al., 1999). Therefore, $I_{Cl(Ca)}$ must play a minor role under these conditions. In the dark, $[Ca^{2+}]_i$ is high (Ratto et al., 1988; Gray-Keller and Detwiler, 1996). Therefore, the Ca^{2+}-activated Cl^- conductance would be highest in darkness when voltage-gated Ca channels and light-sensitive cation channels are open, and lowest in bright light when both are closed.

7.2.1 $I_{Cl(Ca)}$ may play a significant role in mediating the effects of synaptic feedback from horizontal cells during surround illumination of a cone

$I_{Cl(Ca)}$ appears to be involved in stabilizing the presynaptic membrane potential, especially under specific conditions, such as during surround illumination of a cone photoreceptor. Lateral inhibitory interactions are essential for the center-surround antagonistic receptive field organization of neurons in the retina. Several retinal neurons have ON- or OFF-center receptive fields with an antagonistic surround, which were discovered by Kuffler (1953). Receptive fields are created by surround-induced

inhibitory feedback to improve edge detection, create colour opponency, and enhance contrast. Cone photoreceptors hyperpolarize in response to a light stimulus. However, these cells are subject to lateral inhibition in which slight depolarizations, resulting in a decreased light responsiveness, occur during the surround, or diffuse illumination of a cone (Baylor, 1971). Horizontal cells have large receptive fields and therefore can integrate a visual stimulus over a large area to provide negative feedback signals to cones via their laterally positioned dendrites embedded at the cone pedicle (O'Bryan, 1973; Verweij et al., 1996; Kraaij et al., 1998). This was well illustrated in a current-clamp experiment by Hirasawa and Kaneko (2003), where central cone photoreceptors hyperpolarized to a spot of light but slightly depolarized upon addition of diffuse illumination. The feedback response results in a membrane conductance increase of the central cone (O'Bryan, 1973; Piccolino and Gerschenfeld, 1980; Lasansky, 1981). It is now known that the targets of the feedback response from horizontal cells to cones during surround illumination are the presynaptic Ca channels. Although the identity of the feedback messenger is still controversial, it has been well established that the feedback response during surround illumination leads to a shift in the Ca channel activation curve to more negative potentials, which results in Ca^{2+} influx. In addition to increasing Ca channel activity at the plasma membrane, feedback during surround illumination also increases a Cl^- conductance and this has been shown by various studies, from turtle to primate (O'Bryan, 1973; Lasansky, 1981; Burkhardt, 1988; Verweij et al., 1996; Kraaij et al., 1998; Verweij et al., 2003). Therefore, horizontal cells provide surround inhibition to cone photoreceptors in part by modulating Ca and Cl(Ca) channel activation.

7.2.2 The role of $I_{Cl(Ca)}$ during the feedback response depends on E_{Cl}

Broad field or surround light stimuli strongly hyperpolarize horizontal cells and this causes, via the feedback synapse, an increase in both Ca channel and Cl(Ca) channel activity. The movement of Cl^- in and out of cells, and therefore, the polarity of the membrane potential response to Cl(Ca) channel activation, depends on the Cl^- equilibrium potential (E_{Cl}). The value of E_{Cl} in cone photoreceptors is not known but has been estimated at values ranging from -65 mV to -36 mV (Attwell et al., 1983; Kaneko and Tachibana, 1986; Thoreson and Burkhardt, 1991; Kraaij et al., 2000; Thoreson et al., 2000). During surround illumination, if E_{Cl} is positive to the resting membrane potential, the Cl^- conductance will enhance and prolong the depolarization created by Ca^{2+} influx. However, if E_{Cl} is more negative, Cl^- influx will stabilize the presynaptic membrane potential, allowing an increase in glutamate release via the increase in $[Ca^{2+}]_i$, but preventing a large depolarization (Maricq and Korenbrot, 1988; Barnes and Deschenes, 1992; Yagi and MacLeish, 1994). Agreement on E_{Cl}, which determines direction and amplitude of Cl^- currents, is a key parameter for understanding the physiological function of Cl(Ca) channels. A recent paper by Thoreson and Bryson (2004) investigated E_{Cl} in red-sensitive large single cones from tiger salamander retinal slice. Using both patch-clamp and Cl^--imaging experiments, their results indicate that E_{Cl} is very close to the dark resting potential, which sat at around -46 mV under their experimental conditions. These data suggest that activation of Cl(Ca) channels in cones when the cell is at its resting potential (although $[Ca^{2+}]_i$ is highest in darkness) would result in minimal intracellular Cl^- changes and stabilization of membrane potential.

Local variations of E_{Cl} exist within cells (Vardi et al., 2000). Approximating a value for E_{Cl} at an electrically isolated area, such as the cone pedicle, to predict the direction of current flow for the cone photoreceptor Cl(Ca) channel is not straightforward. However, $I_{Cl(Ca)}$ appears to play a role in limiting membrane depolarization during periods of significant Ca^{2+} influx, such as during feedback responses, where neurotransmitter release is increased without significant changes in membrane potential. Therefore, to stabilize presynaptic depolarizations, E_{Cl} is likely to be more negative than the membrane potential, in which case Ca^{2+} influx through voltage-gated Ca channels activates Cl(Ca) channels and facilitates an outward Cl^- current (influx of Cl^- ions). However, unless a physiological value is indisputably obtained, the direction of the conductance and its role in the feedback mechanism between horizontal cells and cone photoreceptors, will remain unknown.

7.3 Finding the molecular identity for Cl(Ca) channels in cone photoreceptors

The molecular identity for Cl(Ca) channels, as well as accessory proteins involved in Cl(Ca) channel expression and function in cone photoreceptors, has not yet been resolved. Revealing the molecular identity of Cl(Ca) channels is important for understanding their distribution, physiological function, and possible role in disease. Although whole-cell $I_{Cl(Ca)}$ seems similar in different tissues, several functional aspects, such as single channel properties (i.e. conductance, rectification, voltage-dependence, sensitivity, antagonists, CaM dependence), point to a considerable molecular diversity among Cl(Ca) channels.

Molecular candidates for Cl(Ca) channels include members of the ClC family of Cl channels (i.e. ClC-3), the bestrophin family, and the CLCA family. The ClC family of Cl channels has been well characterized, although the function of ClC-3 remains controversial (Duan et al., 1997; Stobrawa et al., 2001; Vessey et al., 2004). Although ClC-3 channels have been shown to be localized in the outer plexiform layer, where cone photoreceptor synaptic terminals reside, the present study suggests that ClC-3 channels are not responsible for cone $I_{Cl(Ca)}$ as a polyclonal antibody directed towards ClC-3 did not reduce $I_{Cl(Ca)}$. Bestrophins form a newly identified family of Cl channels (Sun et al., 2002) and are therefore less understood. These proteins, which are the product of the vitelliform macular dystrophy (*VMD2*) gene, have been identified as Ca^{2+}-activated Cl^- channel (Sun et al., 2002; Tsunenari et al., 2003; Qu et al., 2004). Although bestrophins have been shown to be sensitive to $[Ca^{2+}]_i$, whether they are related to the Cl(Ca) channels of interest in the present study remains to be studied.

7.3.1 Is the channel responsible for $I_{Cl(Ca)}$ a member of the CLCA family?

Several members of the CLCA gene family have been cloned from different mammalian species (i.e. bovine, mouse, and human). The very first gene encoding a Cl(Ca) channel was cloned by Cunningham et al. (1995) from bovine tracheal epithelium (*bCLCA1*). The primary structure of *bCLCA1* shows no similarity to any other cloned Cl^- -selective channel. Analysis of the primary amino acid sequence of cloned bCLCA1 predicts at least four putative transmembrane domains with extracellular N and C terminals, and structural models suggest that it co-assembles as a homotetrameric protein complex (see review by Jentsch et al., 2002). Since the identification of bCLCA1, a new

family member called lung-endothelial cell adhesion molecule-1, an endothelial adhesion protein that mediates cell adhesion of metastasic tumour cells, (Lu-ECAM-1; also called bCLCA2) was cloned from bovine aortic endothelial cells (Elble et al., 1997). In addition to the two bovine isoforms, three mouse (mCLCA1, Gandhi et al., 1998; Romio et al., 1999; mCLCA2, Lee et al., 1999; and mCLCA3, also called gob-5, Komiya et al., 1999), and four human (hCLCA1, Gruber et al., 1998b; hCLCA2, Gruber et al., 1999; hCLCA3, Gruber and Pauli 1999; hCLCA4, Agnel et al., 1999) CLCA family members have also been cloned. More recently, a pig CLCA protein (pCLCA1) has been cloned and shown to be located in several porcine exocrine tissues (Gaspar et al., 2000).

Although members of the CLCA family have been identified in different mammalian species, the biophysical properties of these channels may differ from those of salamander cone Cl(Ca) channels when expressed in a heterologous system. For example, when expressed in *Xenopus* oocytes, bCLCA1 is characterized by an outwardly rectifying Cl^- conductance, which is observed without raising $[Ca^{2+}]_i$ (Qu and Hartzell, 2000). On the other hand, currents in transfected in COS-7 cells are characterized by a linear *I-V* relation and are only observed upon raising $[Ca^{2+}]_i$ (Cunningham et al., 1995). Once the molecular identity is established, site-directed mutagenesis, cloning, and expression studies will enable investigators to link structural features to functional properties of Cl(Ca) channels.

Appendix 1

Ionomycin Increases $[Ca^{2+}]_i$ in a Sustained Manner in Salamander Cone Photoreceptors

Appendix 1 has been previously published in the following publication:

Lalonde MR, Barnes S. 2004. Inhibition of Cl(Ca) Channels in Response to High Intracellular Calcium Levels Due to Dephosphorylation-Mediated Ca channel Inhibition in Cone Photoreceptors. Society for Neuroscience, E-Abstract 65.12.

Goal: Investigate $[Ca^{2+}]_i$ changes in salamander cone photoreceptors in the presence of ionomycin using Ca^{2+}-imaging experiments.

Methods: Isolated salamander cone photoreceptors were loaded with the ratiometric calcium indicator dye Fura-4F (5 μM; 30 min incubation at room temperature). Ionomycin (10 μM) was added to the standard extracellular solution, which was delivered by a peristaltic pump. Changes in fluorescence before and during ionomycin superfusion were captured using a Sensicam cooled CCD camera following excitation at 340 and 380 nm (emission 510 nm). An increase in the Fura-4F ratio (340/380 nm) is indicative of increased $[Ca^{2+}]_i$.

Results: Ionomycin increased $[Ca^{2+}]_i$ in a sustained manner in all cells tested (n=4). On average, the measured ratio after 4 min of 10 μM ionomycin superfusion was 1.33 ± 0.11 compared to 0.24 ± 0.01 at baseline (n=4). A representative example is shown in the figure below, where the Fura-4F ratio is plotted against time.

Acknowledgment: I would like to thank Andrew Hartwick for performing these calcium-imaging experiments.

Appendix 1

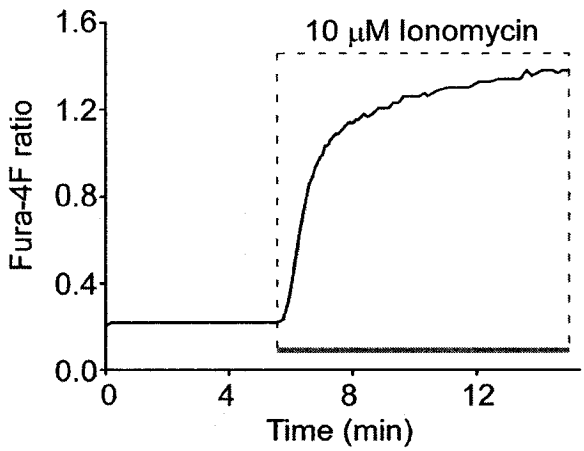

Appendix 2

IP_3-Induced Oscillations in $I_{Cl(Ca)}$

Appendix 2 has been previously published in the following publications:

Lalonde MR, Barnes S. 2003. Contribution of Calcium Stores to Activation of Chloride Current in Cone Photoreceptors. Society for Neuroscience, E-Abstract 791.18.

Lalonde MR, Barnes S. 2004. Inhibition of Cl(Ca) Channels in Response to High Intracellular Calcium Levels Due to Dephosphorylation-Mediated Ca channel Inhibition in Cone Photoreceptors. Society for Neuroscience, E-Abstract 65.12.

Goal: To demonstrate how inositol trisphosphate (IP_3), which generally did not modulate Ca^{2+}-activated Cl^- currents in cone photoreceptors (see Chapter 4; Section 4.2, Fig. 4.2), induced notable $I_{Cl(Ca)}$ oscillations in one out of six recordings from cones under the same conditions.

Methods: In the presence of IP_3 (100 μM; introduced with the recording pipette solution) this cell was held at -60 mV and subjected to the standard depolarizing protocol, which consisted of 10 mV voltage steps of 100 ms duration, from -70 mV to +60 mV every 5 sec.

Results and Discussion: The time course of current amplitude (current remaining plotted against time) illustrates the IP_3-induced self-regenerating cycles in the current during the step to -20 mV and the corresponding Ca^{2+}-activated Cl^- tail, which was recorded at -60 mV. The current traces and *I-V* relations at four time points (indicated in A) are highlighted in B and C, respectively. With IP_3 in the recording pipette solution, the current oscillated through different states. The current, which was of normal appearance 4 min following rupture of the whole-cell patch (solid line), was greatly enhanced at both the depolarizing voltage step and corresponding Ca^{2+}-activated Cl^- tail 5.5 min post-rupture (dotted line; B). At 6.5 min following rupture of the whole-cell patch (dashed line), the current recorded during depolarizing voltage steps was reduced. However, sustained activation of $I_{Cl(Ca)}$ was recorded at this time, which usually reflects a high $[Ca^{2+}]_i$ in the submembrane microdomains. Alternative interpretations, including IP_3-induced long-lived open states of Cl(Ca) channels, are possible. The large Ca^{2+}-

activated Cl^- conductance is reflected in the *I-V* relation as the current reverses close to E_{Cl} at 0 mV (dashed line; C). These data suggest that that the inhibited state of whole-cell current at 6.5 min was initiated via a decrease in Ca^{2+} influx through voltage-gated Ca channels. Interestingly, 8 min post-rupture (dotted dashed line), the Ca^{2+}-activated Cl^- tail current was completely inhibited, and inward current measured during depolarizing voltage steps to -20 mV was abolished. The inhibition of voltage-gated Ca channels, indirectly inhibiting the activation of Cl(Ca) channels at the plasma membrane, is a likely explanation for the inhibition of $I_{Cl(Ca)}$.

Conclusion: IP_3 induced oscillations in Cl(Ca) channel activation that ranged from maximum activation to complete inhibition within an approximate period of 3 minutes, was observed in one out of six recordings from cones. The present results are consistent with the presence of IP_3-sensitive Ca^{2+} stores in cone photoreceptors (Peng et al., 1991; Stella et al., 2003). The reason why Ca^{2+} ions, released from IP_3-sensitive Ca^{2+} stores, reached the submembrane level at a concentration high enough to modulate $I_{Cl(Ca)}$ in this particular cell is unknown and the interpretation of the oscillations can only be hypothesized. The regenerative release of Ca^{2+} from IP_3-sensitive Ca^{2+} stores (Berridge, 1993) is a plausible explanation for the observed oscillations in $I_{Cl(Ca)}$. Rhythmic Ca^{2+} release and re-uptake induced by IP_3 receptor activation have been described in a host of cell types (Berridge, 1993). The release of Ca^{2+} from IP_3-sensitive Ca^{2+} stores may have a positive feedback effect of $[Ca^{2+}]_i$ on the IP_3 receptors located at the endoplasmic reticulum membrane, causing them to cycle through Ca^{2+} release refractory periods.

Appendix 2 On one occasion, IP_3 produced oscillating responses in $I_{Cl(Ca)}$, possibly reflecting changes in $[Ca^{2+}]_i$ at the submembrane level. A cone photoreceptor was subjected to successive depolarizing voltage steps elicited by the standard depolarizing protocol in the presence of IP_3 (100 μM in the pipette solution). (**A**) Time course of current remaining (expressed as a percentage of control) measured during depolarizing voltage steps to -20 mV (Steps; black circles) and during repolarization following those steps (Tails; white circles). In the presence of IP_3, $I_{Cl(Ca)}$ oscillations were observed. (**B**) Current traces elicited by -20 mV depolarizing voltage steps at the corresponding time points identified in (**A**). In the presence of IP_3, the cell oscillated through four different states. Both step and tail currents, which were of normal appearance at 4 min post-rupture (solid line), were increased at 5.5 min following rupture of the whole-cell patch (dotted line). At 6.5 min post-rupture, although the current measured in response to the depolarizing voltage step to -20 mV was reduced, $I_{Cl(Ca)}$ was fully activated as the Ca^{2+}-activated Cl^- tail current was non-deactivating (dashed line). At 8 min post-rupture, both the current measured at the depolarizing voltage step and Ca^{2+}-activated Cl^- tail current were abolished (dotted dashed line). (**C**) Leak-subtracted *I-V* relations of the current measured at depolarizing voltage steps, corresponding to the time points identified in (**A**). At 4 min post-rupture (solid line), the typical *I-V* relation, reflecting a combination of I_{Ca} and $I_{Cl(Ca)}$, was increased 1.5 min later (dotted line). At 6.5 min, the *I-V* relation reversed close to E_{Cl} at 0 mV, reflecting the large $I_{Cl(Ca)}$ contribution. The strong inhibition at 8 min (dotted dashed line), is shown in the *I-V* relation, where no inward current can be detected.

Appendix 2

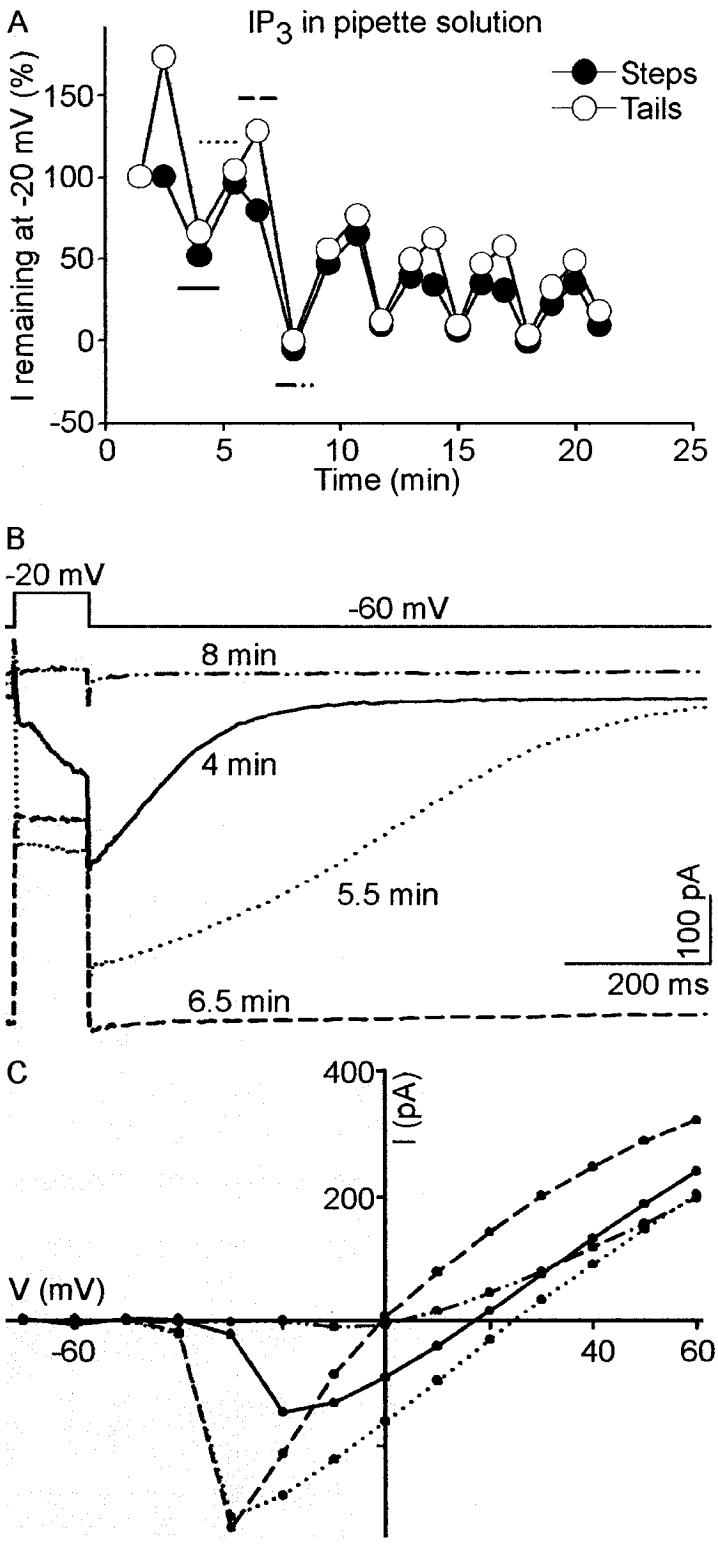
A
IP3 in pipette solution
Steps
Tails
I remaining at -20 mV (%)
150
100
50
0
-50
0
5
10
15
20
25
Time (min)
B
-20 mV
-60 mV
8 min
4 min
5.5 min
6.5 min
100 pA
200 ms
C
400
200
I (pA)
V (mV)
-60
40
60

References

Adly MA, Spiwoks-Becker I, Vollrath L (1999) Ultrastructural changes of photoreceptor synaptic ribbons in relation to time of day and illumination. Invest Ophthalmol Vis Sci 40:2165-2172.

Agnel M, Vermat T, Culouscou JM (1999) Identification of three novel members of the calcium-dependent chloride channel (CaCC) family predominantly expressed in the digestive tract and trachea. FEBS Lett 455:295-301.

Akasu T, Nishimura T, Tokimasa T (1990) Calcium-dependent chloride current in neurones of the rabbit pelvic parasympathetic ganglia. J Physiol 422:303-320.

Akbarali HI, Giles WR (1993) Ca2+ and Ca(2+)-activated Cl- currents in rabbit oesophageal smooth muscle. J Physiol 460:117-133.

Alonso MT, Barrero MJ, Michelena P, Carnicero E, Cuchillo I, Garcia AG, Garcia-Sancho J, Montero M, Alvarez J (1999) Ca2+-induced Ca2+ release in chromaffin cells seen from inside the ER with targeted aequorin. J Cell Biol 144:241-254.

Arreola J, Melvin JE, Begenisich T (1996) Activation of calcium-dependent chloride channels in rat parotid acinar cells. J Gen Physiol 108:35-47.

Arreola J, Melvin JE, Begenisich T (1998) Differences in regulation of Ca(2+)-activated Cl- channels in colonic and parotid secretory cells. Am J Physiol 274:C161-166.

Attwell D, Werblin FS, Wilson M (1982) The properties of single cones isolated from the tiger salamander retina. J Physiol 328:259-283.

Attwell D, Wilson M, Wu SM (1984) A quantitative analysis of interactions between photoreceptors in the salamander (Ambystoma) retina. J Physiol 352:703-737.

Baba-Aissa F, Raeymaekers L, Wuytack F, De Greef C, Missiaen L, Casteels R (1996) Distribution of the organellar Ca2+ transport ATPase SERCA2 isoforms in the cat brain. Brain Res 743:141-153.

Bader CR, Bertrand D, Schwartz EA (1982) Voltage-activated and calcium-activated currents studied in solitary rod inner segments from the salamander retina. J Physiol 331:253-284.

Bader CR, Bertrand D, Schlichter R (1987) Calcium-activated chloride current in cultured sensory and parasympathetic quail neurones. J Physiol 394:125-148.

Barish ME (1983) A transient calcium-dependent chloride current in the immature Xenopus oocyte. J Physiol 342:309-325.

Barnes S, Hille B (1989) Ionic channels of the inner segment of tiger salamander cone photoreceptors. J Gen Physiol 94:719-743.

Barnes S, Bui Q (1991) Modulation of calcium-activated chloride current via pH-induced changes of calcium channel properties in cone photoreceptors. J Neurosci 11:4015-4023.

Barnes S, Deschenes MC (1992) Contribution of Ca and Ca-activated Cl channels to regenerative depolarization and membrane bistability of cone photoreceptors. J Neurophysiol 68:745-755.

Barrero MJ, Montero M, Alvarez J (1997) Dynamics of [Ca2+] in the endoplasmic reticulum and cytoplasm of intact HeLa cells. A comparative study. J Biol Chem 272:27694-27699.

Baylor DA, Fuortes MG (1970) Electrical responses of single cones in the retina of the turtle. J Physiol 207:77-92.

Baylor DA, Fuortes MG, O'Bryan PM (1971) Receptive fields of cones in the retina of the turtle. J Physiol 214:265-294.

Beard NA, Sakowska MM, Dulhunty AF, Laver DR (2002) Calsequestrin is an inhibitor of skeletal muscle ryanodine receptor calcium release channels. Biophys J 82:310-320.

Bech-Hansen NT, Naylor MJ, Maybaum TA, Pearce WG, Koop B, Fishman GA, Mets M, Musarella MA, Boycott KM (1998) Loss-of-function mutations in a calcium-channel alpha1-subunit gene in Xp11.23 cause incomplete X-linked congenital stationary night blindness. Nat Genet 19:264-267.

Beech DJ, Barnes S (1989) Characterization of a voltage-gated K+ channel that accelerates the rod response to dim light. Neuron 3:573-581.

Bennett MK, Scheller RH (1994) Molecular correlates of synaptic vesicle docking and fusion. Curr Opin Neurobiol 4:324-329.

Berridge MJ (1993) Inositol trisphosphate and calcium signalling. Nature 361:315-325.

Berridge MJ (1998) Neuronal calcium signaling. Neuron 21:13-26.

Berridge MJ, Irvine RF (1984) Inositol trisphosphate, a novel second messenger in cellular signal transduction. Nature 312:315-321.

Berridge MJ, Lipp P, Bootman MD (2000) The versatility and universality of calcium signalling. Nat Rev Mol Cell Biol 1:11-21.

Bers DM, Patton CW, Nuccitelli R (1994) A practical guide to the preparation of Ca2+ buffers. Methods Cell Biol 40:3-29.

Bian JH, Ghosh TK, Wang JC, Gill DL (1991) Identification of intracellular calcium pools. Selective modification by thapsigargin. J Biol Chem 266:8801-8806.

Birnbaumer L, Campbell KP, Catterall WA, Harpold MM, Hofmann F, Horne WA, Mori Y, Schwartz A, Snutch TP, Tanabe T, et al. (1994) The naming of voltage-gated calcium channels. Neuron 13:505-506.

Bootman MD, Berridge MJ, Taylor CW (1992) All-or-nothing Ca2+ mobilization from the intracellular stores of single histamine-stimulated HeLa cells. J Physiol 450:163-178.

Bosl MR, Stein V, Hubner C, Zdebik AA, Jordt SE, Mukhopadhyay AK, Davidoff MS, Holstein AF, Jentsch TJ (2001) Male germ cells and photoreceptors, both dependent on close cell-cell interactions, degenerate upon ClC-2 Cl(-) channel disruption. Embo J 20:1289-1299.

Boton R, Dascal N, Gillo B, Lass Y (1989) Two calcium-activated chloride conductances in Xenopus laevis oocytes permeabilized with the ionophore A23187. J Physiol 408:511-534.

Boycott BB, Kolb H (1973) The connections between bipolar cells and photoreceptors in the retina of the domestic cat. J Comp Neurol 148:91-114.

Braekevelt CR (1993) Fine structure of the retinal photoreceptors of the tiger salamander (Ambystoma tigrinum). Histol Histopathol 8:265-272.

Brandstatter JH, Koulen P, Wassle H (1998) Diversity of glutamate receptors in the mammalian retina. Vision Res 38:1385-1397.

Brorson JR, Bleakman D, Gibbons SJ, Miller RJ (1991) The properties of intracellular calcium stores in cultured rat cerebellar neurons. J Neurosci 11:4024-4043.

Brown JE, Blazynski C, Cohen AI (1987) Light induces a rapid and transient increase in inositol-trisphosphate in toad rod outer segments. Biochem Biophys Res Commun 146:1392-1396.

Buck E, Zimanyi I, Abramson JJ, Pessah IN (1992) Ryanodine stabilizes multiple conformational states of the skeletal muscle calcium release channel. J Biol Chem 267:23560-23567.

Burkhardt DA, Gottesman J, Thoreson WB (1988) Prolonged depolarization in turtle cones evoked by current injection and stimulation of the receptive field surround. J Physiol 407:329-348.

Burns ME, Baylor DA (2001) Activation, deactivation, and adaptation in vertebrate photoreceptor cells. Annu Rev Neurosci 24:779-805.

Calkins DJ, Tsukamoto Y, Sterling P (1996) Foveal cones form basal as well as invaginating junctions with diffuse ON bipolar cells. Vision Res 36:3373-3381.

Callaway C, Seryshev A, Wang JP, Slavik KJ, Needleman DH, Cantu C, 3rd, Wu Y, Jayaraman T, Marks AR, Hamilton SL (1994) Localization of the high and low affinity [3H]ryanodine binding sites on the skeletal muscle Ca2+ release channel. J Biol Chem 269:15876-15884.

Cervetto L, Lagnado L, Perry RJ, Robinson DW, McNaughton PA (1989) Extrusion of calcium from rod outer segments is driven by both sodium and potassium gradients. Nature 337:740-743.

Chad JE, Eckert R (1984) Calcium domains associated with individual channels can account for anomalous voltage relations of CA-dependent responses. Biophys J 45:993-999.

Cheek TR, Moreton RB, Berridge MJ, Stauderman KA, Murawsky MM, Bootman MD (1993) Quantal Ca2+ release from caffeine-sensitive stores in adrenal chromaffin cells. J Biol Chem 268:27076-27083.

Chu A, Diaz-Munoz M, Hawkes MJ, Brush K, Hamilton SL (1990) Ryanodine as a probe for the functional state of the skeletal muscle sarcoplasmic reticulum calcium release channel. Mol Pharmacol 37:735-741.

Chun MH, Han SH, Chung JW, Wassle H (1993) Electron microscopic analysis of the rod pathway of the rat retina. J Comp Neurol 332:421-432.

Chun MH, Grunert U, Martin PR, Wassle H (1996) The synaptic complex of cones in the fovea and in the periphery of the macaque monkey retina. Vision Res 36:3383-3395.

Cohen AI, Todd RD, Harmon S, O'Malley KL (1992) Photoreceptors of mouse retinas possess D4 receptors coupled to adenylate cyclase. Proc Natl Acad Sci U S A 89:12093-12097.

Collier ML, Ji G, Wang Y, Kotlikoff MI (2000) Calcium-induced calcium release in smooth muscle: loose coupling between the action potential and calcium release. J Gen Physiol 115:653-662.

Copenhagen DR, Jahr CE (1989) Release of endogenous excitatory amino acids from turtle photoreceptors. Nature 341:536-539.

Cornwall MC, MacNichol EF, Jr., Fein A (1984) Absorptance and spectral sensitivity measurements of rod photoreceptors of the tiger salamander, Ambystoma tigrinum. Vision Res 24:1651-1659.

Coronado R, Morrissette J, Sukhareva M, Vaughan DM (1994) Structure and function of ryanodine receptors. Am J Physiol 266:C1485-1504.

Cseresnyes Z, Bustamante AI, Klein MG, Schneider MF (1997) Release-activated Ca2+ transport in neurons of frog sympathetic ganglia. Neuron 19:403-419.

Cunningham SA, Awayda MS, Bubien JK, Ismailov, II, Arrate MP, Berdiev BK, Benos DJ, Fuller CM (1995) Cloning of an epithelial chloride channel from bovine trachea. J Biol Chem 270:31016-31026.

Currie KP, Scott RH (1992) Calcium-activated currents in cultured neurones from rat dorsal root ganglia. Br J Pharmacol 106:593-602.

Currie KP, Wootton JF, Scott RH (1995) Activation of Ca(2+)-dependent Cl- currents in cultured rat sensory neurones by flash photolysis of DM-nitrophen. J Physiol 482 (Pt 2):291-307.

Danoff SK, Ferris CD, Donath C, Fischer GA, Munemitsu S, Ullrich A, Snyder SH, Ross CA (1991) Inositol 1,4,5-trisphosphate receptors: distinct neuronal and nonneuronal forms derived by alternative splicing differ in phosphorylation. Proc Natl Acad Sci U S A 88:2951-2955.

Dawson DC, Smith SS, Mansoura MK (1999) CFTR: mechanism of anion conduction. Physiol Rev 79:S47-75.

Detwiler PB, Gray-Keller MP (1992) Some unresolved issues in the physiology and biochemistry of phototransduction. Curr Opin Neurobiol 2:433-438.

DeVries SH (2001) Exocytosed protons feedback to suppress the Ca2+ current in mammalian cone photoreceptors. Neuron 32:1107-1117.

Dingledine R, Borges K, Bowie D, Traynelis SF (1999) The glutamate receptor ion channels. Pharmacol Rev 51:7-61.

Dowling JE (1987) The Retina: An approachable part of the brain. Cambridge, MA.: Belknap Press.

Dowling JE (1996) Retinal processing of vision. In: Comprehensive human physiology. (Eds. RGUW, ed), pp 773-788. New York: Springer-Verlag Berlin Heidelberg.

Dowling JE, Boycott BB (1966) Organization of the primate retina: electron microscopy. Proc R Soc Lond B Biol Sci 166:80-111.

Duan D, Winter C, Cowley S, Hume JR, Horowitz B (1997) Molecular identification of a volume-regulated chloride channel. Nature 390:417-421.

Duan D, Zhong J, Hermoso M, Satterwhite CM, Rossow CF, Hatton WJ, Yamboliev I, Horowitz B, Hume JR (2001) Functional inhibition of native volume-sensitive outwardly rectifying anion channels in muscle cells and Xenopus oocytes by anti-ClC-3 antibody. J Physiol 531:437-444.

Duncan RR, Westwood PK, Boyd A, Ashley RH (1997) Rat brain p64H1, expression of a new member of the p64 chloride channel protein family in endoplasmic reticulum. J Biol Chem 272:23880-23886.

Dutzler R, Campbell EB, Cadene M, Chait BT, MacKinnon R (2002) X-ray structure of a ClC chloride channel at 3.0 A reveals the molecular basis of anion selectivity. Nature 415:287-294.

Ehrlich BE, Kaftan E, Bezprozvannaya S, Bezprozvanny I (1994) The pharmacology of intracellular Ca(2+)-release channels. Trends Pharmacol Sci 15:145-149.

Elble RC, Ji G, Nehrke K, DeBiasio J, Kingsley PD, Kotlikoff MI, Pauli BU (2002) Molecular and functional characterization of a murine calcium-activated chloride channel expressed in smooth muscle. J Biol Chem 277:18586-18591.

Elble RC, Widom J, Gruber AD, Abdel-Ghany M, Levine R, Goodwin A, Cheng HC, Pauli BU (1997) Cloning and characterization of lung-endothelial cell adhesion molecule- 1 suggest it is an endothelial chloride channel. J Biol Chem 272:27853-27861.

Endo M (1977) Calcium release from the sarcoplasmic reticulum. Physiol Rev 57:71-108.

Enyedi A, Vorherr T, James P, McCormick DJ, Filoteo AG, Carafoli E, Penniston JT (1989) The calmodulin binding domain of the plasma membrane Ca2+ pump interacts both with calmodulin and with another part of the pump. J Biol Chem 264:12313-12321.

Enz R, Ross BJ, Cutting GR (1999) Expression of the voltage-gated chloride channel ClC-2 in rod bipolar cells of the rat retina. J Neurosci 19:9841-9847.

Ertel EA, Campbell KP, Harpold MM, Hofmann F, Mori Y, Perez-Reyes E, Schwartz A, Snutch TP, Tanabe T, Birnbaumer L, Tsien RW, Catterall WA (2000) Nomenclature of voltage-gated calcium channels. Neuron 25:533-535.

Estevez R, Boettger T, Stein V, Birkenhager R, Otto E, Hildebrandt F, Jentsch TJ (2001) Barttin is a Cl- channel beta-subunit crucial for renal Cl- reabsorption and inner ear K+ secretion. Nature 414:558-561.

Evans MG, Marty A (1986) Calcium-dependent chloride currents in isolated cells from rat lacrimal glands. J Physiol 378:437-460.

Fahlke C (2001) Ion permeation and selectivity in ClC-type chloride channels. Am J Physiol Renal Physiol 280:F748-757.

Fain GL, Matthews HR, Cornwall MC, Koutalos Y (2001) Adaptation in vertebrate photoreceptors. Physiol Rev 81:117-151.

Famiglietti EV, Jr., Kolb H (1975) A bistratified amacrine cell and synaptic cirucitry in the inner plexiform layer of the retina. Brain Res 84:293-300.

Ferris CD, Cameron AM, Huganir RL, Snyder SH (1992) Quantal calcium release by purified reconstituted inositol 1,4,5-trisphosphate receptors. Nature 356:350-352.

Fill M, Coronado R (1988) Ryanodine receptor channel of sarcoplasmic reticulum. Trends Neurosci 11:453-457.

Fill M, Copello JA (2002) Ryanodine receptor calcium release channels. Physiol Rev 82:893-922.

Fong P, Jentsch TJ (1995) Molecular basis of epithelial Cl channels. J Membr Biol 144:189-197.

Freihofer D, Kortje KH, Rahmann H (1990) Ultrastructural localization of endogenous calcium in the teleost retina. Histochem J 22:63-72.

Friel DD, Tsien RW (1992) A caffeine- and ryanodine-sensitive Ca2+ store in bullfrog sympathetic neurones modulates effects of Ca2+ entry on [Ca2+]i. J Physiol 450:217-246.

Frings S, Reuter D, Kleene SJ (2000) Neuronal Ca2+ -activated Cl- channels--homing in on an elusive channel species. Prog Neurobiol 60:247-289.

Fuller CM, Ji HL, Tousson A, Elble RC, Pauli BU, Benos DJ (2001) Ca(2+)-activated Cl(-) channels: a newly emerging anion transport family. Pflugers Arch 443:S107-110.

Furuichi T, Kohda K, Miyawaki A, Mikoshiba K (1994) Intracellular channels. Curr Opin Neurobiol 4:294-303.

Furuichi T, Simon-Chazottes D, Fujino I, Yamada N, Hasegawa M, Miyawaki A, Yoshikawa S, Guenet JL, Mikoshiba K (1993) Widespread expression of inositol 1,4,5-trisphosphate receptor type 1 gene (Insp3r1) in the mouse central nervous system. Receptors Channels 1:11-24.

Gadsby DC, Nairn AC (1994) Regulation of CFTR channel gating. Trends Biochem Sci 19:513-518.

Gan J, Iuvone PM (1997) Depolarization and activation of dihydropyridine-sensitive Ca2+ channels stimulate inositol phosphate accumulation in photoreceptor-enriched chick retinal cell cultures. J Neurochem 68:2300-2307.

Gandhi R, Elble RC, Gruber AD, Schreur KD, Ji HL, Fuller CM, Pauli BU (1998) Molecular and functional characterization of a calcium-sensitive chloride channel from mouse lung. J Biol Chem 273:32096-32101.

Garaschuk O, Yaari Y, Konnerth A (1997) Release and sequestration of calcium by ryanodine-sensitive stores in rat hippocampal neurones. J Physiol 502 (Pt 1):13-30.

Gaspar KJ, Racette KJ, Gordon JR, Loewen ME, Forsyth GW (2000) Cloning a chloride conductance mediator from the apical membrane of porcine ileal enterocytes. Physiol Genomics 3:101-111.

Ghalayini A, Anderson RE (1984) Phosphatidylinositol 4,5-bisphosphate: light-mediated breakdown in the vertebrate retina. Biochem Biophys Res Commun 124:503-506.

Ghalayini AJ, Anderson RE (1987) Activation of bovine rod outer segment phospholipase C by ATP and GTP. Neurosci Res Commun 1:119.

Goeger DE, Riley RT (1989) Interaction of cyclopiazonic acid with rat skeletal muscle sarcoplasmic reticulum vesicles. Effect on Ca2+ binding and Ca2+ permeability. Biochem Pharmacol 38:3995-4003.

Gola M, Crest M (1993) Colocalization of active KCa channels and Ca2+ channels within Ca2+ domains in helix neurons. Neuron 10:689-699.

Golovina VA, Blaustein MP (1997) Spatially and functionally distinct Ca2+ stores in sarcoplasmic and endoplasmic reticulum. Science 275:1643-1648.

Grant GB, Werblin FS (1996) A glutamate-elicited chloride current with transporter-like properties in rod photoreceptors of the tiger salamander. Vis Neurosci 13:135-144.

Gray-Keller MP, Detwiler PB (1996) Ca2+ dependence of dark- and light-adapted flash responses in rod photoreceptors. Neuron 17:323-331.

Groschner K, Schuhmann K, Baumgartner W, Pastushenko V, Schindler H, Romanin C (1995) Basal dephosphorylation controls slow gating of L-type Ca2+ channels in human vascular smooth muscle. FEBS Lett 373:30-34.

Gruber AD, Pauli BU (1999) Molecular cloning and biochemical characterization of a truncated, secreted member of the human family of Ca2+-activated Cl- channels. Biochim Biophys Acta 1444:418-423.

Gruber AD, Gandhi R, Pauli BU (1998a) The murine calcium-sensitive chloride channel (mCaCC) is widely expressed in secretory epithelia and in other select tissues. Histochem Cell Biol 110:43-49.

Gruber AD, Schreur KD, Ji HL, Fuller CM, Pauli BU (1999) Molecular cloning and transmembrane structure of hCLCA2 from human lung, trachea, and mammary gland. Am J Physiol 276:C1261-1270.

Gruber AD, Elble RC, Ji HL, Schreur KD, Fuller CM, Pauli BU (1998b) Genomic cloning, molecular characterization, and functional analysis of human CLCA1, the first human member of the family of Ca2+-activated Cl- channel proteins. Genomics 54:200-214.

Grunder S, Thiemann A, Pusch M, Jentsch TJ (1992) Regions involved in the opening of CIC-2 chloride channel by voltage and cell volume. Nature 360:759-762.

Guerini D, Garcia-Martin E, Zecca A, Guidi F, Carafoli E (1998) The calcium pump of the plasma membrane: membrane targeting, calcium binding sites, tissue-specific isoform expression. Acta Physiol Scand Suppl 643:265-273.

Gutierrez LM, Zhao XL, Hosey MM (1994) Protein kinase C-mediated regulation of L-type Ca channels from skeletal muscle requires phosphorylation of the alpha 1 subunit. Biochem Biophys Res Commun 202:857-865.

Gyorke I, Gyorke S (1998) Regulation of the cardiac ryanodine receptor channel by luminal Ca2+ involves luminal Ca2+ sensing sites. Biophys J 75:2801-2810.

Haase W, Friese W, Gordon RD, Muller H, Cook NJ (1990) Immunological characterization and localization of the Na+/Ca2(+)-exchanger in bovine retina. J Neurosci 10:1486-1494.

Hagiwara S, Takahashi K (1967) Surface density of calcium ions and calcium spikes in the barnacle muscle fiber membrane. J Gen Physiol 50:583-601.

Hamill OP, Marty A, Neher E, Sakmann B, Sigworth FJ (1981) Improved patch-clamp techniques for high-resolution current recording from cells and cell-free membrane patches. Pflugers Arch 391:85-100.

Haque R, Uchida K, Iuvone PM (1998) 8-Br-cGMP and cCMP phosphodiesterase (PDE) inhibitors stimulate intracellular calcium levels and inositol phosphate accumulation in cultured chick photoreceptor cells. Invest Ophthalmol Vis Sci 39:S1056.

Hare WA, Owen WG (1995) Similar effects of carbachol and dopamine on neurons in the distal retina of the tiger salamander. Vis Neurosci 12:443-455.

Harosi FI (1975) Absorption spectra and linear dichroism of some amphibian photoreceptors. J Gen Physiol 66:357-382.

Haverkamp S, Grunert U, Wassle H (2000) The cone pedicle, a complex synapse in the retina. Neuron 27:85-95.

Hayashi F, Amakawa T (1985) Light-mediated breakdown of phosphatidylinositol-4,5-bisphosphate in isolated rod outer segments of frog photoreceptor. Biochem Biophys Res Commun 128:954-959.

He L, Poblenz AT, Medrano CJ, Fox DA (2000) Lead and calcium produce rod photoreceptor cell apoptosis by opening the mitochondrial permeability transition pore. J Biol Chem 275:12175-12184.

Hernandez-Cruz A, Sala F, Adams PR (1990) Subcellular calcium transients visualized by confocal microscopy in a voltage-clamped vertebrate neuron. Science 247:858-862.

Hernandez-Cruz A, Diaz-Munoz M, Gomez-Chavarin M, Canedo-Merino R, Protti DA, Escobar AL, Sierralta J, Suarez-Isla BA (1995) Properties of the ryanodine-sensitive release channels that underlie caffeine-induced Ca2+ mobilization from intracellular stores in mammalian sympathetic neurons. Eur J Neurosci 7:1684-1699.

Herscher CJ, Rega AF (1996) Pre-steady-state kinetic study of the mechanism of inhibition of the plasma membrane Ca(2+)-ATPase by lanthanum. Biochemistry 35:14917-14922.

Hicks D, Molday RS (1986) Differential immunogold-dextran labeling of bovine and frog rod and cone cells using monoclonal antibodies against bovine rhodopsin. Exp Eye Res 42:55-71.

Hille B (2001) Ion Channels of Excitable Membranes, 3rd Edition. Sunderland, MA.: Sinauer Associates, Inc.

Hirasawa H, Kaneko A (2003) pH Changes in the Invaginating Synaptic Cleft Mediate Feedback from Horizontal Cells to Cone Photoreceptors by Modulating Ca2+ Channels. J Gen Physiol 122:657-671.

Inesi G, Sagara Y (1992) Thapsigargin, a high affinity and global inhibitor of intracellular Ca2+ transport ATPases. Arch Biochem Biophys 298:313-317.

Ishikawa T, Cook DI (1993) A Ca(2+)-activated Cl- current in sheep parotid secretory cells. J Membr Biol 135:261-271.

Ivanenko A, Baring MD, Airey JA, Sutko JL, Kenyon JL (1993) A caffeine- and ryanodine-sensitive Ca2+ store in avian sensory neurons. J Neurophysiol 70:710-722.

James P, Maeda M, Fischer R, Verma AK, Krebs J, Penniston JT, Carafoli E (1988) Identification and primary structure of a calmodulin binding domain of the Ca2+ pump of human erythrocytes. J Biol Chem 263:2905-2910.

Jenden DJ, Fairhurst AS (1969) The pharmacology of ryanodine. Pharmacol Rev 21:1-25.

Jentsch TJ, Gunther W (1997) Chloride channels: an emerging molecular picture. Bioessays 19:117-126.

Jentsch TJ, Steinmeyer K, Schwarz G (1990) Primary structure of Torpedo marmorata chloride channel isolated by expression cloning in Xenopus oocytes. Nature 348:510-514.

Jentsch TJ, Friedrich T, Schriever A, Yamada H (1999) The CLC chloride channel family. Pflugers Arch 437:783-795.

Jentsch TJ, Stein V, Weinreich F, Zdebik AA (2002) Molecular structure and physiological function of chloride channels. Physiol Rev 82:503-568.

Jin LQ, Goswami S, Cai G, Zhen X, Friedman E (2003) SKF83959 selectively regulates phosphatidylinositol-linked D1 dopamine receptors in rat brain. J Neurochem 85:378-386.

Jindrova H, Detwiler PB (1998) Protein kinase C and IP3 in photoresponses of functionally intact rod outer segments: constraints about their role. Physiol Res 47:285-290.

Johansen J, Kleinhaus AL (1988) Voltage clamp characterization of a calcium-dependent chloride conductance in a putative invertebrate motoneuron. J Comp Physiol [A] 162:57-65.

Juusola M, French AS, Uusitalo RO, Weckstrom M (1996) Information processing by graded-potential transmission through tonically active synapses. Trends Neurosci 19:292-297.

Kamermans M, Fahrenfort I, Schultz K, Janssen-Bienhold U, Sjoerdsma T, Weiler R (2001) Hemichannel-mediated inhibition in the outer retina. Science 292:1178-1180.

Kamp TJ, Hell JW (2000) Regulation of cardiac L-type calcium channels by protein kinase A and protein kinase C. Circ Res 87:1095-1102.

Kaneko A (1971) Electrical connexions between horizontal cells in the dogfish retina. J Physiol 213:95-105.

Kaneko A, Tachibana M (1986) Effects of gamma-aminobutyric acid on isolated cone photoreceptors of the turtle retina. J Physiol 373:443-461.

Kawasaki M, Uchida S, Monkawa T, Miyawaki A, Mikoshiba K, Marumo F, Sasaki S (1994) Cloning and expression of a protein kinase C-regulated chloride channel abundantly expressed in rat brain neuronal cells. Neuron 12:597-604.

Kenyon JL, Goff HR (1998) Temperature dependencies of Ca2+ current, Ca(2+)-activated Cl- current and Ca2+ transients in sensory neurones. Cell Calcium 24:35-48.

Khodakhah K, Ogden D (1993) Functional heterogeneity of calcium release by inositol trisphosphate in single Purkinje neurones, cultured cerebellar astrocytes, and peripheral tissues. Proc Natl Acad Sci U S A 90:4976-4980.

Kidd JF, Thorn P (2000) Intracellular Ca2+ and Cl- channel activation in secretory cells. Annu Rev Physiol 62:493-513.

Kim TS, Reid DM, Molday RS (1998) Structure-function relationships and localization of the Na/Ca-K exchanger in rod photoreceptors. J Biol Chem 273:16561-16567.

Kleene SJ (1997) High-gain, low-noise amplification in olfactory transduction. Biophys J 73:1110-1117.

Klockner U (1993) Intracellular calcium ions activate a low-conductance chloride channel in smooth-muscle cells isolated from human mesenteric artery. Pflugers Arch 424:231-237.

Koch MC, Steinmeyer K, Lorenz C, Ricker K, Wolf F, Otto M, Zoll B, Lehmann-Horn F, Grzeschik KH, Jentsch TJ (1992) The skeletal muscle chloride channel in dominant and recessive human myotonia. Science 257:797-800.

Kolb H (1974) The connections between horizontal cells and photoreceptors in the retina of the cat: electron microscopy of Golgi preparations. J Comp Neurol 155:1-14.

Kolb H (1994) The architecture of functional neural circuits in the vertebrate retina. The Proctor Lecture. Invest Ophthalmol Vis Sci 35:2385-2404.

Kolb H, Famiglietti EV (1974) Rod and cone pathways in the inner plexiform layer of cat retina. Science 186:47-49.

Kolb H, Nelson R (1983) Rod pathways in the retina of the cat. Vision Res 23:301-312.

Komiya T, Tanigawa Y, Hirohashi S (1999) Cloning and identification of the gene gob-5, which is expressed in intestinal goblet cells in mice. Biochem Biophys Res Commun 255:347-351.

Korn SJ, Weight FF (1987) Patch-clamp study of the calcium-dependent chloride current in AtT-20 pituitary cells. J Neurophysiol 58:1431-1451.

Korn SJ, Horn R (1989) Influence of sodium-calcium exchange on calcium current rundown and the duration of calcium-dependent chloride currents in pituitary cells, studied with whole cell and perforated patch recording. J Gen Physiol 94:789-812.

Kornak U, Kasper D, Bosl MR, Kaiser E, Schweizer M, Schulz A, Friedrich W, Delling G, Jentsch TJ (2001) Loss of the ClC-7 chloride channel leads to osteopetrosis in mice and man. Cell 104:205-215.

Koumi S, Sato R, Aramaki T (1994) Characterization of the calcium-activated chloride channel in isolated guinea-pig hepatocytes. J Gen Physiol 104:357-373.

Kraaij DA, Kamermans M, Spekreijse H (1998) Spectral sensitivity of the feedback signal from horizontal cells to cones in goldfish retina. Vis Neurosci 15:799-808.

Kraaij DA, Spekreijse H, Kamermans M (2000) The nature of surround-induced depolarizing responses in goldfish cones. J Gen Physiol 115:3-16.

Krizaj D, Witkovsky P (1993) Effects of submicromolar concentrations of dopamine on photoreceptor to horizontal cell communication. Brain Res 627:122-128.

Krizaj D, Copenhagen DR (1998) Compartmentalization of calcium extrusion mechanisms in the outer and inner segments of photoreceptors. Neuron 21:249-256.

Krizaj D, Copenhagen DR (2002) Calcium regulation in photoreceptors. Front Biosci 7:d2023-2044.

Krizaj D, Lai FA, Copenhagen DR (2003) Ryanodine stores and calcium regulation in the inner segments of salamander rods and cones. J Physiol 547:761-774.

Krizaj D, Liu X, Copenhagen DR (2004) Expression of calcium transporters in the retina of the tiger salamander (Ambystoma tigrinum). J Comp Neurol 475:463-480.

Krizaj D, Gabriel R, Owen WG, Witkovsky P (1998) Dopamine D2 receptor-mediated modulation of rod-cone coupling in the Xenopus retina. J Comp Neurol 398:529-538.

Krizaj D, Bao JX, Schmitz Y, Witkovsky P, Copenhagen DR (1999) Caffeine-sensitive calcium stores regulate synaptic transmission from retinal rod photoreceptors. J Neurosci 19:7249-7261.

Krizaj D, Demarco SJ, Johnson J, Strehler EE, Copenhagen DR (2002) Cell-specific expression of plasma membrane calcium ATPase isoforms in retinal neurons. J Comp Neurol 451:1-21.

Kuffler SW (1953) Discharge patterns and functional organization of mammalian retina. J Neurophysiol 16:37-68.

Lara B, Lopez MG, Villarroya M, Gandia L, Cleeman L, Morad M, Garcia AG (1997) A caffeine-sensitive Ca2+ store modulates K+-evoked secretion in chromaffin cells. Am J Physiol 272:C1211-1221.

Larsson HP, Picaud SA, Werblin FS, Lecar H (1996) Noise analysis of the glutamate-activated current in photoreceptors. Biophys J 70:733-742.

Lasansky A (1973) Organization of the outer synaptic layer in the retina of the larval tiger salamander. Philos Trans R Soc Lond B Biol Sci 265:471-489.

Lasansky A (1981) Synaptic action mediating cone responses to annular illumination in the retina of the larval tiger salamander. J Physiol 310:205-214.

Lasater EM, Witkovsky P (1991) The calcium current of turtle cone photoreceptor axon terminals. Neurosci Res Suppl 15:S165-173.

Lattanzio FA, Jr., Schlatterer RG, Nicar M, Campbell KP, Sutko JL (1987) The effects of ryanodine on passive calcium fluxes across sarcoplasmic reticulum membranes. J Biol Chem 262:2711-2718.

Laughlin SB (1989) The role of sensory adaptation in the retina. J Exp Biol 146:39-62.

Lee D, Ha S, Kho Y, Kim J, Cho K, Baik M, Choi Y (1999) Induction of mouse Ca(2+)-sensitive chloride channel 2 gene during involution of mammary gland. Biochem Biophys Res Commun 264:933-937.

Liebman PA, Entine G (1968) Visual pigments of frog and tadpole (Rana pipiens). Vision Res 8:761-775.

Lipscombe D, Madison DV, Poenie M, Reuter H, Tsien RW, Tsien RY (1988) Imaging of cytosolic Ca2+ transients arising from Ca2+ stores and Ca2+ channels in sympathetic neurons. Neuron 1:355-365.

Liu C, Hermann TE (1978) Characterization of ionomycin as a calcium ionophore. J Biol Chem 253:5892-5894.

Llinas R, Sugimori M, Silver RB (1992) Microdomains of high calcium concentration in a presynaptic terminal. Science 256:677-679.

Ludewig U, Pusch M, Jentsch TJ (1996) Two physically distinct pores in the dimeric ClC-0 chloride channel. Nature 383:340-343.

Lytton J, Westlin M, Hanley MR (1991) Thapsigargin inhibits the sarcoplasmic or endoplasmic reticulum Ca-ATPase family of calcium pumps. J Biol Chem 266:17067-17071.

MacLeish PR, Nurse CA (2000) Ion channel compartments in photoreceptors. Invest Ophthalmol Vis Sci 41:S494.

MacLeish PR, Barnstable CJ, Townes-Anderson E (1983) Use of a monoclonal antibody as a substrate for mature neurons in vitro. Proc Natl Acad Sci U S A 80:7014-7018.

MacLennan DH, Rice WJ, Green NM (1997) The mechanism of Ca2+ transport by sarco(endo)plasmic reticulum Ca2+-ATPases. J Biol Chem 272:28815-28818.

Maduke M, Miller C, Mindell JA (2000) A decade of CLC chloride channels: structure, mechanism, and many unsettled questions. Annu Rev Biophys Biomol Struct 29:411-438.

Makino CL, Dodd RL (1996) Multiple visual pigments in a photoreceptor of the salamander retina. J Gen Physiol 108:27-34.

Makino CL, Taylor WR, Baylor DA (1991) Rapid charge movements and photosensitivity of visual pigments in salamander rods and cones. J Physiol 442:761-780.

Mansergh F, Orton NC, Vessey JP, Lalonde MR, Stell WK, Tremblay F, Barnes S, Rancourt DE, Bech-Hansen NT Mutation of the Calcium Channel Gene Cacna1f Disrupts Calcium Signaling, Synaptic Transmission and Cellular Organization in Mouse Retina. J Neurosci Submitted.

Mariani AP (1986) Photoreceptors of the larval tiger salamander retina. Proc R Soc Lond B Biol Sci 227:483-492.

Maricq AV, Korenbrot JI (1988) Calcium and calcium-dependent chloride currents generate action potentials in solitary cone photoreceptors. Neuron 1:503-515.

Maricq AV, Korenbrot JI (1990a) Potassium currents in the inner segment of single retinal cone photoreceptors. J Neurophysiol 64:1929-1940.

Maricq AV, Korenbrot JI (1990b) Inward rectification in the inner segment of single retinal cone photoreceptors. J Neurophysiol 64:1917-1928.

Marmorstein AD, Marmorstein LY, Rayborn M, Wang X, Hollyfield JG, Petrukhin K (2000) Bestrophin, the product of the Best vitelliform macular dystrophy gene (VMD2), localizes to the basolateral plasma membrane of the retinal pigment epithelium. Proc Natl Acad Sci U S A 97:12758-12763.

Marmorstein LY, McLaughlin PJ, Stanton JB, Yan L, Crabb JW, Marmorstein AD (2002) Bestrophin interacts physically and functionally with protein phosphatase 2A. J Biol Chem 277:30591-30597.

Marrion NV, Adams PR (1992) Release of intracellular calcium and modulation of membrane currents by caffeine in bull-frog sympathetic neurones. J Physiol 445:515-535.

Martin DK (1993) Small conductance chloride channels in acinar cells from the rat mandibular salivary gland are directly controlled by a G-protein. Biochem Biophys Res Commun 192:1266-1273.

Martinez-Pinna J, McLachlan EM, Gallego R (2000) Distinct mechanisms for activation of Cl- and K+ currents by Ca2+ from different sources in mouse sympathetic neurones. J Physiol 527 Pt 2:249-264.

Marty A, Tan YP, Trautmann A (1984) Three types of calcium-dependent channel in rat lacrimal glands. J Physiol 357:293-325.

Masland RH (2001) The fundamental plan of the retina. Nat Neurosci 4:877-886.

Matchkov VV, Aalkjaer C, Nilsson H (2004) A cyclic GMP-dependent calcium-activated chloride current in smooth-muscle cells from rat mesenteric resistance arteries. J Gen Physiol 123:121-134.

Matsumura Y, Uchida S, Kondo Y, Miyazaki H, Ko SB, Hayama A, Morimoto T, Liu W, Arisawa M, Sasaki S, Marumo F (1999) Overt nephrogenic diabetes insipidus in mice lacking the CLC-K1 chloride channel. Nat Genet 21:95-98.

Mayer ML (1985) A calcium-activated chloride current generates the after-depolarization of rat sensory neurones in culture. J Physiol 364:217-239.

McBride DW, Jr., Roper SD (1991) Ca(2+)-dependent chloride conductance in Necturus taste cells. J Membr Biol 124:85-93.

McNulty TJ, Taylor CW (1993) Caffeine-stimulated Ca2+ release from the intracellular stores of hepatocytes is not mediated by ryanodine receptors. Biochem J 291 (Pt 3):799-801.

McPherson PS, Kim YK, Valdivia H, Knudson CM, Takekura H, Franzini-Armstrong C, Coronado R, Campbell KP (1991) The brain ryanodine receptor: a caffeine-sensitive calcium release channel. Neuron 7:17-25.

Meldolesi J, Pozzan T (1998) The endoplasmic reticulum Ca2+ store: a view from the lumen. Trends Biochem Sci 23:10-14.

Mercurio AM, Holtzman E (1982) Smooth endoplasmic reticulum and other agranular reticulum in frog retinal photoreceptors. J Neurocytol 11:263-293.

Middleton RE, Pheasant DJ, Miller C (1996) Homodimeric architecture of a ClC-type chloride ion channel. Nature 383:337-340.

Mignery GA, Sudhof TC (1990) The ligand binding site and transduction mechanism in the inositol-1,4,5-triphosphate receptor. Embo J 9:3893-3898.

Mikoshiba K, Furuichi T, Miyawaki A (1994) Structure and function of IP3 receptors. Semin Cell Biol 5:273-281.

Miledi R (1982) A calcium-dependent transient outward current in Xenopus laevis oocytes. Proc R Soc Lond B Biol Sci 215:491-497.

Mindell JA, Maduke M (2001) ClC chloride channels. Genome Biol 2.

Mironov SL, Usachev Yu M, Lux HD (1993) Spatial and temporal control of intracellular free Ca2+ in chick sensory neurons. Pflugers Arch 424:183-191.

Missiaen L, Taylor CW, Berridge MJ (1991) Spontaneous calcium release from inositol trisphosphate-sensitive calcium stores. Nature 352:241-244.

Missiaen L, De Smedt H, Droogmans G, Casteels R (1992) Luminal Ca2+ controls the activation of the inositol 1,4,5-trisphosphate receptor by cytosolic Ca2+. J Biol Chem 267:22961-22966.

Missotten L (1965) The ultrastructure of the human retina. Arscia S.A.

Mogami H, Tepikin AV, Petersen OH (1998) Termination of cytosolic Ca2+ signals: Ca2+ reuptake into intracellular stores is regulated by the free Ca2+ concentration in the store lumen. Embo J 17:435-442.

Monteith GR, Roufogalis BD (1995) The plasma membrane calcium pump--a physiological perspective on its regulation. Cell Calcium 18:459-470.

Montero M, Alvarez J, Scheenen WJ, Rizzuto R, Meldolesi J, Pozzan T (1997) Ca2+ homeostasis in the endoplasmic reticulum: coexistence of high and low [Ca2+] subcompartments in intact HeLa cells. J Cell Biol 139:601-611.

Montero M, Brini M, Marsault R, Alvarez J, Sitia R, Pozzan T, Rizzuto R (1995) Monitoring dynamic changes in free Ca2+ concentration in the endoplasmic reticulum of intact cells. Embo J 14:5467-5475.

Morgan AJ, Jacob R (1994) Ionomycin enhances Ca2+ influx by stimulating store-regulated cation entry and not by a direct action at the plasma membrane. Biochem J 300 (Pt 3):665-672.

Morgans CW (1999) Calcium channel heterogeneity among cone photoreceptors in the tree shrew retina. Eur J Neurosci 11:2989-2993.

Morgans CW (2000) Presynaptic proteins of ribbon synapses in the retina. Microsc Res Tech 50:141-150.

Morgans CW (2001) Localization of the alpha(1F) calcium channel subunit in the rat retina. Invest Ophthalmol Vis Sci 42:2414-2418.

Morgans CW, El Far O, Berntson A, Wassle H, Taylor WR (1998) Calcium extrusion from mammalian photoreceptor terminals. J Neurosci 18:2467-2474.

Morigiwa K, Vardi N (1999) Differential expression of ionotropic glutamate receptor subunits in the outer retina. J Comp Neurol 405:173-184.

Naka KI (1971) Receptive field mechanism in the vertebrate retina. Science 171:691-693.

Nakagawa T, Okano H, Furuichi T, Aruga J, Mikoshiba K (1991) The subtypes of the mouse inositol 1,4,5-trisphosphate receptor are expressed in a tissue-specific and developmentally specific manner. Proc Natl Acad Sci U S A 88:6244-6248.

Nakatani K, Yau KW (1988) Calcium and light adaptation in retinal rods and cones. Nature 334:69-71.

Nawy S, Jahr CE (1991) cGMP-gated conductance in retinal bipolar cells is suppressed by the photoreceptor transmitter. Neuron 7:677-683.

Neher E (1998) Vesicle pools and Ca2+ microdomains: new tools for understanding their roles in neurotransmitter release. Neuron 20:389-399.

Nelson R, Famiglietti EV, Jr., Kolb H (1978) Intracellular staining reveals different levels of stratification for on- and off-center ganglion cells in cat retina. J Neurophysiol 41:472-483.

Nilius B, Droogmans G (2003) Amazing chloride channels: an overview. Acta Physiol Scand 177:119-147.

Nilius B, Prenen J, Voets T, Van den Bremt K, Eggermont J, Droogmans G (1997a) Kinetic and pharmacological properties of the calcium-activated chloride-current in macrovascular endothelial cells. Cell Calcium 22:53-63.

Nilius B, Prenen J, Szucs G, Wei L, Tanzi F, Voets T, Droogmans G (1997b) Calcium-activated chloride channels in bovine pulmonary artery endothelial cells. J Physiol 498:381-396.

Nomura A, Shigemoto R, Nakamura Y, Okamoto N, Mizuno N, Nakanishi S (1994) Developmentally regulated postsynaptic localization of a metabotropic glutamate receptor in rat rod bipolar cells. Cell 77:361-369.

Nucifora FC, Jr., Li SH, Danoff S, Ullrich A, Ross CA (1995) Molecular cloning of a cDNA for the human inositol 1,4,5-trisphosphate receptor type 1, and the identification of a third alternatively spliced variant. Brain Res Mol Brain Res 32:291-296.

O'Bryan PM (1973) Properties of the depolarizing synaptic potential evoked by peripheral illumination in cones of the turtle retina. J Physiol 235:207-223.

Ogden DC, Capiod T, Walker JW, Trentham DR (1990) Kinetics of the conductance evoked by noradrenaline, inositol trisphosphate or Ca2+ in guinea-pig isolated hepatocytes. J Physiol 422:585-602.

Okada T, Horiguchi H, Tachibana M (1995) Ca(2+)-dependent Cl- current at the presynaptic terminals of goldfish retinal bipolar cells. Neurosci Res 23:297-303.

Orkand RK, Thomas RC (1995) Effects of low doses of caffeine on [Ca2+]i in voltage-clamped snail (Helix aspersa) neurones. J Physiol 489 (Pt 1):19-28.

Owen DG, Segal M, Barker JL (1986) Voltage-clamp analysis of a Ca2+- and voltage-dependent chloride conductance in cultured mouse spinal neurons. J Neurophysiol 55:1115-1135.

Palmer MJ, Hull C, Vigh J, von Gersdorff H (2003) Synaptic cleft acidification and modulation of short-term depression by exocytosed protons in retinal bipolar cells. J Neurosci 23:11332-11341.

Partridge LD (1994) Cytoplasmic Ca2+ activity regulation as measured by a calcium-activated current. Brain Res 647:76-82.

Patel S, Joseph SK, Thomas AP (1999) Molecular properties of inositol 1,4,5-trisphosphate receptors. Cell Calcium 25:247-264.

Peng YW, Sharp AH, Snyder SH, Yau KW (1991) Localization of the inositol 1,4,5-trisphosphate receptor in synaptic terminals in the vertebrate retina. Neuron 6:525-531.

Perry RJ, McNaughton PA (1991) Response properties of cones from the retina of the tiger salamander. J Physiol 433:561-587.

Pessah IN, Zimanyi I (1991) Characterization of multiple [3H]ryanodine binding sites on the Ca2+ release channel of sarcoplasmic reticulum from skeletal and cardiac muscle: evidence for a sequential mechanism in ryanodine action. Mol Pharmacol 39:679-689.

Picaud S, Larsson HP, Wellis DP, Lecar H, Werblin F (1995) Cone photoreceptors respond to their own glutamate release in the tiger salamander. Proc Natl Acad Sci U S A 92:9417-9421.

Piccolino M, Gerschenfeld HM (1980) Characteristics and ionic processes involved in feedback spikes of turtle cones. Proc R Soc Lond B Biol Sci 206:439-463.

Pin JP, Duvoisin R (1995) The metabotropic glutamate receptors: structure and functions. Neuropharmacology 34:1-26.

Piwon N, Gunther W, Schwake M, Bosl MR, Jentsch TJ (2000) ClC-5 Cl- -channel disruption impairs endocytosis in a mouse model for Dent's disease. Nature 408:369-373.

Pozzan T, Rizzuto R, Volpe P, Meldolesi J (1994) Molecular and cellular physiology of intracellular calcium stores. Physiol Rev 74:595-636.

Putney JW, Jr. (1986) A model for receptor-regulated calcium entry. Cell Calcium 7:1-12.

Putney JW, Jr. (1990) Capacitative calcium entry revisited. Cell Calcium 11:611-624.

Qin P, Pourcho RG (1999) Localization of AMPA-selective glutamate receptor subunits in the cat retina: a light- and electron-microscopic study. Vis Neurosci 16:169-177.

Qu Z, Hartzell HC (2000) Anion permeation in Ca(2+)-activated Cl(-) channels. J Gen Physiol 116:825-844.

Qu Z, Fischmeister R, Hartzell C (2004) Mouse bestrophin-2 is a bona fide Cl(-) channel: identification of a residue important in anion binding and conduction. J Gen Physiol 123:327-340.

Qu Z, Wei RW, Mann W, Hartzell HC (2003) Two bestrophins cloned from Xenopus laevis oocytes express Ca(2+)-activated Cl(-) currents. J Biol Chem 278:49563-49572.

Rabl K, Thoreson WB (2002) Calcium-dependent inactivation and depletion of synaptic cleft calcium ions combine to regulate rod calcium currents under physiological conditions. Eur J Neurosci 16:2070-2077.

Rao-Mirotznik R, Harkins AB, Buchsbaum G, Sterling P (1995) Mammalian rod terminal: architecture of a binary synapse. Neuron 14:561-569.

Ratto GM, Payne R, Owen WG, Tsien RY (1988) The concentration of cytosolic free calcium in vertebrate rod outer segments measured with fura-2. J Neurosci 8:3240-3246.

Reid DM, Friedel U, Molday RS, Cook NJ (1990) Identification of the sodium-calcium exchanger as the major ricin-binding glycoprotein of bovine rod outer segments and its localization to the plasma membrane. Biochemistry 29:1601-1607.

Rhee SG, Bae YS (1997) Regulation of phosphoinositide-specific phospholipase C isozymes. J Biol Chem 272:15045-15048.

Rieke F, Schwartz EA (1996) Asynchronous transmitter release: control of exocytosis and endocytosis at the salamander rod synapse. J Physiol 493 (Pt 1):1-8.

Rios E, Stern MD (1997) Calcium in close quarters: microdomain feedback in excitation-contraction coupling and other cell biological phenomena. Annu Rev Biophys Biomol Struct 26:47-82.

Ripps H, Chappell RL (1991) Ultrastructural and electrophysiological changes associated with K(+)-evoked release of neurotransmitter at the synaptic terminals of skate photoreceptors. Vis Neurosci 7:597-609.

Rogawski MA, Inoue K, Suzuki S, Barker JL (1988) A slow calcium-dependent chloride conductance in clonal anterior pituitary cells. J Neurophysiol 59:1854-1870.

Romio L, Musante L, Cinti R, Seri M, Moran O, Zegarra-Moran O, Galietta LJ (1999) Characterization of a murine gene homologous to the bovine CaCC chloride channel. Gene 228:181-188.

Rossi D, Sorrentino V (2002) Molecular genetics of ryanodine receptors Ca2+-release channels. Cell Calcium 32:307-319.

Rousseau E, Smith JS, Meissner G (1987) Ryanodine modifies conductance and gating behavior of single Ca2+ release channel. Am J Physiol 253:C364-368.

Sagara Y, Wade JB, Inesi G (1992) A conformational mechanism for formation of a dead-end complex by the sarcoplasmic reticulum ATPase with thapsigargin. J Biol Chem 267:1286-1292.

Sampath AP, Matthews HR, Cornwall MC, Bandarchi J, Fain GL (1999) Light-dependent changes in outer segment free-Ca2+ concentration in salamander cone photoreceptors. J Gen Physiol 113:267-277.

Sanchez-Vives MV, Gallego R (1994) Calcium-dependent chloride current induced by axotomy in rat sympathetic neurons. J Physiol 475:391-400.

Schaeffer SF, Raviola E, Heuser JE (1982) Membrane specializations in the outer plexiform layer of the turtle retina. J Comp Neurol 204:253-267.

Schiavo G, Rossetto O, Montecucco C (1994) Clostridial neurotoxins as tools to investigate the molecular events of neurotransmitter release. Semin Cell Biol 5:221-229.

Schmid A, Dehlinger-Kremer M, Schulz I, Gogelein H (1990) Voltage-dependent InsP3-insensitive calcium channels in membranes of pancreatic endoplasmic reticulum vesicles. Nature 346:374-376.

Schmitz Y, Witkovsky P (1996) Glutamate release by the intact light-responsive photoreceptor layer of the Xenopus retina. J Neurosci Methods 68:55-60.

Schnetkamp PP, Basu DK, Szerencsei RT (1989) Na+-Ca2+ exchange in bovine rod outer segments requires and transports K+. Am J Physiol 257:C153-157.

Schultz K, Goldman DJ, Ohtsuka T, Hirano J, Barton L, Stell WK (1997) Identification and localization of an immunoreactive AMPA-type glutamate receptor subunit (GluR4) with respect to identified photoreceptor synapses in the outer plexiform layer of goldfish retina. J Neurocytol 26:651-666.

Scott RH, McGuirk SM, Dolphin AC (1988) Modulation of divalent cation-activated chloride ion currents. Br J Pharmacol 94:653-662.

Scott RH, Sutton KG, Griffin A, Stapleton SR, Currie KP (1995) Aspects of calcium-activated chloride currents: a neuronal perspective. Pharmacol Ther 66:535-565.

Seidler NW, Jona I, Vegh M, Martonosi A (1989) Cyclopiazonic acid is a specific inhibitor of the Ca2+-ATPase of sarcoplasmic reticulum. J Biol Chem 264:17816-17823.

Sheppard DN, Welsh MJ (1999) Structure and function of the CFTR chloride channel. Physiol Rev 79:S23-45.

Sherry DM, Bui DD, Degrip WJ (1998) Identification and distribution of photoreceptor subtypes in the neotenic tiger salamander retina. Vis Neurosci 15:1175-1187.

Shmigol A, Svichar N, Kostyuk P, Verkhratsky A (1996) Gradual caffeine-induced Ca2+ release in mouse dorsal root ganglion neurons is controlled by cytoplasmic and luminal Ca2+. Neuroscience 73:1061-1067.

Simon DB, Bindra RS, Mansfield TA, Nelson-Williams C, Mendonca E, Stone R, Schurman S, Nayir A, Alpay H, Bakkaloglu A, Rodriguez-Soriano J, Morales JM, Sanjad SA, Taylor CM, Pilz D, Brem A, Trachtman H, Griswold W, Richard GA, John E, Lifton RP (1997) Mutations in the chloride channel gene, CLCNKB, cause Bartter's syndrome type III. Nat Genet 17:171-178.

Sitsapesan R, Williams AJ (1997) Regulation of current flow through ryanodine receptors by luminal Ca2+. J Membr Biol 159:179-185.

Slaughter MM, Miller RF (1985) Identification of a distinct synaptic glutamate receptor on horizontal cells in mudpuppy retina. Nature 314:96-97.

Smith JS, Imagawa T, Ma J, Fill M, Campbell KP, Coronado R (1988) Purified ryanodine receptor from rabbit skeletal muscle is the calcium-release channel of sarcoplasmic reticulum. J Gen Physiol 92:1-26.

Snutch TP, Leonard JP, Gilbert MM, Lester HA, Davidson N (1990) Rat brain expresses a heterogeneous family of calcium channels. Proc Natl Acad Sci U S A 87:3391-3395.

Solessio E, Lasater EM (2002) Calcium-induced calcium release and calcium buffering in retinal horizontal cells. Vis Neurosci 19:713-725.

Solovyova N, Veselovsky N, Toescu EC, Verkhratsky A (2002) Ca(2+) dynamics in the lumen of the endoplasmic reticulum in sensory neurons: direct visualization of Ca(2+)-induced Ca(2+) release triggered by physiological Ca(2+) entry. Embo J 21:622-630.

Somlyo AP, Walz B (1985) Elemental distribution in Rana pipiens retinal rods: quantitative electron probe analysis. J Physiol 358:183-195.

Sorrentino V (1995) The ryanodine receptor family of intracellular calcium release channels. Adv Pharmacol 33:67-90.

Sorrentino V, Rizzuto R (2001) Molecular genetics of Ca(2+) stores and intracellular Ca(2+) signalling. Trends Pharmacol Sci 22:459-464.

Steele EC, Chen X, Nurse CA, MacLeish PR (2002) Functional colocalization of calcium channels, calcium-dependent anion channels, and intracellular calcium stores in the presynaptic terminals of vertebrate photoreceptors. Society for Neuroscience 115.5 (Abstr.).

Steinmeyer K, Klocke R, Ortland C, Gronemeier M, Jockusch H, Grunder S, Jentsch TJ (1991) Inactivation of muscle chloride channel by transposon insertion in myotonic mice. Nature 354:304-308.

Stella SL, Jr., Thoreson WB (2000) Differential modulation of rod and cone calcium currents in tiger salamander retina by D2 dopamine receptors and cAMP. Eur J Neurosci 12:3537-3548.

Stella SL, Jr., Bryson EJ, Thoreson WB (2002) A2 adenosine receptors inhibit calcium influx through L-type calcium channels in rod photoreceptors of the salamander retina. J Neurophysiol 87:351-360.

Stella SL, Jr., Hirano AH, Vila A, Sabatini A, Brecha NC (2003) IP_3 receptors are localized to ribbon synapses within terminals of photoreceptors and bipolar cells in mammalian retina. Society for Neuroscience 263.8 (Abstr.).

Stern MD (1998) Exploring local calcium feedback: trying to fool mother nature. J Gen Physiol 112:259-262.

Stobrawa SM, Breiderhoff T, Takamori S, Engel D, Schweizer M, Zdebik AA, Bosl MR, Ruether K, Jahn H, Draguhn A, Jahn R, Jentsch TJ (2001) Disruption of ClC-3, a chloride channel expressed on synaptic vesicles, leads to a loss of the hippocampus. Neuron 29:185-196.

Streb H, Irvine RF, Berridge MJ, Schulz I (1983) Release of Ca2+ from a nonmitochondrial intracellular store in pancreatic acinar cells by inositol-1,4,5-trisphosphate. Nature 306:67-69.

Strehler EE, Zacharias DA (2001) Role of alternative splicing in generating isoform diversity among plasma membrane calcium pumps. Physiol Rev 81:21-50.

Strehler EE, Treiman M (2004) Calcium pumps of plasma membrane and cell interior. Curr Mol Med 4:323-335.

Strom TM, Nyakatura G, Apfelstedt-Sylla E, Hellebrand H, Lorenz B, Weber BH, Wutz K, Gutwillinger N, Ruther K, Drescher B, Sauer C, Zrenner E, Meitinger T, Rosenthal A, Meindl A (1998) An L-type calcium-channel gene mutated in incomplete X-linked congenital stationary night blindness. Nat Genet 19:260-263.

Stuhmer W, Conti F, Suzuki H, Wang XD, Noda M, Yahagi N, Kubo H, Numa S (1989) Structural parts involved in activation and inactivation of the sodium channel. Nature 339:597-603.

Sun H, Tsunenari T, Yau KW, Nathans J (2002) The vitelliform macular dystrophy protein defines a new family of chloride channels. Proc Natl Acad Sci U S A 99:4008-4013.

Sutko JL, Ito K, Kenyon JL (1985) Ryanodine: a modifier of sarcoplasmic reticulum calcium release in striated muscle. Fed Proc 44:2984-2988.

Szegedi C, Sarkozi S, Herzog A, Jona I, Varsanyi M (1999) Calsequestrin: more than 'only' a luminal Ca2+ buffer inside the sarcoplasmic reticulum. Biochem J 337 (Pt 1):19-22.

Szerencsei RT, Prinsen CF, Schnetkamp PP (2001) Stoichiometry of the retinal cone Na/Ca-K exchanger heterologously expressed in insect cells: comparison with the bovine heart Na/Ca exchanger. Biochemistry 40:6009-6015.

Takahashi T, Neher E, Sakmann B (1987) Rat brain serotonin receptors in Xenopus oocytes are coupled by intracellular calcium to endogenous channels. Proc Natl Acad Sci U S A 84:5063-5067.

Taleb O, Feltz P, Bossu JL, Feltz A (1988) Small-conductance chloride channels activated by calcium on cultured endocrine cells from mammalian pars intermedia. Pflugers Arch 412:641-646.

Taylor CW (1998) Inositol trisphosphate receptors: Ca2+-modulated intracellular Ca2+ channels. Biochim Biophys Acta 1436:19-33.

Taylor CW, da Fonseca PC, Morris EP (2004) IP(3) receptors: the search for structure. Trends Biochem Sci 29:210-219.

Taylor R, Roper S (1994) Ca(2+)-dependent Cl- conductance in taste cells from Necturus. J Neurophysiol 72:475-478.

Taylor WR, Morgans C (1998) Localization and properties of voltage-gated calcium channels in cone photoreceptors of Tupaia belangeri. Vis Neurosci 15:541-552.

Thastrup O, Cullen PJ, Drobak BK, Hanley MR, Dawson AP (1990) Thapsigargin, a tumor promoter, discharges intracellular Ca2+ stores by specific inhibition of the endoplasmic reticulum Ca2(+)-ATPase. Proc Natl Acad Sci U S A 87:2466-2470.

Thayer SA, Miller RJ (1990) Regulation of the intracellular free calcium concentration in single rat dorsal root ganglion neurones in vitro. J Physiol 425:85-115.

Thayer SA, Perney TM, Miller RJ (1988a) Regulation of calcium homeostasis in sensory neurons by bradykinin. J Neurosci 8:4089-4097.

Thayer SA, Hirning LD, Miller RJ (1988b) The role of caffeine-sensitive calcium stores in the regulation of the intracellular free calcium concentration in rat sympathetic neurons in vitro. Mol Pharmacol 34:664-673.

Thayer SA, Usachev YM, Pottorf WJ (2002) Modulating Ca2+ clearance from neurons. Front Biosci 7:d1255-1279.

Thiemann A, Grunder S, Pusch M, Jentsch TJ (1992) A chloride channel widely expressed in epithelial and non-epithelial cells. Nature 356:57-60.

Thoreson WB, Burkhardt DA (1991) Ionic influences on the prolonged depolarization of turtle cones in situ. J Neurophysiol 65:96-110.

Thoreson WB, Miller RF (1996) Removal of extracellular chloride suppresses transmitter release from photoreceptor terminals in the mudpuppy retina. J Gen Physiol 107:631-642.

Thoreson WB, Bryson EJ (2004) Chloride equilibrium potential in salamander cones. BMC Neurosci 5:53.

Thoreson WB, Nitzan R, Miller RF (2000) Chloride efflux inhibits single calcium channel open probability in vertebrate photoreceptors: chloride imaging and cell-attached patch- clamp recordings. Vis Neurosci 17:197-206.

Thurman CL, Burns JS, O'Neil RG (2000) Identifying the Ca(++) signalling sources activating chloride currents in Xenopus oocytes using ionomycin and thapsigargin. Cell Signal 12:629-635.

Tinker A, Williams AJ (1993) Probing the structure of the conduction pathway of the sheep cardiac sarcoplasmic reticulum calcium-release channel with permeant and impermeant organic cations. J Gen Physiol 102:1107-1129.

Townes-Anderson E, MacLeish PR, Raviola E (1985) Rod cells dissociated from mature salamander retina: ultrastructure and uptake of horseradish peroxidase. J Cell Biol 100:175-188.

Toyoda J, Hashimoto H, Anno H, Tomita T (1970) The rod response in the frog and studies by intracellular recording. Vision Res 10:1093-1100.

Toyoshima C, Nakasako M, Nomura H, Ogawa H (2000) Crystal structure of the calcium pump of sarcoplasmic reticulum at 2.6 A resolution. Nature 405:647-655.

Tripathy A, Meissner G (1996) Sarcoplasmic reticulum lumenal Ca2+ has access to cytosolic activation and inactivation sites of skeletal muscle Ca2+ release channel. Biophys J 70:2600-2615.

Tsien RW, Lipscombe D, Madison DV, Bley KR, Fox AP (1988) Multiple types of neuronal calcium channels and their selective modulation. Trends Neurosci 11:431-438.

Tsunenari T, Sun H, Williams J, Cahill H, Smallwood P, Yau KW, Nathans J (2003) Structure-function analysis of the bestrophin family of anion channels. J Biol Chem 278:41114-41125.

Ungar F, Piscopo I, Letizia J, Holtzman E (1984) Uptake of calcium by the endoplasmic reticulum of the frog photoreceptor. J Cell Biol 98:1645-1655.

Vardi N, Morigiwa K (1997) ON cone bipolar cells in rat express the metabotropic receptor mGluR6. Vis Neurosci 14:789-794.

Vardi N, Zhang LL, Payne JA, Sterling P (2000) Evidence that different cation chloride cotransporters in retinal neurons allow opposite responses to GABA. J Neurosci 20:7657-7663.

Vardi N, Morigiwa K, Wang TL, Shi YJ, Sterling P (1998) Neurochemistry of the mammalian cone 'synaptic complex'. Vision Res 38:1359-1369.

Verboomen H, Wuytack F, De Smedt H, Himpens B, Casteels R (1992) Functional difference between SERCA2a and SERCA2b Ca2+ pumps and their modulation by phospholamban. Biochem J 286 (Pt 2):591-595.

Verweij J, Kamermans M, Spekreijse H (1996) Horizontal cells feed back to cones by shifting the cone calcium-current activation range. Vision Res 36:3943-3953.

Verweij J, Hornstein EP, Schnapf JL (2003) Surround antagonism in macaque cone photoreceptors. J Neurosci 23:10249-10257.

Vessey JP, Shi C, Jollimore CA, Stevens KT, Coca-Prados M, Barnes S, Kelly ME (2004) Hyposmotic activation of ICl,swell in rabbit nonpigmented ciliary epithelial cells involves increased ClC-3 trafficking to the plasma membrane. Biochem Cell Biol 82:708-718.

Wagenknecht T, Samso M (2002) Three-dimensional reconstruction of ryanodine receptors. Front Biosci 7:d1464-1474.

Wagner HJ (1997) Presynaptic bodies ("ribbons"): from ultrastructural observations to molecular perspectives. Cell Tissue Res 287:435-446.

Walker D, De Waard M (1998) Subunit interaction sites in voltage-dependent Ca2+ channels: role in channel function. Trends Neurosci 21:148-154.

Wang TL, Sterling P, Vardi N (1999) Localization of type I inositol 1,4,5-triphosphate receptor in the outer segments of mammalian cones. J Neurosci 19:4221-4228.

Ward SM, Kenyon JL (2000) The spatial relationship between Ca2+ channels and Ca2+-activated channels and the function of Ca2+-buffering in avian sensory neurons. Cell Calcium 28:233-246.

Wassle H, Boycott BB (1991) Functional architecture of the mammalian retina. Physiol Rev 71:447-480.

Wheeler JJ, Veiro JA, Cullis PR (1994) Ionophore-mediated loading of Ca2+ into large unilamellar vesicles in response to transmembrane pH gradients. Mol Membr Biol 11:151-157.

Wictome M, Michelangeli F, Lee AG, East JM (1992) The inhibitors thapsigargin and 2,5-di(tert-butyl)-1,4-benzohydroquinone favour the E2 form of the Ca2+,Mg(2+)-ATPase. FEBS Lett 304:109-113.

Wilkinson MF, Barnes S (1996) The dihydropyridine-sensitive calcium channel subtype in cone photoreceptors. J Gen Physiol 107:621-630.

Witkovsky P, Schmitz Y, Akopian A, Krizaj D, Tranchina D (1997) Gain of rod to horizontal cell synaptic transfer: relation to glutamate release and a dihydropyridine-sensitive calcium current. J Neurosci 17:7297-7306.

Wu KD, Lee WS, Wey J, Bungard D, Lytton J (1995) Localization and quantification of endoplasmic reticulum Ca(2+)-ATPase isoform transcripts. Am J Physiol 269:C775-784.

Wu SM (1991) Input-output relations of the feedback synapse between horizontal cells and cones in the tiger salamander retina. J Neurophysiol 65:1197-1206.

Wuytack F, Raeymaekers L, Missiaen L (2002) Molecular physiology of the SERCA and SPCA pumps. Cell Calcium 32:279-305.

Yagi T, Macleish PR (1994) Ionic conductances of monkey solitary cone inner segments. J Neurophysiol 71:656-665.

Yamashita M, Wassle H (1991) Responses of rod bipolar cells isolated from the rat retina to the glutamate agonist 2-amino-4-phosphonobutyric acid (APB). J Neurosci 11:2372-2382.

Yamoah EN, Lumpkin EA, Dumont RA, Smith PJ, Hudspeth AJ, Gillespie PG (1998) Plasma membrane Ca2+-ATPase extrudes Ca2+ from hair cell stereocilia. J Neurosci 18:610-624.

Yarfitz S, Hurley JB (1994) Transduction mechanisms of vertebrate and invertebrate photoreceptors. J Biol Chem 269:14329-14332.

Yazulla S, Studholme KM (1999) Co-localization of Shaker A-type K+ channel (Kv1.4) and AMPA-glutamate receptor (GluR4) immunoreactivities to dendrites of OFF-bipolar cells of goldfish retina. J Neurocytol 28:63-73.

Yoshida S, Plant S (1992) Mechanism of release of Ca2+ from intracellular stores in response to ionomycin in oocytes of the frog Xenopus laevis. J Physiol 458:307-318.

Yoshizaki K, Hoshino T, Sato M, Koyano H, Nohmi M, Hua SY, Kuba K (1995) Ca(2+)-induced Ca2+ release and its activation in response to a single action potential in rabbit otic ganglion cells. J Physiol 486 (Pt 1):177-187.

Zhang L, Franzini-Armstrong C, Ramesh V, Jones LR (2001) Structural alterations in cardiac calcium release units resulting from overexpression of junctin. J Mol Cell Cardiol 33:233-247.

Zimanyi I, Buck E, Abramson JJ, Mack MM, Pessah IN (1992) Ryanodine induces persistent inactivation of the Ca2+ release channel from skeletal muscle sarcoplasmic reticulum. Mol Pharmacol 42:1049-1057.

Zygmunt AC, Gibbons WR (1992) Properties of the calcium-activated chloride current in heart. J Gen Physiol 99:391-414.